Università degli Studi di Ferrara

INTERNATIONAL DOCTORAL COURSE IN
"EARTH AND MARINE SCIENCES (EMAS)"

CYCLE XXXV

COORDINATOR Prof. Ciavola Paolo

# GEOCHEMICAL INVESTIGATION OF THE SOIL ORGANIC CARBON AND EVALUATION OF ITS DEPLETION: THE CASE STUDY OF FERRARA PROVINCE (NORTHERN ITALY)

Scientific/Disciplinary Sector (SDS) GEO/09

**Candidate**
Dott. Salani Gian Marco

**Supervisor**
Prof. Bianchini Gianluca

**Co-Supervisor**
Dr. Brombin Valentina

Years 2019/2022

# Table of contents

**Abbreviation list** ..... **5**

**1. Introduction** ..... **7**

1.1 The nature of Soil Organic Matter ..... 7

1.2 The factors influencing the Soil Organic Matter ..... 9

1.3 Carbon and nitrogen in soil ..... 13

1.4 SOC sequestration ..... 15

1.5 Aim of the thesis ..... 18

**2. Study area** ..... **21**

2.1 The Ferrara province and its reclamation history ..... 21

**3. Material and methods** ..... **25**

3.1 Soil sampling ..... 25

3.1.1 Selection of inventoried samples for the study of Po and Reno sediment provenance ..... 25

3.1.2 Soil sampling to estimate SOC depletions after 85 years ..... 26

3.1.3 Sampling of burning peat in Mezzano Valley ..... 27

3.1.4 The experimental field of Malborghetto di Boara ..... 29

3.1.5 Sampling of 100 topsoil in Jolanda di Savoia ..... 31

3.2 Laboratory analyses ..... 33

3.2.1 Loss On Ignition ..... 33

3.2.2 Elemental analysis coupled with Isotope Ratio Mass Spectrometry (EA-IRMS) technique ..... 33

3.2.3 Smart combustion elemental analysis (Elementar SoliTOC cube) ..... 39

3.2.4 Further methods applied on peaty soils of the Mezzano Lowland ..... 40

3.3 Geophysical methods ..... 41

3.4 Remotely sensed data ..... 42

3.4.1 The Sentinel-2 NDVI ..... 42

3.4.2 PRISMA imagery ..... 42

3.4.3 Artificial Neural Networks ..... 44
3.5 Statistical methods and Geographic Information System ..... 45
3.5.1 Mapping of soil carbon loss ..... 46
**4. Isotopic proxies to verify the provenance of the Ferrara province topsoils ..... 49**
4.1 Introduction ..... 50
4.2 Results ..... 52
4.3 Discussion ..... 55
4.4 Conclusions ..... 62
Appendix 4 ..... 63
**5. The SOC depletion in the Ferrara province from 1937 to 2022 ..... 65**
5.1 Introduction ..... 66
5.2 Results ..... 67
5.3 Discussion ..... 69
5.3.1 Comparison of TC, IC, OC, and N contents after 85 years ..... 69
5.3.2 SOC stocks and GHGs loss ..... 72
5.3.3 $\delta^{13}C$ spatial distribution in Ferrara province ..... 74
5.4 Conclusions ..... 77
Appendix 5 ..... 79
**6. Accelerated SOM degradation in the peatlands of Mezzano Valley: a particular case ..... 91**
6.1 Introduction ..... 92
6.2 Results ..... 93
6.2.1 pH, Electrical Conductivity and Bulk Density ..... 93
6.2.2 Soil Carbon Pools on F and NF Profiles ..... 96
6.2.3. Soil Carbon Pools of the Experimentally Fired Profiles ..... 99
6.3 Discussion ..... 103
6.3.1 Effects of Soil Burning in the Mezzano Lowland ..... 103
6.3.2 Triggering Mechanisms of Soil Burning in the Mezzano Lowland ..... 104
6.3.3 Environmental Consequences of Peat Burning in the Mezzano Lowland ..... 105

6.3.4 Impacts of Peat Burning on the Human Health ..... 106
6.4 Conclusions ..... 107
Appendix 6 ..... 108
**7. A new geochemical-geophysical method for the SOC evaluation at farm scale: the Malborghetto di Boara case ..... 111**
7.1 Introduction ..... 112
7.2 Results ..... 114
7.3 Discussion ..... 118
7.3.1 Soil carbon elemental and isotopic speciation ..... 118
7.3.2 Insights from soil organic carbon and geophysical data ..... 121
7.4 Conclusions ..... 125
Appendix 7 ..... 127
**8. Assessing the soil organic carbon contents through a combination of geochemical soil investigations and remote-sensing by data of Sentinel-2 and PRISMA ..... 129**
8.1 Introduction ..... 130
8.1.1 Soil Organic Carbon in the critical zone ..... 130
8.1.2 Soil Organic Carbon changes in agricultural context ..... 132
8.2 Results and discussions ..... 132
8.2.1 Laboratory analyses ..... 133
8.2.2 Time series of the Sentinel-2 NDVI ..... 133
8.2.3 Artificial Neural Network results ..... 135
8.3 Conclusions ..... 136
Appendix 8 ..... 139
**9. General conclusions ..... 143**
**References ..... 145**
**Acknowledgments ..... 180**

## Abbreviation list

AFOLU, Agriculture, Forestry and Other Land Use;

C, Carbon;

CAP, Common Agricultural Policy;

CFI, Carbon Farming Initiative;

$CO_2$ eq, carbon dioxide equivalent;

$CO_2$, carbon dioxide;

Cr, Chromium;

EA-IRMS, Elemental Analyzer Isotopic Ratio Mass Spectrometry;

EC, Electrical Conductivity;

EU, European Union;

F or FE, Ferrara;

FL, littoral lands of Ferrara;

FM, Ferrara municipality;

GAECs, Standards of Good Agricultural Environmental Conditions;

GHG, Greenhouse gas;

GIS, Geographic Information System;

IC, Inorganic carbon;

IPCC, Intergovernmental Panel on Climate Change;

LOI, Loss On Ignition;

LULCC, Land-Use Land-Cover-Change;

LV, leftward Po di Volano;

MB, Malborghetto di Boara;

ML, Mezzano Lowland;

N, Nitrogen;

Ni, Nichel

OC, Organic carbon;

OM, Organic Matter;

PCA, Principal Component Analysis;

REE, Rare Earth Elements;

ROC, Residual Oxidizable Carbon;

RV, rightward Po di Volano;

S, Sulphur;

SDGs, Sustainable Deveolpment Goals;

SOC, Soil Organic Carbon;

SOM, Soil Organic Matter;

TC, Total Carbon;

TIC, Total Inorganic Carbon;

TOC, Total Organic Carbon;

$TOC_{400}$, Thermally Labile Organic Carbon;

VM or VP, Vigarano Mainarda.

# 1. Introduction

## 1.1 The nature of Soil Organic Matter

The first appropriate definition of soil organic matter (SOM) was described by Allison (1973): “Soil organic matter has over the centuries been considered by many as an elixir of life. Ever since the dawn of history, some eight thousand or more years ago, man has appreciated the fact that dark soils, commonly found in the river valleys and broad level plains, are usually productive soils. He also realized at a very early date that color and productivity are commonly associated with organic matter derived chiefly from decaying plant materials”.

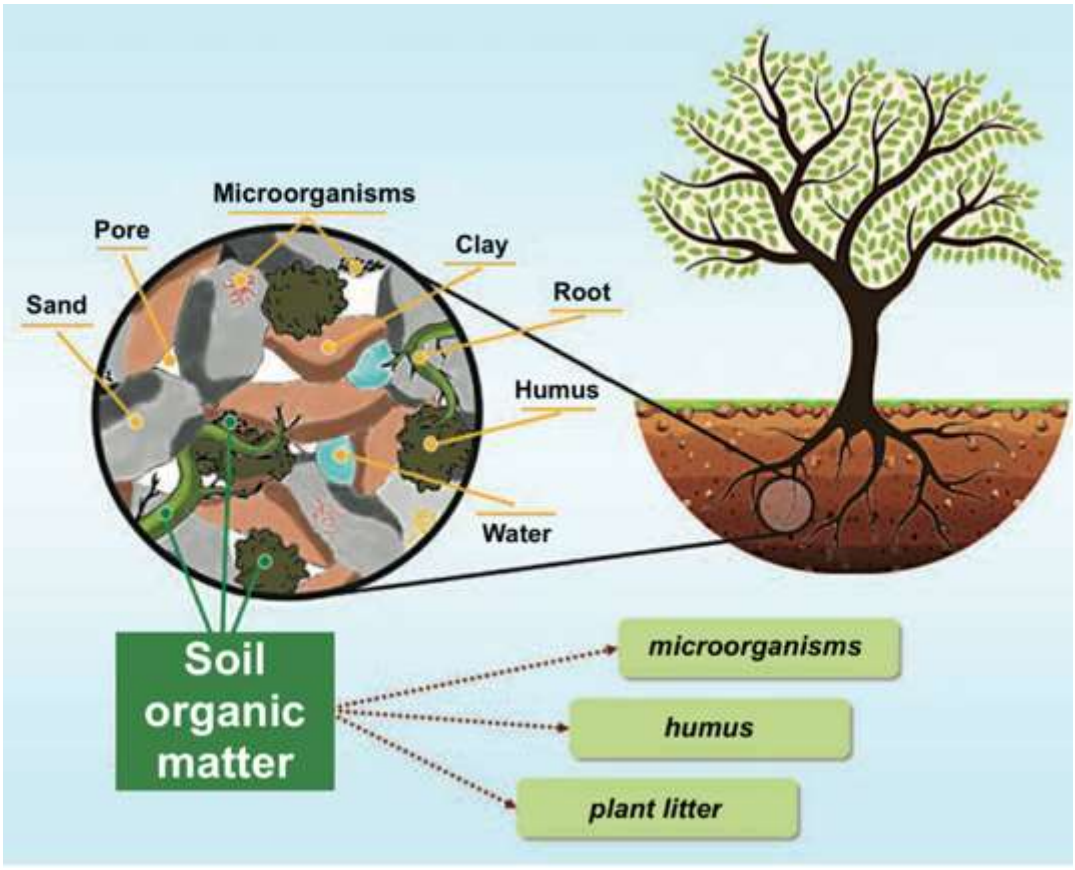


**Figure 1.** Simplified representation of the organic material of a soil (modified from Mistri and De Feudis, 2021).

The complex framework of the SOM (Figure 1) derived from the decomposition of plants, animals, and microorganisms (von Lützow et al., 2006; Paul, 2014; Lal, 2018b), which are constitutes by soluble organic compounds (*i.e.,* sugars, proteins, and other metabolites), and amorphous organic compounds (*i.e.,* humic acids, fats, waxes, oils, lignin, and

polyuronides). Moreover, these organic compounds contain fundamental elements for the biogeochemical processes such as carbon (C), hydrogen (H), oxygen (O), nitrogen (N), sulfur (S), and phosphorus (P) (Johnston et al., 2009). Once in the soil, OM can decompose relatively rapidly to provide nutrients to the soil biota, or slowly to be stored as reservoir. In line with this, according to literature, whole SOM is commonly separated into "labile" (or "active") and "stable" (or "passive") pools (Gulde et al., 2008 for a review). Labile SOM pool is characterized by a rapid turnover (less than one year), mainly consists of young organic material, such as root exudates and rapidly decomposed components of fresh plant litter. Labile SOM is sensitive to land management and environmental conditions. Due to these characteristics, labile SOM pool plays an important role in short-term C and N cycling in terrestrial ecosystems. Stable or "passive" pool is stabilized organic matter that persists in soils over several thousands of years. In this case the organic matter is hosted into macro- or micro-aggregates, which protect them from the decomposition. This pool represents an important sink of SOM, which is slowly released in the soils and became available to the soil biota during time.

Both labile and stable SOM play a key role in soil fertility, crop yields, and agronomic sustainability, but they are also significative tools for climate mitigation and ecosystem preservation (Jackson et al., 2017; Johnston et al., 2009; Chen et al., 2019; Bossio et al., 2020). In fact, the whole SOM can support different physical, chemical, and biological processes sustaining vital ecosystem (Hoffland et al., 2020; Figure 2), which are related to:

- soil structure (physics): water retention, aeration, aggregation;
- soil life (biology): promotion of plant health;
- elemental cycles (chemistry): mineralization, C sequestration, compound retention.

These processes favor the ecosystem services such as erosion protection, provision of a habitat for biodiversity, primary production, climate regulation and compound retention.

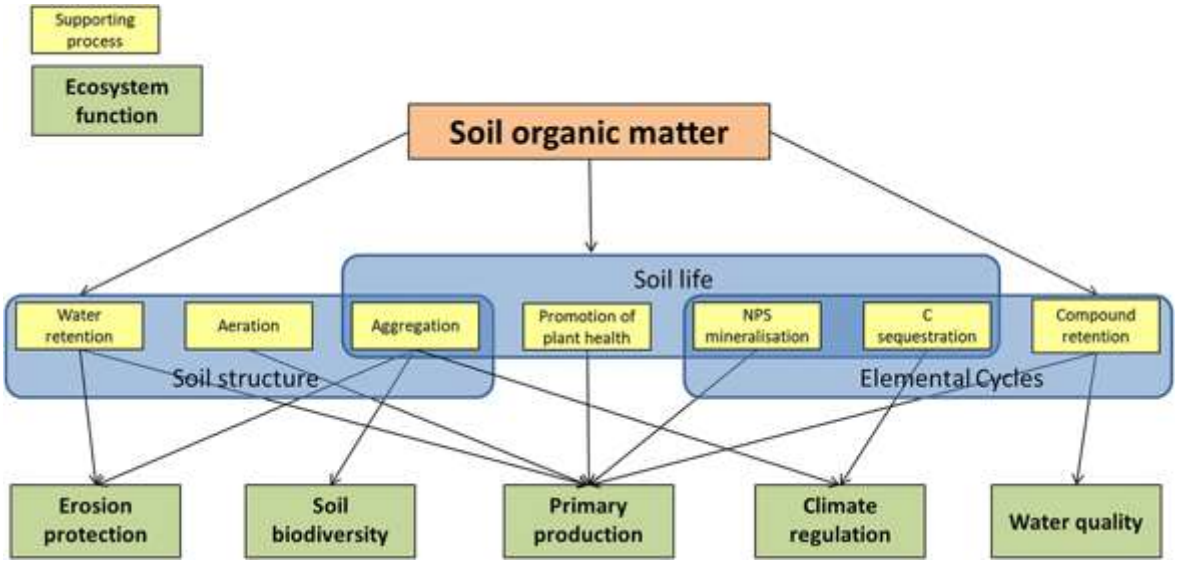


**Figure 2.** Ecosystem functions of SOM and the processes supporting them (Hoffland et al., 2020).

## 1.2 The factors influencing the Soil Organic Matter

The preservation of OM in soils is fundamental, and several parameters influence its accumulation. In general, SOM concentration can be affected by soil biota and vegetation cover, soil texture and parent material, water availability and hydrology, topography, and climate (Figure 3).

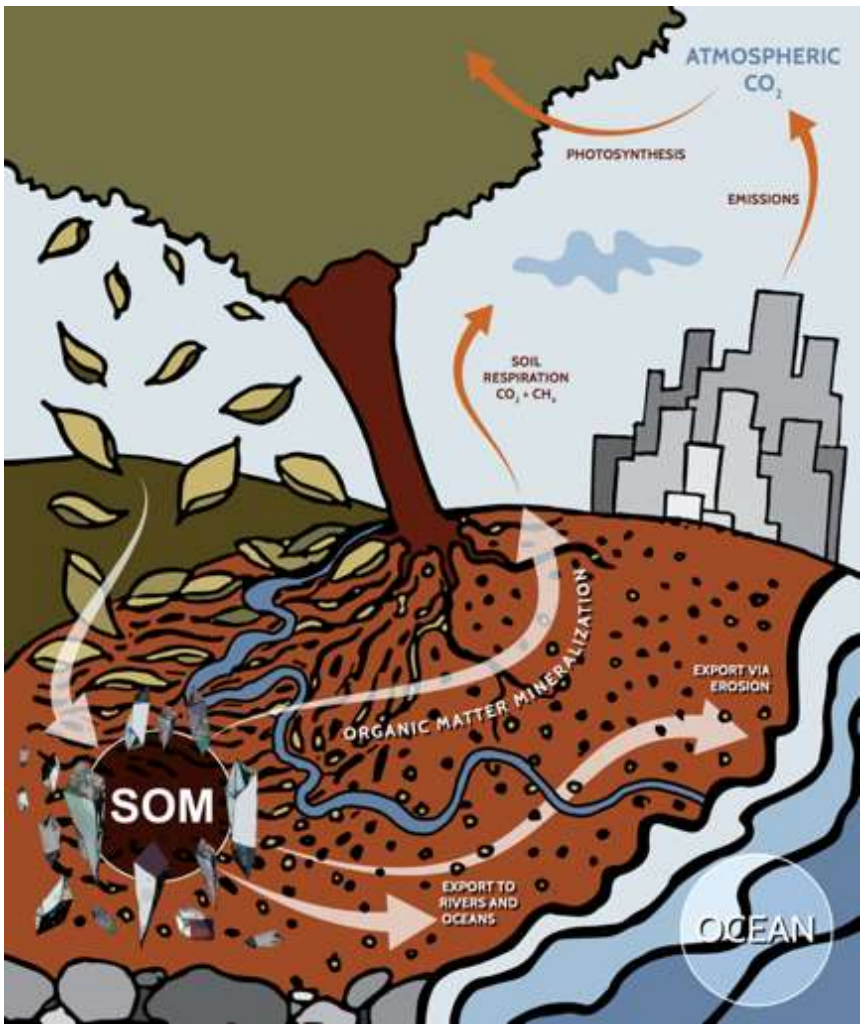


**Figure 3.** Dynamics affecting SOM concentration (modified from Lefèvre et al., 2017).

The first parameter influencing the SOM accumulation is soil biota (*i.e.*, living organisms in soil), which has direct role of producer/consumer of the organic material; soil organisms can be subdivided in: autotrophic and heterotrophic. The former are represented by plants and autotrophic bacteria, such as sulfur and iron bacteria, which build up SOM by synthesis of the atmospheric $CO_2$ into organic material. The latter are represented by animals and heterotrophic microorganisms that use the organic material and transform it into $CO_2$ and water. Overall, plant litter compounds and microbial decomposition products in various stages of decomposition involve the magnitude of these transformation processes of the organic material (von Lützow et al., 2006; Paul, 2014; Lefèvre et al., 2017). In particular, soil biota affects the degree of decomposition of SOM. From insoluble macromolecules microorganisms can produce stabilized C (*i.e.*, C with long turnover; van der Wal and de Boer, 2017) or induce carbon loss ($CO_2$ and $CH_4$ are emitted back into the atmosphere) from the decomposition (or mineralization) of SOM through the microbial heterotrophic respiration. More in general, bacterial communities play a key role in soil

processes such as nutrient cycling, SOM decomposition, building persistent SOM stocks, and plant growth. Changes in soil properties, such as organic matter content, pH, and nutrient availability affect the microbial communities. Therefore, they are considered a proxy for understanding the dynamics of soil organic matter and nutrients (Qiu et al., 2021). In fact, changes in bacterial community composition and diversity are associated with changes in soil organic matter and nutrient dynamics. For example, a decrease in bacterial diversity has been linked to a decline in soil organic matter content and nutrient availability, while an increase in bacterial diversity has been associated with improved soil health and fertility. Microbial community composition drives also the chemical fingerprint of soil carbon. In fact, bacteria-only communities lead to more thermally labile soil C pools than communities with bacteria and fungi, that stabilize the SOM (Domeignoz-Horta et al., 2021).

In addition, vegetation cover can improve SOM preservation with the plant canopy and the root system, which increases soil structural stability and aggregation and offers a physical protection of the soil surface (Six et al., 1998; Bronick and Lal, 2005). Moreover, an absence of plant cover and, consequently, of roots, prevents the accumulation or maintenance of SOM, also leading to increased runoff (Cammeraat and Imeson, 1999) and sediment movement (Ruiz-Colmenero et al., 2013).

The other factors that influence the accumulation of SOM through the control of the decomposition rates rather than to the productivity of ecosystems are soil texture, parent material, water availability, topography, and climate.

Soil texture influences SOM quality and quantity, also within soil depth. The decomposition of SOM is particularly limited when SOM form organo-mineral complexes with clays, which are the most reactive soil particles for their permanent and variable surface charges (Sarkar et al., 2018). In this way, clays are able to protect soil organic matter against microbial decomposition for decades, centuries or even millennia (Schmidt et al., 2011; Lefèvre et al., 2017). More in general, at similar climatic conditions, the SOM sequestration rates in a loamy-soil will be larger than in a sandy-soil.

Parent material may influence SOM accumulation through its effect on soil fertility. In fact, accumulation of organic materials is more abundant in soils formed by base cation-rich mafic rocks (*e.g.*, basalt) with respect of soils derived from felsic materials with lower inherent mineral-derived nutrients (*e.g.*, granite) (Quideau, 2018).

Soil water availability influences microbial decomposition of SOM (Moyano et al., 2012) and it is more abundant with high amounts of SOM (Libohova et al., 2018). In fact, hydrology under normal rainfall condition provides water availability favoring SOM

accumulation through the increase of quantity of living plants, whose inputs accumulate more plant litter in form of above and belowground biomass (Thiébeau et al., 2021). On the contrary, strong rainfall events and flooding may lead to soil erosion and SOM loss (Lal, 2003). More in general, mutual interactions between water and biogeochemical cycles at all scales affect SOM stabilization and destabilization impacting on plants and soil microbiology (Védère et al., 2022).

Across the landscape SOM varies vertically (within the soil profile 39–70% of the global organic carbon in the upper 1 m are stored in the first 30 cm; Batjes, 1996), horizontally and, temporally due to the human influence (Janzen et al., 2018), affecting the ecosystem behavior. In particular, at local scale, SOM is influenced by topography, through effects on microclimate and water movement with lowest amount of SOM on mountaintops and highest in lowlands (Schimel et al., 1985; Burke et al., 1995; Gregorich et al., 1998), where there is a prevalence of palustrine environment. In fact, variations in microclimate produce a differentiation in plant communities across topographical gradients; and generally, soil erosion move SOM to in depositional sites such as foothills and valleys (Doetterl et al., 2016; Janzen et al., 2018). Topography affects SOM also on the basis of drainage, and degree of slope.

Climate plays a key role on SOM accumulation by controlling the balance between litter production and decomposition rates (Quideau, 2018). Similar to many other biochemical reactions, the decomposition of SOM is temperature dependent, as it is mediated by microbial enzymes, which increase their activity with the increase of temperature. However, different experimental studies demonstrates that the temperature sensitivity of SOM decomposition decreases with increasing stability (Plante and Conant, 2014; Qin et al., 2019; Moinet et al., 2020). In fact, the recalcitrant SOM, hosted in microaggregates, is more protected from the microbial decomposition than the labile SOM. This means that the SOM in subsoil is less affected by the decomposition than that of the topsoil as, across soil depths, microbial abundance is lower and SOM protection is stronger. According to Qin et al. (2019), the temperature affects more the active pools than the slow pools, as microbial communities dominated in the former, whereas aggregate protection was more important in the latter. Given that the slow C pool is the largest component of SOM with a longer turnover time, SOM protection via microaggregates could be the key mechanism that regulates the long-term response of SOM decomposition to global warming.

## 1.3 Carbon and nitrogen in soil

The principal element of soil is carbon, and it is present as soil organic carbon (SOC), which is related to the SOM, and soil inorganic carbon (IC), which is largely found in carbonate minerals (Nelson and Sommers, 1996). In SOM carbon ranges between 48% and 58% (Nelson and Sommers, 1996). Both SOC and IC are implied in the global carbon cycle. As described before, the SOC pools vary through years, decades, centuries and millennia, which make soils alternatively a source or a sink of C (Bouwman, 1990; Wisniewski and Sampson, 1993; Lal et al., 1998; Schmidt et al., 2011). On the other hand, IC has a role in the carbon cycle represented by both pedogenic and geogenic carbonates (Batjes, 1996; Nordt et al., 1998; Lal et al., 1999).

In terrestrial ecosystems, the first meter of soil storing ~2700 Pg of C, and ~1500 Pg of which (57%) are sequestered by SOM, approximately two and three times much more than the atmosphere the vegetation, respectively (Lal, 2004b, 2008). Despite SOC are not uniformly distributed above the Earth surface, there are hotspots where SOC is largely stored, such as wetlands and peatlands of tropics and permafrost regions (Gougoulias et al., 2014; Köchy et al., 2015). In fact, these two environments store 30% of the world's SOC in only 3% of the Earth's land area (Lefèvre et al., 2017).

Due by root and microbial emissions, the amount of SOC stock can be naturally yet reduced by the soil respiration that emitted C in the atmosphere as one of the main greenhouse gases (GHGs), the carbon dioxide ($CO_2$; Oertel et al., 2016). Unfortunately, with climate change and unsustainable management, also the fertile areas with high SOC content could become a potential source of GHG emissions. Moreover, after the last glaciation, 220 Pg C were emitted in the atmosphere, with an increasing rate of global C emissions of about 4.4 Pg C/year (Baldocchi et al., 2016). As described by Le Quéré et al. (2016) for the period 2006–2015, the emissions of C as GHG exponentially increased after the global introduction of fossil fuels and industry. However, since the industrial revolution, the change in land use, which is developing agricultural land, contributes to one third of greenhouse gas emissions (IPCC, 2014b).

Globally, soils also contain 0.01% of atmospheric nitrogen (N), both organic and inorganic (Tamm, 1991). N is extremely related to C in SOM and for the activity of bacteria and fungi of a soil (Stevenson, 1994). Such microorganisms have a key role in regulating C/N ratio. In fact, they transform these elements and provide fluxes from the soil to the

atmosphere. In particular, the condition of aerobic processes also leads to $CO_2$ production and, in case of anaerobic conditions, to methanogenesis.

In environmental geochemistry, the use of stable isotopes to trace sources of C and N is widely used (Cloern et al., 2002). In particular, $^{13}C/^{12}C$ (expressed as $\delta^{13}C$) and $^{15}N/^{14}N$ (expressed as $\delta^{15}N$) are relevant in the soil studies to characterize the nature and evolution of soils and the related SOM, as well as the anthropic or natural effects which influence the OM quantity and quality in soils. In fact, the OC/IC ratio in a bulk soil affects the $^{13}C/^{12}C$ signature: soil samples with higher of SOM are $^{12}C$-enriched, and therefore exhibit more negative isotopic signature, whereas soil samples with IC predominance show $^{12}C$-depleted, and therefore exhibit less negative isotopic signature (Natali et al., 2018b; Brombin et al, 2020; Salani et al., 2021; Bianchini et al., 2022). Also $^{15}N/^{14}N$ could represent a proxy to study the degree of maturity of a soil, as mature soils are more $^{15}N$-enriched.

Wada (2009) suggested that each biogenic material has its own isotopic composition. Therefore, considering the stable carbon isotopic signature of SOM is mainly related to that of the decomposed plants, the $^{13}C/^{12}C$ can be used to recognize the type of vegetation which produced SOM (Figure 4). Based on the fact that during transfer from plant to sediment, the vegetal residua conserve the stable carbon isotopic signature of its photosynthetic pathway, stable carbon isotopic composition of OC is preserved in soils or sediments and may be a valuable proxy of local environmental conditions (Evans et al., 1986; Craine et al., 2015b; Wang et al., 2015). In particular, plants can be discriminated according to their different photosynthetic pathways into $C_3$, $C_4$, and CAM (Crassulacean acid metabolism) plants. The $C_3$ plants fix $CO_2$ using the Calvin–Benson cycle and prevalently grow in relatively cold and humid environments (Kirkels et al., 2022). On the contrary, $C_4$ plants add a preventive phase to fix and concentrate $CO_2$ useful to maintain relatively high photosynthesis rates also in arid environments as typically occur to CAM plants, like pineapples (Sage, 2004; Kirkels et al., 2022). In an agricultural soil the isotopic signature of OC is contribution of plant residua associated prevalently to a mix of $C_3$ plants such as rice, wheat, soybeans and barley and $C_4$ plants such as maize, sugar cane, and sorghum. The distribution of $C_4$ vegetation frequently occurs at the expense of the population of $C_3$ and is influenced by a number of natural and anthropogenic drivers, including climate, land cover and land use changes, variations in the fire frequency, nitrogen deposition, nocturnal global warming, and increasing $CO_2$ (Still et al., 2003). These group of plants have characteristic isotopic signature, because they fractionate

carbon isotopes to a different extent. The $\delta^{13}C$ values of $C_3$ range from −37 to −20‰ and those of $C_4$ range from −20‰ to −9‰ (O'Leary, 1988; Kohn, 2010; Figure 4).

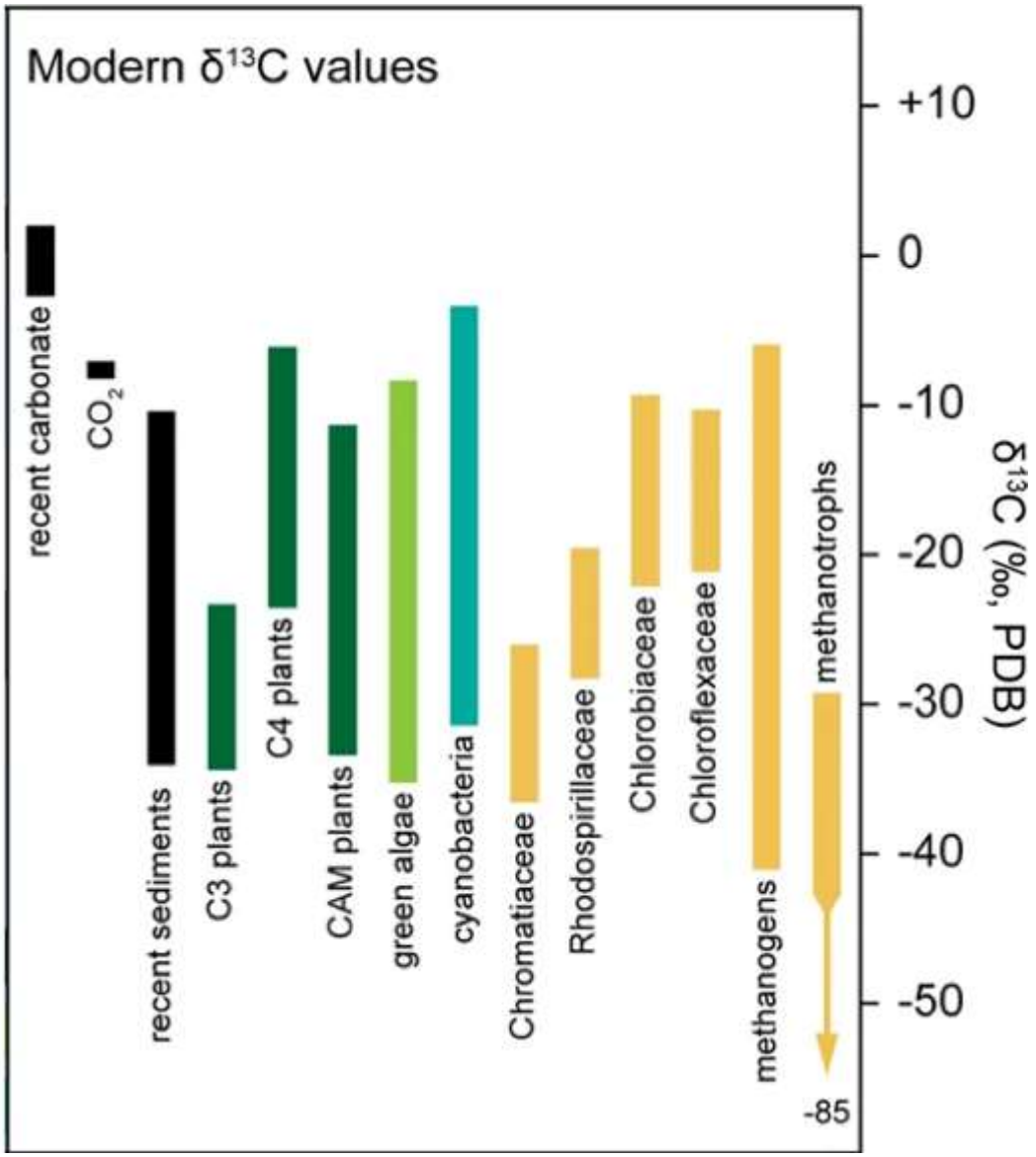


**Figure 4.** Modern $\delta^{13}C$ values from Schidlowski (2001; modified from Garcia et al., 2021). Bars are colored as follows: black: geologic reservoirs; dark green: land plants; light green: green algae; teal: cyanobacteria; other taxa: yellow.

## 1.4 SOC sequestration

Anthropic activities which interfere with natural environments, such as urbanization and agricultural practices, produce SOM losses (Tiessen et al., 1994; Solomon et al., 2000). Considering the abuse of not-sustainable agricultural practices, Davidson and Ackerman (1993) estimated a loss of about 30% of original SOC content for change of land use, for

example the conversion of grasslands and forestlands to arable lands, which implies the loss of vegetation producing biomass. Then, in arable soils, tillage causes SOM oxidation (and mineralization), which contributes to the releasing of $CO_2$ and other GHGs (*i.e.,* methane ($CH_4$), and nitrous oxide ($N_2O$)) in atmosphere (Soane and van Ouwerkerk, 1995; Ball et al., 1999). On the other hand, the use of sustainable agricultural practices can promote the SOC sequestration, improving soil health and sustainability and favoring the GHG emission mitigation, through the removal of $CO_2$ from the atmosphere due to the increase soil quality (Paustian, 2014; Minasny et al., 2017). In arable soils, a reduction of tillage intensity can reduce the SOC depletion (Alvarez et al., 2014; Franko and Spiegel, 2016; Prasad et al., 2016). For this reason, the initiative "4 per 1000" (per year) proposed by the French government at COP-21-UNFCCC in 2015 is based on the global restoration of the SOC concentration to create a positive C-balance through best management practices (*e.g.,* conservation agriculture; Lal et al., 2015).

In association with the above mentioned, to contrast the phenomenon of Climate Change (*i.e.,* the Paris Agreement Article 2.1: "to well below 2 °C above pre-industrial levels and to pursue efforts to limit the temperature increase to 1.5 °C"), the Intergovernmental Panel on Climate Change (IPCC) defined appropriate adjustments to promote the action of decarbonization for the energy, industry, urban and land-use systems (de Coninck et al., 2018). In particular, the agriculture, forestry and other land use (AFOLU) sector, responsible for 22% of global emissions (Shukla et al., 2019), could produce a relevant process to decarbonize sources of GHG emissions with increasing SOC sequestration and the producing of bioenergy (IPCC, 2014a). As described by de Coninck et al. (2018), there is a link, both in form of benefits and trade-offs, between decarbonization in AFOLU and some Sustainable Development Goals (SDGs), such as food security, biodiversity, soil rights, jobs and poverty. However, the synergy actions of decarbonization and SDGs (notably food security, biodiversity preservation, poverty alleviation and job creation) should be maximize and the trade-offs minimized, with simplifying the programming plans and strategies with main stakeholders (Svensson et al., 2021). The common objective, suggested by evidence from IPCC, are to limit global temperature increase to 1.5°C, with global emissions will have to fall to net-zero by 2050 (Burke et al., 2019). The meaning of net-zero emission is balancing carbon emissions with carbon removal.
Nowadays, reducing GHGs from industrial sector are disincentivized with *ad-hoc* taxes ruled by carbon pricing (Zakeri et al., 2015), but does not yet efficient to reach net-zero targets.

In the agricultural sector a change of land use and management practices can limit (Smith et al., 2001; Horowitz and Gottlieb, 2010) and potentially even abate GHGs (Kragt et al., 2012; Powlson et al., 2012; Lal, 2018a). To incentive the use of sustainable practices in agriculture, a price for each abated or sequestered tonne of $CO_2$ was applied for the first time in 2011 by the Carbon Farming Initiative (CFI) supported by Australian Carbon Pricing Scheme (Carbon Credits – CFI, 2011; Macintosh and Waugh, 2012; Murray, 2012; Verschuuren, 2017; Evans, 2018; Copland, 2020). Through the project of "Carbon farming", the biggest $CO_2$ emitters such as factories and business companies (*e.g.*, Google, Apple, Amazon) can buy carbon credits sold by farmers in carbon markets (Beka et al, 2022). Unfortunately to certify these farms, a method to measure and to provide real increasing SOC storage is still a challenge.

In the European Union (EU) LUCAS Soil data show that cultivated and permanent crops have the lowest SOC levels of all major land cover classes (around 17 g $kg^{-1}$ of C; Figure 5). It was estimated that 60-70% of soils are degraded as a direct result of unsustainable management practices and have lost significant capacity to provide ecological functions for various forms of life (European Commission, 2020). In 2017, 25% of European land (411,000 $km^2$), particularly in southern Europe, was identified as being at high or very high risk of desertification, a 14% increase since 2008 (Prăvălie et al., 2017; Ferreira et al., 2022). For these reasons, in the 1990's the EU policies moved to a series of economic measures to improve and encourage the use of sustainable best-practices as replacement of the conventional approaches in agriculture (Marraccini et al., 2012). In 2003, with the adoption of the Common Agricultural Policy (CAP) were introduced Standards of Good Agricultural and Environmental Conditions (GAECs) (Angileri et al., 2011). Since 2005, the Member States implemented CAP reform, while only one year late in Italy (DM 12541/2006) listing the standard GAECs (Bazzoffi and Zaccarini Bonelli, 2011). One of the main aims of CAP is to preserve soil quality by maintaining a high level of SOM. In rural agricultural systems, characterized by low yield, these measurements were successful applied (Agnoletti et al., 2011; Borrelli et al., 2011), therefore since the 2010's these approaches take places also in more intensive or specialized systems (Farina et al., 2011; Fumagalli et al., 2011; Brombin et al., 2020). In the future, CAP could promote incentives like the CFI approach (Beka et al, 2022). However, not all EU countries maintain a systematic monitoring of the SOC and more in general a soil monitoring service. Indeed, examples of EU nations that have a national service of soil monitoring could be France, Sweden, and Poland. By contrast, Mediterranean nations as Italy, Spain and Greece have

monitoring services undeveloped or regional database without linkage, but there is awareness of achieving a higher level of soil monitoring.

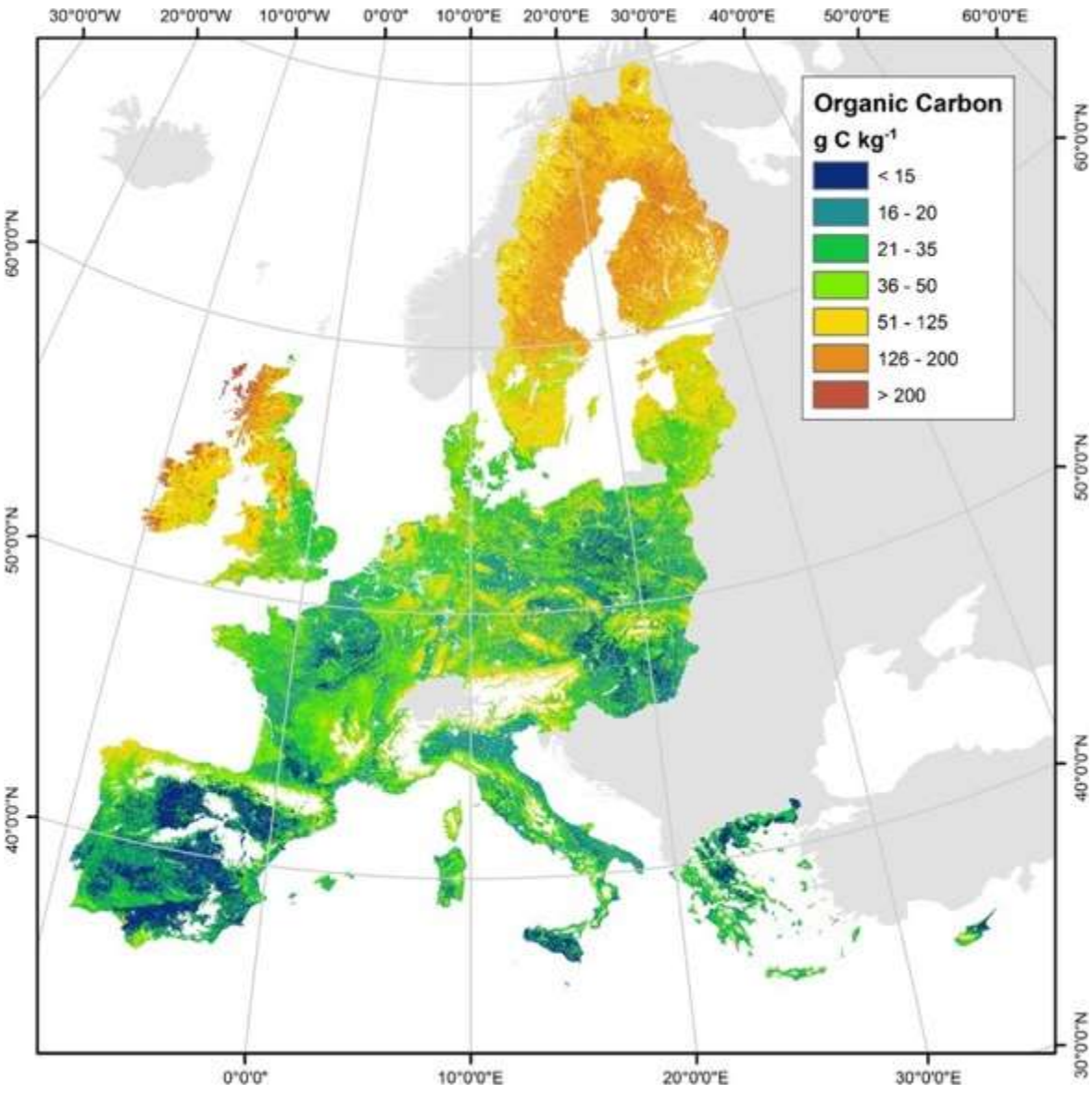


**Figure 5.** Organic carbon (in g $kg^{-1}$) distribution in the European member states provided by the Land Resource Management Unit (Institute for Environment & Sustainability) of the Joint Research Centre (JRC) of the European Commission (de Brogniez et al., 2015).

## 1.5 Aim of the thesis

In order to demonstrate the importance of a continuous monitoring of the organic matter in soils, this thesis aimed to reconstruct the depletion of SOM and the relative C in Ferrara province (Northeastern Italy), which was affected by a strong agricultural development in the last century. Since the XIX century, and in particular before and after the World War

II, the Ferrara province was affected by reclamation activities which dried the palustrine environments located in most of this area. It is known that since then, the abuse of land use change and conventional agricultural practices reduced the SOM of the Ferrara province. In addition, since the industrial revolution, the soils of Ferrara province, like those of the rest of the planet, started to face the "climate-change" threat due to the exponential increase of GHG emissions. This situation has been exasperated in the last 30 years, where the advent of globalization promoted the production increase globally in all the sectors (agriculture, industry, tourism). Therefore, this thesis aimed to reconstruct the nature, evolution, a distribution of SOM and the relative carbon contents, considering the strong agricultural development occurred in the century in Ferrara. In particular, in this project the SOM distribution and characteristics was evaluated through the measurement and mapping of C, both organic and inorganic, contents and the estimation of respective isotopic signatures with the most innovative techniques to discriminate the organic and inorganic pools. To better define the quality of soil, the labile and stable organic pools of SOC were also analyzed. In this thesis, Chapter 2 explains in detail the study area and the several reclamation processes which took place since the XIX century. Chapter 3 describes the soil sampling procedure and the innovative elemental and isotopic methods used for the investigation of the soil samples. The chapters 4–8 host the main scientific activities carried out during these 3 years, whose most of their results are already published in international scientific high-impact factor journals. In Chapter 4, the C, N, and S isotopic measurements of the soils of Ferrara province are presented, mapped, and, for the first time, used as innovative proxies to reconstruct the source of the sediments which composed the Ferrara soils (Salani et al., 2021). Chapters 5 reconstructs and maps the SOC depletion occurred in the entire Ferrara province in 85 years comparing the OC data of a report prepared in 1937 with the OC data collected in 2022 for this thesis (Salani et al., submitted). Chapter 6 shows an interesting case of a strong SOC depletion in a restricted area of the Ferrara Province, *i.e.*, the Mezzano Valley, where a natural phenomenon of peat burning was documented (Natali et al., 2021), with a great release of OC in the atmosphere. Chapters 7 and 8 are pilot studies to introduce new methods for a continuous monitoring of the SOC quality and quantity, which can be used by farmers to make their farm more sustainable and obtain the carbon credits by CAP. Chapter 7 explains a new method to map the SOC benchmark at the farm scale combining measurement of OC contents and isotopic signature performed in laboratory with *in-situ* geophysical measurements (Salani et al., in preparation). Finally, Chapter 8 describes a preliminary OC contents prediction through remote-sensing combining OC measurement of Ferrara soil

samples with hyper-spectral satellite sensors and artificial neural networks (Salani et al., in preparation).

# 2. Study area

## 2.1 The Ferrara province and its reclamation history

The Padanian Plain is the widest alluvial plain (~48,000 $km^2$) of the Italian peninsula (Campo et al., 2020). It is the morphological expression of the homonymous basin, which is bounded by the Alpine and Apennine chains, at north and south respectively (Figure 6). The plain was characterized by marine sedimentation in the Pliocene to Early Pleistocene before progradation of fluvial sediments that was enhanced during glaciation periods (Amorosi et al., 2019, 2021; Campo et al., 2020). The easternmost part of the plain, where the Ferrara province is located, received sedimentary contributes from i) the Po River, which is the principal Italian fluvial system crossing from west to east the Padanian Plain with numerous tributaries from distinct parts of the Alps and the north-western Apennines (Marchina et al., 2015, 2016, 2018), and ii) several torrents flowing from the north-eastern Apennines (Figure 6; Bianchini et al., 2002, 2012, 2014). The sediments of Po River mainly derive from the western and central Alps and north-western Apennines, where limestones, sandstones, as well as mafic and ultramafic rocks (*i.e.*, ophiolites) crop out (Amorosi et al., 2002). On the other hand, sediments from north-eastern Apenninic rivers derive from Cretaceous to Pliocene sedimentary rocks, such as sandstones, marls, and evaporites (Amorosi et al., 2002; Manzi et al., 2007).


**Figure 6.** The studied area (pink field) in the Padanian Plain (boarded by black dashed line). Main course and tributaries of Po River and Reno River are also reported (modified from Salani et al., 2021).

The Ferrara province is a lowland area including 2636 km² of the Padanian plain within the Emilia-Romagna region, and it is located in the southern part of the Po River delta (Figure 6). The area is characterized by a mostly flat terrain staring as an alluvial plain 20m above sea level (a.s.l) to the west, transitioning into to a deltaic plain that ends at –4m a.s.l in the coastal plain of the Adriatic Sea to the east (Di Giuseppe et al., 2014a, b). Generally, this sector of the Padanian Plain was filled by sediments eroded from the Alps and the Apennines, which have been transported and deposited by the Po River (Amorosi et al., 2002; Garzanti et al., 2012; Bianchini et al., 2002, 2012, 2013). In particular, the soils of the Ferrara province are medium and medium-fine textured soils (68% of the territory), medium-fine sands (9% of the territory) and peaty soils (23% of the territory), formed by

recent sediment deposition (Holocene, <10,000 years; Amorosi et al., 2002; Bianchini et al., 2014) composed by recent sediments from the interfering fluvial systems of the Po and Apennine rivers including the Reno River and its tributaries (Amorosi et al., 2002; Mastrocicco et al., 2010; Colombani et al., 2011; Bianchini et al., 2013). The heterogeneous nature of the soils in the province originates from the various landforms and sediment deposition processes as well as from the presence of paleo-channels interconnected with crevasses splay and marsh lagoon environments (Mastrocicco et al., 2010; Colombani et al., 2011; Bianchini et al., 2019; Figure 7).

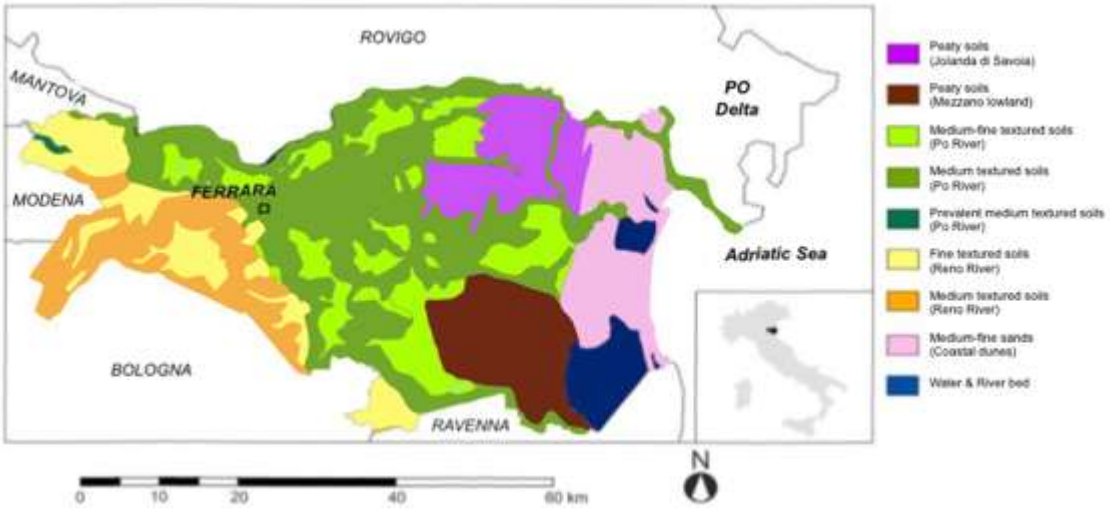


**Figure 7.** Soil classification map of the Ferrara province (modified from Colombani et al., 2011).

From the foundation of the town of Ferrara (VII century; *e.g.,* Bianchini et al., 2006), the human settlements concentrated along the ancient main courses of the Po branches: Po di Primaro and Po di Volano. Since the XIX century, pioneering reclamation activities dried out ~51000 ha of the land below sea level from the palustrine environment to create new agricultural territories (Simeoni and Corbau, 2009; Targetti et al., 2021). In particular, the last wetland reclamation event ~60–70 years ago was the Mezzano Lowland (ML; Figure 10a; see section 3.1.3) discussed in Chapter 6. ML represents the terminal (deltaic) portion of the Po River catchment close to the Adriatic Sea and has been historically characterized by wetlands. The ML soils therefore evolved from alluvial and deltaic lacustrine sediments (Di Giuseppe et al., 2014a, 2014b; Natali et al., 2018b; Simeoni and Corbau, 2009; Stefani and Vincenzi, 2005) and are organic-rich, including repeated levels of peats (Miola et al., 2006). The total ML peat volume is estimated to be 177 × 106 $m^3$ (Cremonini et al., 2008). The ML peat soils are also renowned for methane seepage and local thermal anomalies

recorded down to a depth of 1 m (Bonzi et al., 2017). Analogous thermal anomalies have been observed in other parts of the Po Plain and ascribed to the exothermal oxidation of $CH_4$ mediated by biochemical processes (Capaccioni et al., 2015).

More than half of the area is dedicated to intensive agricultural production of winter cereals (~32%) and maize (~22%) (Colombani et al., 2011), with the lowlands reclaimed in the last 150 years cultivated as rice paddies. The climate of the region, influenced by the coast on the Adriatic Sea, is a typical sub-coastal temperate climate with cold winters and warm summers, moderate precipitations, elevated humidity, low wind speed, and moderate daily and seasonal temperature excursions (Mastrocicco et al., 2010).

# 3. Material and methods

## 3.1 Soil sampling

The strategy of sampling was adapted for each study of this thesis (Chapters 4-8).

### 3.1.1 Selection of inventoried samples for the study of Po and Reno sediment provenance

For this thesis 21 samples were selected from alluvial sediments carried by the Po and Reno Rivers that were already sampled and geochemically characterized by Bianchini et al. (2012, 2013). The Authors collected soil samples at two distinct depths: one representative of the plough horizon (just beneath the roots zone, at a depth of 30-40 cm) and the other representative of the underlying undisturbed layer (at a depth of 100-120 cm). As shown in Figure 8, such agricultural soils were collected close to i) the town of Ferrara (labels FE, F), and ii) the nearby village of Vigarano Mainarda (labels VM, VP). These samples were subject of the study reported in Chapter 4.

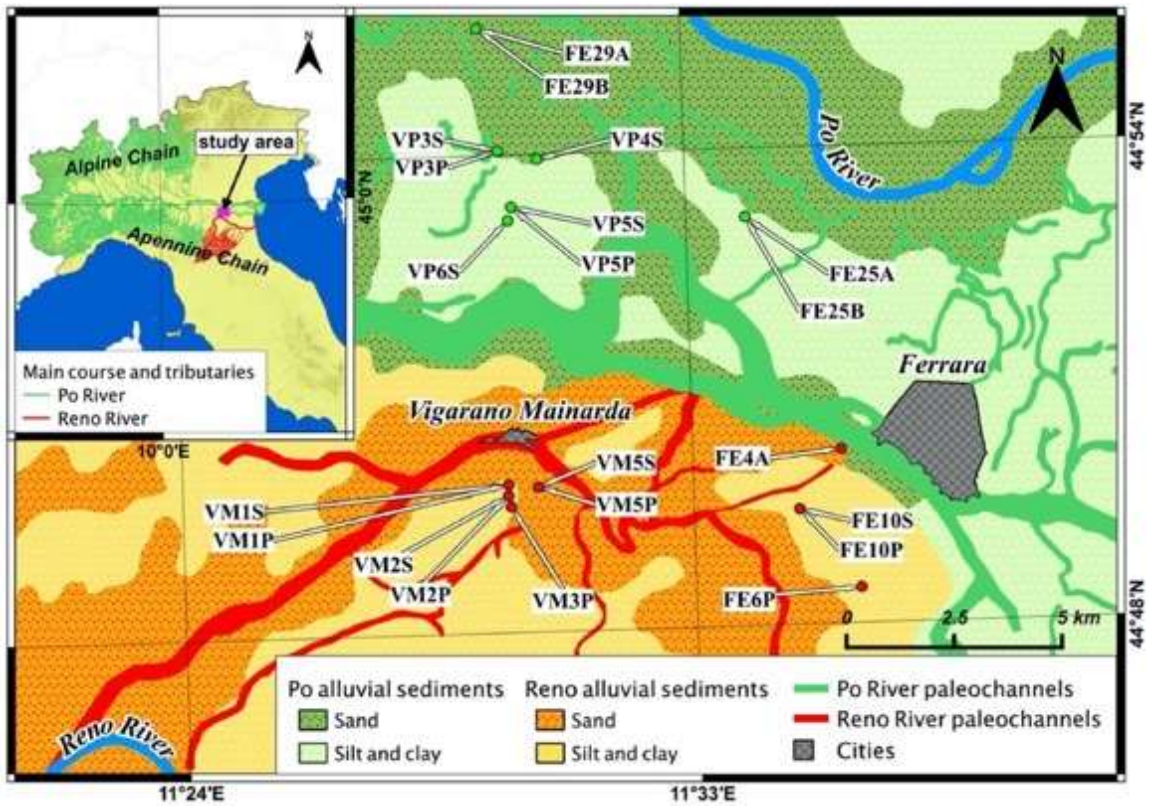


**Figure 8.** Sedimentological map (modified from Bertolini et al., 2008) of the study area reporting the paleochannels and the location of the sediment samples. Samples collected near Ferrara are labelled FE, F; samples collected near Vigarano Mainarda are labelled VM, VP. The inset reports the location of the study area in Northern Italy and the main courses and tributaries of the Po and Reno fluvial systems.

### 3.1.2 Soil sampling to estimate SOC depletions after 85 years

To estimate the SOC depletion of the Ferrara province in Chapter 5, the SOC data reported in an agricultural report of Ferrari et al. (1937) in 1937 were compared with soil samples were collected in 2022 over the same agricultural districts of the Ferrara province (Figure 9). Ferrari et al. (1937), on their survey to assess the soil properties in the Ferrara province, divided the territory into four main regions according to the reclamation activities at the time, drainage patterns and land morphology (Simeoni and Corbau, 2009; Targetti et al. 2021). The four regions were i) the central municipalities of the province related to Po di Primaro (FM), which include Ferrara, Portomaggiore, and Argenta, ii) the reclaimed lands of the leftward Po di Volano (LV), which include the municipalities of Copparo and Codigoro, iii) the reclaimed lands of the rightward Po di Volano (RV), which include the surroundings of Ostellato, and iv) the littoral lands of the province (FL) which include the municipality of Comacchio. For this new sampling, 138 topsoils (0-30 cm in depth; Figure 9) were collected with a gouge auger (Eijkelkamp®, Giesbeek, Netherlands) in the same locations previously investigated by Ferrari et al. (1937).

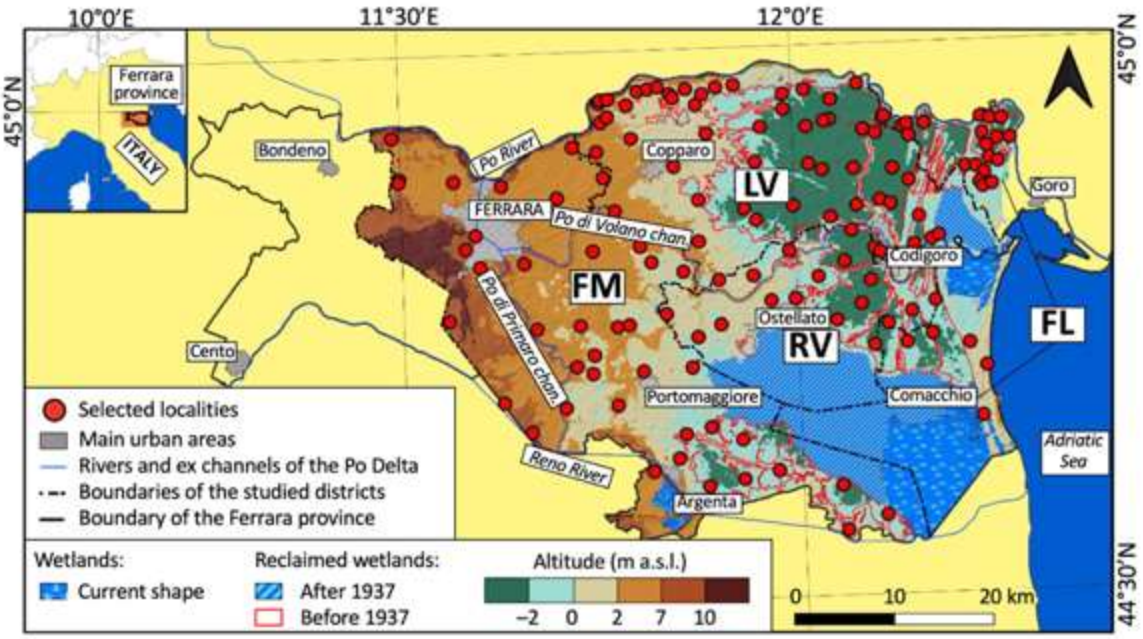


**Figure 9.** The Ferrara province (Northeastern Italy) divided by Ferrari et al. (1937) in the agricultural districts (bounded by the black dashed line): FM (central municipalities of the province), LV (leftward Po di Volano reclamation land), RV (rightward Po di Volano reclamation land), and FL (littoral municipalities of the province). Red dots represent the 138 topsoils (0-30 cm in depth) investigated by Ferrari et al. in 1937, and again in this study. Main cities, rivers, wetlands, and reclaimed wetlands (before and after 1937) are also reported. The shape of all the reclaimed wetlands was defined using historical land use map from 1853. The altitude data in the map, showing a range of elevation from –2 m to 10 m a.s.l., was derived from the elevation point vector file developed by the Emilia-Romagna region (2011) Servizio Statistica e Sistemi informativi geografici (https://geoportale.regione.emilia-romagna.it/catalogo/dati-cartografici/cartografia-di-base/database-topografico-regionale/orografia/altimetria/layer-1).

### 3.1.3 Sampling of burning peat in Mezzano Valley

For Chapter 6, which investigated the peat burning phenomena in Mezzano Valley, the sampling area was sub-rectangular in shape and extended from 44°41′17.08″N, 12°00′09.34″E (upper left corner) to 44°40′35.45″N, 12°00′51.96″E (lower right corner) (Figure 10). It was investigated in July 2018 (Figure 11), when the area experienced ongoing peat fires at its southern edge. The northern edge was instead affected by fires in the past (Martinelli et al., 2015). Each peat fire event was confined to a subcircular area of approximately 3–4 m in diameter, characterized by the absence of vegetation (Figure 10b). Five trenches, approximately 2 m long, 1 m wide and 1 m deep, were dug to access the soil profile for inspection, and the well-exposed sides of the pits were observed carefully to determine the different soil horizons. Soil profile TOR1 was the only one dug in the sector affected by the active fire, while other two profiles (TOR2 and TOR3, Figure 10b) were dug in the sector affected by past fire events. They were characterized by horizons having

reddish color (Figure 10c), consisting of very fine ashy particles that obliterated the original structural characteristics. Other two profiles (TOR4 and TOR5) were dug in sectors of the investigated area not interested by peat smoldering, to perceive the original soil condition preceeding the burning processes.

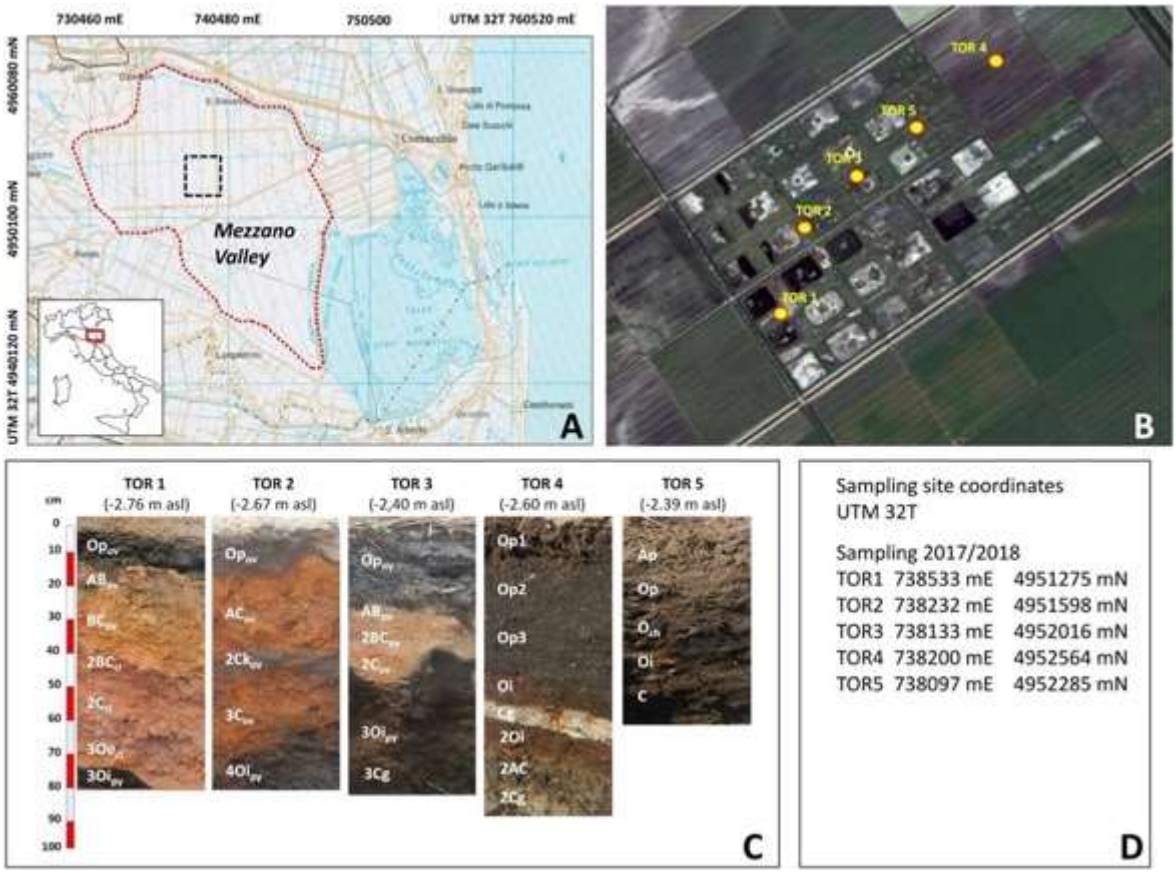


**Figure 10.** (a) Geographic location of the study area (black dashed line) within the Mezzano Lowland (red dashed line) in the easternmost Padanian plain (Northern Italy), facing the Adriatic Sea. (b) Satellite image (Google Earth, year 2010) showing the study area and the sampling locations of the investigated soil profiles. Note the presence of several fired elliptical areas. (c) Photographs of the fired (TOR1, TOR2, TOR3) and non-fired (TOR4 and TOR5) soil profiles and (d) relative geographic coordinates.

Thirty-four representative samples (of about 1–2 kg) were collected from horizons of the soil profiles TOR1– TOR3 variously affected (F) by peat burning, and soil profiles TOR4 and TOR5 unaffected (NF) by peat burning.

The soil horizons were described according to Schoeneberger et al. (2012), attributing specific suffixes to the horizons where peat smoldering induced different effects due to the temperature increase; for example, Oipy was attributed to the pyrolyzed organic horizon with peat carbonization, 2Ccl to the calcined mineral horizon, and ABov to the overheated organo-mineral horizon.


**Figure 11**. Pictures showing an ongoing peat fire phenomenon in the neighbors of profile TOR1. (a and c) Note that the inner part of the fired elliptical area is depressed with respect to the neighbors, and (d) that smoke developed at depth escapes from the superficial layer of unburned peat.

### 3.1.4 The experimental field of Malborghetto di Boara

For the pilot study of Chapter 7 was taken into account as experimental field a conservative managed hazel orchard (3 ha) with cover crop grassland (Figure 12). This study area is located in Malborghetto di Boara (MB; 44°51'18.8"N 11°39'25.2"E), a rural locality of the Po Plain at ~4 m above sea level (a.s.l.) close to the city of Ferrara (Northeast Italy; Figure 13a). The field is crossed by a minor paleochannel of the Po River (Figure 13b).

**Figure 12.** The hazel orchard in MB area.

The soil sampling was carried out in MB in October 2021. 15 composite samples were collected in the grasslands within the hazel rows (Figure 13b). For each composite sample, 5 aliquots of soils were collected using a gouge auger (Eijkelkamp®, Giesbeek, Netherlands) in the layer 0-30 cm within a square of 3x3 $m^2$ area and mixed together (Figure 13c).

In addition to the soil sampling, here geophysical detection of the superficial soil EC was simultaneously carried out using a Profiler EMP-400 (GSSI company, Nashua, NH; USA) along several parallel lines with a spacing of about 5m (Figure 13d and e).

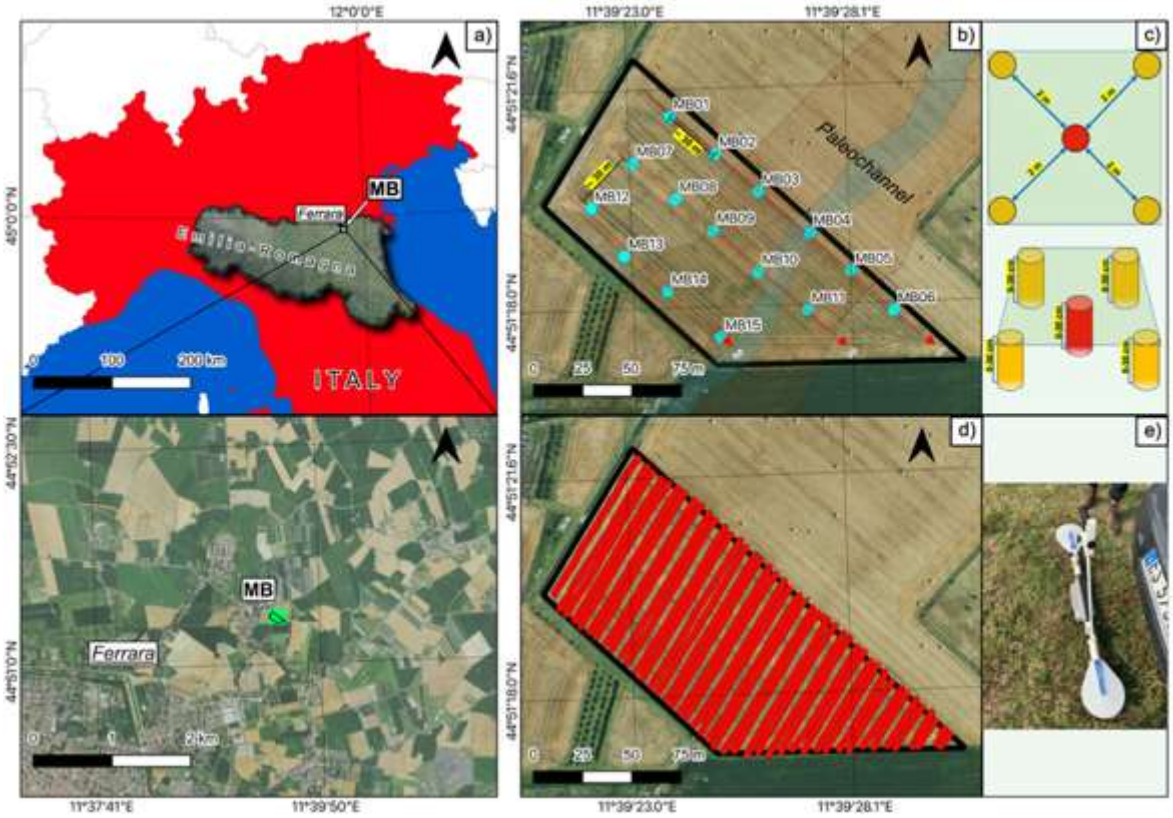


**Figure 13.** a) Location of the sampling area (MB) in Emilia-Romagna region (Northeastern Italy) and zoom of the location of MB area in the north-east sector of the municipality of Ferrara; b) soil sampling location represented by light blue dots; c) in each location sample was collected and mixed five aliquots of soil per square probed at the depth of 0-30 cm; d) location of the geophysical measurement of the superficial electrical conductivity (EC) provided by e) a Profiler EMP-400 (GSSI).

### 3.1.5 Sampling of 100 topsoil in Jolanda di Savoia

For the pilot study of Chapter 8, which aimed to combine the SOC data with the remote-sensing, soil samples were collected over the area in the surroundings of the municipality of Jolanda di Savoia (JDS) in the middle eastern part of the Ferrara province (Emilia-Romagna region; Figure 14a). The JDS area is covered by several PRISMA acquisitions (each image has a size 30 × 30 km and is tilted of ~15°). In particular, the sampling campaign was planned to cover only the land at the south of the Po River, also excluding the southernmost part. 100 composite topsoils (0-15 cm in depth; Figure 14a) were collected in October 2021 over a square parcel of 30 × 30 m (Figure 14b). For composite samples, sampling was carried out by a gouge auger (Eijkelkamp®, Giesbeek, Netherlands) and mixing 5 aliquots collected over the parcel for each sample. The sampled parcel has the size of a pixel of a PRISMA hyperspectral image.

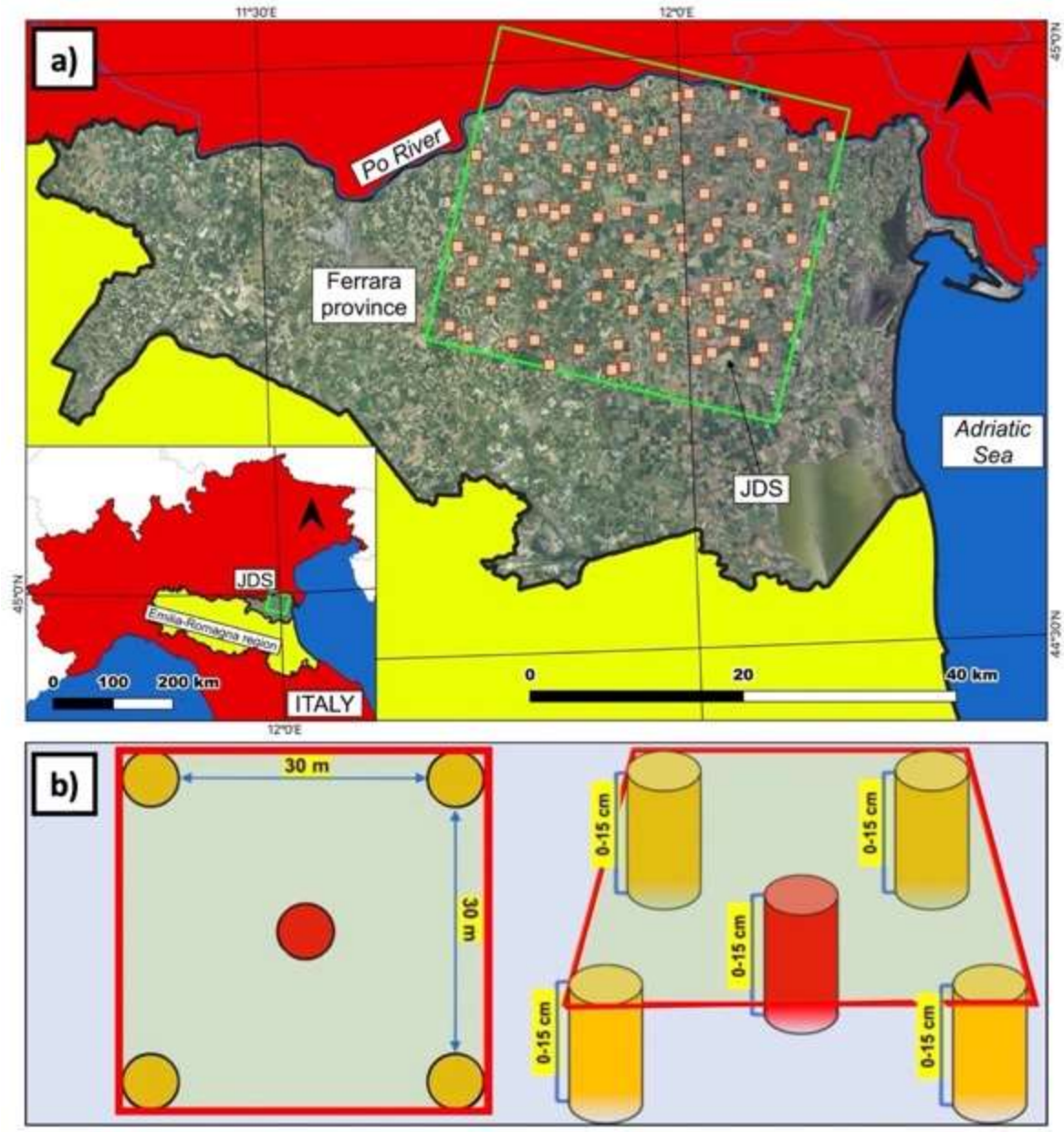


**Figure 14.** a) Location of the sampling area (JDS; represented by a 30 x 30 $km^2$ square with green border) in the Ferrara province, Emilia-Romagna region (Northeastern Italy); b) in each location sample was collected and mixed five aliquots of soil per square (30 x 30 $m^2$) probed at the depth of 0-15 cm.

## 3.2 Laboratory analyses

### 3.2.1 Loss On Ignition

At the Department of Physics and Earth Sciences of the University of Ferrara, soil samples were air-dried, sieved at < 2 mm, and powdered using an agate mortar. Sequential loss on ignition (LOI) was performed, heating the soil samples in a muffle furnace at different temperatures (Dean, 1974). The gypsum and the hygroscopic water content (LOI 105°C) was estimated after heating the soil samples at 105°C for 12 h and calculated as follow:

$$\text{LOI 105°C (wt\%)} = [ ( WS - DW_{105} ) / WS ] \times 100$$

where: WS is the air-dried weight, and $DW_{105}$ is the dry weight after the heating at 105°C.
After the evaluation of LOI 105°C, the same soil samples were heated at 550°C to determine the content of soil organic matter (LOI 550°C) as follow:

$$\text{LOI 550°C (wt\%)} = [ ( DW_{105} - DW_{550} ) / DW_{105} ] \times 100$$

where: $DW_{105}$ is the dry weight after the heating at 105°C and $DW_{550}$ is the weight of the exsolved SOM.
Finally, the same soil samples were heated at 1000°C to calculate the soil inorganic fraction (LOI 1000°C) as follow:

$$\text{LOI 1000°C (wt\%)} = [ ( DW_{550} - DW_{1000} ) / DW_{550} ] \times 100$$

where: $DW_{550}$ is the dry weight after the heating at 550°C and $DW_{1000}$ is the weight of destabilized of the inorganic fraction (carbonates and clay minerals).

### 3.2.2 Elemental analysis coupled with Isotope Ratio Mass Spectrometry (EA-IRMS) technique

For the estimation of C (including OC and IC), N, S contents in soil samples and the respective isotopic ratio values, the innovative elemental analysis coupled with Isotope Ratio Mass Spectrometry (EA-IRMS) technique was used. According to the elemental species to analyze (TC, OC, IC, N, or S), different instruments and/or procedure were implied. All of them are described below in detail.

3.2.2.1 Elementar PYRO Cube-precisION for elemental and isotopic analysis of C, N, S

The analyses of C, N, S contents (expressed in wt%) and the relative isotope ratios ($^{13}C/^{12}C$, $^{15}N/^{14}N$, and $^{34}S/^{32}S$) discussed in Chapter 4 were carried out at the Department of Physics and Earth Science of University of Ferrara (Italy) using an elemental analyser (EA) Vario PYRO Cube (Elementar®) operating in combustion mode and coupled with the isotope ratio mass spectrometer (IRMS) precisION (Elementar®) (Figure 15). Homogenous powdered samples (around 40 mg) were weighed in tin capsules, wrapped, and finally loaded in the EA autosampler to be analyzed.

The Vario PYRO Cube consists of a combustion oven operating at 1150°C. After the sample has been burnt, the released C, N, and S gaseous species are transferred in a reduction column operating at 850° C that contains chips of native copper to reduce the nitrogen oxides ($NO_x$) to $N_2$. The analyte gases pass into the original purge and trap module before to enter in the IRMS. Only $N_2$ is not trapped and is introduced directly in the IRMS to be analyzed for isotopic composition determination. $CO_2$ and $SO_2$ are trapped respectively in two distinct traps. When the N isotopic analysis terminated, the $CO_2$ trap is heated at 110°C to release $CO_2$ which flows in the IRMS to start the isotopic C analyses. After that, the $SO_2$ trap is heated at 220°C to release the gas.

In the mass spectrometer the molecules of the sample gas are ionized by the source (*i.e.,* a thorium oxide filament), and the ions pass through a magnet, which deflects and sorts them into beams with distinctive mass/ charge ratios (m/z). Then ion beams arrive at the collector where 3 Faraday cups detect the ions of each of the three different masses of analyzed gas simultaneously (*i.e.,* for $N_2$ the masses 28, 29, and 30, for $CO_2$ the masses are 44, 45, and 46 and for $SO_2$ the masses 64 and 66). The detection of the distinct isotopic masses of the sample is bracketed between those of reference gases ($N_2$, $CO_2$, $SO_2$, 5 grade purity), which have been calibrated using reference materials. In the cups, the impact of the ions is translated into a recordable electrical signal, forming peaks, which area is proportional to the number of incident ions. The isotope ratios are calculated through peak definition and integration through the ionOS software. The signal intensity is amplified by an integrated Amplifier and is expressed in nano-ampere (nA). The signal intensity is referred as “peak height”, and the minimum acceptable signal is 1 nA (optimum between 2 and 10 nA) in amplitude and at least 5 s in duration. Additional data on the distinct carbon fractions (organic carbon, OC; inorganic carbon IC) were carried out with the EA Vario MICRO cube coupled with the IRMS Isoprime 100 (Elementar®), following the thermal speciation analytical approach defined by Natali et al. (2018a).

Calibration of the instruments were performed using several standards: the limestone JLs-1 (Kusaka and Nakano, 2014), the Carrara Marble (Natali and Bianchini, 2015), the Jacupiranga carbonatite (Beccaluva et al., 2017), the peach leaves NIST SRM1547 (Dutta et al., 2006), the caffeine IAEA-600, the Tibetan human hair powder USGS42 (Coplen and Qi, 2011), the Barium Sulphate IAEA–SO–5 (Halas and Szaran, 2001).

The C, N, and S isotope ratios (*i.e.,* $^{13}C/^{12}C$, $^{15}N/^{14}N$, and $^{34}S/^{32}S$) were expressed with the δ notation in per mil (‰), relative to the international standards: Vienna Pee Dee Belemnite (PDB), air $N_2$, and Canyon Diablo troilite (CDT) for C, N, and S respectively. (Gonfiantini et al., 1995). The isotopic signature was calculated as follow:

$$\boldsymbol{\delta} = [\ (\ R_{sam} / R_{std}\ ) - 1\ ] \times 1000$$

Where: $R_{sam}$ is the isotope ratio of the sample and $R_{std}$ is the isotope ratio of the international isotope standards.

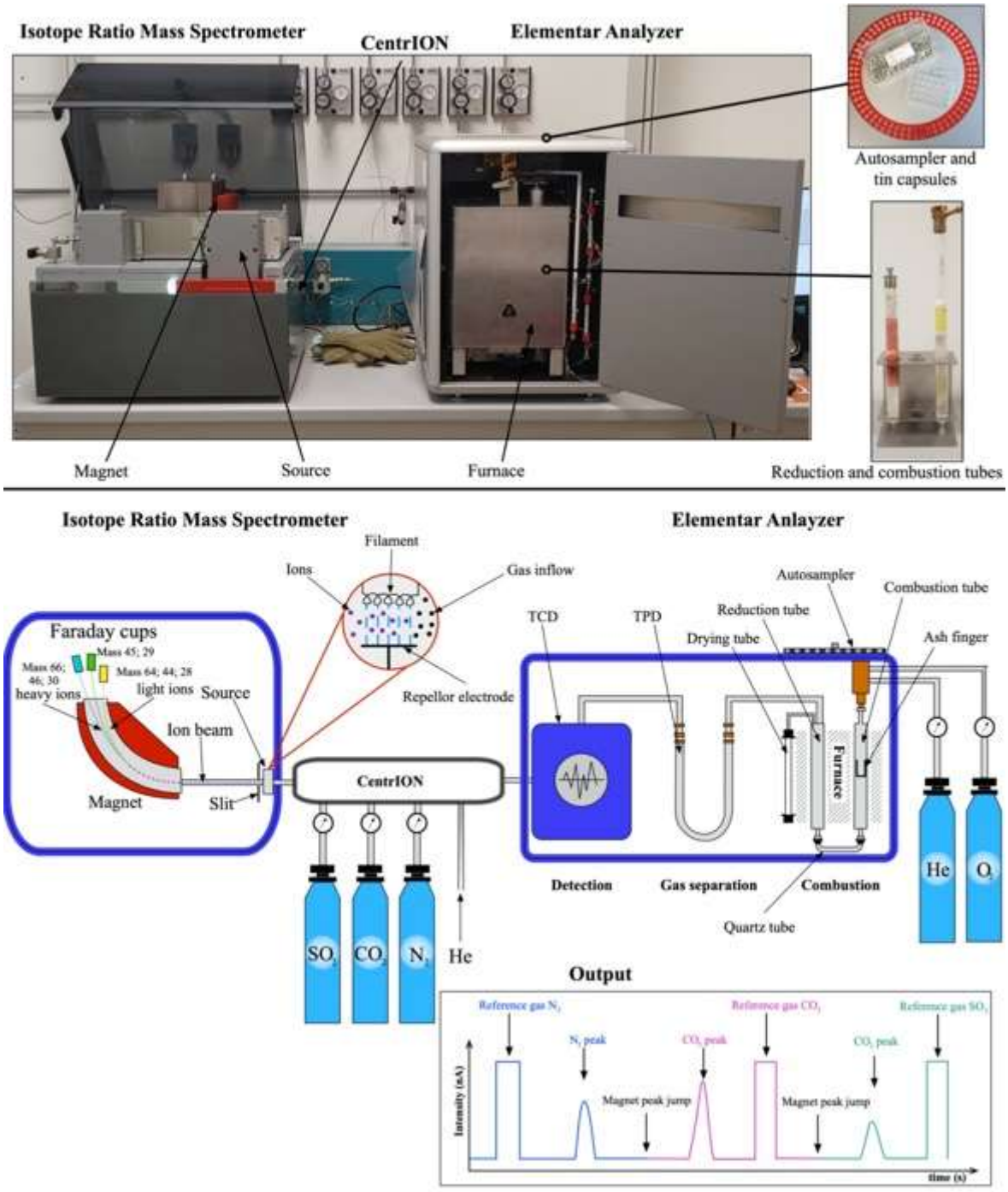


**Figure 15.** a) The Elementar® PYRO Cube (EA) in line with the PrecisION (IRMS) at the Department of Physics and Earth Sciences of the University of Ferrara; b) simplified scheme of an EA-IRMS analysis of C, N, and S.

### 3.2.2.2 Elementar Vario Micro Cube-Isoprime 100 for elemental and isotopic analysis of C (OC and IC), N

At the Department of Physics and Earth Sciences of the University of Ferrara the Elementar® Vario MICRO Cube elemental analyzer (EA) coupled with the IsoPrime100

isotope ratio mass spectrometer (IRMS) in the continuous-flow mode (Figure 16a) was used to measure the C (including OC and IC) and N contents and the relative isotopic ratios (Figure 16b). Powdered samples were weighed and wrapped in tin capsules. These capsules allowed loading of up to 40 mg of sample material and were subsequently introduced into the Vario MICRO Cube autosampler for the analysis. Flash combustion occurred in a sealed quartz tube filled with copper oxide grains in an excess of high-purity $O_2$ gas (grade purity 6). The carbon and nitrogen gaseous species were released by the burnt samples and were transferred to another tube maintained at 550°C. This tube contained chips of native copper, which reduced the nitrogen oxides ($NO_X$) to $N_2$. The formed $CO_2$ and $N_2$ gases were carried by He (grade purity 5) gas flow within a trap containing Sicapent® to remove $H_2O$. The $CO_2$ and $N_2$ gases were finally separated by a temperature programmable desorption column, and they were quantitatively determined using a thermo-conductivity detector (TCD).

The $CO_2$ gas was conveyed to the IRMS to determine carbon isotopic ratios. The detected isotopic masses of the sample were compared to those of the reference $CO_2$ (grade purity 5) gas. The reference gas was previously calibrated using various reference materials such as the limestone JLs-1 (Kusaka and Nakano, 2014), the peach leaves NIST SRM1547 (Dutta et al., 2006), the Carrara Marble (calibrated at the Institute of Geoscience and Georesources of the Italian National Research Council), the Jacupiranga carbonatite (Beccaluva et al., 2017; Santos and Clayton, 1995) and the synthetic sulfanilamide provided by Isoprime Ltd. Mass peaks were recalculated as isotopic ratios using the Ion Vantage software package.

Elemental precision was estimated by repeated standard analyses. Accuracy was evaluated by comparing the reference and measured values. Both parameters were approximately 5% for C and 7 % for N of the absolute measured value, but uncertainty increased for contents approaching the detection limit (0.001 wt%) (Natali et al., 2018b; 2021).

As for the abovementioned EA–IRMS system, C and N isotope ratios (*i.e.,* $^{13}C/^{12}C$ and $^{15}N/^{14}N$) were expressed with the δ notation in per mil (‰), relative to PDB and air $N_2$, respectively.

Regulating the temperature of combustion of the instrument is possible to perform the C speciation, *i.e.*, the definition of elemental and isotopic composition of the total carbon (TC), and its subfraction: OC and IC. The speciation has been carried out following method proposed by Natali and Bianchini (2015) and Natali et al. (2018a).

According to this analytical protocol:

- TC is measured by EA-IRMS, with a sample combustion at 950 °C;

- OC is measured by EA-IRMS, with a sample combustion set at a lower temperature (tests at 450, 500 and 550 °C);
- IC is measured by EA-IRMS, with combustion at 950 °C in samples where organic matter has been previously removed by combustion in a muffle furnace (at 450 for 12 h); the relative gravimetric loss (LOI) was also determined to correct the elemental concentration of the IC fraction.

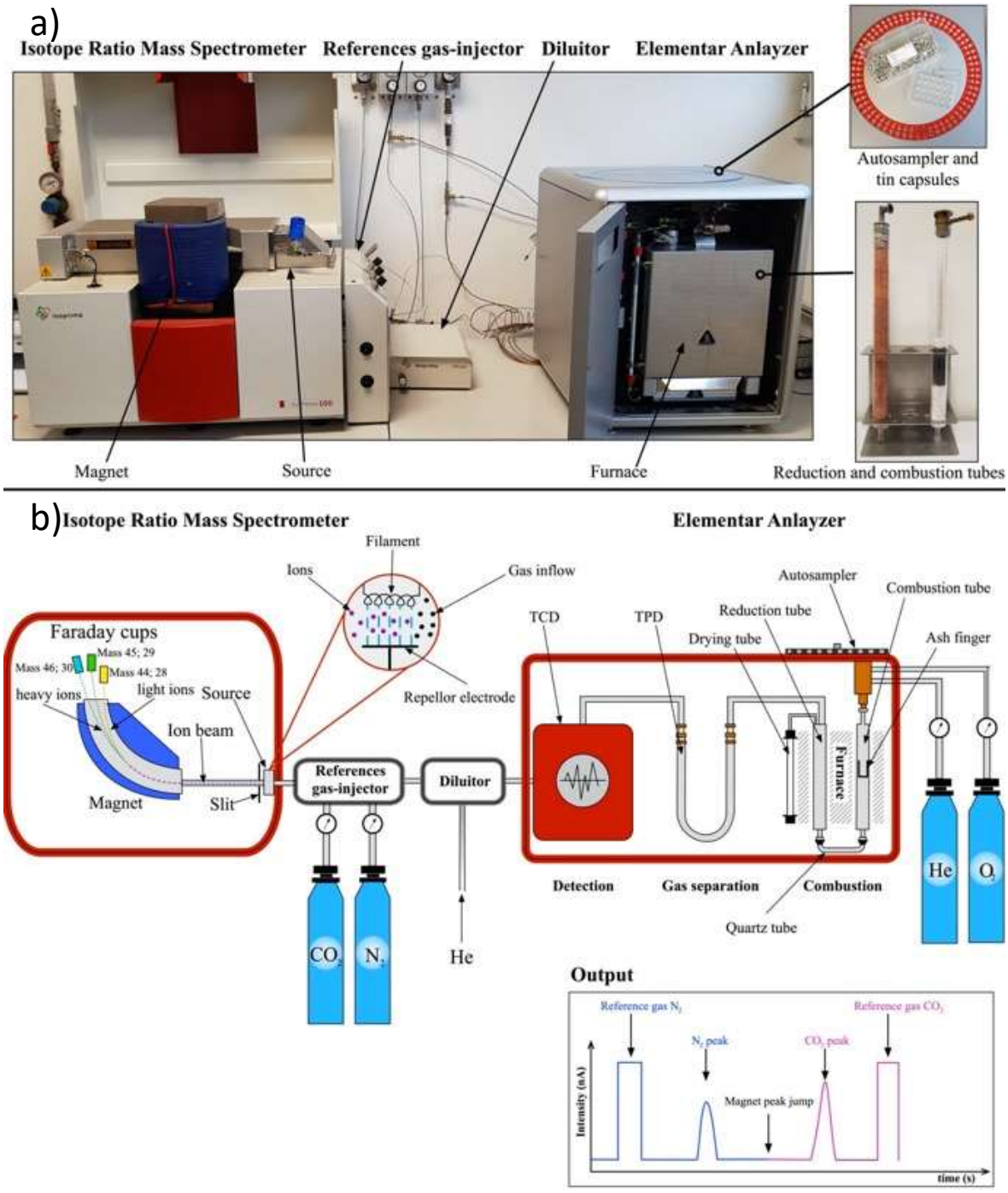


**Figure 16.** a) The Elementar® Vario MICRO Cube (EA) coupled with the IsoPrime100 (IRMS) at the Department of Physics and Earth Sciences of the University of Ferrara; b) simplified scheme of an EA-IRMS analysis of C and N (Bianchini et al., 2021).

### 3.2.3 Smart combustion elemental analysis (Elementar SoliTOC cube)

Elemental analyses of C were carried out at the Department of Physics and Earth Sciences of the University of Ferrara and at CREA (Council for Agricultural Research and Economics, Gorizia, Italy) using the SoliTOC Cube elemental analyzer (Elementar®, Langenselbold, Germany; Figure 17a), in compliance with the DIN 19539 standard, to carry out the temperature-dependent differentiation of total carbon (TC) in the investigated soil samples. This method is also known as "smart combustion" (Zethof et al., 2019). Powdered samples were loaded in stainless steel crucibles and placed in an 80-position autosampler. The crucibles were picked up by a stainless steel arm and placed in the dynamically heated portion of the combustion column at an initial temperature of 60°C. The analytical run required approximately 1,600 s and involved a three-step heating of the samples to 400, 600, and 900°C with holding time of 230, 120, and 150 s, respectively. The $CO_2$ produced during the sample combustion was collected by two dedicated traps and sent to an IR detector for the continuous measurement of carbon. The DIN 19539 (Figure 17b) standard involves the separation and analysis of two oxidizable soil carbon pools with different thermal stabilities (*i.e.,* thermally labile organic carbon—$TOC_{400}$— stripped out at temperatures below 400°C, and residual oxidizable carbon—ROC—at temperatures of 500–600°C) and one carbon pool derived from the thermal breakdown of carbonate minerals at 650–850°C (total inorganic carbon – TIC). At the end of the analytical run, an internal fan reset the temperature of the dynamically heated portion of the column to 60°C. The same analytical device was used by Natali et al. (2020) to quantify the carbon pools in a soil sample set characterized by substantial textural and geochemical variability. They defined TOC as the sum of the $TOC_{400}$ and ROC organic carbon pools.

A standard of calcium carbonate ($CaCO_3$, Calciumcarbonat, Elementar®) and a soil standard (Bodenstandard, Elementar®) were analyzed prior, between, and after each run. Analytical precision and accuracy of the instrument were better than 5% of the absolute measured value (Natali et al., 2021).

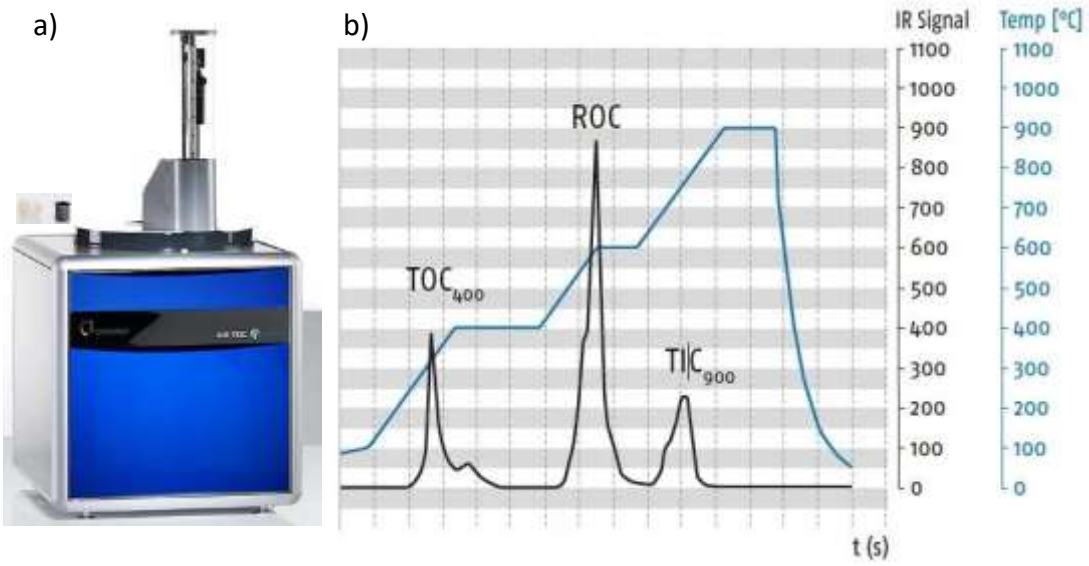


**Figure 17.** a) The Elementar® SoliTOC cube and b) a graphic panel of a single run with DIN 19539 method showing the different carbon fractions: $TOC_{400}$ (thermally labile organic carbon), ROC (residual oxidizable carbon), and TIC (total inorganic carbon).

### 3.2.4 Further methods applied on peaty soils of the Mezzano Lowland

#### 3.2.4.1 Experimental Firing of unaffected Soil Profiles

In the laboratory of the Department of Agricultural and Food Sciences of the University of Bologna, samples were burnt from horizons of the profile TOR4 which is located in a sector unaffected by natural fire, to simulate the processes and to evaluate the thermal transformation of soil samples induced by peat burning, following the method by Gonzalez-Vila and Galmedros (2003). Thermal heating was applied for 12 h at different temperatures using an electric muffle. Three replicates were prepared using 100-ml porcelain crucibles, each containing 20 g of soil sample. After isothermal heating at 105, 200, 400, and 600°C, 4 g of heated soil was used to quantitatively determine the different carbon fractions.

#### 3.2.4.2 pH, Electrical Conductivity and Bulk Density

Soil pH was measured by potentiometric titration on a 1:2.5 (w/v) soil:distilled water suspension with a Crison pH meter. Soil electrical conductivity (EC), expressed as deciSiemens per meter (dS $m^{-1}$), was obtained on a 1:2.5 (w/v) aqueous suspension filtered with a Whatman® 42 filter paper using an Orion conductivity-meter. Undisturbed soil samples collected in the steel cylinders of known volume were weighed after drying at

105°C for 24 h to calculate the bulk density (BD), which is the weight of dry soil divided by the total soil volume expressed in grams per cubic centimeter (g $cm^{-3}$).

## 3.3 Geophysical methods

*In-situ* detection of the apparent electrical conductivity (EC) using a non-invasive electromagnetic induction (EMI) discussed in Chapter 7 was simultaneously carried out using a Profiler EMP-400 (GSSI company, Nashua, NH; USA) along several parallel lines with a spacing of about 5m (Figure 13d and e; see section 3.1.4). The EMI survey was conducted in MB test site where the geochemical analyses were applied. In detail, the geophysical survey was carried out along 42 parallel lines with an interval spacing of about 5m. Each data was georeferenced with a horizontal accuracy of less than 0.5m and the number of readings was two per second, acquiring around 4000 values for each used frequency (16 kHz, 14 kHz and 10 kHz). The whole survey took approximately 1h to cover the study site. The estimation of the soil EC is obtained according to the Biot-Savart law, where a uniform electrical current (I) defines a magnetic field (B) in the vacuum:

$$B = \frac{\mu_0}{4\pi} I \int \frac{dl\ x\ r}{r^2}$$

*r* is the radius-vector between the current line and the measurement point, $\mu_0$ is the magnetic permeability of the vacuum ($4\pi 10^{-7}$ $NA^{-2}$), *dl* is the unit vector along the current line. In frequency domain EM instruments, the alternating current induces an alternating magnetic field, which induces the electromotive force (e.m.f.) according to the Faraday's law. Moreover, in EC soils the induced primary field (Hp) e.m.f. produces secondary electrical eddy currents.

The secondary currents cause, in turn, a secondary magnetic field (Hs), which is a complicated function of coils configuration and electro-magnetic properties of the ground. However, the Hs should be associated to a simple function of these variables for non-magnetic layered earth (so called "low induction number"). Therefore, the apparent ground conductivity ($\sigma_a$) becomes:

$$\sigma_a = \frac{4}{\omega \mu s^2} \frac{H_s}{H_p}$$

Where: $\omega$ is angular frequency ($2\pi f$), $\mu$ is permeability of the vacuum, *s* is the intercoil spacing. The depth of investigation depends on the generated electromagnetic forces; however, the magnitude of primary and secondary fields decreases with the increased distance. This introduces the concept of exploration skin depth, which defines the depth at

which the primary field strength is reduced $1/e$ times its original value. In detail, the skin depth depends on the ground conductivity and the used frequency (Telford et al., 1976).

## 3.4 Remotely sensed data

This section is exclusively related to the research summarized in Chapter 8.

### 3.4.1 The Sentinel-2 NDVI

Using a reserved API key on the ADAM platform (https://adamplatform.eu), for each investigated locality (discussed in Chapter 8) the normalized difference vegetation index (NDVI) with a dimension of a 10 × 10 m pixel of Copernicus Sentinel-2 (European Spatial Agency) was collected, also with masking of pixels affected by cloud cover and sun gliding, to reconstruct time series for the period December 2017 – December 2021. The bands acquired by the Sentinel-2 multispectral instrument, which also allows acquisition in other 11 bands in VNIR and SWIR, are used to calculate NDVI as follow:

$$NDVI_{Sentinel\text{-}2} = (B08 - B04) / (B08 + B04)$$

Where: B04 is red and B08 is near infrared.
Therefore, NDVI time series guarantee a coverage each 2-3 days of JDS area for an average of 169 acquisitions.

### 3.4.2 PRISMA imagery

JDS (discussed in Chapter 8) is also the most covered area of the Ferrara province by the acquisition of PRISMA (Italian Space Agency, ASI) that every 29 days detects with a "pushbroom" motion (Figure 18): a 1000 × 1000 30 m pixels hyperspectral image and a co-registered 6000 × 6000 5 m pixel panchromatic image.

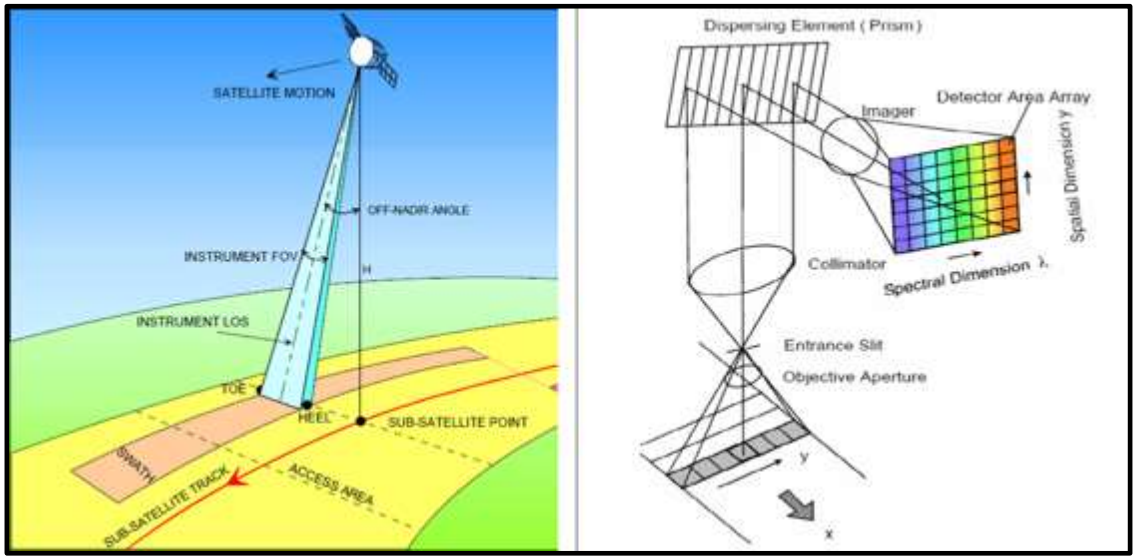


**Figure 18.** PRISMA 'pushbroom' image acquisition concept (ASI, 2020).

The spectrometer imaging has the capability to collect 240 spectral bands in the wavelength range 400-2450 nm: 66 bands in the visible and near-infrared (VNIR) spectral range (400-1010 nm) and 173 bands in the short-wave infrared (SWIR) range (920-2500 nm) (Pignatti et al., 2013). Therefore, 12 PRISMA images were collected in correspondence of Sentinel-2 acquisition (Table 1). Thus, the much more reliable Sentinel-2 NDVI value was compared for each pixel of PRISMA in the date closest to the acquisition time of each of the available JDS PRISMA images. Table 1 shows the number of sampling locations having a Sentinel-2 NDVI smaller than the two possible thresholds of bare soil (*i.e.*, 0.2 and 0.3), for each PRISMA image.

**Table 1.** Number of sampling locations (out of 100) for which, in each date corresponding to a JDS PRISMA image, the Sentinel-2 NDVI value is smaller than the indicated thresholds (*i.e.*, 0.2 and 0.3). The numbers do not take into consideration the possibility that some of the sampling locations might be outside the area imaged by PRISMA on each date.

| PRISMA image | Sentinel-2 date | NDVI | |
|---|---|---|---|
| | | < 0.2 | < 0.3 |
| 20191021 | 2019-10-21 | 93 | 96 |
| 20200407 | 2020-04-08 | 99 | 100 |
| 20200517 | 2020-05-18 | 80 | 99 |
| 20200523 | 2020-05-23 | 45 | 69 |
| 20200626 | 2020-06-27 | 5 | 9 |
| 20200731 | 2020-08-01 | 1 | 5 |
| 20200916 | 2020-09-15 | 52 | 68 |
| 20210214 | 2021-02-14 | 7 | 12 |
| 20210424 | 2021-04-23 | 68 | 76 |
| 20210523 | 2021-05-23 | 46 | 61 |
| 20210604 | 2021-06-04 | 6 | 6 |
| 20210911 | 2021-09-10 | 54 | 65 |

### 3.4.3 Artificial Neural Networks

Artificial neural networks are a powerful and versatile machine learning system that can be configured to tackle a wide variety of tasks, particularly those involving large amounts of data (Géron, 2019). They thus appear to be the best technique to handle the wealth of data made available by a hyperspectral sensor. We tested the data on a Multi-Layer Perceptron (MLP) architecture.

Preprocessing steps were applied to adapt the spectrum of each image as described by Meng et al. (2020). Firstly, we applied an atmospheric window, considering hyperspectral data with the following requirements: < 1350 nm, between 1451 nm and 1771 nm, and > 1982 nm. As second step, we computed the first derivative curve of each spectrum to reduce systematic errors in spectral data. Finally, to smooth the spectra a Discrete Wavelet Transform (DWT) with its two processes of signal decomposition of the spectral signal (into low- and high-frequencies using a set of wavelets) and a signal reconstruction also to eliminate noise at high-frequencies, as described by Meng et al. (2020). Then, we perform a Principal Component Analysis (PCA) and select only the principal components which the total spectral variance is greater than 85%. Thus, as spectral indices, we applied the normalized difference index (NDI), ratio index (RI) and difference index (DI) equations in the contour map method and selected the optimal spectral index as a predictor in the SOC prediction model.

$$NDI = ( R_i - R_j ) / ( R_i + R_j )$$

$$RI = R_i / R_j$$

$$DI = R_i - R_j$$

Where: R is spectral data and $_i \neq _j$

We attempted on the starting configuration composed by 1 hidden layer of 12 neurons. The input for the ANN were 3 bands with the highest weight computed after DWT process and the computed NDI, the RI, and the DI with the highest Pearson coefficient of correlation to the associated OC values. Overall, we used the 100 soil OC values: 70% to train and 30% to test the ANN, respectively. We iterated the training and testing process multiple times, always making a different random selection of the training and testing data. To avoid a significative fluctuation of the results between one iteration and the next, we always performed 100 iterations. Therefore, to evaluate the ANN, we tested the regression performance of the ANN used only the $R^2$ coefficient, averaged over the iterations, as follow:

$$R^2 = 1 - \{ [ \sum_j ( y_j - \hat{y}_j )^2 ] / [ \sum_j ( y_j - \bar{y} )^2 ] \}$$

Where: $\hat{y}_j$ is the predicted value by the model and $\bar{y}$ is the average values.

### 3.5 Statistical methods and Geographic Information System

The data interpretation was supported by a statistical analysis that was carried out by R (R Core Team, 2017). The analysis of variance (ANOVA test) was applied to test if element composition and/or isotopic ratios were affected by the provenance of the sediments. The PCA was applied to examine differences in elemental and isotopic parameters between sediments having Po and Reno affinity (package “FactoMineR” [Le et al., 2008]; package “factoextra” [Kassambara, 2017]).

Interpolated raster data discussed in Chapter 7 were obtained to represent the spatial variation at the resolution of 1 m of the physicochemical parameters investigated along the site using ordinary kriging and cokriging (Ahmed et al., 2017), we adopted a gaussian semivariogram model on a power transformed data like Box and Cox (1964) approach. The maps reported in Chapter 7 of the OC concentration (interpolated using kriging and cokriging) and the EC measured at 10 kHz were edited with Q-GIS 3.16.13 (QGIS.org,

2021). Map of the isotopic signatures in Chapter 5 that appears influenced by the depositional facies, were prepared with Q-GIS 3.14.

### 3.5.1 Mapping of soil carbon loss

In this section are reported exclusively the GIS procedures related to the activities described in Chapter 5.

Using Q–GIS 3.22.12, the database of results from the 1937 (Ferrari et al., 1937) digitized soil survey report was used to create a point shapefile that included the following fields: i) sample identifier, ii) sampling coordinates, iii) SOM (wt%), iv), carbonates (wt%), and v) nitrogen (wt%) (Supplementary Table B1; See appendix 5). The SOM was converted to OC content using the van Bemmelen factor (0.58), and the IC content was calculated considering the 12% of total carbonate concentration. TC was obtained by the sum of OC and IC fractions. Next, interpolated maps of SOC distribution in 1937 and 2022 were obtained from the point shape files using the ordinary kriging with spherical semivariogram model in the Geostatistical Analyst tool of ArcMap 10.8.2 (ESRI, 2022). In addition, a spatial distribution map of $\delta^{13}C$ was created using the isotopic data from the 2022 soil sample campaign following the technique described by Bowen (2010). The SOC stock (in Mg $ha^{-1}$) distributions in 1937 and 2022 were predicted using the geoprocessing tool of raster calculator on QGIS 3.22.12 with the product:

$$SOC\ stock_{raster} = BD \times SOC_{raster} \times Thk$$

where: BD is the bulk density (in g $cm^{-3}$) value of the 0-30cm Ferrara province soils, downloaded from by the Emilia-Romagna region geological and soil survey (Emilia-Romagna region, 2015). In the resulting spatial map shown in Figure 24 (see section 5.3.1), $SOC_{raster}$ (in wt%; each pixel is 1ha) is the organic carbon concentration distribution predicted using 2022 and 1937 datasets; Thk is the considered soil thickness (*i.e.*, 30 cm).

The estimation of the $\Delta\ CO_2\ eq_{\ 85\ years}$ (in Mg $ha^{-1}$) was also calculated using the raster calculator, as follow:

$$\Delta\ CO_2\ eq_{\ 85\ years} = \Delta\ SOC\ stock \times 44/12$$

Where $\Delta$ SOC stock is the difference between $SOC\ stock_{raster}$ calculated in 2022 and 1937.

Soil delineations of the Ferrara province provided by the Soil survey service of the Emilia-Romagna region (1:50,000 Soil map) were imported on QGIS as shapefile. Because each delineation can be a mix of different percentages of several characteristic soils of the Emilia-Romagna region, the type of soil texture has been recognized (see Supplementary Figure B1a in appendix B) with a weighted average of the textures of each characteristic

soil described in the soil catalog of the Emilia-Romagna region. In order to obtain the average ΔOC after 85 years (see Supplementary Figure B1b in appendix 5) of each delineation, the difference (using the processing tool raster calculator) between the averaged OC in 1937 and 2022 (both carried out using the processing tool of statistical zone) was calculated.

# 4. Isotopic proxies to verify the provenance of the Ferrara province topsoils

Enclosed:

SALANI, G.M., Brombin, V., Natali, C., Bianchini, G., 2021. Carbon, nitrogen, and sulphur isotope analysis of the Padanian Plain sediments: Backgrounds and provenance indication of the alluvial components. *Applied Geochemistry, 135,* 105130. https://doi.org/10.1016/J.APGEOCHEM.2021.105130.

## 4.1 Introduction

The geochemical signatures of sediments in alluvial plains record the geochemistry of the parent rocks and the weathering mechanisms occurred in the source areas. However, geochemical signatures are often complex to be interpreted because distinct rivers (and tributaries) drain geologically different sub-basins, sometimes conveying different sediments in the same alluvial plain. Trace elements ratios, Rare Earth Element (REE) contents, and Sr-Nd isotopic composition are in general considered as the best provenance tracers (Bianchini et al., 2012; Balabanova et al., 2016; Nyobe et al., 2018; Salomão et al.,2020; Vicente et al., 2021) although care must be taken if they are affected by sedimentary sorting effect (Bouchez et al., 2011; Roddaz et al., 2014). In addition, the primary signature of sediments could be modified by secondary pedological processes, in turn related to local climatic conditions (Costantini et al., 2002; Caporale and Violante, 2016). The natural (geogenic) geochemical fingerprint of the alluvial sediments can be also overprinted by anthropogenic contributions in agricultural, industrial, and urban areas (Galán et al., 2014; Barbieri et al., 2018). Therefore, in order to better constrain the sources of alluvial sediments, new geochemical proxies have to be tested to delineate the provenance of sediments and features of the relative depositional environments. Among the various case-studies, alluvial sediments in the province of Ferrara, located in the easternmost sector of the Padanian Plain (Northern Italy), have been widely studied from a geochemical point of view (Amorosi et al., 2002; Amorosi, 2012; Bianchini et al., 2012, 2013, 2019; Di Giuseppe et al., 2014a, 2014b, 2014c). The soils of this specific sector of the plain are composed by young (Holocene in age) alluvial deposits transported by Po and Reno fluvial systems. Previous investigations on these sediments were mainly focused on major elements having lithophile affinity (Si, Al, Ti, Fe, Mn, Mg, Ca, Na, K, P) and heavy metals (Ni, Co, Cr, V, Sc, Cu, Pb, Zn) to constrain the distribution of potentially toxic elements (Di Giuseppe et al., 2014a, 2014b, 2014c; Bianchini et al., 2012, 2013, 2019). They were important to define the local geochemical backgrounds, and interestingly, also the sediments provenance, *i.e.,* which fluvial system conveyed its alluvial load in the plain (Bianchini et al., 2012, 2013). In fact, specific trace element such as nickel (Ni) and chromium (Cr) were effective in discriminating between alluvial sediments from Po and Reno Rivers, the two fluvial systems that are interacting in the area (Bianchini et al., 2012, 2013, 2019). The Po River sediments are richer in Cr and Ni than Reno River sediments because the parent rocks outcropping in the Po River catchment include mafic and ultramafic lithologies rich in heavy metals (Amorosi, 2012). In the above-mentioned

studies essential elements such as carbon (C), nitrogen (N), and sulphur (S) have been scarcely investigated, and information on their isotopic ratios ($^{13}C/^{12}C$, $^{15}N/^{14}N$, $^{34}S/^{32}S$) is missing. The stable isotope compositions of C, N, and S of soils and sediments vary significantly, reflecting the nature of the parent rock material, the current and past climates and vegetation, and the effects of other organisms (Anderson, 1988). Therefore, they could be used as additional proxies to trace the source areas of the weathered material, which was mobilized by erosion, transported by rivers in the catchments and finally deposited in alluvial plains.

In order to test the effectiveness of CNS elemental and isotopic data in the provenance analysis, sediment samples were selected from the collections of previous geochemical studies that emphasized the origin of Padanian alluvial sediments on the basis of Cr and Ni content (Bianchini et al., 2012, 2013; Di Giuseppe et al., 2014a, 2014b, 2014c). This new investigation deals with the analysis of the elemental and isotopic composition of C, N, and S of selected sample sediments having "Po affinity" (*i.e.,* high Ni-Cr contents) and "Reno affinity" (*i.e.,* low Ni-Cr contents). The goal is to define CNS elemental and isotopic backgrounds and to verify if these tracers can be used as additional proxies to define the sediment provenance.

## 4.2 Results

The contents of C, N, and S as well as the respective isotopic ratios of alluvial sediments with Po or Reno River affinity are reported in Table 2. The Total Carbon (TC) concentration of the whole sample population varies between 1.2 and 3.1 wt% and $\delta^{13}C_{TC}$ ranges from −7.3 to −21.4‰.

**Table 2.** Total C (TC), N, and S elemental and isotopic values and relative standard deviations of alluvial sediments in the surroundings of Ferrara. Sediments are ascribed to Po and Reno River contributions on the basis of Cr and Ni contents according to previous studies (Bianchini et al., 2012, 2013).

| | Depth (cm) | Ni* ppm | Cr* ppm | TC (wt%) | $\delta^{13}C_{TC}$ (‰) | N (wt%) | $\delta^{15}N$ (‰) | S (wt%) | $\delta^{34}S$ (‰) |
|---|---|---|---|---|---|---|---|---|---|
| **Po River affinity** | | | | | | | | | |
| VP3S | 30-40 | 212 | 127 | 2.81 ± 0.03 | –10.9 ± 0.1 | 0.13 ± 0.02 | 9.7 ± 0.3 | 0.05 ± 0.01 | 1.9 ± 0.3 |
| VP3P | 100-120 | 204 | 137 | 3.10 ± 0.03 | –7.5 ± 0.1 | 0.06 ± 0.02 | 9.8 ± 0.3 | 0.04 ± 0.01 | 2.8 ± 0.3 |
| VP4S | 30-40 | 190 | 103 | 2.55 ± 0.04 | –10.5 ± 0.1 | 0.10 ± 0.02 | 8.9 ± 0.3 | 0.03 ± 0.01 | 3.0 ± 0.3 |
| VP5S | 30-40 | 215 | 122 | 2.76 ± 0.06 | –14.4 ± 0.1 | 0.14 ± 0.02 | 8.7 ± 0.3 | 0.03 ± 0.01 | 2.6 ± 0.3 |
| VP5P | 100-120 | 266 | 149 | 1.23 ± 0.15 | –21.4 ± 0.1 | 0.08 ± 0.02 | 7.3 ± 0.3 | 0.03 ± 0.01 | 0.2 ± 0.3 |
| VP6S | 30-40 | 232 | 144 | 2.63 ± 0.03 | –13.0 ± 0.1 | 0.12 ± 0.02 | 8.1 ± 0.3 | 0.03 ± 0.00 | 2.9 ± 0.3 |
| FE25A | 30-40 | 150 | 221 | 2.04 ± 0.06 | –12.0 ± 0.1 | 0.12 ± 0.02 | 8.2 ± 0.3 | < 0.01 ± 0.00 | 0.5 ± 0.3 |
| FE25B | 100-120 | 128 | 193 | 2.55 ± 0.03 | –8.2 ± 0.1 | 0.08 ± 0.02 | 10.7 ± 0.3 | < 0.01 ± 0.00 | 0.8 ± 0.3 |
| FE29A | 30-40 | 112 | 206 | 2.48 ± 0.13 | –9.8 ± 0.1 | 0.12 ± 0.02 | 12.5 ± 0.3 | < 0.01 ± 0.00 | 1.8 ± 0.3 |
| FE29B | 100-120 | 178 | 265 | 2.04 ± 0.04 | –9.4 ± 0.1 | 0.12 ± 0.05 | 10.3 ± 0.3 | < 0.01 ± 0.00 | 0.7 ± 0.3 |
| **Average** | | | | **2.42** | **–11.7** | **0.11** | **9.4** | **0.04** | **1.7** |
| **Reno River affinity** | | | | | | | | | |
| VM1S | 30-40 | 102 | 50 | 2.62 ± 0.05 | –11.0 ± 0.1 | 0.10 ± 0.02 | 6.4 ± 0.3 | 0.04 ± 0.01 | –2.0 ± 0.3 |
| VM1P | 100-120 | 105 | 59 | 2.58 ± 0.09 | –7.3 ± 0.1 | 0.05 ± 0.02 | 7.0 ± 0.3 | 0.03 ± 0.01 | –1.9 ± 0.3 |
| VM2S | 30-40 | 111 | 54 | 2.45 ± 0.13 | –8.7 ± 0.1 | 0.06 ± 0.02 | 6.3 ± 0.3 | 0.04 ± 0.01 | –2.6 ± 0.3 |
| VM2P | 100-120 | 98 | 51 | 2.64 ± 0.07 | –8.0 ± 0.1 | 0.05 ± 0.02 | 6.7 ± 0.3 | 0.05 ± 0.01 | –4.0 ± 0.3 |
| VM3P | 100-120 | 103 | 56 | 2.71 ± 0.03 | –9.9 ± 0.1 | 0.07 ± 0.02 | 5.7 ± 0.3 | 0.03 ± 0.01 | –3.1 ± 0.3 |
| VM5S | 30-40 | 76 | 39 | 2.47 ± 0.03 | –7.6 ± 0.1 | 0.06 ± 0.02 | 7.6 ± 0.3 | 0.03 ± 0.01 | –4.1 ± 0.3 |
| VM5P | 100-120 | 90 | 48 | 2.50 ± 0.06 | –5.9 ± 0.1 | 0.03 ± 0.02 | 9.0 ± 0.3 | 0.03 ± 0.01 | –1.6 ± 0.3 |
| F6P | 100-120 | 77 | 135 | 2.43 ± 0.03 | –9.9 ± 0.1 | 0.13 ± 0.00 | 8.0 ± 0.3 | < 0.01 ± 0.01 | –0.9 ± 0.3 |
| F10S | 30-40 | 74 | 125 | 2.74 ± 0.01 | –11.0 ± 0.1 | 0.15 ± 0.01 | 7.3 ± 0.3 | < 0.01 ± 0.01 | –0.1 ± 0.3 |
| F10P | 100-120 | 77 | 124 | 2.41 ± 0.02 | –7.6 ± 0.1 | 0.10 ± 0.01 | 7.8 ± 0.3 | 0.11 ± 0.01 | –4.5 ± 0.3 |
| FE4A | 30-40 | 54 | 89 | 2.74 ± 0.01 | –9.2 ± 0.1 | 0.15 ± 0.06 | 9.0 ± 0.3 | < 0.01 ± 0.01 | –0.4 ± 0.3 |
| **Average** | | | | **2.57** | **–8.7** | **0.09** | **7.3** | **0.04** | **–2.3** |

The sediments with Po and Reno affinity show similar C contents (Figure 19a), but their relative isotopic compositions are different (Figure 19b).

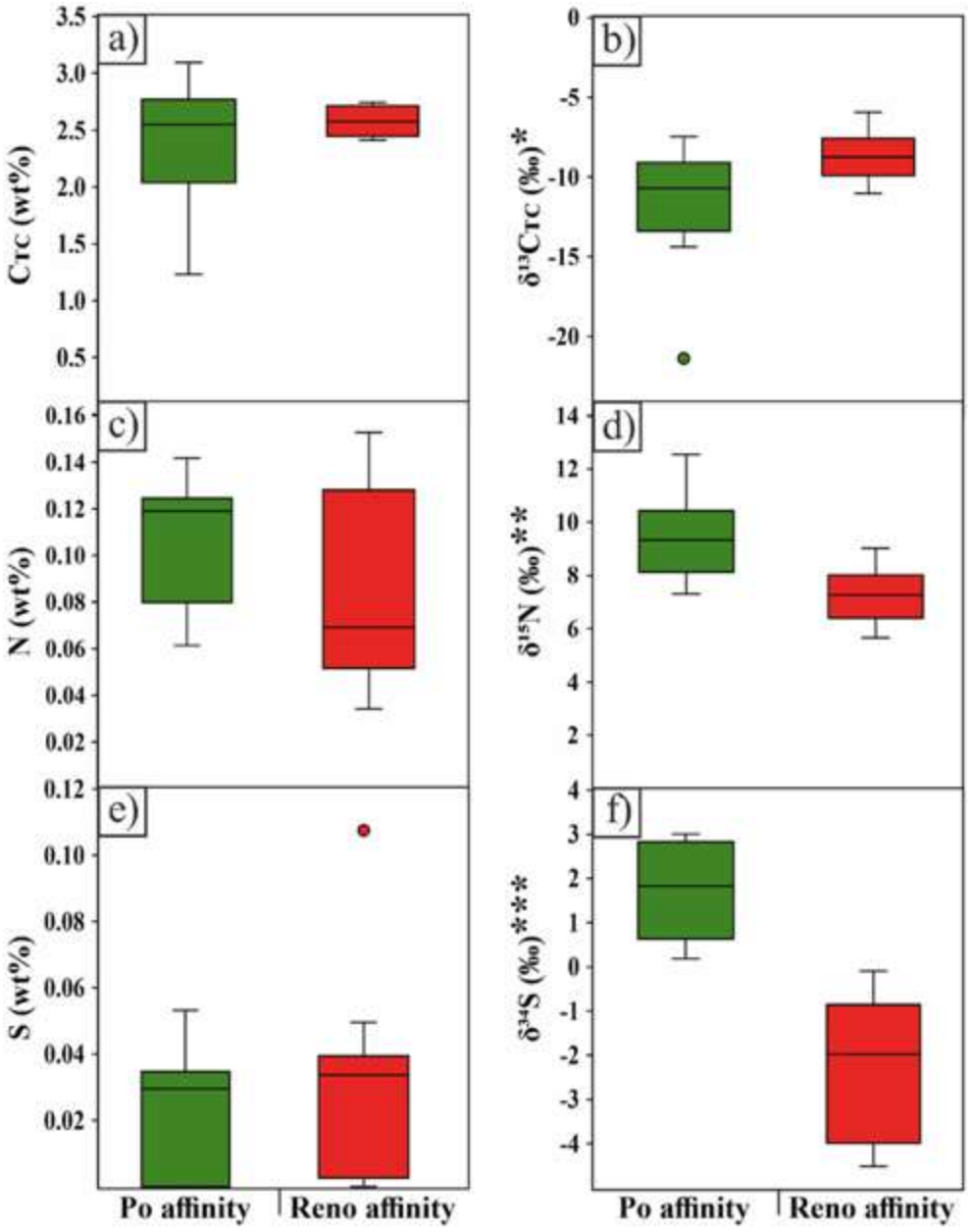


**Figure 19.** Box plots of the C, N, and S elemental and isotopic composition of alluvial sediments in the surroundings of Ferrara. Sediments are ascribed to Po and Reno River contributions according to previous studies (Bianchini et al., 2012, 2013). For the isotopic parameters, the one-way ANOVA results are also reported (*p < 0.01; **p < 0.001; ***p < 0.0001), while for the elemental contents, the one-way ANOVA results are not significant.

In particular, Po River sediments are characterized by TC between 1.2 and 3.1 wt% and $\delta^{13}C_{TC}$ between −7.5 and −21.4‰ with average value of 2.4 wt% and −11.7‰, respectively. Reno River sediments are characterized by more restricted elemental and

isotopic ranges than those of Po River, having TC between 2.4 and 2.7 wt% and $\delta^{13}C_{TC}$ between −7.3 and −11.0‰, with average values of 2.6 wt% and −8.7‰, respectively. This difference is primarily related to the inorganic and organic carbon (IC and OC, respectively) ratios, as IC typically has $\delta^{13}C_{IC}$ approaching 0‰ and OC typically has very negative $\delta^{13}C_{OC}$ down to −25‰ (Natali and Bianchini, 2015). However, our analyses of the distinct carbon fractions (Table 3) revealed that also OC and IC are characterized by distinct isotopic values in Po and Reno River sediments.

**Table 3.** Elemental and isotopic composition of distinct carbon fractions (Organic Carbon, OC; Inorganic Carbon, IC) of alluvial sediments in the surroundings of Ferrara. Sediments are ascribed to Po and Reno River contributions according to previous studies (Bianchini et al., 2012, 2013).

| | Depth (cm) | OC (wt%) | $\delta^{13}C_{OC}$ (‰) | IC (wt%) | $\delta^{13}C_{IC}$ (‰) |
|---|---|---|---|---|---|
| **Po River affinity** | | | | | |
| VP3S | 30-40 | 0.85 | –21.8 | 1.73 | –1.2 |
| VP3P | 100-120 | 0.39 | –20.5 | 2.32 | –1.5 |
| VP4S | 30-40 | 0.77 | –21.1 | 1.64 | –1.4 |
| VP5S | 30-40 | 1.13 | –22.0 | 1.36 | –2.2 |
| VP5P | 100-120 | 0.60 | –28.1 | 0.43 | –4.1 |
| VP6S | 30-40 | 0.93 | –22.4 | 1.48 | –2.7 |
| FE25A | 30-40 | 0.70 | –24.5 | 2.75 | –3.3 |
| FE25B | 100-120 | 0.31 | –23.6 | 0.77 | –0.4 |
| FE29A | 30-40 | 0.84 | –22.8 | 1.32 | 0.2 |
| FE29B | 100-120 | 0.56 | –22.8 | 1.32 | –0.5 |
| **Average** | | **0.71** | **–23.0** | **1.51** | **–1.7** |
| **Reno River affinity** | | | | | |
| VM1S | 30-40 | 0.75 | –22.5 | 1.59 | –0.5 |
| VM1P | 100-120 | 0.43 | –21.3 | 1.98 | –0.5 |
| VM2S | 30-40 | 0.48 | –22.1 | 1.72 | –1.0 |
| VM2P | 100-120 | 0.49 | –22.1 | 1.88 | –1.1 |
| VM3P | 100-120 | 0.34 | –20.0 | 1.86 | –0.8 |
| VM5S | 30-40 | 0.54 | –20.7 | 1.88 | –0.2 |
| VM5P | 100-120 | 0.63 | –21.7 | 1.92 | –0.1 |
| F6P | 100-120 | 0.76 | –23.1 | 1.27 | –0.9 |
| F10S | 30-40 | 0.90 | –22.7 | 1.32 | –1.5 |
| F10P | 100-120 | 0.50 | –22.5 | 1.53 | –1.3 |
| FE4A | 30-40 | 0.80 | –22.3 | 1.80 | 0.2 |
| **Average** | | **0.60** | **–21.9** | **1.70** | **–0.7** |

Samples with Po affinity have on average 0.7 wt% of OC characterized by $\delta^{13}C_{OC}$ of −23.0‰ and 1.5 wt% of IC with $\delta^{13}C_{IC}$ of −1.7‰, whereas those with Reno affinity have

on average 0.6 wt% of OC characterized by $\delta^{13}C_{OC}$ of −21.9‰ and 1.7 wt% of IC characterized by $\delta^{13}C_{IC}$ of −0.7‰.

The N concentration of the whole sample population varies between 0.03 and 0.15 wt% and $\delta^{15}N$ varies between 5.7 and 12.5‰. From the elemental point of view Po and Reno River sediments are indistinct (0.0–0.1 wt%), but they differ in the isotopic composition (Figure 19c, d). Po River sediments are characterized by $\delta^{15}N$ between 7.3 and 12.5‰ with average of 9.4‰, whereas Reno River sediments are characterized by $\delta^{15}N$ between 5.7 and 9.0‰ with average of 7.3‰. The S concentration of the whole sample population varies from <0.01 wt% up to 0.11 wt%, whereas $\delta^{34}S$ varies between −4.5 and 3.0‰. Po River sediments are characterized by positive $\delta^{34}S$ values (between 0.2 and 3.0‰, average of 1.7‰), whereas Reno River sediments are characterized by negative $\delta^{34}S$ values (between −4.5 and −0.1‰, average of −2.3‰; Figure 19e, f).

The one-way ANOVA test was used to verify if the composition and/ or isotopic ratios were affected by the provenance of the sediments (Po or Reno River catchment). The test showed that TC, N, S, OC, IC, and $\delta^{13}C_{OC}$ of alluvial sediments were not significantly influenced ($p$-values > 1) by fluvial system which transported and deposited the sediments on the Padanian Plain. On the other hand, the $\delta^{13}C_{TC}$, $\delta^{13}C_{TC}$, are moderately affected ($p$-values < 0.01) by the fluvial system, and $\delta^{15}N$, $\delta^{34}S$ are significantly ($p$-value < 0.001) and extremely ($p$-value < 0.0001) influenced by the origin of the alluvial sediments, respectively.

## 4.3 Discussion

The difference between Reno and Po River sediments was already pointed out based on selected trace elements such as Cr and Ni as their high concentration is related to the presence of the ophiolite rock sequences in the Po River hydrological basin and are largely subordinate in the Reno River catchment (Bianchini et al., 2012, 2013, 2019). However, following the ANOVA results and the box plots, the isotopic ratios of C, N, and S are further good parameters to discriminate the sediments for their provenance. Such discrimination is also emphasized by the multivariate statistical analysis (PCA, Figure 20), where the isotopic ratios of C, N, and S were used as principal components. The PCA plot explains more than 80% of the total variance and well clusters the samples according to the Po and Reno River affinity. In the PCA plot the arrays show a similar length indicating that the isotopic parameters contribute equally to discriminate the two sample populations.

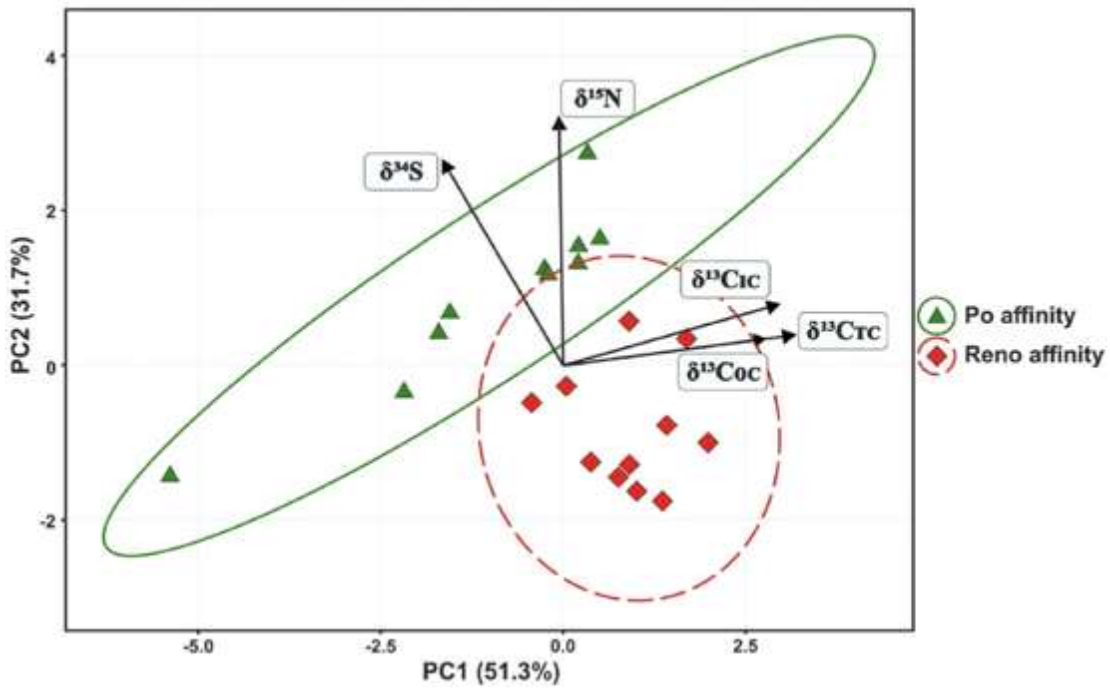


**Figure 20.** Principal Component Analysis (PCA) for the isotopic ratios of C, N, and S of alluvial sediments in the surroundings of Ferrara having Po and Reno affinity.

In order to test the role of these isotopic tracers in the provenance analysis, $\delta^{13}C_{TC}$, $\delta^{15}N$ and $\delta^{34}S$ are plotted vs. the Cr content, *i.e.,* one of the most appropriate geochemical markers to discriminate between Po and Reno River sediments according to Bianchini et al. (2012; 2013, 2019; Figure 21a–c). The enrichment of metals is a common geochemical feature of finer grain size sediments, often affecting the discrimination of the different sediment sources in the provenance analysis. The use of the least mobile elements (*i.e.,* Al, Th, Sc) in these systems as normalizing factors of metals concentrations has been widely used to avoid the grainsize effect on the metal enrichment leading to a correct identification of the alluvial sediment provenance (Bouchez et al., 2011). In particular, the variation of the Al/Si ratio, which represents a grain size index (*e.g.,* Bouchez et al., 2011; Roddaz et al., 2014), shows a wide overlap between the Po (0.28–0.40) and Reno (0.20–0.33) River sediments implying a comparable textural range for the two sample populations. Its distribution with respect to the CNS elemental and isotopic composition doesn't highlight any significant correlation suggesting that they are independent from the sample grain-size, and in turn that this latter does not affect the signature of the sediment provenance (Supplementary Figure A1 in appendix 4). The best correlation observed between the Al/Si ratio and the analyzed trace elements is with V, indicating that it is the most immobile element for the investigated sediments, and can be used as an alternative

and effective tracer of the sole grain size variation, being unaffected by the sediment provenance such as Cr and Ni (Supplementary Figure A2 in appendix 4). Therefore, in order to emphasize the distinct geochemical trends of the two sediment sources, the CNS isotopic ratios are also plotted against the Cr/V ratio, which is related to the rate of ophiolite contribution to the investigated sediments (Figure 21d–f). In particular, it can be observed a general decrease of $\delta^{13}C$ (Figure 21d) and a marked increase of $\delta^{15}N$ and $\delta^{34}S$ (Figure 21e–f), suggesting a complementary role of these isotopic tracers in the sediment provenance analysis.

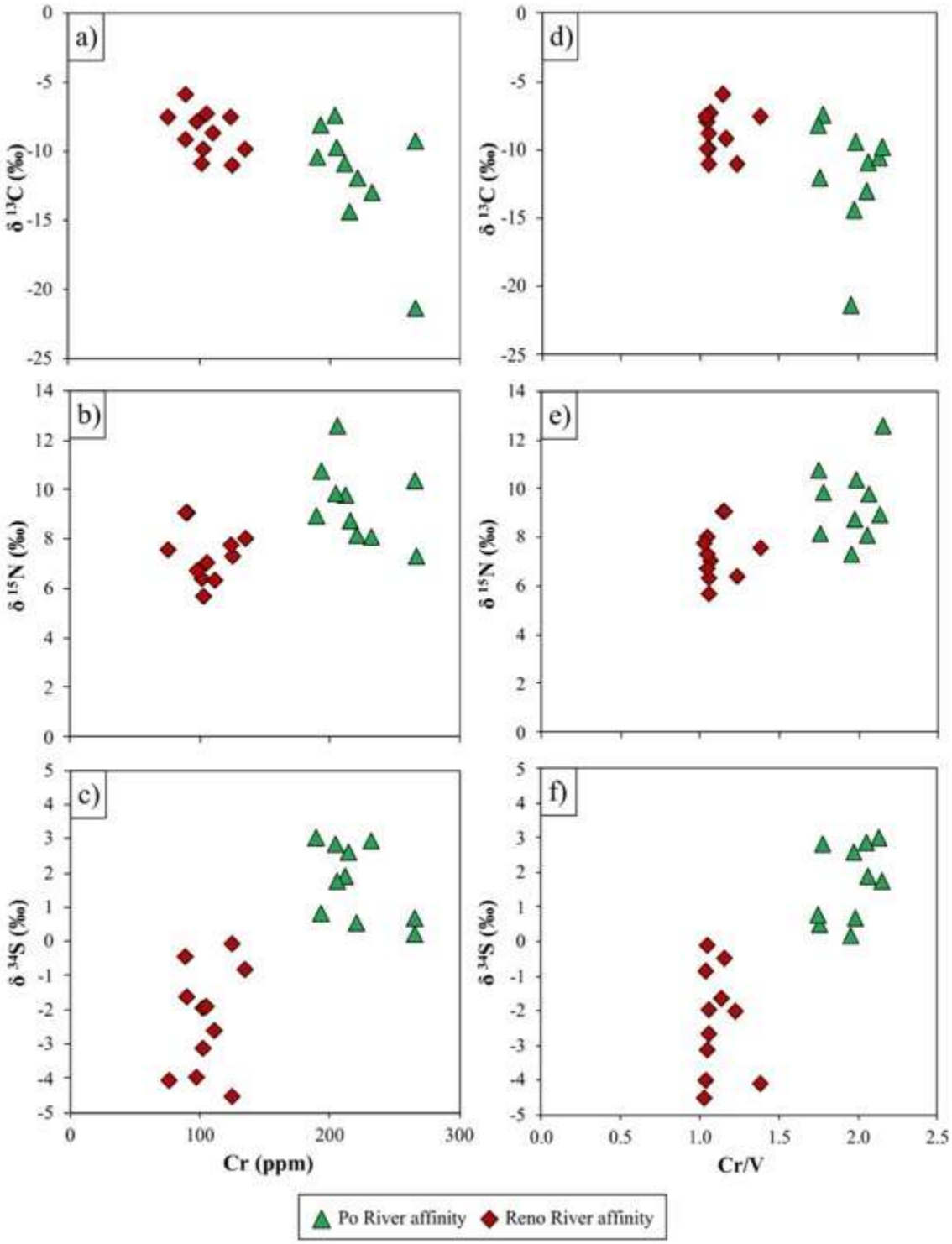


**Figure 21.** Cr (ppm) and Cr/V vs $\delta^{13}C_{TC}$ (a and d), $\delta^{15}N$ (b and e) and $\delta^{34}S$ (c and f) biplot diagrams discriminating the Po and Reno alluvial affinities in the surroundings of Ferrara on the basis of the geochemical composition (from Bianchini et al., 2012, 2013).

Hypotheses can be done to explain for the different C, N, and S isotopic fingerprint on the Po and Reno River alluvial sediments.

For carbon, the TC isotopic fingerprint depends on the OC and IC contents and their relative isotopic ratio. The difference cannot be related to a distinct fertilization history as

proposed for other study cases (Kanstrup et al., 2011) and must be interpreted as a distinctive character of the sediment source area, which is peculiar for every hydrological basin (Li et al., 2020). In general, the $\delta^{13}C_{OC}$ is controlled by the distribution of $C_3$ and $C_4$ plants, as according to their photosynthetic pathways the $\delta^{13}C_{TC}$ ranges from − 21‰ and − 35‰ for $C_3$ plants and from −9‰ to −20‰ for $C_4$ plants (O'Leary, 1988; Meier et al., 2014; Brombin et al., 2020). Moreover, in aquatic ecosystems the isotopic composition of the transported organic matter is also influenced by the autochthon growth of biomass constituted by algae and plankton (Finlay and Kendall, 2007). On the other hand, the $\delta^{13}C_{IC}$ is controlled by the presence of lithogenic (*i.e.,* primary) or pedogenic (*i.e.,* secondary) carbonates, which have $\delta^{13}C_{TC}$ values close to 0‰ or negative, respectively (Gao et al., 2017).

Summarizing, the TC isotopic ratios of Po River sediments are generally more negative than those recorded in Reno River sediments (Table 2; Figures 19b and 21a). This evidence cannot be related to a different proportion of organic and inorganic compounds, because i) the OC and IC contents of Po and Reno River sediments are similar (Table 3) and ii) both $\delta^{13}C_{OC}$ and $\delta^{13}C_{IC}$ values of Po River sediments are comparatively more negative respect to those of Reno River sediments (Table 3). Indeed, the different distribution of $C_3$ and $C_4$ plants could be responsible for the different $\delta^{13}C_{OC}$ of the Po and Reno sediments. The Po River hydrological basin comparatively extends at higher latitude and altitude and is plausibly characterized by a higher $C_3/C_4$ biomass ratio, with respect to the Reno River ratio. Moreover, it has to be noted that, the embankments of Po River are dominated by *Cyperus* vegetation (Pellizzari, 2020), which are $C_3$-plants whose $\delta^{13}C$ signature is extremely negative (Puttock et al., 2012; Laceby et al., 2014; Meier et al., 2014). In addition, $\delta^{13}C$ negativization in suspended particles of Po River water can also be induced by comparatively higher development of freshwater plankton (Søballe and Kimmel, 1987; Finlay and Kendall, 2007). The significant presence of such biomass could be responsible for the more negative $\delta^{13}C$ signature recorded in the Po River alluvial sediments. In addition, the samples collected in the interfluvial areas of Po River (VP5S, VP5P, VP6S, FE25A) have comparatively negative $\delta^{13}C_{IC}$ values, which are indicative of the presence of pedogenic carbonates that enhance the difference of the TC isotopic fingerprint of the two sample populations.

Interestingly, the $\delta^{13}C_{TC}$ appears effective, not only to discriminate Po and Reno River sediments, but also to precisely constrain the depositional facies. According to the geochemical map of Figure 22, irrespectively to the provenance of sediments (Po or Reno Rivers catchment), the paleo-channel deposits, mainly composed of sandy sediments, have

less negative $\delta^{13}C_{TC}$ signature respect to the surrounding interfluvial areas which are mainly composed of clayey sediments. In fact, clays usually form aggregates in which the organic matter remains protected from microbial decomposition, and the organic carbon can therefore preserve its original signature (von Lützow et al., 2006; Gunina and Kuzyakov, 2014; De Clercq et al., 2015; Guillaume et al., 2015).

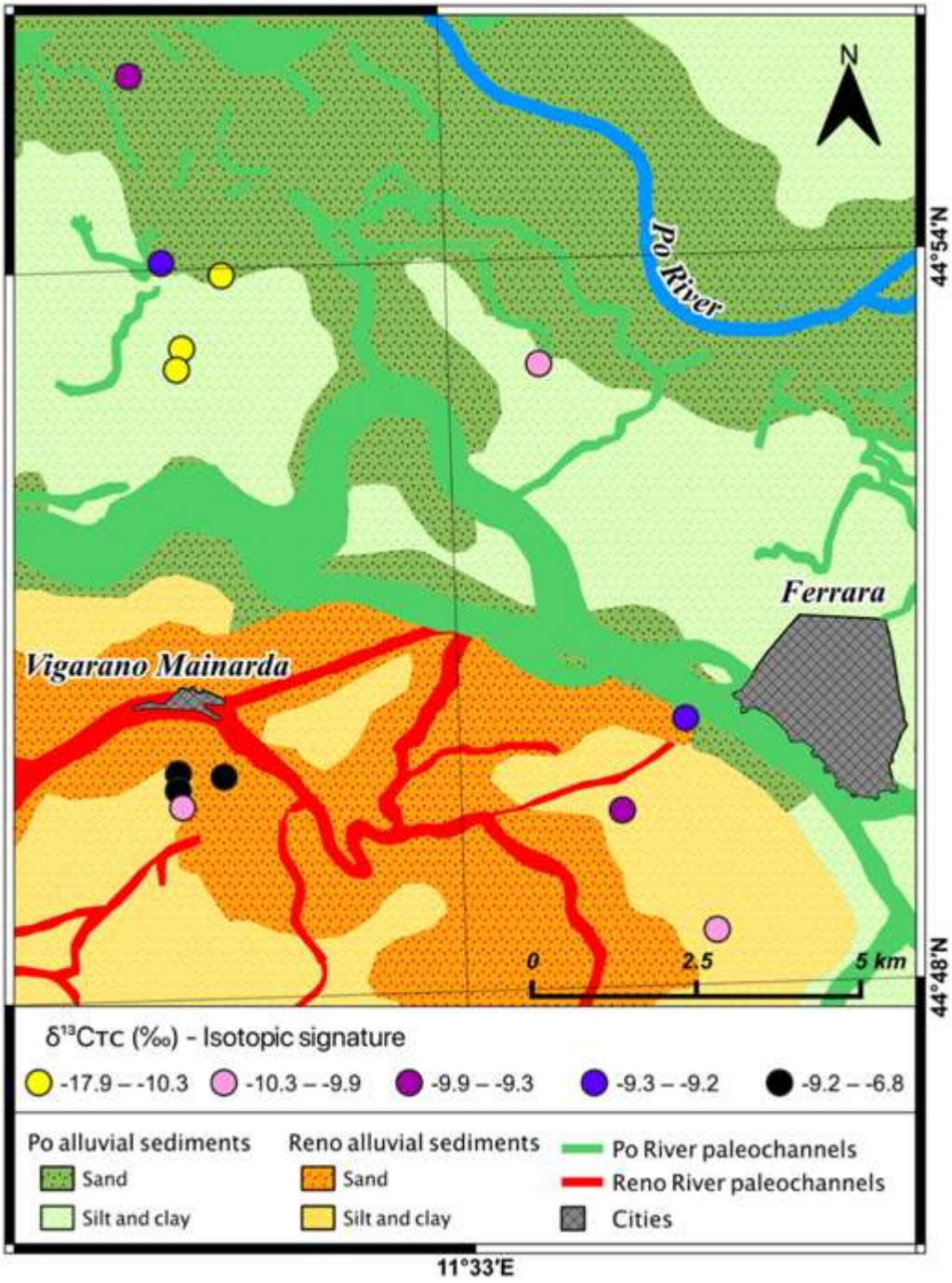


**Figure 22.** Geochemical map of the $\delta^{13}C_{TC}$ (‰) showing the distribution of the isotopic signatures near Ferrara and Vigarano Mainarda.

The observed differences on the nitrogen isotopic composition of Reno and Po River sediments can be in principle related to that of the organic matter, but soil $\delta^{15}N$ value can be also deeply affected by the agricultural practices and the related fertilization history (Bateman and Kelly, 2007; Xu et al., 2012). Noteworthy, in this case-study the observed difference of the two sample populations indicates that the anthropogenic activities did not obliterate the pristine compositions. In fact, the Po River sediments appear to be systematically enriched in $^{15}N$ with respect to those from the Reno River, a pristine difference of the associated organic matter that generally tends to develop higher $\delta^{15}N$ as result of the intense biogeochemical transformations (Hobbie and Ouimette, 2009; Craine et al., 2015a; Szpak, 2014) occurring in the Po soils which are more mature than those of Reno.

The difference on the sulphur isotopic composition of Reno and Po River sediments is also intriguing. As observed for N, the isotopic differences of S could also be explained in terms of soil maturity, since most of soil sulphur should be hosted in the organic matter (*e.g.,* Edwards et al., 1998). In this case, S isotopic fractionation should be controlled by biogeochemical processes producing fugitive gaseous compounds that are generally $\delta^{34}S$-depleted (Raven et al., 2015) and leave $\delta^{34}S$ -enriched residua (Norman et al., 2002). This occurs because during soil biogeochemical processes bacteria preferentially utilize $^{32}S$ during their metabolism, producing fugitive $\delta^{34}S$ -depleted products (Strauss, 1997). Therefore, as the Po River alluvial soils are more mature than those of Reno River, they developed higher $\delta^{34}S$ in response to biochemical isotopic fractionation. Noteworthy, among the biogeochemical processes a particular role is represented by sulphate reduction, where anaerobic bacteria reduce the sulphates into sulphides with more negative $\delta$ S fingerprint (Guo et al., 2016). This process is associated with the depletion of $\delta^{34}S$ up to 70‰ in the sediments (Habicht and Canfield, 2001), therefore the produced sulphide is depleted in $^{34}S$ compared to the sulphate from which is formed. This process could explain the different isotopic signature between the alluvial sediments of the surrounding of Ferrara.

On the whole, alluvial soils formed by the deposition of Po River sediments are more mature than those of Reno alluvial soils. This is mainly related to the physiographic difference of the two catchments, as the Po River catchment has a length (652 km) which is four times greater than that of the Reno River catchment (212 km), but also to the timing of sedimentation which appear older for Po River sediments. In fact, locally the interfluvial basins of Po River was definitely reclaimed during the fifteenth century (Bondesan, 1989), whereas the course of Reno River was changed several times until the eighteenth century,

when anthropic hydraulic activities defined the actual riverbed (Cremonini, 1989). These different depositional ages are plausibly recorded by the organic matter; Po River soils experienced more complete biogeochemical reactions than that of Reno River sediments. This fact affects the N and S cycles, because as proposed by previous studies organic matter plays a key role in the processes responsible for gaseous loss of nitrogen and sulphur light isotopes (Hobbie and Ouimette, 2009; Norman et al., 2002; Raven et al., 2015).

## 4.4 Conclusions

This paper demonstrates that, although intimately associated and interlayered, alluvial sediments having distinct provenance show different CNS isotope signature. This is validated for alluvial sediments of the easternmost sector of Padanian Plain, where the distinction between Alpine and Apennine contributions (conveyed Po and Reno Rivers, respectively) was known on the basis of heavy metals concentration.

We found out that the different CNS isotope fingerprint of Po and Reno River sediments is natural and not induced by anthropogenic contributions, but doesn't necessarily reflect a lithogenic signature, *i.e.,* it is not solely related to different parent rock types in the Po and Reno River catchments. In fact, we infer that bio-geochemical processes, characterized by distinct ecological conditions in the Po and Reno River catchments, are recorded in the CNS isotopic signatures. Po River sediments are generally few hundreds of years older and pertain to a basin having a path of nearly seven hundred kilometers, much longer that of Reno River. Consequently, soils developed on Po River sediments are comparatively more mature and record more complete biogeochemical processes that were more intense and affected nitrogen/sulphur compounds generating the distinctive isotope signatures.

The important evidence is that the CNS systematics preserve a "memory" of the environment of formation of the conveyed particles, which differs in the distinct basins that feed the alluvial plains. In the considered case-study, this "memory" is not overprinted by the existing anthropogenic activities.

More in general, the reported data increase knowledge on the local elemental and isotopic backgrounds. This is important because many pollutants contain significant CNS concentrations and specific isotope compositions. Therefore, the presented data will serve as baseline and provide new tools to recognize possible anthropogenic anomalies in the studied area.

Appendix 4

Figures:

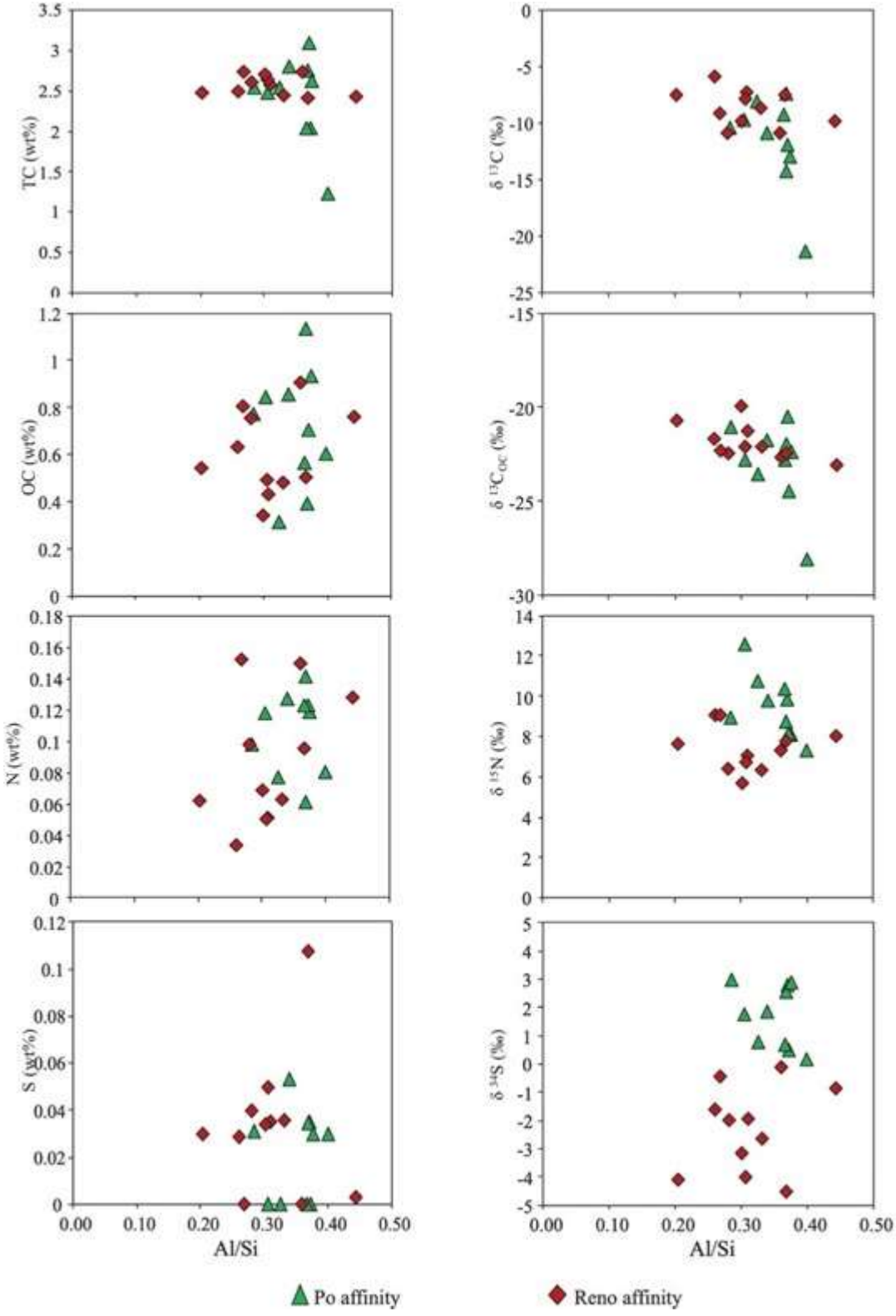


**Supplementary Figure A1.** Al/Si with respect to the CNS elemental and isotopic composition.

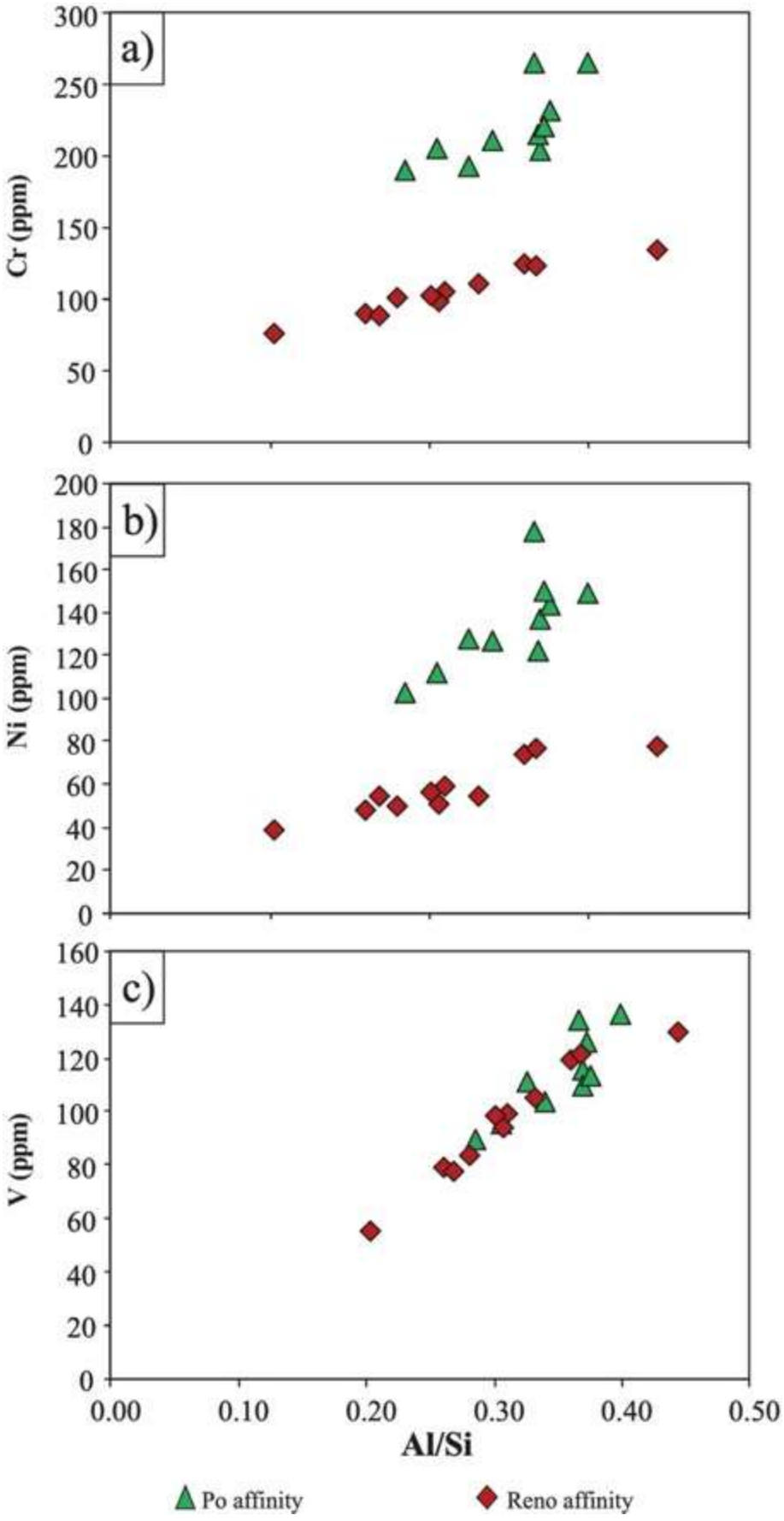


**Supplementary Figure A2.** Correlation observed between the Al/Si ratio and the analyzed trace elements (in ppm): a) Cr, b) Ni, and c) V.

# 5. The SOC depletion in the Ferrara province from 1937 to 2022

Enclosed manuscript (re-submitted at the Journal of Environmental Quality after the first round of revision, 17 February 2023; manuscript ID: JEQ-2022-12-0341-TR).
Soil Organic Carbon Data Comparison After 85 Years and New $^{13}C/^{12}C$ Compositions: the Case Study of the Ferrara Province (Northeastern Italy)

Gian Marco Salani[a], Gianluca Bianchini[b,a], Valentina Brombin[a], Claudio Natali[b,c]

[a] Department of Physics and Earth Sciences, University of Ferrara, Ferrara, 44122, Italy

[b] Department of Earth Sciences, University of Florence, Florence, 50121, Italy

[c] CNR-IGAG CNR-IGAG, Area della Ricerca di Roma-1, SP 35d, 9, 00010, Montelibretti RM, Italy

## 5.1 Introduction

Global warming is accelerating soil organic matter (SOM) degradation and increasing the release of greenhouse gases (GHGs; *e.g.*, $CO_2$, $CH_4$, $N_2O$) into the atmosphere (Crowther et al., 2016; Pries et al., 2017). Unsustainable agricultural practices, agricultural land use and land cover change (LULCC) exacerbate the process and account for 20% of the total $CO_2$ emissions (Lal, 2001; Arneth et al., 2017; Friedlingstein et al., 2019). Among the agricultural practices, the conventional tillage is considered one of the most unsustainable activity for the environment. In fact, plough tillage accelerates organic matter decomposition by breaking soil aggregates and the exposition of them to the air increasing soil aeration, which in turn promotes microbial activity, SOM mineralization and the consequent release of $CO_2$ (Wang et al., 2011; Kibet et al., 2016). Moreover, soil microbial activity is accelerated as temperature increases with the warmest regions of the world having the highest SOM decomposition rates (Wang et al., 2011). The Mediterranean area, characterized by warm and dry climate, have SOM contents that are low (<2%) and very low (<1%) (EIP-AGRI, 2015) and the soil organic carbon (SOC) is particularly vulnerable to oxidation (Ferreira et al., 2022). Thus, conservation of SOM is a critical issue in the Mediterranean to preserve soil fertility and limit GHG emissions. Over the last century conventional agriculture and LULCC have reduced SOM and released $CO_2$ in Norther Italy (Gardi and Sconosciuto, 2007; Fantappié at al., 2011; Brombin et al., 2020). The Ferrara province, located in the easternmost part of the Po River plain in Northern Italy, has soils with a large range of SOM content that include peatlands with very high SOM (Martinelli et al., 2013). Most of the SOM content variability found in the soils of the Ferrara province is the result of a wetland reclamation program of palustrine environment that ended in the 1970s and increased the agricultural production area by ~78000 ha (Simeoni and Corbau, 2009; Targetti et al., 2021). Reclamation projects started before the World War II, with ~51000 ha of land dried (Simeoni and Corbau, 2009; Targetti et al., 2021). In 1937 Ferrari et al. (1937) conducted a survey of the entire Ferrara province to assess the physico-chemical properties of the soils; the survey included SOM content in the 0-30 cm top soil layer. Recent soil surveys in the Ferrara province (Argenta municipality, Natali et al., 2018b; Bondeno and Mezzano lowland, Brombin et al., 2020; Mezzano lowland, Natali et al., 2021; Ferrara and Vigarano municipalities, Salani et al., 2021) reported a topsoils SOC range from ~0.4 wt% to ~24.4 wt% with a median of ~1.1 wt%, with the highest values recorded in peats from reclaimed wetlands. The research described in this paper offers a comparison of SOM content data collected by Ferrari et al. (1937)

with new topsoil chemical data collected from the same sample locations in 2022. In addition, the carbon isotopic signature ($\delta^{13}C$) of the samples obtained in 2022 was measured. Soil $\delta^{13}C$ has been used to determine the C turn over in soils and to better understand the C sources and the magnitude of the transformation of SOM by biogeochemical processes (Ehleringer et al., 2000; Wang et al., 2015; Mäkelä et al., 2022; Vittori Antisari et al., 2016; Wang et al., 2018; Camino-Serrano et al., 2019; Bianchini et al., 2022).

## 5.2 Results

The range and average of the measured TC, OC, IC, N, and $\delta^{13}C$ values in soils sampled in 2022 for each district of the Ferrara province are summarized in Table 4. The complete analytical dataset, including the C and N elemental and isotopic analyses of soil sampled in 2022, is reported in Supplementary Table B2 (see Appendix 5).

**Table 4.** Range and average (avg) of TC, OC, IC, N contents and $\delta^{13}C$ values for each district in 2022 and in the Ferrara province. The complete database is reported in Supplementary Table B2 (see Appendix 5).

| District | TC | | OC | | IC | | N | | $\delta^{13}C$ | |
|---|---|---|---|---|---|---|---|---|---|---|
| | range | avg | range | avg | range | avg | range | avg | range | avg |
| | wt% | | wt% | | wt% | | wt% | | ‰ | |
| **FM** | 1.52 - 6.72 | 2.74 | 0.71 - 5.81 | 1.31 | 0.12 - 2.28 | 1.42 | 0.03 - 0.45 | 0.14 | −23.1 - −2.4 | –11.1 |
| **LV** | 1.72 - 24.64 | 3.86 | 0.79 - 24.52 | 2.82 | 0.04 - 1.98 | 1.04 | 0.05 - 1.49 | 0.24 | −26.6 - −4.2 | –15.9 |
| **RV** | 1.99 - 6.02 | 3.21 | 0.66 - 5.46 | 2.04 | 0.17 - 1.85 | 1.17 | 0.04 - 0.45 | 0.20 | −25.4 - −4.0 | –14.0 |
| **FL** | 1.20 - 4.46 | 2.38 | 0.42 - 4.35 | 1.31 | 0.11 - 1.67 | 1.07 | 0.05 - 0.38 | 0.14 | −24.8 - −5.3 | –11.7 |
| **Ferrara province** | 1.20 - 24.64 | 3.18 | 0.42 - 24.52 | 2.01 | 0.04 - 2.28 | 1.18 | 0.03 - 1.49 | 0.19 | −26.6 - −2.4 | −13.5 |

The TC varied between 1.20 wt% (FL) and 24.64 wt% (LV), with an average of 3.18 wt%. The OC varied between 0.42 wt% (FL) and 24.52 wt% (LV), with an average of 2.01 wt%, whereas the IC varied between 0.04 wt% (LV) and 2.28 wt% (FM), with an average of 1.18 wt%. From Table 4 and Figure 23 it is evident that the observed variation in TC content is mainly due to the OC, since IC is a largely subordinate to the OC the topsoil of this province. The present-day (year 2022) spatial distribution of OC in topsoils displayed highest contents in the LV area, characterized by the presence of peatland soils derived from wetlands reclaimed since 1872, whereas all the other areas show maximum OC contents lower than 6 wt%.

The contents of N varied between 0.03 wt% (FM) and 1.49 wt% (LV), with an average of 0.19 wt%. A strong OC vs N relationship ($r^2$ ~0.9, not shown) confirmed that most of the measured N is concentrated in SOM.

The $\delta^{13}C$ varied from –26.6‰ (LV) to –2.4‰ (FM), with an average of –13.5‰.

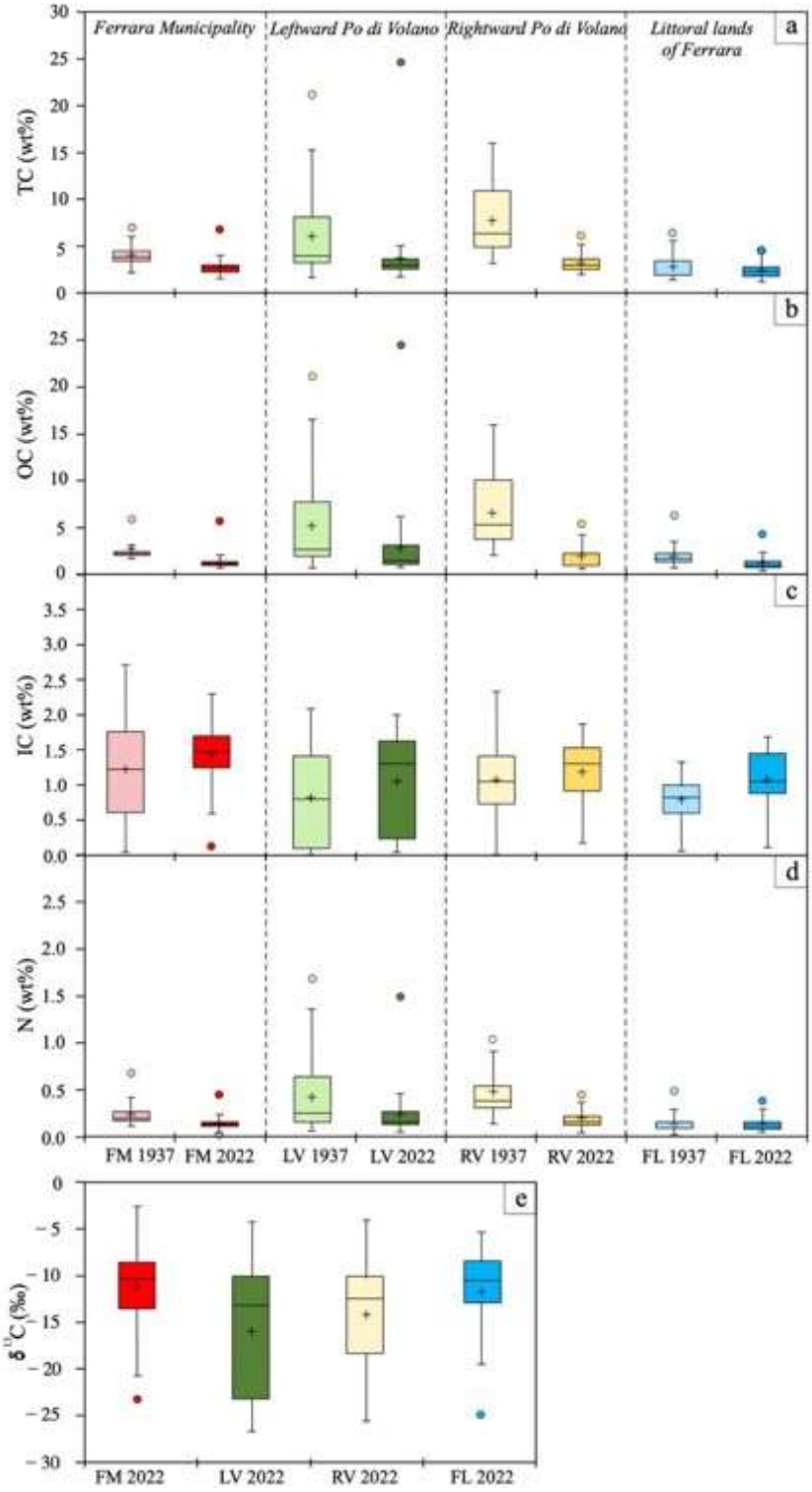


**Figure 23.** Distribution for each district in 1937 (light color) and 2022 (dark color) of: the elemental contents of a) TC, b) OC, c) IC, d) N, and, for 2022, the isotopic signature of e) $\delta^{13}C$. Average (black cross) and median (black line) values are also reported.

## 5.3 Discussion

### 5.3.1 Comparison of TC, IC, OC, and N contents after 85 years

The comparison of top soil TC, IC, OC and N composition in the Ferrara province from 1937 and 2022 is reported in Figure 23. The box and whiskers plot shows that TC and OC variably decreased from the 1937 to 2022 in all districts, whereas the IC approximatively remains stable or slightly increased by 2022 from 1937 for the addition of carbonates to correct the low pH of the soils. In the last 85 years the SOC decreased in average of 1.44 wt% in FM, 2.36 wt% in LV, 4.62 wt% in RV, and 0.68 wt% in FL; only a fraction of the reclaimed lands in LV has maintained the high values of OC. The geographic distribution of SOC in 1937 and 2022 are shown in Figure 24. In 1937 SOC distribution appears to be directly related to the soil landform. In fact, the lowest SOC values (0.75 wt% in FM and 0.70 wt% in LV areas) were measured in soils with coarse textures corresponding to ancient coastal and dunes in proximity to paleochannels and leeves of the Po River. On the contrary the highest SOC values (21.14 wt% in LV and 15.96 wt% RV) were measured in peaty deposits, typical of low energy depositional processes, that are currently managed as rice paddy thanks to their hydromorphic features.

The comparison of SOC values of 1937 with those of present-day (year 2022) indicates a variable significant depletion of the SOM during this period (Figure 24a and b). The negative SOC balance is caused by the intensification of cropland employment since the 1940s using unsustainable agriculture practices (*e.g.*, conventional tillage) which increased SOM oxidation and the release of C in atmosphere. According to Kumar et al. (2018), intensive agriculture globally impacted on the soil carbon cycle, favoring a large emission of $CO_2$ (Reicosky et al., 2005). Such leaks were also responsible for soil compaction as evidenced by local subsidence in the region (Gambolati et al., 2005, 2006; Corbau et al., 2019).

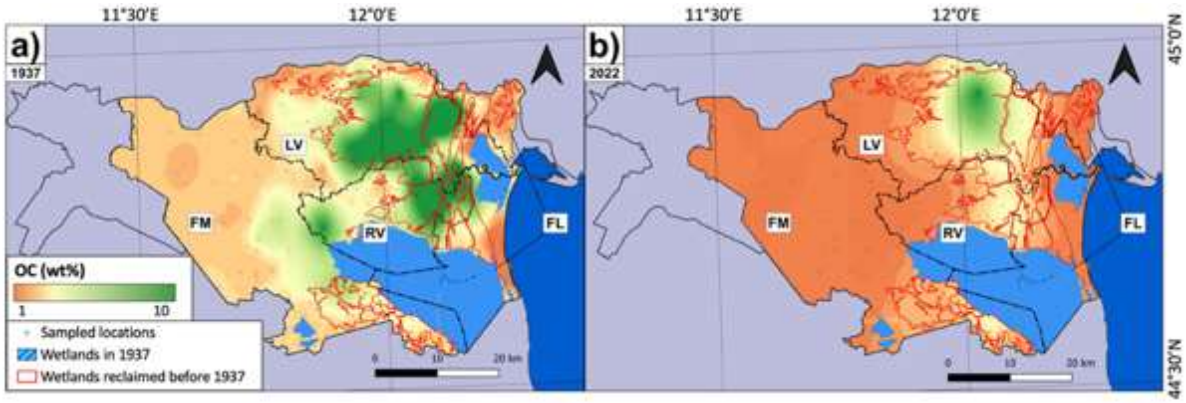


**Figure 24.** SOC distribution in a) 1937 and b) 2022. Sampled locations and wetland surfaces in 1937 and study districts boundary are also reported.

Figure 25a shows the linear correlation between the SOM concentration measured in 1937 and the SOC depletion (calculated by the difference of OC concentrations between 1937 and 2022; expressed as $\Delta OC_{85\ years}$). The maximum SOC depletions ($\Delta OC_{85\ years} > 10$ wt%) occurred in LV and RV soils, which recorded the highest SOM values in 1937, where land use changed from wetland to cropland, resulting in an increase of the oxidation of peaty soils. This trend is confirmed by the N depletion ($\Delta N_{85\ years}$) shown in Figure 25b, as consequence of the decrease of SOM.

The few exceptions to this trend characterized by higher OC and N values in 2022 (Figure 25), can be attributed to seasonal fertilization occurred in these locations, in which farmers reintegrated organic material (*e.g.*, slurry and manure) in the topsoils (Natali et al., 2018b).

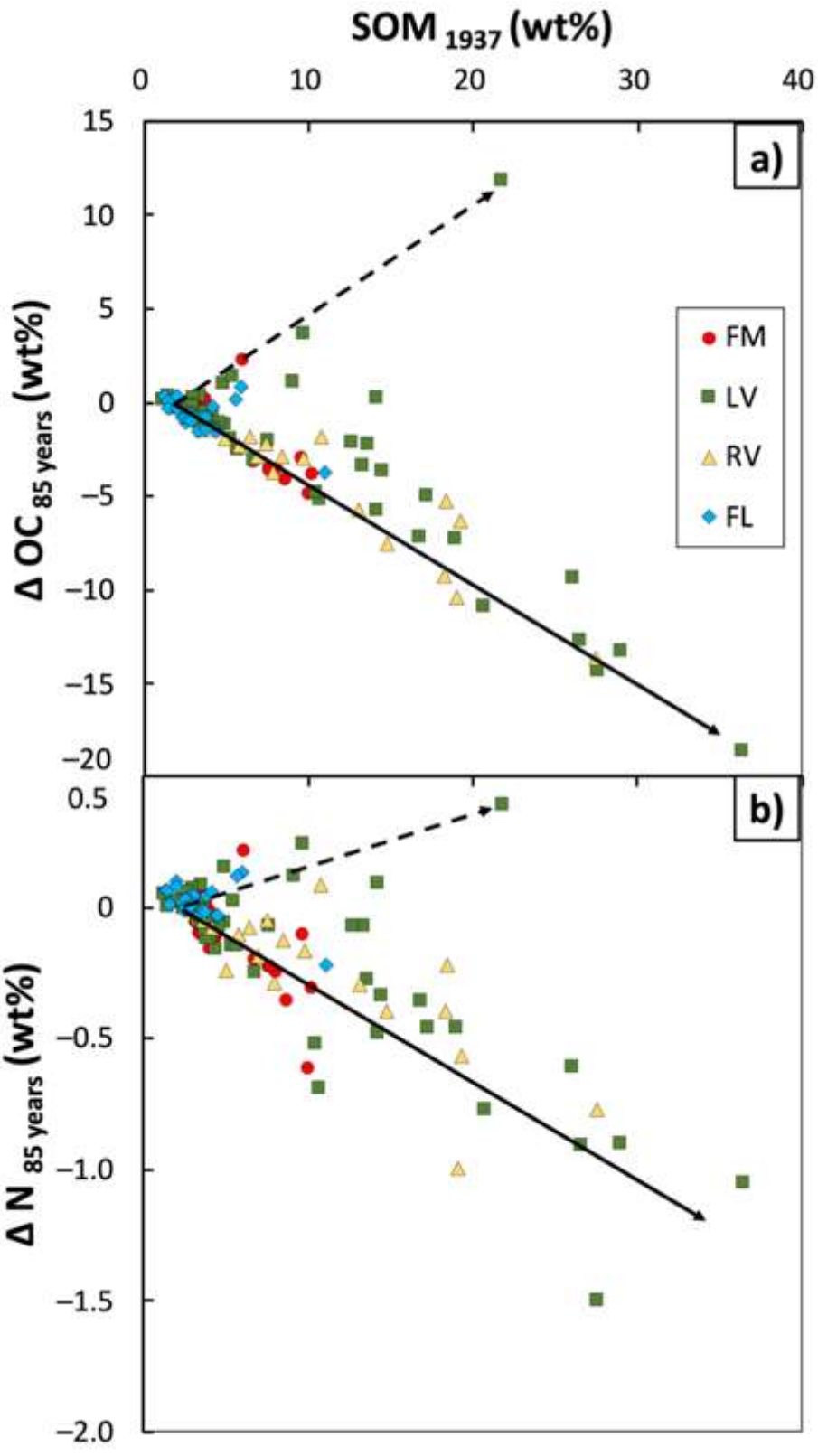


**Figure 25.** SOM concentrations of 1937 related to changes in OC (Δ OC) and N (ΔN) content after 85 years. Differences (Δ) of concentration of a) OC and b) N after 85 years. Arrows has have been placed to indicate the samples affected by SOM degradation (solid line) and SOM increase through fertilization.

To better understand how the C losses are influenced by the soil type, a map elaboration was carried out using the shapefile of the soil delineations provided by the Emilia-Romagna soil survey service (1:50,000 Soil map) and reported in Appendix 5. In the first map (Supplementary Figure B1a) each delineation is classified on the basis of the soil texture type (*i.e.*, clay, silty clay, silty clay loam, clay loam, loam, silt loam, sandy loam, loamy sand, and sand); the second map (Supplementary Figure B1b) describe for each delineation the average of $\Delta OC_{85\ years}$. The soil delineations that lost more than 5 wt% of OC in 85 years are in an area with a mix of fine granulometries (Silt Clay Loam) and salinized water, which are soil conditions that favor the SOM degradation. In fact, observing the Supplementary Table B3 and the Supplementary Figure B2 (a and b): "JOLANDA Silt Clay Loam, with mixed Organic Matter and mineral fraction / CANALE DEL SOLE Silt Clay Loam Complex (JOL2/CDS2)" and "JOLANDA Silty Clay Consociation (JOL1)" lost on average 6.84 and 5.47 wt% of OC in 85 years. On the contrary, "CANALE LEONE Silt Clay Loam Consociation (CLN1)" on average increase of 2.39 wt%, probably for the semi-humid (paddy rice) and high acidic conditions (pH 5) that preserve the SOM.

### 5.3.2 SOC stocks and GHGs loss

The calculated present-day (year 2022) and in 1937 SOC stock for each district, as well as the difference between the two years ($\Delta$ SOCstock $_{85\ years}$) are reported in Table 5.

**Table 5.** Average SOC stocks calculated for each district in 2022 and 1937, and the differences of SOC stocks between the two years ($\Delta$ SOCstock $_{85\ years}$). The $CO_2$ eq emitted in 85 years was also reported ($\Delta$ $CO_2$ eq $_{85\ years}$).

| **District** | **SOCstock$_{2022}$** | **SOCstock$_{1937}$** | **$\Delta$ SOCstock $_{85\ years}$** | **$\Delta$ $CO_2$ eq $_{85\ years}$** |
|---|---|---|---|---|
| | **(Mg ha$^{-1}$)** | **(Mg ha$^{-1}$)** | **(Mg ha$^{-1}$)** | **(Mg ha$^{-1}$)** |
| **FM** | 54 | 117 | –63 | 231 |
| **LV** | 95 | 198 | –103 | 376 |
| **RV** | 77 | 247 | –169 | 621 |
| **FL** | 61 | 122 | –61 | 224 |
| **Ferrara province** | 70 | 158 | –88 | 324 |

SOC stocks were especially reduced in RV (–169 Mg OC ha$^{-1}$) and in LV (–103 Mg OC ha$^{-1}$) and in smaller proportions in FM (–63 Mg OC ha$^{-1}$) and in FL (–61 Mg OC ha$^{-1}$), with an average for the entire area of –88 Mg OC ha$^{-1}$. This corresponds to $CO_2$ emitted in

85 years ranging from 224 to 621 Mg $ha^{-1}$ (Table 5); the spatial distribution of the released $CO_2$ is also described in the map presented in Figure 26. Topsoils that suffered the highest OC loss with time are located in the reclaimed wetland of RV and LV areas. As observed in Figures 24 and 25, the topsoils that suffered the highest OC loss with time, and in turn released most of the $CO_2$, are located in the reclaimed wetland of RV and LV areas. In these districts the effects of land use change by wetland reclamation, and intensive agriculture, increased SOM decomposition and oxidation. However, in some northern localities of LV district, where high OC contents still persists at present-days (according to map of Figure 24b), the $CO_2$ emissions after 85 years were comparatively low, probably because they have been seasonally flooded for the rice cultivation. In fact, anaerobic conditions induced by water saturation, slow down organic matter decomposition, and promote the SOC accumulation (Wu, 2011; Liu et al., 2021). A modest $\Delta CO_2$ eq $_{85\ years}$ (< 200 Mg $ha^{-1}$) occurred in northern lands of LV (in presence of rice cultivations), and similarly, in FM and FL districts as these areas have been poor in SOM since 1937, and released less GHGs in 85 years than the districts with peatlands (Figure 26). In fact, a sizeable loss of $CO_2$ eq (up to > 1200 Mg $ha^{-1}$) occurred especially on soils within the reclaimed lands of RV and LV and at the border between FM and RV. Here the mineralization of high amount of SOM was due to farming, encouraged by the high fertility of these soils.

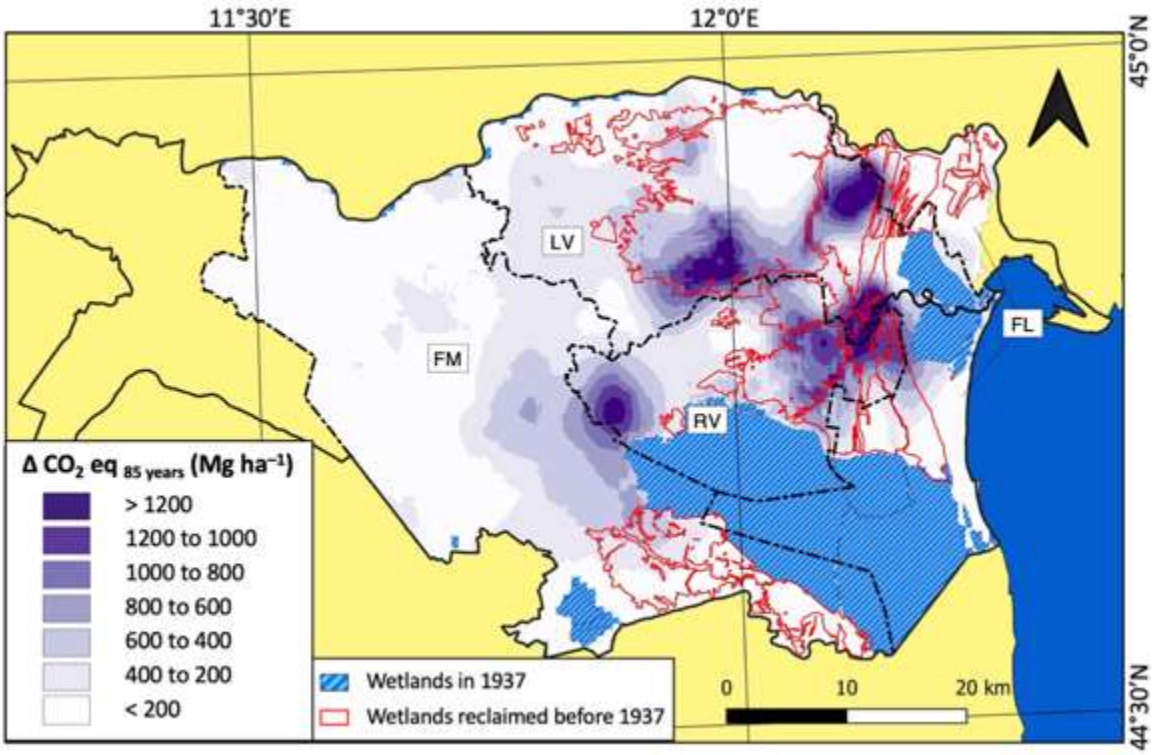


**Figure 26.** Estimated equivalent $CO_2$ ($\Delta$ $CO_2$ eq) released in the atmosphere from 1937. Each pixel has dimension of 100 x 100m.

### 5.3.3 $\delta^{13}C$ spatial distribution in Ferrara province

Using the isotopic data from 2022, we reconstructed the C isotopic ratio for the soils in the Ferrara province (Figure 27). The C isotopic ratio can be used to discern soil carbon fractions, with the IC fraction characterized by values around 0‰, and the OC by more negative isotopic ratios varying according to the photosynthetic pathways of the vegetation form which the OM was derived, from those of $C_4$ (−9‰ to −20‰) to those of $C_3$ (−20 to −37‰) (O'Leary, 1988; Kohn, 2010). Literature data on soil OC isotopic ratio in the Ferrara province that ranges from −21 to −29 ‰ (Brombin et al., 2020; Natali et al., 2018b, 2021; Salani et al., 2021) indicating a preponderance of $C_3$ plant derived OM. Moreover, a thorough investigation on the SOM dynamics in these soils by Natali et al. (2018b) revealed that the original OC isotopic ratio can be affected the decomposition process and could produce a shift toward less negative isotopic $\delta^{13}C$ values. SOM decomposition would be minimized either by the amount of clay fraction (Smith and Chalk, 2021) or by the soil water saturation acting as protection from oxidation and bacterial activity. In fact, according to Figure 27, the most negative values of $\delta^{13}C$ were measured in the easternmost part of the province, in the RL and LV districts, which lay below the sea level and is used for rice paddy production nowadays. These soils derived from the land reclamation of marshes and swamps, had the highest OC measured (Figure

24b). These soils lay below the sea level and were deposited in marshes and swamps environments before the land reclamation and used as paddy soils up nowadays.

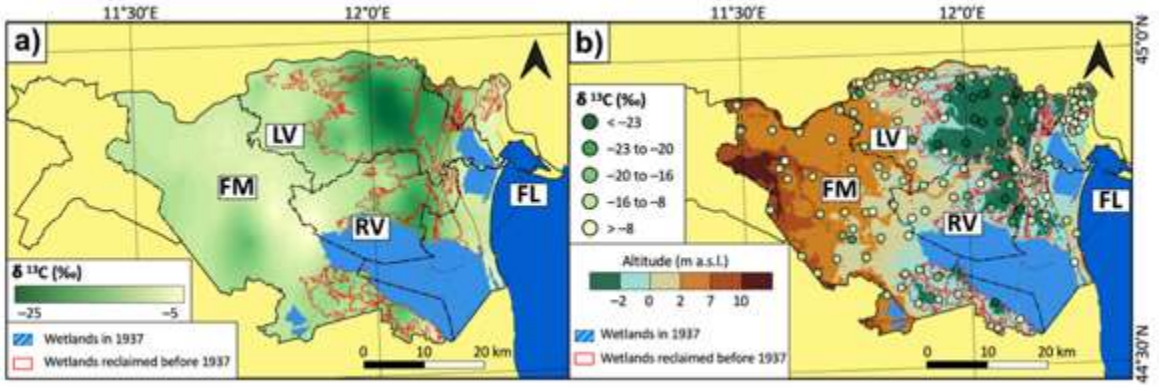


**Figure 27.** Distribution of the $^{13}C$ isotopic signature of the topsoils in the Ferrara province in 2022 represented as a) isoscape and b) compared with the altitude.

The distribution of OC content *vs* $\delta^{13}C$ are plotted in Figure 28. In the figure two sample groups are evident: one is characterized by the lowest OC contents associated to isotopic ratios near to 0‰, representative of the samples collected from the FM and FL districts. The other is characterized by the highest OC concentrations (> 20 wt%) and the most negative $\delta^{13}C$ values (–26.6‰), representative of the samples collected from the LV district. Samples from the LV region included reclaimed marshes and swamps, with many samples having more than 5wt% OC and $\delta^{13}C$ values less than –25.5 ‰. Natali et al. (2018b and 2021; Figure 28). On the contrary, the least negative C isotopic values (close to 0‰) indicate soils with low OC content, where IC fraction is the most abundant C fraction, which is instead typical of high-energy alluvial (*e.g.*, paleo-channel) and coastal (*e.g.*, sand dunes) depositional environments (Salani et al., 2021).

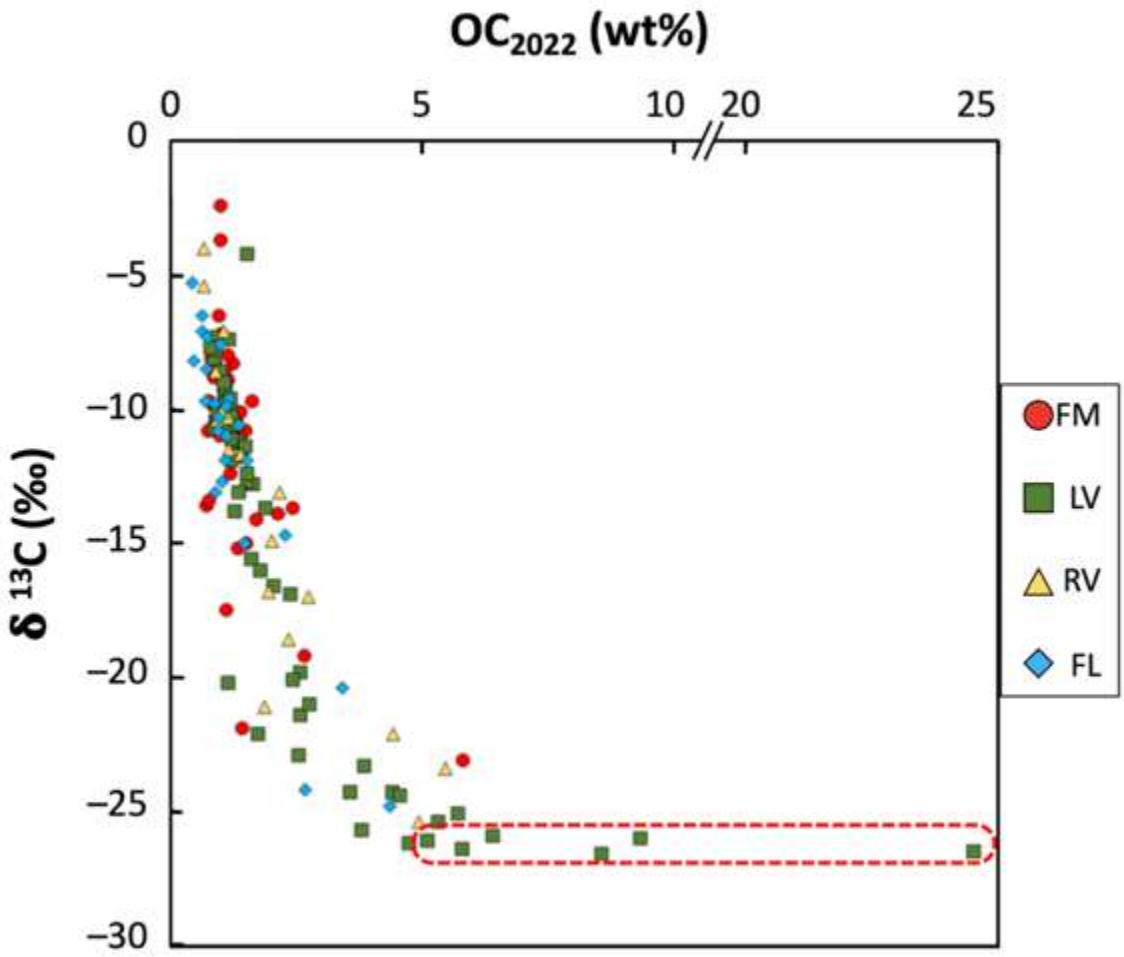


**Figure 28.** Scatterplot of the complete soil dataset between OC and $\delta^{13}C$. Red dashed field clustered peatlands of the Ferrara province (Natali et al., 2018b; 2021).

The relationships between the soil carbon isotopic composition and the depositional processes identified by Salani et al. (2021) are reinforced by Figure 27b, in which sampling points with less negative $\delta^{13}C$ values are related to relatively high-altitude areas typical of paleo-channel, whereas samples with more negative $\delta^{13}C$ values are located in the lowest altitude areas in the proximity of interfluvial basins. In summary, use of soil $\delta^{13}C$ is an opportunity to evaluate net and gross C changes in carbon stocks over a long time scales. In particular, shifts in $\delta^{13}C$ signatures can be an useful tool to understand the residence time of C in soils (Smith and Chalk, 2021).

## 5.4 Conclusions

This work analyzes the degradation of soil organic matter (SOM) during a very long period and after a massive land-use land-cover-change from wetlands to croplands. In particular, it estimates the loss of SOM and the associated release of $CO_2$ in the Ferrara province during the last century due to the effects of LULCC and the conventional agriculture, by comparing past (1937) and modern (2022) soil OC to measurements. Only the peaty soil in northern zones of the Ferrara province are still characterized by high OC contents, but they also are high emitters of $CO_2$ due to production that have prevailed over 85 years. This work demonstrated that OC content inventories are useful to estimate the SOC stock loss after several years and to calculate the amount of $CO_2$ eq released in the atmosphere. Moreover, the isotopic present-day $\delta^{13}C$ signature can be used to verify if LULCC has caused a shift in isotopic signature of SOC stocks (Figure 29). Research like this is useful to demonstrate to farmers the negative effects of unsustainable agricultural practices with which future generations will have to deal. Therefore, the adoption of best-practices such as no- or minimum-tillage, reduction of the tillage in organic farming, burying crop residues deeper, restoring degraded soils and increasing biodiversity, should be promoted to farmers, as these practices are still not widespread adopted in Italy. This is particularly urgent in nowadays, considering the prediction of 7.4% decline in the SOC stock on agricultural soils by 2100 due to the climate change (Mondini et al., 2012). Agricultural sustainable practices would the increase of soil fertility, restore degraded soils and increasing biodiversity, and will play a significant role in the mitigation of climate change, reducing the greenhouse gas emission.

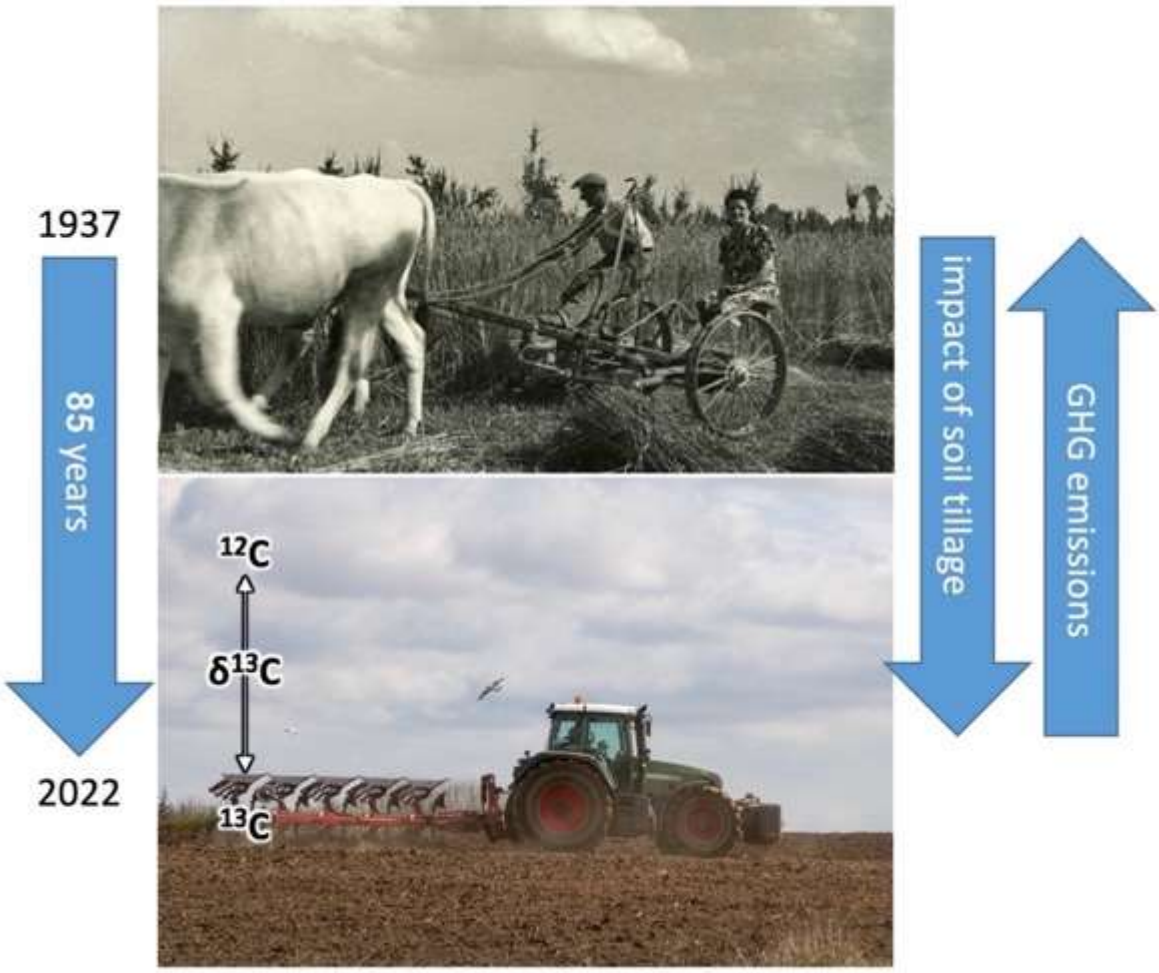


**Figure 29.** Unsustainable tillage practices over a long period can cause unconstrained GHG emissions and SOC stock shifts which can be verified observing $\delta^{13}C$ signatures variations.

Appendix 5

Figures:

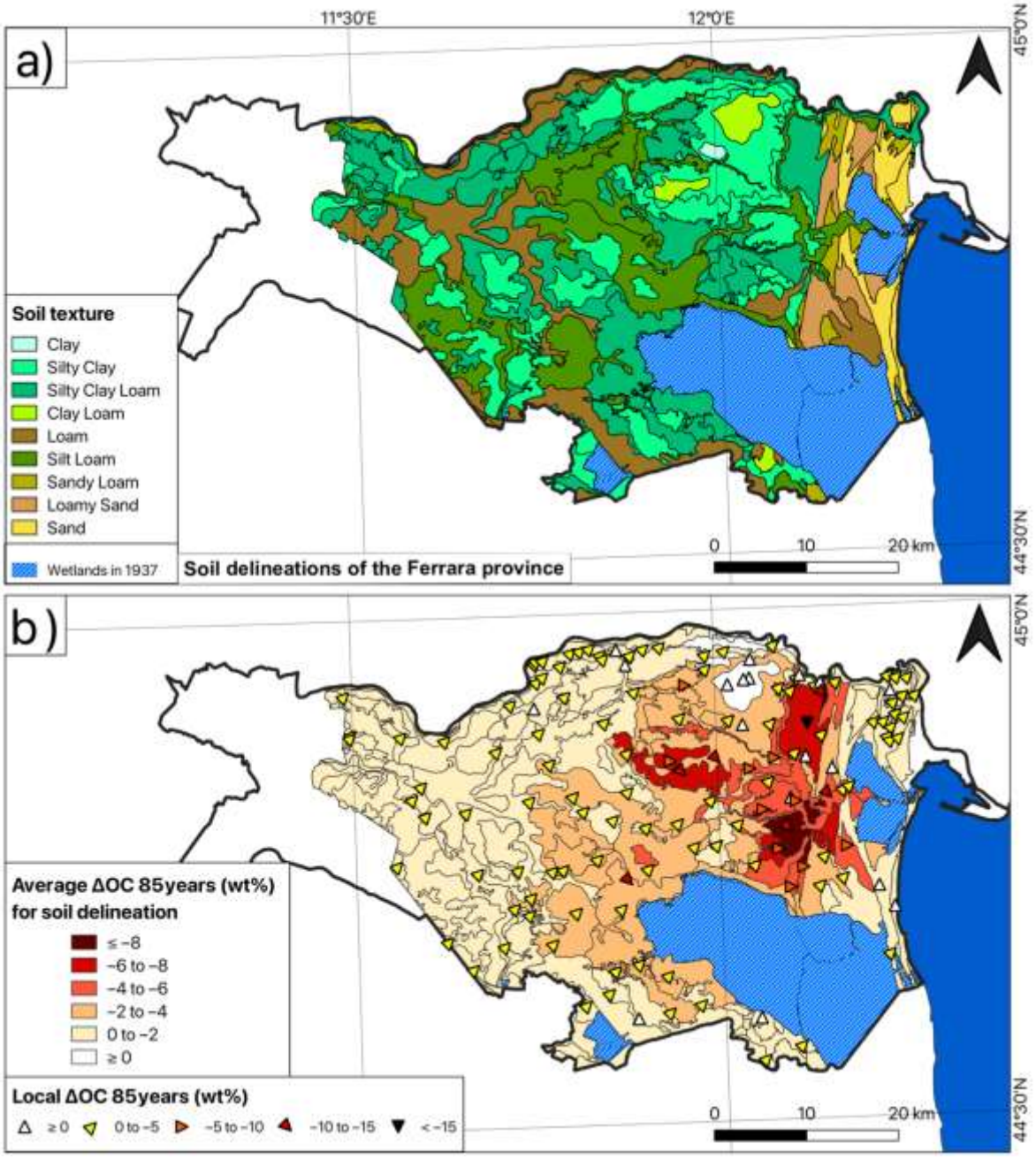


**Supplementary Figure B1.** Soil delineations (1:50,000) of the Ferrara Province (Emilia-Romagna soil survey service): a) Texture; b) Averaged ΔOC (wt%) after 85 years calculated using statistical geoprocessing on raster files of 1937 and 2022 OC distribution (for each investigated soil, local Δ OC are also reported).

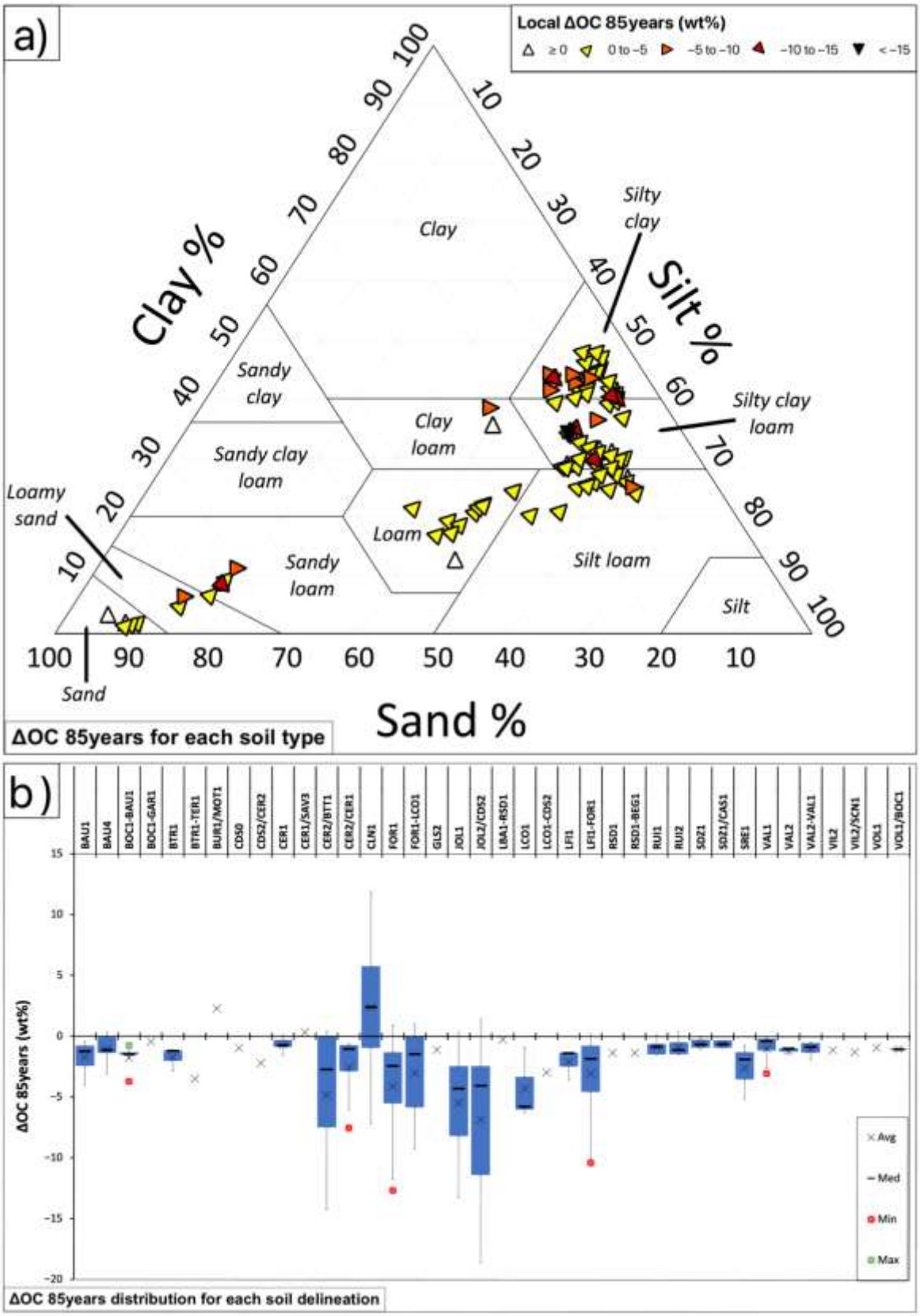


**Supplementary Figure B2.** ΔOC after 85 (wt%): a) observed in function of the soil texture type of each investigated location; b) box-plot distributions for each soil delineation.

Tables:

**Supplementary Table B1.** The complete dataset of the soil samples investigated in 1937 by Ferrari et al. The districts reported are: i) central municipalities of the Ferrara province (FM), ii) leftward Po di Volano reclamation (LV), iii) rightward Po di Volano reclamation (RV), and iv) littoral of the Ferrara province (FL).

| Sample | District | Latitude | Longitude | N (wt%) | TC (wt%) | OC (wt%) | IC (wt%) |
|---|---|---|---|---|---|---|---|
| 158 | FM | 44.889125 | 11.498803 | 0.18 | 3.43 | 2.35 | 1.08 |
| 157 | FM | 44.886261 | 11.497686 | 0.20 | 3.22 | 2.26 | 0.96 |
| 180 a | FM | 44.824150 | 11.580890 | 0.15 | 3.87 | 1.86 | 2.02 |
| 215 | FM | 44.809752 | 11.654369 | 0.20 | 3.04 | 2.20 | 0.84 |
| 185 | FM | 44.807420 | 11.598400 | 0.15 | 3.78 | 2.04 | 1.74 |
| 238 a | FM | 44.798139 | 11.855923 | 0.17 | 3.97 | 2.03 | 1.94 |
| 236 a | FM | 44.807510 | 11.815753 | 0.18 | 3.42 | 2.33 | 1.09 |
| 233 a | FM | 44.822186 | 11.801964 | 0.20 | 3.36 | 2.33 | 1.03 |
| 241 | FM | 44.819049 | 11.741971 | 0.15 | 3.29 | 2.09 | 1.20 |
| 203 | FM | 44.885429 | 11.757781 | 0.18 | 3.44 | 2.18 | 1.26 |
| 187 | FM | 44.868268 | 11.698416 | 0.17 | 3.38 | 2.24 | 1.14 |
| 197 a | FM | 44.750012 | 11.668228 | 0.20 | 3.96 | 1.97 | 1.99 |
| 168 | FM | 44.880632 | 11.627875 | 0.15 | 3.15 | 2.13 | 1.02 |
| 191 | FM | 44.885613 | 11.567477 | 0.16 | 3.72 | 2.22 | 1.50 |
| 167 a | FM | 44.926666 | 11.490126 | 0.22 | 3.44 | 2.33 | 1.10 |
| 209 | FM | 44.836480 | 11.593620 | 0.11 | 3.79 | 1.75 | 2.04 |
| 223 | FM | 44.759310 | 11.557540 | 0.16 | 3.52 | 2.08 | 1.44 |
| 245 a | FM | 44.751795 | 11.723265 | 0.21 | 3.15 | 2.20 | 0.95 |
| 334 | FM | 44.749850 | 11.770686 | 0.34 | 4.66 | 4.42 | 0.24 |
| 248 | FM | 44.751210 | 11.785584 | 0.39 | 5.45 | 5.03 | 0.42 |
| 289 | FM | 44.724757 | 11.740191 | 0.40 | 4.83 | 4.67 | 0.16 |
| 312 | FM | 44.708938 | 11.801655 | 0.30 | 4.44 | 3.90 | 0.54 |
| 347 | FM | 44.710978 | 11.863649 | 0.68 | 5.84 | 5.80 | 0.04 |
| 332 | FM | 44.678744 | 11.768149 | 0.15 | 2.54 | 1.94 | 0.60 |
| 386 | FM | 44.650605 | 11.852853 | 0.32 | 4.71 | 4.44 | 0.26 |
| 391 | FM | 44.656401 | 11.885351 | 0.48 | 6.24 | 5.94 | 0.30 |
| 502 | FM | 44.708054 | 11.737525 | 0.24 | 2.68 | 2.26 | 0.42 |
| 508 | FM | 44.714816 | 11.717215 | 0.23 | 2.81 | 2.51 | 0.30 |
| 570 | FM | 44.677751 | 11.701990 | 0.19 | 2.17 | 2.11 | 0.06 |
| 524 | FM | 44.656496 | 11.658208 | 0.27 | 4.63 | 2.59 | 2.04 |
| 405 a | FM | 44.683956 | 11.624367 | 0.20 | 4.14 | 2.39 | 1.75 |
| 425 | FM | 44.608345 | 11.925477 | 0.30 | 3.63 | 2.31 | 1.32 |
| 605 | FM | 44.615300 | 11.969137 | 0.22 | 4.23 | 2.01 | 2.22 |
| 652 | FM | 44.559522 | 12.054107 | 0.15 | 3.72 | 1.71 | 2.02 |
| 622 | FM | 44.572060 | 12.104472 | 0.16 | 3.97 | 1.86 | 2.11 |
| 639 | FM | 44.600067 | 12.049003 | 0.24 | 5.19 | 3.50 | 1.69 |
| 586 | FM | 44.644199 | 11.924477 | 0.39 | 6.91 | 5.59 | 1.31 |
| 458 | FM | 44.617752 | 11.810665 | 0.22 | 3.84 | 2.16 | 1.68 |
| 564 | FM | 44.602977 | 11.880437 | 0.21 | 4.35 | 2.19 | 2.16 |
| 445 | FM | 44.628828 | 11.843292 | 0.29 | 3.84 | 2.40 | 1.44 |
| 182 | FM | 44.913801 | 11.719727 | 0.24 | 5.19 | 2.49 | 2.70 |
| 1011 | LV | 44.909010 | 11.750479 | 0.11 | 3.28 | 1.21 | 2.07 |
| 990 a | LV | 44.952901 | 11.754979 | 0.17 | 3.39 | 1.97 | 1.42 |
| 1012 | LV | 44.955863 | 11.756856 | 0.23 | 3.36 | 2.13 | 1.23 |

| Sample | District | Latitude | Longitude | N (wt%) | TC (wt%) | OC (wt%) | IC (wt%) |
|---|---|---|---|---|---|---|---|
| 1013 | LV | 44.935234 | 11.756671 | 0.14 | 3.35 | 1.94 | 1.41 |
| 1015 | LV | 44.940094 | 11.765371 | 0.13 | 3.34 | 1.66 | 1.68 |
| 1010 | LV | 44.956149 | 11.766471 | 0.07 | 2.96 | 1.10 | 1.86 |
| 1006 | LV | 44.950383 | 11.790166 | 0.15 | 3.41 | 1.73 | 1.68 |
| 999 | LV | 44.962704 | 11.804413 | 0.12 | 2.76 | 1.38 | 1.38 |
| 997 | LV | 44.964251 | 11.817555 | 0.11 | 2.82 | 1.14 | 1.68 |
| 996 | LV | 44.966157 | 11.830376 | 0.16 | 2.84 | 2.00 | 0.84 |
| 992 | LV | 44.959594 | 11.845096 | 0.12 | 2.19 | 1.59 | 0.60 |
| 994 | LV | 44.955863 | 11.849034 | 0.22 | 3.47 | 2.03 | 1.44 |
| 656 | LV | 44.963626 | 11.866070 | 0.17 | 3.58 | 2.02 | 1.56 |
| 657 | LV | 44.948752 | 11.878066 | 0.06 | 1.96 | 0.70 | 1.26 |
| 661 | LV | 44.958293 | 11.886557 | 0.17 | 3.55 | 2.05 | 1.50 |
| 664 | LV | 44.964185 | 11.904519 | 0.17 | 3.27 | 1.89 | 1.38 |
| 656 a | LV | 44.965709 | 11.927102 | 0.16 | 3.26 | 1.97 | 1.28 |
| 658 a | LV | 44.956331 | 11.989441 | 0.25 | 3.55 | 2.85 | 0.70 |
| 668 | LV | 44.959590 | 12.015996 | 0.31 | 4.03 | 2.41 | 1.62 |
| 670 | LV | 44.950136 | 12.049881 | 0.15 | 3.65 | 1.73 | 1.92 |
| 682 | LV | 44.963720 | 12.083993 | 0.13 | 2.30 | 1.46 | 0.84 |
| 928 | LV | 44.825024 | 11.876928 | 0.15 | 2.74 | 1.60 | 1.14 |
| 920 a | LV | 44.789672 | 11.900814 | 0.18 | 3.26 | 2.24 | 1.02 |
| 869 | LV | 44.920106 | 11.794804 | 0.34 | 4.50 | 3.90 | 0.60 |
| 835 | LV | 44.893408 | 11.848129 | 0.25 | 4.04 | 3.29 | 0.74 |
| 830 | LV | 44.922566 | 11.890490 | 0.29 | 3.99 | 3.09 | 0.90 |
| 852 | LV | 44.926989 | 11.959315 | 0.71 | 8.46 | 8.22 | 0.24 |
| 849 | LV | 44.942559 | 11.989174 | 0.51 | 7.97 | 7.37 | 0.60 |
| 945 a | LV | 44.926154 | 12.017818 | 0.38 | 5.74 | 5.63 | 0.12 |
| 892 | LV | 44.854939 | 11.771370 | 0.17 | 3.94 | 2.26 | 1.68 |
| 914 | LV | 44.862692 | 11.877883 | 0.31 | 4.44 | 4.38 | 0.06 |
| 957 att. | LV | 44.853481 | 11.935913 | 0.79 | 11.00 | 10.97 | 0.03 |
| 962 att. | LV | 44.842861 | 11.950548 | 0.86 | 12.01 | 12.01 | 0.00 |
| 969 | LV | 44.895680 | 11.951527 | 0.17 | 2.79 | 2.22 | 0.57 |
| 949 | LV | 44.854644 | 11.998364 | 1.06 | 16.84 | 16.81 | 0.03 |
| 790 | LV | 44.914953 | 12.147985 | 1.15 | 15.39 | 15.39 | 0.00 |
| 694 | LV | 44.918489 | 12.105491 | 0.77 | 8.19 | 7.89 | 0.30 |
| 696 | LV | 44.922047 | 12.089885 | 0.23 | 3.10 | 2.68 | 0.42 |
| 944 att. | LV | 44.931930 | 12.048026 | 0.39 | 5.39 | 5.27 | 0.12 |
| 986 | LV | 44.930597 | 12.040108 | 1.10 | 12.64 | 12.64 | 0.00 |
| 699 a | LV | 44.874768 | 12.146296 | 0.40 | 7.72 | 7.71 | 0.00 |
| 776 | LV | 44.885761 | 12.125902 | 1.29 | 21.14 | 21.14 | 0.01 |
| 815 | LV | 44.887086 | 12.076348 | 0.72 | 8.38 | 8.38 | 0.00 |
| 692 a | LV | 44.886649 | 12.036640 | 0.60 | 8.28 | 8.24 | 0.05 |
| 965 att. | LV | 44.892269 | 12.019184 | 0.76 | 10.02 | 9.99 | 0.03 |
| 696 a | LV | 44.843461 | 12.045211 | 0.62 | 9.74 | 9.74 | 0.00 |
| 816 | LV | 44.853376 | 12.078876 | 1.08 | 15.10 | 15.10 | 0.00 |
| 732 | LV | 44.857767 | 12.108506 | 0.66 | 6.19 | 6.07 | 0.12 |
| 757 | LV | 44.853980 | 12.121955 | 0.39 | 4.36 | 3.16 | 1.20 |
| 739 | LV | 44.841676 | 12.157641 | 0.12 | 1.64 | 0.86 | 0.78 |
| 728 | LV | 44.814015 | 12.099344 | 0.21 | 4.08 | 2.82 | 1.26 |
| 726 | LV | 44.810490 | 12.106870 | 0.81 | 6.51 | 6.18 | 0.32 |
| 723 | LV | 44.816580 | 12.150140 | 1.68 | 16.04 | 15.99 | 0.05 |

| Sample | District | Latitude | Longitude | N (wt%) | TC (wt%) | OC (wt%) | IC (wt%) |
|---|---|---|---|---|---|---|---|
| 725 | LV | 44.820880 | 12.172965 | 0.31 | 3.60 | 2.52 | 1.08 |
| 733 | LV | 44.824098 | 12.181888 | 0.23 | 3.71 | 2.33 | 1.38 |
| 1216 | RV | 44.760181 | 11.832940 | 0.33 | 4.96 | 4.00 | 0.96 |
| 1183 | RV | 44.738442 | 11.872246 | 1.04 | 12.00 | 11.04 | 0.96 |
| 1234 | RV | 44.749169 | 11.901934 | 0.40 | 5.18 | 4.58 | 0.60 |
| 1130 a | RV | 44.792586 | 11.944757 | 0.26 | 4.54 | 3.36 | 1.18 |
| 1149 | RV | 44.814220 | 11.991167 | 0.36 | 3.84 | 2.88 | 0.96 |
| 1137 | RV | 44.769392 | 11.966501 | 0.21 | 4.15 | 2.38 | 1.77 |
| 1140 | RV | 44.770426 | 11.997239 | 0.30 | 4.92 | 3.75 | 1.17 |
| 1091 | RV | 44.790004 | 12.027398 | 0.14 | 3.17 | 2.08 | 1.09 |
| 1075 | RV | 44.803146 | 12.060869 | 0.56 | 11.36 | 10.64 | 0.72 |
| 1044 | RV | 44.830924 | 12.071213 | 0.34 | 7.47 | 6.24 | 1.23 |
| 1277 | RV | 44.749861 | 12.049242 | 0.45 | 6.37 | 5.65 | 0.72 |
| 1119 | RV | 44.764202 | 12.080905 | 1.02 | 11.20 | 11.19 | 0.00 |
| 1115 | RV | 44.785149 | 12.093580 | 0.99 | 15.96 | 15.96 | 0.00 |
| 1041 | RV | 44.745881 | 12.114071 | 0.63 | 13.01 | 10.70 | 2.31 |
| 1035 | RV | 44.756279 | 12.144506 | 0.32 | 6.36 | 4.88 | 1.47 |
| 1023 a | RV | 44.765108 | 12.174620 | 0.50 | 8.69 | 8.58 | 0.11 |
| 1163 | RV | 44.726499 | 12.095818 | 0.46 | 9.81 | 7.60 | 2.21 |
| 1026 | RV | 44.735004 | 12.169465 | 0.25 | 6.00 | 4.34 | 1.66 |
| 1389 | FL | 44.930938 | 12.114850 | 0.49 | 6.45 | 6.39 | 0.05 |
| 1391 | FL | 44.933274 | 12.117352 | 0.25 | 4.75 | 3.45 | 1.31 |
| 1489 | FL | 44.923399 | 12.140089 | 0.14 | 3.29 | 2.18 | 1.11 |
| 1488 | FL | 44.925728 | 12.145545 | 0.21 | 3.88 | 3.25 | 0.63 |
| 1497 | FL | 44.925816 | 12.168057 | 0.17 | 3.57 | 2.42 | 1.15 |
| 1427 | FL | 44.930087 | 12.239994 | 0.16 | 3.81 | 2.59 | 1.23 |
| 1424 | FL | 44.928440 | 12.251839 | 0.08 | 2.35 | 1.51 | 0.83 |
| 1396 | FL | 44.927807 | 12.266598 | 0.08 | 1.80 | 1.32 | 0.48 |
| 1437 | FL | 44.915298 | 12.241501 | 0.08 | 1.83 | 1.16 | 0.67 |
| 1413 | FL | 44.910016 | 12.260015 | 0.08 | 2.58 | 1.80 | 0.78 |
| 1407 | FL | 44.910149 | 12.276879 | 0.18 | 3.59 | 2.58 | 1.01 |
| 1463 | FL | 44.903524 | 12.246444 | 0.17 | 3.07 | 2.09 | 0.98 |
| 1443 | FL | 44.892475 | 12.249402 | 0.03 | 2.08 | 1.48 | 0.60 |
| 1446 | FL | 44.889116 | 12.260430 | 0.08 | 1.92 | 1.37 | 0.55 |
| 1479 | FL | 44.885729 | 12.219166 | 0.03 | 1.91 | 1.16 | 0.75 |
| 1455 | FL | 44.885478 | 12.232096 | 0.09 | 2.63 | 1.71 | 0.93 |
| 1451 | FL | 44.879393 | 12.242479 | 0.08 | 2.97 | 1.95 | 1.02 |
| 1475 | FL | 44.870443 | 12.236581 | 0.10 | 2.72 | 2.16 | 0.56 |
| 1474 | FL | 44.866690 | 12.240187 | 0.09 | 2.56 | 1.66 | 0.90 |
| 1453 | FL | 44.869002 | 12.251907 | 0.09 | 2.07 | 1.47 | 0.60 |
| 1296 | FL | 44.728023 | 12.137467 | 0.09 | 1.76 | 1.65 | 0.11 |
| 1374 | FL | 44.725712 | 12.216481 | 0.03 | 1.40 | 0.85 | 0.54 |
| 1362 | FL | 44.704669 | 12.237037 | 0.02 | 1.64 | 0.75 | 0.89 |
| 1387 | FL | 44.659236 | 12.229865 | 0.05 | 1.84 | 0.88 | 0.96 |

**Supplementary Table B2.** The complete analytical dataset, including the C and N elemental and isotopic analyses of soil sampled in 2022. The districts reported are: i) central municipalities of the Ferrara province (FM), ii) leftward Po di Volano reclamation (LV), iii) rightward Po di Volano reclamation (RV), and iv) littoral of the Ferrara province (FL).

| Sample | Disticts | Latitude | Longitude | TC (wt%) | OC (wt%) | IC (wt%) | N (wt%) | $\delta^{13}C$ (‰) |
|---|---|---|---|---|---|---|---|---|
| VP5 | FM | 44.889125 | 11.498803 | 2.77 | 1.41 | 1.36 | 0.16 | –11.8 |
| VP6 | FM | 44.886261 | 11.497686 | 2.73 | 1.29 | 1.44 | 0.16 | –10.3 |
| F10 | FM | 44.824150 | 11.580890 | 2.73 | 1.62 | 1.29 | 0.16 | –9.7 |
| F13 | FM | 44.809752 | 11.654369 | 2.13 | 0.89 | 1.24 | 0.12 | –10.3 |
| F6 | FM | 44.807420 | 11.598400 | 2.91 | 0.71 | 1.28 | 0.20 | –13.6 |
| FE10 | FM | 44.798139 | 11.855923 | 2.22 | 0.92 | 1.81 | 0.07 | –8.6 |
| FE11 | FM | 44.807510 | 11.815753 | 2.31 | 1.14 | 1.32 | 0.10 | –8.9 |
| FE12 | FM | 44.822186 | 11.801964 | 2.18 | 0.81 | 1.68 | 0.10 | –8.1 |
| FE13 | FM | 44.819049 | 11.741971 | 2.22 | 1.14 | 1.51 | 0.08 | –8.0 |
| FE15 | FM | 44.885429 | 11.757781 | 2.46 | 0.91 | 1.15 | 0.14 | –10.6 |
| FE17 | FM | 44.868268 | 11.698416 | 2.49 | 1.01 | 1.36 | 0.11 | –7.2 |
| FE2 | FM | 44.750012 | 11.668228 | 1.98 | 1.23 | 1.50 | 0.10 | –8.3 |
| FE22 | FM | 44.880632 | 11.627875 | 2.66 | 1.36 | 0.95 | 0.15 | –10.7 |
| FE25 | FM | 44.885613 | 11.567477 | 2.06 | 0.74 | 1.47 | 0.11 | –10.8 |
| FE29 | FM | 44.926666 | 11.490126 | 2.37 | 0.86 | 1.46 | 0.13 | –9.9 |
| FE4 | FM | 44.836480 | 11.593620 | 2.72 | 0.85 | 1.33 | 0.11 | –7.7 |
| FE7 | FM | 44.759310 | 11.557540 | 2.31 | 0.76 | 1.46 | 0.19 | –13.4 |
| BA1 | FM | 44.751795 | 11.723265 | 2.13 | 1.50 | 0.63 | 0.11 | –15.0 |
| BA2 | FM | 44.749850 | 11.770686 | 2.61 | 0.89 | 1.72 | 0.11 | –8.3 |
| BA3 | FM | 44.751210 | 11.785584 | 2.82 | 0.98 | 1.84 | 0.03 | –2.4 |
| BA7 | FM | 44.724757 | 11.740191 | 2.48 | 1.18 | 1.30 | 0.15 | –12.4 |
| BA8 | FM | 44.708938 | 11.801655 | 1.80 | 0.76 | 1.04 | 0.10 | –9.7 |
| BA9 | FM | 44.710978 | 11.863649 | 2.60 | 0.99 | 1.61 | 0.06 | –3.7 |
| BA10 | FM | 44.678744 | 11.768149 | 2.16 | 0.97 | 1.18 | 0.11 | –11.0 |
| BA11 | FM | 44.650605 | 11.852853 | 2.45 | 0.86 | 1.59 | 0.09 | –8.8 |
| BA12 | FM | 44.656401 | 11.885351 | 3.58 | 2.13 | 1.45 | 0.17 | –13.9 |
| AR16 | FM | 44.708054 | 11.737525 | 1.52 | 1.41 | 0.12 | 0.16 | –21.9 |
| AR17 | FM | 44.714816 | 11.717215 | 1.56 | 1.10 | 0.46 | 0.15 | –17.5 |
| AR19 | FM | 44.677751 | 11.701990 | 2.35 | 1.34 | 1.00 | 0.16 | –15.2 |
| AR23 | FM | 44.656496 | 11.658208 | 3.55 | 1.49 | 2.06 | 0.16 | –10.8 |
| AR26 | FM | 44.683956 | 11.624367 | 2.95 | 1.14 | 1.81 | 0.15 | –9.7 |
| AR30 | FM | 44.608345 | 11.925477 | 3.57 | 1.38 | 2.19 | 0.14 | –10.1 |
| AR32 | FM | 44.615300 | 11.969137 | 3.18 | 1.07 | 2.11 | 0.11 | –8.6 |
| AR34 | FM | 44.559522 | 12.054107 | 3.29 | 1.29 | 2.00 | 0.15 | –10.4 |
| AR36 | FM | 44.572060 | 12.104472 | 3.23 | 0.95 | 2.28 | 0.10 | –6.5 |
| AR38 | FM | 44.600067 | 12.049003 | 6.72 | 5.81 | 0.91 | 0.45 | –23.1 |
| AR41 | FM | 44.644199 | 11.924477 | 3.41 | 2.66 | 0.75 | 0.28 | –19.2 |
| AR42 | FM | 44.617752 | 11.810665 | 2.67 | 1.08 | 1.59 | 0.13 | –10.2 |
| AR6 | FM | 44.602977 | 11.880437 | 4.68 | 2.43 | 2.25 | 0.22 | –13.7 |
| AR8A | FM | 44.628828 | 11.843292 | 3.09 | 1.69 | 1.41 | 0.19 | –14.1 |
| LG1A | FM | 44.913801 | 11.719727 | 2.55 | 1.03 | 1.51 | 0.12 | –10.2 |
| LG3A | LV | 44.909010 | 11.750479 | 2.93 | 1.35 | 1.59 | 0.15 | –13.1 |
| LG2A | LV | 44.952901 | 11.754979 | 2.86 | 1.08 | 1.77 | 0.13 | –9.8 |
| LG4A | LV | 44.955863 | 11.756856 | 2.89 | 1.18 | 1.71 | 0.14 | –9.6 |
| LG6A | LV | 44.935234 | 11.756671 | 2.04 | 0.88 | 1.16 | 0.11 | –10.7 |
| LG5A | LV | 44.940094 | 11.765371 | 2.78 | 1.14 | 1.64 | 0.13 | –20.2 |

| Sample | Districts | Latitude | Longitude | TC (wt%) | OC (wt%) | IC (wt%) | N (wt%) | $\delta^{13}C$ (‰) |
|---|---|---|---|---|---|---|---|---|
| LG7A | LV | 44.956149 | 11.766471 | 2.56 | 0.79 | 1.77 | 0.09 | –7.7 |
| LG8A | LV | 44.950383 | 11.790166 | 2.91 | 1.52 | 1.38 | 0.16 | –12.4 |
| LG9A | LV | 44.962704 | 11.804413 | 2.26 | 1.06 | 1.20 | 0.11 | –9.0 |
| LG10A | LV | 44.964251 | 11.817555 | 2.61 | 1.09 | 1.52 | 0.13 | –9.2 |
| LG11A | LV | 44.966157 | 11.830376 | 2.68 | 1.06 | 1.61 | 0.13 | –10.5 |
| LG12A | LV | 44.959594 | 11.845096 | 2.96 | 1.48 | 1.48 | 0.17 | –11.4 |
| LG13A | LV | 44.955863 | 11.849034 | 2.80 | 1.52 | 1.29 | 0.19 | –12.7 |
| LG1B | LV | 44.963626 | 11.866070 | 3.39 | 2.38 | 1.01 | 0.26 | –16.9 |
| LG2B | LV | 44.948752 | 11.878066 | 2.81 | 0.92 | 1.89 | 0.11 | –7.3 |
| LG3B | LV | 44.958293 | 11.886557 | 2.83 | 1.60 | 1.23 | 0.19 | –15.6 |
| LG4B | LV | 44.964185 | 11.904519 | 2.51 | 1.07 | 1.45 | 0.12 | –9.4 |
| LG5B | LV | 44.965709 | 11.927102 | 3.10 | 1.36 | 1.74 | 0.16 | –11.3 |
| LG6B | LV | 44.956331 | 11.989441 | 3.21 | 1.73 | 1.48 | 0.19 | –22.1 |
| LG7B | LV | 44.959590 | 12.015996 | 3.46 | 1.88 | 1.58 | 0.21 | –13.7 |
| LG8B | LV | 44.950136 | 12.049881 | 3.38 | 2.05 | 1.34 | 0.22 | –16.6 |
| LG9B | LV | 44.963720 | 12.083993 | 3.29 | 1.30 | 1.98 | 0.16 | –10.6 |
| MC1 | LV | 44.825024 | 11.876928 | 2.42 | 1.21 | 1.21 | 0.16 | –11.1 |
| MC2 | LV | 44.789672 | 11.900814 | 2.25 | 0.92 | 1.33 | 0.13 | –10.2 |
| CJ1 | LV | 44.920106 | 11.794804 | 2.73 | 0.89 | 1.83 | 0.09 | –7.8 |
| CJ2 | LV | 44.893408 | 11.848129 | 2.53 | 0.85 | 1.68 | 0.10 | –8.1 |
| CJ3 | LV | 44.922566 | 11.890490 | 2.63 | 1.21 | 1.42 | 0.14 | –11.9 |
| CJ4 | LV | 44.926989 | 11.959315 | 2.75 | 2.54 | 0.20 | 0.23 | –22.9 |
| CJ5 | LV | 44.942559 | 11.989174 | 5.39 | 5.32 | 0.07 | 0.44 | –25.4 |
| CJ6 | LV | 44.926154 | 12.017818 | 9.49 | 9.35 | 0.15 | 0.62 | –26.0 |
| CJ7 | LV | 44.854939 | 11.771370 | 2.83 | 1.19 | 1.64 | 0.13 | –9.8 |
| CJ8 | LV | 44.862692 | 11.877883 | 3.00 | 2.43 | 0.58 | 0.24 | –20.1 |
| CJ9 | LV | 44.853481 | 11.935913 | 3.85 | 3.79 | 0.06 | 0.33 | –25.7 |
| CJ10 | LV | 44.842861 | 11.950548 | 2.78 | 1.15 | 1.63 | 0.09 | –7.4 |
| CJ11 | LV | 44.895680 | 11.951527 | 1.72 | 1.51 | 0.21 | 0.05 | –4.2 |
| CJ12 | LV | 44.854644 | 11.998364 | 3.75 | 3.57 | 0.18 | 0.16 | –24.3 |
| SG1A | LV | 44.914953 | 12.147985 | 3.32 | 2.75 | 0.58 | 0.24 | –21.0 |
| SG2A | LV | 44.918489 | 12.105491 | 5.96 | 5.72 | 0.24 | 0.49 | –25.1 |
| SG3A | LV | 44.922047 | 12.089885 | 3.08 | 1.63 | 1.45 | 0.16 | –12.8 |
| SG4A | LV | 44.931930 | 12.048026 | 6.55 | 6.41 | 0.14 | 0.51 | –25.9 |
| SG5A | LV | 44.930597 | 12.040108 | 24.64 | 24.52 | 0.12 | 1.49 | –26.5 |
| SG6A | LV | 44.874768 | 12.146296 | 4.61 | 4.41 | 0.20 | 0.33 | –24.3 |
| SG7A | LV | 44.885761 | 12.125902 | 2.97 | 2.57 | 0.40 | 0.24 | –21.4 |
| SG8A | LV | 44.887086 | 12.076348 | 4.78 | 4.74 | 0.04 | 0.38 | –26.2 |
| SG9A | LV | 44.886649 | 12.036640 | 8.68 | 8.57 | 0.11 | 0.69 | –26.6 |
| SG10A | LV | 44.892269 | 12.019184 | 5.17 | 5.10 | 0.07 | 0.30 | –26.1 |
| EM1A | LV | 44.843461 | 12.045211 | 3.34 | 2.58 | 0.76 | 0.26 | –19.8 |
| EM2A | LV | 44.853376 | 12.078876 | 5.88 | 5.80 | 0.08 | 0.47 | –26.4 |
| EM3A | LV | 44.857767 | 12.108506 | 2.64 | 1.31 | 1.33 | 0.14 | –11.2 |
| EM4A | LV | 44.853980 | 12.121955 | 4.77 | 4.55 | 0.22 | 0.41 | –24.4 |
| EM5A | LV | 44.841676 | 12.157641 | 2.29 | 1.27 | 1.02 | 0.12 | –13.8 |
| EM6A | LV | 44.814015 | 12.099344 | 4.26 | 3.85 | 0.42 | 0.36 | –23.3 |
| EM7A | LV | 44.810490 | 12.106870 | 2.72 | 1.05 | 1.67 | 0.12 | –9.1 |
| EM8A | LV | 44.816580 | 12.150140 | 2.58 | 1.78 | 0.80 | 0.18 | –16.0 |
| EM9A | LV | 44.820880 | 12.172965 | 2.81 | 1.20 | 1.60 | 0.15 | –10.2 |
| EM10A | LV | 44.824098 | 12.181888 | 2.65 | 0.98 | 1.67 | 0.11 | –8.6 |

| Sample | Districts | Latitude | Longitude | TC (wt%) | OC (wt%) | IC (wt%) | N (wt%) | $\delta^{13}C$ (‰) |
|---|---|---|---|---|---|---|---|---|
| BA4 | RV | 44.760181 | 11.832940 | 2.43 | 1.15 | 1.28 | 0.14 | –11.5 |
| BA5 | RV | 44.738442 | 11.872246 | 2.19 | 0.66 | 1.53 | 0.04 | –4.0 |
| BA6 | RV | 44.749169 | 11.901934 | 2.53 | 0.89 | 1.65 | 0.11 | –8.6 |
| MC3 | RV | 44.792586 | 11.944757 | 2.48 | 1.13 | 1.36 | 0.15 | –10.3 |
| MC4 | RV | 44.814220 | 11.991167 | 2.69 | 1.01 | 1.68 | 0.12 | –10.1 |
| MC5 | RV | 44.769392 | 11.966501 | 1.99 | 0.92 | 1.06 | 0.13 | –10.4 |
| MC6 | RV | 44.770426 | 11.997239 | 3.05 | 1.94 | 1.11 | 0.22 | –16.8 |
| MC7 | RV | 44.790004 | 12.027398 | 2.51 | 0.66 | 1.85 | 0.09 | –5.4 |
| MC8 | RV | 44.803146 | 12.060869 | 2.89 | 1.38 | 1.51 | 0.16 | –11.7 |
| MC9 | RV | 44.830924 | 12.071213 | 4.96 | 4.42 | 0.54 | 0.42 | –22.1 |
| MC10 | RV | 44.749861 | 12.049242 | 4.02 | 2.74 | 1.28 | 0.28 | –17.0 |
| MC11 | RV | 44.764202 | 12.080905 | 5.11 | 4.93 | 0.17 | 0.45 | –25.4 |
| MC12 | RV | 44.785149 | 12.093580 | 3.20 | 2.35 | 0.85 | 0.22 | –18.6 |
| GN1AS | RV | 44.745881 | 12.114071 | 6.02 | 5.46 | 0.56 | 0.41 | –23.4 |
| GN1BS | RV | 44.756279 | 12.144506 | 3.15 | 2.02 | 1.14 | 0.19 | –14.9 |
| GN1CS | RV | 44.765108 | 12.174620 | 2.91 | 1.05 | 1.85 | 0.10 | –7.1 |
| GN2AS | RV | 44.726499 | 12.095818 | 2.06 | 1.86 | 0.20 | 0.16 | –21.1 |
| GN2CS | RV | 44.735004 | 12.169465 | 3.66 | 2.16 | 1.50 | 0.20 | –13.1 |
| LG10B | FL | 44.930938 | 12.114850 | 2.80 | 2.68 | 0.11 | 0.27 | –24.2 |
| LG11B | FL | 44.933274 | 12.117352 | 4.46 | 4.35 | 0.12 | 0.38 | –24.8 |
| LG12B | FL | 44.923399 | 12.140089 | 2.61 | 1.47 | 1.14 | 0.18 | –15.0 |
| LG13B | FL | 44.925728 | 12.145545 | 4.31 | 3.42 | 0.90 | 0.33 | –20.4 |
| LG14B | FL | 44.925816 | 12.168057 | 3.70 | 2.27 | 1.43 | 0.23 | –14.7 |
| LG1C | FL | 44.930087 | 12.239994 | 2.55 | 1.10 | 1.45 | 0.13 | –9.9 |
| LG2C | FL | 44.928440 | 12.251839 | 2.32 | 0.87 | 1.45 | 0.11 | –9.8 |
| LG3C | FL | 44.927807 | 12.266598 | 1.96 | 0.96 | 1.01 | 0.10 | –10.3 |
| LG4C | FL | 44.915298 | 12.241501 | 2.99 | 1.52 | 1.47 | 0.18 | –11.9 |
| LG5C | FL | 44.910016 | 12.260015 | 1.83 | 1.02 | 0.81 | 0.12 | –12.7 |
| LG6C | FL | 44.910149 | 12.276879 | 2.82 | 1.15 | 1.67 | 0.14 | –9.6 |
| LG7C | FL | 44.903524 | 12.246444 | 2.96 | 1.35 | 1.62 | 0.16 | –10.6 |
| LG8C | FL | 44.892475 | 12.249402 | 1.20 | 0.46 | 0.74 | 0.06 | –8.2 |
| LG9C | FL | 44.889116 | 12.260430 | 1.56 | 0.63 | 0.93 | 0.07 | –6.5 |
| LG10C | FL | 44.885729 | 12.219166 | 1.58 | 0.89 | 0.68 | 0.11 | –13.1 |
| LG11C | FL | 44.885478 | 12.232096 | 2.58 | 0.98 | 1.60 | 0.10 | –7.6 |
| LG12C | FL | 44.879393 | 12.242479 | 1.38 | 0.42 | 0.95 | 0.05 | –5.3 |
| LG13C | FL | 44.870443 | 12.236581 | 2.15 | 0.72 | 1.42 | 0.08 | –7.3 |
| LG14C | FL | 44.866690 | 12.240187 | 1.58 | 0.69 | 0.89 | 0.09 | –9.7 |
| LG15C | FL | 44.869002 | 12.251907 | 1.79 | 0.71 | 1.08 | 0.08 | –8.5 |
| GN2BS | FL | 44.728023 | 12.137467 | 1.84 | 1.08 | 0.77 | 0.13 | –11.9 |
| GN2DS | FL | 44.725712 | 12.216481 | 1.87 | 0.94 | 0.94 | 0.09 | –10.8 |
| GN2ES | FL | 44.704669 | 12.237037 | 2.50 | 1.11 | 1.39 | 0.08 | –11.0 |
| GN3DS | FL | 44.659236 | 12.229865 | 1.75 | 0.62 | 1.12 | 0.06 | –7.1 |

**Supplementary Table B3.** Soil delineations (1:50,000) of the investigated locations in the Ferrara Province (Emilia-Romagna soil survey service) and the averaged ΔOC (wt%) after 85 years.

| Soil Delineation | Description | Average Δ OC 85years (wt%) |
|---|---|---|
| **BAU1** | BAURA Silt Clay Loam Consociation | –1.70 |
| **BAU4** | BAURA Silt Loam Consociation | –1.04 |
| **BOC1-BAU1** | BOCCALEONE Silt Loam Silt - BAURA Clay Loam Association | –1.75 |
| **BOC1-GAR1** | BOCCALEONE Silt Loam Silt - Garusola Sandy Loam Association | –0.42 |
| **BTR1** | BORGO TREBBI Silt Clay Consociation | –1.72 |
| **BTR1-TER1** | BORGO TREBBI Silt Clay - TERZANA Clay Association | –3.49 |
| **BUR1/MOT1** | BURANO fine Sandy Loam / MOTTALUNGA fine Sandy Loam Complex | 2.31 |
| **CDS0** | CANALE DEL SOLE Consociation | –0.94 |
| **CDS2/CER2** | CANALE DEL SOLE Silt Clay Loam / CERBA fine Sandy Loam Complex | –2.18 |
| **CER1** | CERBA fine Sand Consociation | –0.70 |
| **CER1/SAV3** | CERBA fine Sand / SAN VITALE fine Sand "decapitati" Complex | 0.36 |
| **CER2/BTT1** | CERBA fine Sand Loam / BOSCHETTO Loam Complex | –4.80 |
| **CER2/CER1** | CERBA fine Sand Loam / CERBA fine Sand Complex | –2.54 |
| **CLN1** | CANALE LEONE Silt Clay Loam Consociation | 2.39 |
| **FOR1** | FORCELLO Silty Clay Consociation | –4.10 |
| **FOR1-LCO1** | FORCELLO - LE CONTANE Silty Clay Association | –2.99 |
| **GLS2** | GALISANO Silty Clay Consociation | –1.08 |

| Soil Delineation | Description | Average Δ OC 85years (wt%) |
|---|---|---|
| **JOL1** | JOLANDA Silty Clay Consociation | –5.47 |
| **JOL2/CDS2** | JOLANDA Silt Clay Loam, with mixed Organic Matter and mineral fraction / CANALE DEL SOLE Silt Clay Loam Complex | –6.84 |
| **LBA1-RSD1** | LA BOARIA / RISAIA DEL DUCA Silt Clay Association | –0.24 |
| **LCO1** | LE CONTANE Silty Clay Consociation | –4.30 |
| **LCO1-CDS2** | LE CONTANE Silty Clay - CANALE DEL SOLE Silt Clay Loam Association | –2.93 |
| **LFI1** | LA FIORANA Silt Loam Consociation | –2.08 |
| **LFI1-FOR1** | LA FIORANA Silt Loam - FORCELLO Silty Clay Association | –3.04 |
| **RSD1** | RISAIA DEL DUCA Silty Clay Consociation | –1.33 |
| **RSD1-BEG1** | RISAIA DEL DUCA Silty Clay - BERGAMASCA Clay Association | –1.32 |
| **RUI1** | Ruina Silty Clay Loam Consociation | –0.84 |
| **RUI2** | Ruina Silty Clay Loam Consociation, with peaty substrate (above the sea level) | –0.83 |
| **SDZ1** | STRADAZZA Loam Consociation | –0.58 |
| **SDZ1/CAS1** | STRADAZZA Loam / CASTELVETRO Complex, on flood areas | –0.62 |
| **SRE1** | STRADA REALE Silt Loam Consociation | –2.57 |
| **VAL1** | VALLONA Silt Clay Loam Consociation | –0.96 |
| **VAL2** | VALLONA Silty Clay Consociation, with thin solum | –1.13 |
| **VAL2-VAL1** | VALLONA Silty Clay, with thin solum - VALLONA Silt Clay Loam Association | –1.00 |
| **VIL2** | VILLALTA Loam Consociation | –1.10 |

| Soil Delineation | Description | Average Δ OC 85years (wt%) |
|---|---|---|
| **VIL2/SCN1** | VILLALTA Loam / ASCENSIONE Silt Loam Complex | –1.25 |
| **VOL1** | VOLANO Consociation | –0.90 |
| **VOL1/BOC1** | VOLANO Loam / BOCCALEONE Silt Loam Complex | –1.01 |

# 6. Accelerated SOM degradation in the peatlands of Mezzano Valley: a particular case

Enclosed:

Natali, C., Bianchini, G., Cremonini, S., SALANI, G.M., Vianello, G., Brombin, V., Ferrari, M., Vittori Antisari, L., 2021. Peat Soil Burning in the Mezzano Lowland (Po Plain, Italy): Triggering Mechanisms and Environmental Consequences. *Geohealth, 5*, e2021GH000444. https://doi.org/10.1029/2021GH000444.

## 6.1 Introduction

Peat soils are organic-rich sedimentary deposits that formed by the accumulation of biomass in water-saturated conditions. Peat bogs minimize organic matter decomposition and serve as important carbon reservoir worldwide (Belyea and Malmer, 2004; Natali et al., 2018b; Rein, 2015; Smith et al., 2004). Globally, peat soils contain one-third of the world's soil carbon; their carbon budget exceeds that of the forests and is comparable to that of the atmosphere (Joosten and Clarke, 2002).

Unfortunately, peat soils are episodically affected by burning, as soil organic matter (SOM) can fuel and sustain the burning process for a long time (Moreno et al., 2011; Rein, 2015). According to the literature, peat smoldering can reach maximum temperatures of 700°C that, although lower than that of flaming combustion (1,500–1,800°C, Rein, 2009; Rein et al., 2008), progressively degrades SOM (Kreye et al., 2011).

Several studies have indicated that peat burning is triggered by surface fires that progressively propagates downward in low oxygen conditions (Joosten and Clarke, 2002), as in the cases of peat fires in Indonesia (Boehm et al., 2001; Page et al., 2002; Usup et al., 2004) and Florida (Monroe et al., 2009; Watts and Kobziar, 2013). Noteworthy, these processes deserve particular attention, as they produce more greenhouse emissions than vegetation fires and become progressively frequent under drought conditions (Langmann and Heil, 2004). Considering that future climate change scenarios predict more frequent and severe drought events in many areas worldwide (IPCC, 2007), soil fires need to be better understood to manage and mitigate their detrimental effects (Abram et al., 2021), which can impact also the human health (Uda et al., 2019).

In Italy, peats (and associated soils) are mainly distributed in the north and were generated in alluvial basins from the late Würm (late Pleistocene) to the Holocene (Martinelli et al., 2015).

This paper presents a case study of peat burning in the Mezzano Lowland (ML; Figure 10; see Section 3.1.3), a reclaimed coastal wetland located in the easternmost Po Plain, which is located in northern Italy (Di Giuseppe et al., 2014a, 2014b). This area is renowned for peat burning since historical times (Cremonini et al., 2008; Martinelli et al., 2015), and is characterized by peat deposits exposed to the Mediterranean climate with frequent and persistent droughts (Marchina et al., 2017, 2019). To assess the effects of burning, we applied an analytical technique based on the distinctive thermal stability of the various carbon bearing-phases (Mörchen et al., 2019; Natali et al., 2020; Zethof et al., 2019, 2020) as well as isotope ratio mass spectrometry (Natali et al., 2018a). With the obtained results

we provide constraints on the effects of burning in the surrounding environment, evaluating the smoldering combustion effects on the local soil carbon stock.

## 6.2 Results

### 6.2.1 pH, Electrical Conductivity and Bulk Density

The physicochemical parameters of the soil horizons from the five investigated soil profiles are shown in Table 6. The pH values generally decreased with depth in all investigated profiles, but the F and NF profile trends (and average values) are characterized by significant differences. The pH of the NF profiles (TOR4 and TOR5) varied from 2.4 (TOR4, 2AC, 63–75 cm depth) to 7.6 (TOR5, Op, 22–30 cm depth), with average pH value of 5.5. The F profiles (TOR1–TOR3) displayed a comparable pH range, varying from 3.3 (TOR3, Cg, 70–90 cm depth) to 8.3 (TOR2, 3Cov, 43–65 cm depth), with an average of pH value of 6.6. A marked increase in pH characterized the horizons at intermediate depths (35–70 cm) of the F profiles, whereas a slight pH decrease was observed in the NF profiles at comparable depths. EC of the F profiles had an average of 8.1 dS $m^{-1}$ generally higher than what observed in NF profiles (average 5.3 dS $m^{-1}$). Noteworthy, EC in F profiles presented an inverse relationship with depth, with a general decrease in EC at depths of 35–70 cm. The BD of the F profiles was heterogeneous, varying between 0.51 and 1.19 g $cm^{-3}$, with the lowest values recorded between depths of 12 cm (TOR2, Acov, 12–38 cm depth) and 43 cm (TOR1, Bcov, 30–43 cm depth). The BD of the NF profiles (average 1 g $cm^{-3}$) generally increased with depth and was higher than that in the F profiles (average 0.8 g $cm^{-3}$) that showed the lowest values in the 30–70 cm depth range.

**Table 6.** Physicochemical Parameters, Carbon Fractions (and Isotope Composition) and Nitrogen of the Soil Profiles Variably Affected (TOR1, TOR2, TOR3) and Unaffected (TOR4, TOR5) by Peat Smoldering

| | | | | | | DIN19539 by SoliTOC Cube | | | | | EA | IRMS |
|---|---|---|---|---|---|---|---|---|---|---|---|---|
| **Profile** | **Horizon** | **Depth** | **pH** | **EC** | **BD** | **$TOC_{400}$** | **ROC** | **TIC** | **TOC** | **TC** | **TN** | **$\delta^{13}C_{TC}$** |
| | | cm | | (ms/cm) | ($g/cm^3$) | (wt%) | (wt%) | (wt%) | (wt%) | (wt%) | (wt%) | (‰) |
| **TOR 1** | Opov | 0-14 | 6.8 ± 0.7 | 1.1 ± 0.1 | 0.74 ± 0.07 | 23.59 ± 0.22 | 1.03 ± 0.24 | 0.24 ± 0.05 | 24.4 ± 0.03 | 24.64 ± 0.07 | 1.56 ± 0.04 | –26.7 ± 0.0 |
| | AB1ov | 14-17 | 7.4 ± 0.6 | 4.5 ± 0.7 | 0.97 ± 0.09 | 5.75 ± 0.30 | 3.60 ± 0.17 | 0.07 ± 0.00 | 6.28 ± 0.14 | 6.35 ± 0.14 | 1.41 ± 0.77 | –26.1 ± 0.0 |
| | Bcov | 17-30 | 7.9 ± 0.5 | 6.5 ± 0.5 | 0.58 ± 0.06 | 1.10 ± 0.13 | 1.22 ± 0.08 | 0.26 ± 0.05 | 2.23 ± 0.05 | 2.49 ± 0.00 | 0.72 ± 0.21 | –24.9 ± 0.2 |
| | 2BCcl | 30-43 | 7.9 ± 0.6 | 2.8 ± 0.2 | 0.60 ± 0.05 | 0.05 ± 0.01 | 0.01 ± 0.01 | 0.01 ± 0.00 | 0.07 ± 0.02 | 0.07 ± 0.02 | 0.02 ± 0.01 | –23.8 ± 1.4 |
| | 2Ccl | 43-65 | 7.8 ± 0.4 | 2.7 ± 0.3 | 1.01 ± 0.08 | 0.03 ± 0.02 | 0.01 ± 0.00 | 0.00 ± 0.00 | 0.05 ± 0.02 | 0.05 ± 0.02 | 0.01 ± 0.01 | –21.5 ± 1.9 |
| | 3Oecl | 65-73 | 5.7 ± 0.3 | 8.7 ± 0.9 | 0.88 ± 0.08 | 0.04 ± 0.01 | 0.01 ± 0.01 | 0.02 ± 0.01 | 0.06 ± 0.01 | 0.08 ± 0.01 | 0.02 ± 0.01 | –22.7 ± 2.4 |
| | 3Oipy | 73-84 | 3.5 ± 0.3 | 11.7 ± 0.8 | 0.69 ± 0.09 | 8.32 ± 0.55 | 2.36 ± 0.46 | 0.08 ± 0.04 | 10.17 ± 0.10 | 10.26 ± 0.06 | 0.67 ± 0.09 | –27.2 ± 0.2 |
| | 4Cg | 84-96+ | 5.9 ± 0.4 | 3.7 ± 0.4 | 1.15 ± 0.11 | 1.62 ± 0.08 | 1.07 ± 0.04 | 0.04 ± 0.01 | 2.66 ± 0.04 | 2.70 ± 0.04 | 0.23 ± 0.01 | –24.5 ± 0.1 |
| **TOR 2** | Opov | 0-12 | 6.9 ± 0.7 | - | 0.83 ± 0.09 | 14.93 ± 0.54 | 0.96 ± 0.12 | 0.58 ± 0.14 | 15.89 ± 0.51 | 16.47 ± 0.36 | 1.33 ± 0.04 | –25.7 ± 0.3 |
| | Acov | 12-38 | 8.1 ± 0.5 | 4.7 ± 0.5 | 0.51 ± 0.07 | 0.12 ± 0.02 | 0.21 ± 0.03 | 2.83 ± 0.03 | 0.36 ± 0.01 | 3.20 ± 0.02 | 0.07 ± 0.01 | –8.2 ± 0.0 |
| | 2Ckov | 38-48 | 8.2 ± 0.5 | 3.0 ± 0.1 | 1.03 ± 0.11 | 0.10 ± 0.01 | 0.31 ± 0.03 | 8.87 ± 0.00 | 0.44 ± 0.02 | 9.31 ± 0.02 | 0.09 ± 0.02 | –6.6 ± 0.2 |
| | 3Cov | 48-65 | 8.3 ± 0.4 | 3.8 ± 0.1 | 0.78 ± 0.04 | 0.18 ± 0.02 | 0.27 ± 0.04 | 0.87 ± 0.02 | 0.48 ± 0.06 | 1.34 ± 0.06 | 0.08 ± 0.01 | –13.1 ± 0.1 |
| | 4Oipy | 65-72 | 4.2 ± 0.3 | 5.5 ± 0.3 | 0.71 ± 0.06 | 22.14 ± 0.06 | 0.73 ± 0.15 | 0.10 ± 0.01 | 22.90 ± 0.10 | 23.1 ± 0.09 | 1.22 ± 0.11 | –26.6 ± 0.1 |
| | 4Cg | 72-90 | 4.9 ± 0.7 | 14.4 ± 0.9 | 1.02 ± 0.09 | 11.30 ± 0.18 | 1.03 ± 0.17 | 0.10 ± 0.01 | 12.15 ± 0.04 | 12.24 ± 0.04 | 0.64 ± 0.02 | –27.0 ± 0.2 |
| **TOR 3** | Opov | 0-28 | 7.2 ± 0.1 | 2.4 ± 0.2 | 0.71 ± 0.07 | 17.49 ± 0.19 | 0.95 ± 0.08 | 1.22 ± 0.13 | 18.35 ± 0.14 | 19.57 ± 0.05 | 1.17 ± 0.04 | –24.9 ± 0.0 |
| | Abov | 28-30 | 7.7 ± 0.4 | 2.2 ± 0.3 | 1.01 ± 0.11 | 2.66 ± 0.46 | 1.31 ± 0.08 | 0.53 ± 0.03 | 3.89 ± 0.43 | 4.42 ± 0.43 | 0.49 ± 0.04 | –24.3 ± 0.3 |
| | 2Bcov | 30-40 | 7.9 ± 0.6 | 2.1 ± 0.1 | 0.60 ± 0.05 | 0.32 ± 0.03 | 0.22 ± 0.03 | 0.54 ± 0.03 | 0.57 ± 0.06 | 1.10 ± 0.04 | 0.04 ± 0.01 | –19.8 ± 0.1 |
| | 2Cov | 40-50 | 7.9 ± 0.5 | 2.9 ± 0.3 | 0.93 ± 0.09 | 0.27 ± 0.02 | 0.26 ± 0.03 | 0.26 ± 0.02 | 0.57 ± 0.05 | 0.83 ± 0.03 | 0.05 ± 0.01 | –23.3 ± 0.2 |
| | 3Oipy | 50-70 | 5.2 ± 0.6 | 3.8 ± 0.4 | 0.70 ± 0.11 | 26.19 ± 0.40 | 0.68 ± 0.19 | 0.11 ± 0.00 | 26.86 ± 0.30 | 26.97 ± 0.30 | 1.41 ± 0.10 | –26.8 ± 0.1 |
| | 3Cg | 70-90 | 3.3 ± 0.2 | 13.8 ± 0.8 | 1.19 ± 0.21 | 8.60 ± 0.10 | 0.63 ± 0.14 | 0.08 ± 0.01 | 9.13 ± 0.05 | 9.21 ± 0.04 | 0.51 ± 0.07 | –26.6 ± 0.1 |
| **TOR 4** | Op1 | 0-12 | 7.0 ± 0.5 | 4.4 ± 0.3 | 0.76 ± 0.09 | 22.03 ± 0.38 | 0.80 ± 0.31 | 0.20 ± 0.03 | 23.08 ± 0.48 | 23.29 ± 0.49 | 1.32 ± 0.02 | –26.5 ± 0.2 |
| | Op2 | 10-25 | 7.1 ± 0.6 | 4.8 ± 0.4 | 0.80 ± 0.07 | 22.19 ± 0.60 | 1.00 ± 0.25 | 0.17 ± 0.01 | 23.23 ± 0.57 | 23.40 ± 0.56 | 1.28 ± 0.07 | –26.4 ± 0.2 |
| | Op3 | 25-38 | 7.0 ± 0.4 | 4.9 ± 0.3 | 0.94 ± 0.09 | 21.43 ± 0.64 | 1.19 ± 0.57 | 0.20 ± 0.03 | 22.80 ± 0.42 | 23.00 ± 0.40 | 1.26 ± 0.13 | –26.1 ± 0.1 |
| | Oi | 38-47 | 4.2 ± 0.2 | 9.0 ± 0.7 | 0.83 ± 0.07 | 23.82 ± 0.98 | 0.57 ± 0.16 | 0.10 ± 0.01 | 24.40 ± 0.96 | 24.51 ± 0.96 | 1.08 ± 0.22 | –26.5 ± 0.0 |
| | Cg | 47-54 | 3.5 ± 0.1 | 7.6 ± 0.4 | 1.09 ± 0.11 | 1.68 ± 0.08 | 0.38 ± 0.05 | 0.03 ± 0.00 | 2.00 ± 0.03 | 2.03 ± 0.03 | 0.21 ± 0.01 | –27.1 ± 0.1 |
| | 2Oi | 54-63 | 4.0 ± 0.3 | 15.0 ± 0.9 | 0.93 ± 0.09 | 32.52 ± 0.47 | 0.86 ± 0.32 | 0.07 ± 0.01 | 33.64 ± 0.51 | 33.71 ± 0.52 | 1.52 ± 0.09 | –27.3 ± 0.1 |
| | 2AC | 63-75 | 2.4 ± 0.2 | 17.0 ± 0.8 | 1.18 ± 0.11 | 13.11 ± 0.23 | 1.05 ± 0.13 | 0.04 ± 0.00 | 14.02 ± 0.11 | 14.06 ± 0.11 | 0.64 ± 0.00 | –26.3 ± 0.1 |
| | 2Cg | 75-85+ | 6.2 ± 0.4 | 10.6 ± 0.6 | 1.21 ± 0.17 | 2.39 ± 0.06 | 0.82 ± 0.06 | 0.04 ± 0.00 | 3.15 ± 0.04 | 3.19 ± 0.05 | 0.27 ± 0.02 | –23.0 ± 0.5 |

| Profile | Horizon | Depth | pH | EC | BD | DIN19539 by SoliTOC Cube | | | | | EA | IRMS |
|---|---|---|---|---|---|---|---|---|---|---|---|---|
| | | | | | | $TOC_{400}$ | ROC | TIC | TOC | TC | TN | $\delta^{13}C_{TC}$ |
| | | cm | | (ms/cm) | ($g/cm^3$) | (wt%) | (wt%) | (wt%) | (wt%) | (wt%) | (wt%) | (‰) |
| **TOR 5** | Ap | 0-22 | 7.2 ± 0.5 | 2.5 ± 0.1 | 0.84 ± 0.05 | 13.56 ± 0.44 | 0.96 ± 0.30 | 2.76 ± 0.12 | 14.78 ± 0.40 | 17.55 ± 0.34 | 1.00 ± 0.06 | –21.5 ± 0.1 |
| | Op | 22-30 | 7.6 ± 0.4 | 5.1 ± 0.2 | 0.98 ± 0.08 | 15.77 ± 0.66 | 1.27 ± 0.20 | 1.43 ± 0.22 | 17.08 ± 0.68 | 18.54 ± 0.49 | 1.08 ± 0.04 | –23.8 ± 0.4 |
| | Och | 30-36 | 6.5 ± 0.4 | 3.5 ± 0.1 | 1.01 ± 0.09 | 22.34 ± 0.17 | 0.80 ± 0.32 | 0.11 ± 0.01 | 23.35 ± 0.47 | 23.47 ± 0.49 | 1.31 ± 0.08 | –26.7 ± 0.1 |
| | Oi | 36-45 | 5.5 ± 0.7 | 7.6 ± 0.7 | 1.01 ± 0.10 | 22.15 ± 1.12 | 0.77 ± 0.03 | 0.11 ± 0.00 | 22.96 ± 1.14 | 23.07 ± 1.15 | 1.25 ± 0.05 | –27.5 ± 0.1 |
| | C | 45-60 | 3.6 ± 0.3 | 13.3 ± 0.1 | 1.27 ± 0.12 | 7.63 ± 0.11 | 0.56 ± 0.07 | 0.06 ± 0.01 | 8.27 ± 0.18 | 8.33 ± 0.17 | 0.48 ± 0.02 | –26.3 ± 0.2 |

### 6.2.2 Soil Carbon Pools on F and NF Profiles

Carbon speciation of the F and NF peat profiles was carried out in compliance with the DIN 19539 standard, where four carbon fractions were measured: TC, $TOC_{400}$, ROC, and TIC. The carbon speciation results are presented in Table 6 and Figures 30 and 31. The two-way ANOVA test showed that all the elemental and isotopic variables of F and NF samples were affected by both the profile and the depth of sampling ($p$-values < 0.0001).

TC of the NF peat profiles was determined to be generally higher than that of the F profiles.

The TC of the NF peat profiles equaled approximately 20–25 wt% from the surface down to a depth of 40 cm, diminished at the Cg and C horizons, and reached the maximum of 34 wt% in the Oi horizon of TOR4 at a depth of 54–63 cm.

The TC of the F peat profiles was comparable with that of the NF profiles in the shallow horizons (16– 25 wt%, down to a depth of 15 cm) and dramatically decreased (down to 0 wt% in some cases) at variable depths between 14–73 cm (TOR1), 12–65 cm (TOR2), 28–50 cm (TOR3). Profile TOR2 presented a notable exception, where the intermediate 2Ckov horizon (38–48 cm depth) was characterized by a TC reaching 9 wt%. The TC of the F profiles increased downward, with values up to 10 wt% at 73–84 cm in TOR1, 23 wt% at 65–72 cm in TOR2, and 27 wt% at a depth of 50–70 cm in TOR3.

The distribution of $TOC_{400}$ with depth was determined to be similar to that of TC, suggesting that most carbon in the investigated peat profiles belongs to the thermally labile organic pool. In the NF profiles, $TOC_{400}$ was on average 20 wt% down to a depth of 50 cm, decreasing in the Cg and 2Cg horizons in TOR4, and in the C horizon in TOR5. The relative amount of the $TOC_{400}$ fraction ($TOC_{400}$%) was always >75% of the TC along the NF profiles.

In the F profiles, the $TOC_{400}$ values (14–24 wt%) were comparable with those of the NF profiles in the shallower horizons down to a depth of 15 cm, dramatically decreasing (approaching zero) at depths between 14–73 cm (TOR1), 12–65 cm (TOR2), and 28–50 cm (TOR3). The deeper horizons of the F profiles were characterized by a marked increase in the $TOC_{400}$ values, varying from 8.3 wt% at 73–84 cm in TOR1, to 22 wt% at 65–72 cm in TOR2, and to 26 wt% at 50–70 cm in TOR3.

The ROC content was similar in the F and NF profiles in the shallow horizons, showing values around 1 wt%. A marked ROC decrease occurred in the lower horizons of the F profiles, where ROC reached approximately 0 wt% at 30–73 cm in TOR1, 0.2–0.3 wt% at 12–65 cm in TOR2, and 0.2–0.3 wt% at 30–50 cm in TOR3, followed by a variable ROC increase with depth.

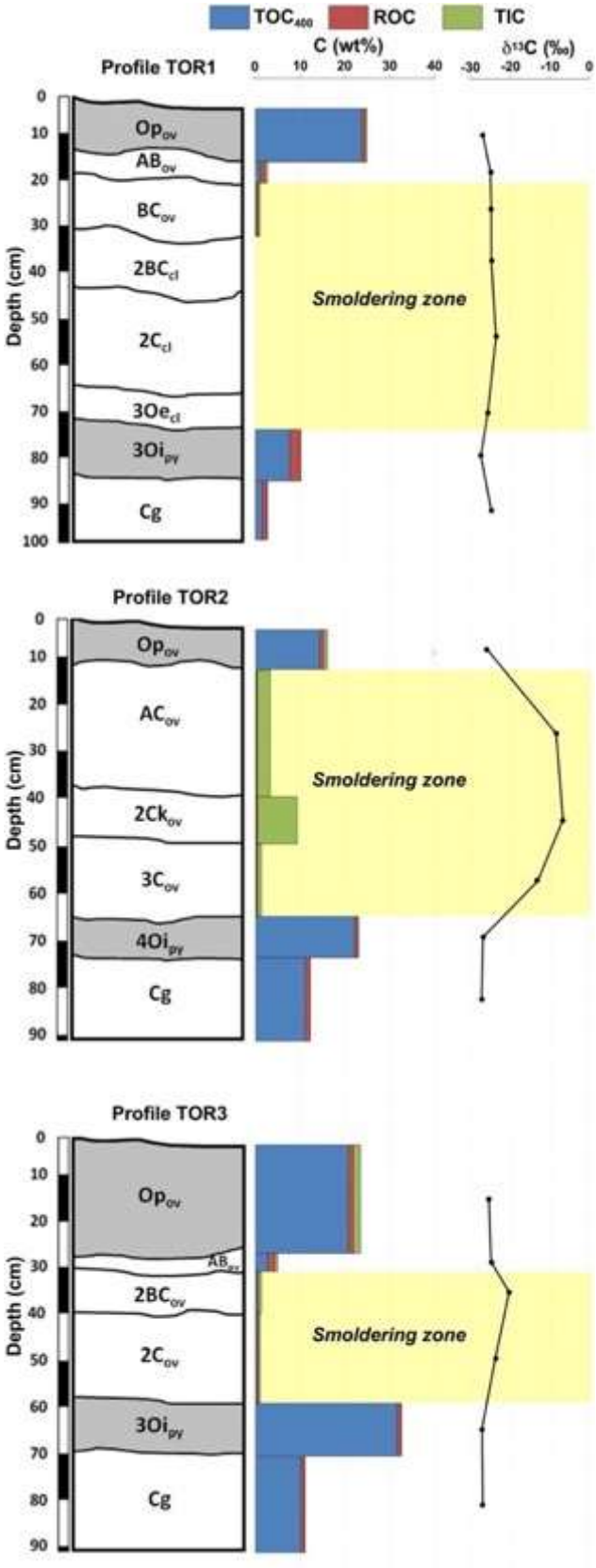


**Figure 30.** Carbon speciation of soil profiles variably affected by peat smoldering (TOR1, TOR2, TOR3). Histograms refer to the three soil carbon pools defined by the DIN 19539 standard ($TOC_{400}$, ROC, total inorganic carbon). The bulk carbon isotopic composition ($\delta^{13}C_{TC}$) is also reported. Note that the depth of the smoldering zone is indicated by the yellow box. See text for further details.

The TIC content varied from 2.8 wt% (TOR5) to 0.2 wt% (TOR2 and TOR4) in the superficial horizons and decreased with depth in both the F and NF profiles. The only exception was represented by the TOR1 profile, characterized by a TIC approaching zero in the intermediate horizons (30–73 cm depth), with a slight increase in the TIC values downward. The relative amount of TIC with respect to TC (TIC%) varied from 0% to 95%, with the highest values recorded in the intermediate horizons of the F profiles.

The bulk carbon Isotopic composition ($\delta^{13}C_{TC}$) of the NF horizons varied between −27.5‰ (TOR5, Oi, 36–45 cm depth) and −21.5‰ (TOR5, Ap, 0–25 cm depth).

A marked variation was observed in the $\delta^{13}C_{TC}$ of the F profiles, where $\delta^{13}C_{TC}$ changed from −27.2‰ (TOR1, 3Oipy, 73–84 cm depth) to −6.6‰ (TOR2, 2Ckov, 38–48 cm depth), with less negative values recorded in the intermediate horizons (Figures 30 and 31).

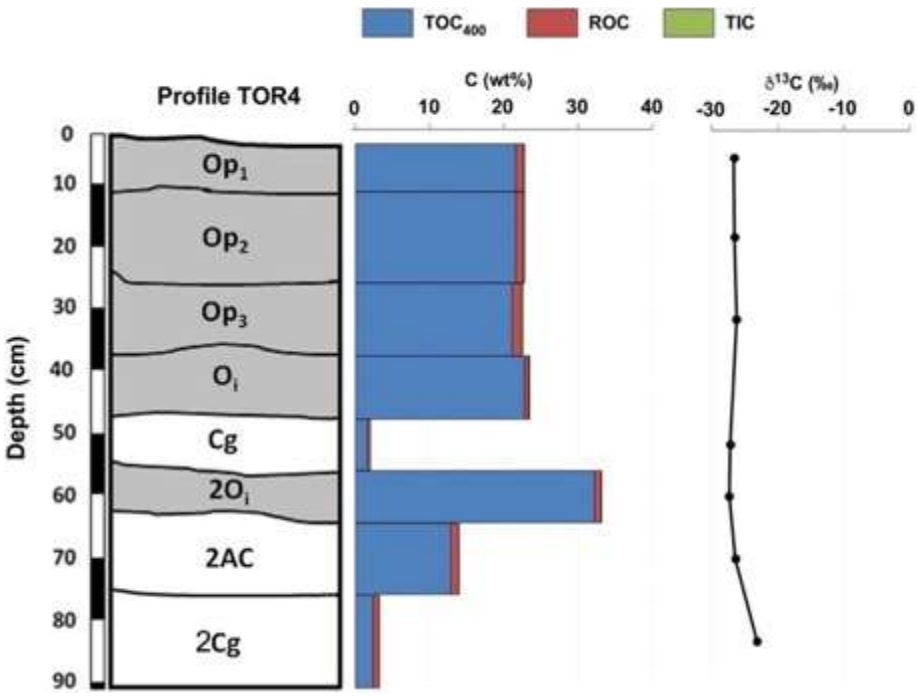


**Figure 31.** Carbon speciation in soil profile TOR4, taken as representative soil profile unaffected by peat smoldering. Histograms refer to the three soil carbon pools defined by the DIN 19539 standard ($TOC_{400}$, ROC, total inorganic carbon). The bulk carbon isotopic composition ($\delta^{13}C_{TC}$) is also reported.

A very good linear correlation between $\delta^{13}C_{TC}$ and TIC% ($r^2$= 0.9) confirmed that the bulk carbon isotopic value is directly related to the relative amount of a carbonate endmember.

The total nitrogen (TN) elemental content was also determined and varied from 1.56 wt% (TOR1, 0–14 cm depth) to 0.01 wt% (TOR1, 30–73 cm depth), showing a significant positive correlation with the TOC ($TOC_{400}$ + ROC) parameter.

Differences between F and NF soil profiles can be emphasized with a statistical elaboration of the available data, as shown in the PCA reported in Figure 32. The PCA is able to group the TOR profiles on the basis of many variables called principal components, which can describe correlations among the studied samples. We considered the $TOC_{400}$, ROC, TC, TIC, N and $\delta^{13}C$ as principal components and we focused the statistical analyses on horizons ranging from 30 to 70 cm where smoldering was effective. Noteworthy, the first and second PCA axes explained 74.6% and 20.3% of the variance, respectively. In the plot the NF profiles showed a clear grouping, which was driven by high content of organic carbon fractions ($TOC_{400}$, ROC, and TOC) and N. On the other hand, F profiles plot in opposite areas of the PCA diagram, reflecting lower content of organic carbon fractions and N.

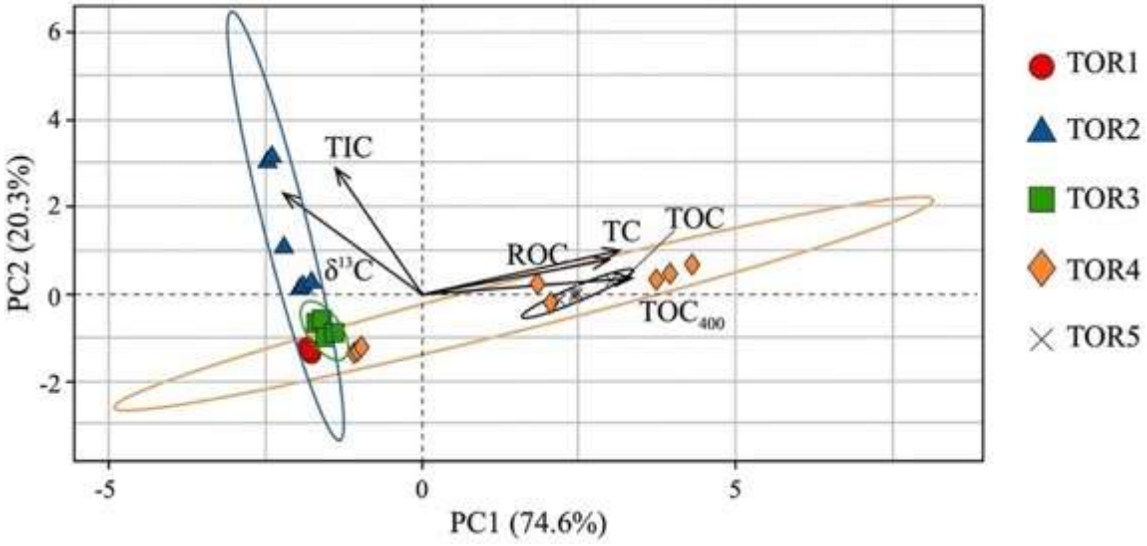


**Figure 32.** Principal component analysis of F and NF soil profiles.

### 6.2.3. Soil Carbon Pools of the Experimentally Fired Profiles

The results of carbon speciation of the experimentally fired soil horizons from the NF profile (TOR4) are presented in Table 7 and Figure 33.

**Table 7.** Carbon Fractions (and Isotope Composition) and Nitrogen of the experimentally fired horizons from soil profile TOR4. Analytical cross-check obtained analyzing the same samples with independent methods are reported in Supplementary Table C1 (see Appendix 6).

| | | | DIN 19539 | by SoliTOC Cube | | | | EA | IRMS |
|---|---|---|---|---|---|---|---|---|---|
| **Profile** | **Horizon** | **Depth** cm | **$TOC_{400}$** (wt%) | **ROC** (wt%) | **TIC** (wt%) | **TOC** (wt%) | **TC** (wt%) | **TN** (wt%) | **$\delta^{13}C_{tC_{exp}}$ (‰)** |
| **TOR4** | 25–38 | 105 | 21.83 ± 0.92 | 0.70 ± 0.01 | 0.19 ± 0.03 | 22.53 ± 0.91 | 22.73 ± 0.94 | 1.20 ± 0.01 | −25.9 ± 0.1 |
| | | 200 | 21.01 ± 0.44 | 1.39 ± 0.51 | 0.21 ± 0.02 | 22.40 ± 0.06 | 22.62 ± 0.06 | 1.30 ± 0.08 | −25.6 ± 0.1 |
| | | 400 | 0.56 ± 0.16 | 1.39 ± 0.14 | 0.26 ± 0.02 | 1.94 ± 0.02 | 2.21 ± 0.03 | 0.30 ± 0.00 | −21.4 ± 0.2 |
| | | 600 | 0.14 ± 0.08 | 0.24 ± 0.12 | 0.15 ± 0.02 | 0.40 ± 0.17 | 0.55 ± 0.15 | 0.02 ± 0.00 | −17.5 ± 0.3 |
| **TOR4** | 47–54 | 105 | 2.09 ± 0.10 | 0.37 ± 0.03 | 0.03 ± 0.00 | 2.46 ± 0.08 | 2.49 ± 0.08 | 0.22 ± 0.03 | −27.0 ± 0.2 |
| | | 200 | 1.83 ± 0.08 | 0.42 ± 0.03 | 0.03 ± 0.00 | 2.26 ± 0.10 | 2.28 ± 0.10 | 0.23 ± 0.02 | −27.0 ± 0.0 |
| | | 400 | 0.09 ± 0.00 | 0.18 ± 0.03 | 0.03 ± 0.00 | 0.27 ± 0.00 | 0.30 ± 0.00 | 0.12 ± 0.01 | −26.1 ± 0.2 |
| | | 600 | 0.04 ± 0.02 | 0.02 ± 0.02 | 0.01 ± 0.00 | 0.08 ± 0.01 | 0.08 ± 0.01 | 0.01 ± 0.01 | −26.6 ± 0.1 |
| **TOR4** | 63–75 | 105 | 11.03 ± 0.69 | 0.44 ± 0.15 | 0.06 ± 0.01 | 11.47 ± 0.58 | 11.54 ± 0.58 | 0.53 ± 0.01 | −26.2 ± 0.1 |
| | | 200 | 5.99 ± 0.09 | 0.73 ± 0.15 | 0.04 ± 0.00 | 6.73 ± 0.20 | 6.76 ± 0.20 | 0.45 ± 0.02 | −26.0 ± 0.1 |
| | | 400 | 0.08 ± 0.02 | 0.25 ± 0.02 | 0.04 ± 0.00 | 0.33 ± 0.00 | 0.37 ± 0.00 | 0.13 ± 0.00 | −24.7 ± 0.3 |
| | | 600 | 0.04 ± 0.03 | 0.01 ± 0.00 | 0.01 ± 0.00 | 0.06 ± 0.01 | 0.08 ± 0.01 | 0.02 ± 0.01 | −26.5 ± 0.3 |
| **TOR4** | 75–5+ | 105 | 1.96 ± 0.00 | 1.30 ± 0.08 | 0.04 ± 0.00 | 3.27 ± 0.08 | 3.31 ± 0.09 | 0.24 ± 0.01 | −21.4 ± 0.3 |
| | | 200 | 2.01 ± 0.03 | 1.11 ± 0.15 | 0.04 ± 0.00 | 3.12 ± 0.17 | 3.16 ± 0.17 | 0.26 ± 0.01 | −21.2 ± 0.4 |
| | | 400 | 0.14 ± 0.00 | 0.59 ± 0.03 | 0.05 ± 0.01 | 0.74 ± 0.03 | 0.79 ± 0.03 | 0.12 ± 0.01 | n.a. |
| | | 600 | 0.06 ± 0.04 | 0.02 ± 0.01 | 0.02 ± 0.00 | 0.10 ± 0.01 | 0.11 ± 0.01 | 0.02 ± 0.00 | −21.5 ± 0.3 |

Abbreviations: EA, elemental analyzer; IRMS, isotope ratio mass spectrometer; n.a., not analyzed; TC, total carbon; TIC, total inorganic carbon; TN, total nitrogen.

TC varied insignificantly in the samples heated to 200°C, except for horizon 2AC, where the TC content was reduced by 40% between 105°C and 200°C. A remarkable TC decrease was recorded in the samples heated to 400°C, and very little carbon was left in the samples after heating them to 600°C. The TC decrease with the increasing temperature was irrespective of the TC content in the untreated samples.

Regarding the carbon fractions, $TOC_{400}$ was the most abundant, and its relative contribution in the untreated samples varied from 93% (Op3) to approximately 75% (2Cg). $TOC_{400}$ did not exhibit any remarkable variation in the samples heated to 200°C, whereas it generally disappeared when the temperatures reached 400°C.

The relative contribution of ROC with respect to TC varied from approximately 5% (Op3) to 26% (2Cg) in the untreated samples. The behavior of ROC in response to thermal treatment was similar to that of $TOC_{400}$ in the samples heated to 200°C. A slight non-systematic variation of ROC was recorded in the samples heated to 400°C, and ROC disappeared when the temperature reached 600°C.

The TIC content remained nearly constant during all heating treatments for all samples and was best represented in the Op3 horizon, where it constituted 0.20 wt% and 0.15 wt% in the untreated and treated (heated to 600°C) samples, respectively.

The relative amount of inorganic carbon with respect to TC (TIC%) increased with increasing temperature, and the highest variations were recorded in the samples heated to 400°C and 600°C when the two organic fractions were exhausted. TIC% was less than 1% in the untreated samples and up to 26% in the samples heated to 600°C.

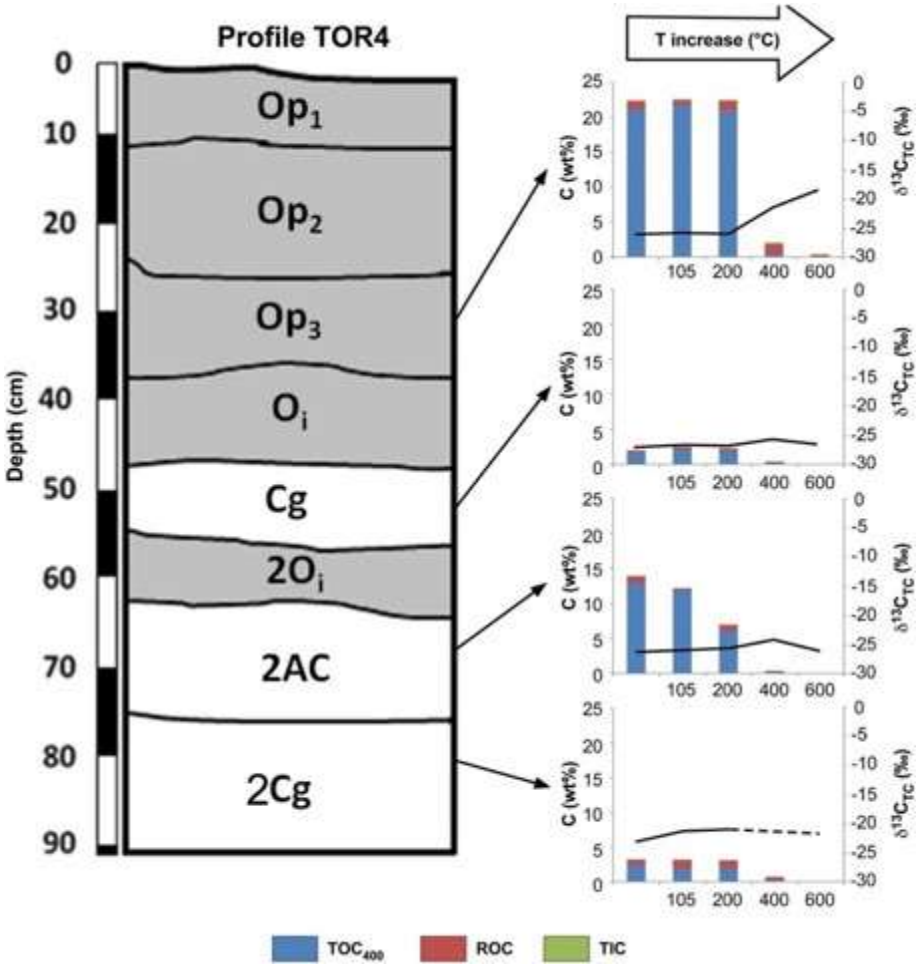


**Figure 33.** Carbon speciation of experimentally fired horizons from soil profile TOR4. Histograms refer to the three soil carbon pools defined by the DIN19539 standard ($TOC_{400}$, ROC, total inorganic carbon). The bulk carbon isotopic composition ($\delta^{13}C_{TC_{exp}}$) is also reported.

The carbon isotopic composition ($\delta^{13}C_{TC_{exp}}$) was less negative when the temperature increased. The greatest variation was recorded in the Op3 horizon, where $\delta^{13}C_{TC_{exp}}$ were −26.1‰ and −17.5‰ in the untreated and treated (heated to 600°C) samples, respectively. This variation is likely related to the loss of $TOC_{400}$ and increased TIC contribution to TC when the temperature escalated.

## 6.3 Discussion

### 6.3.1 Effects of Soil Burning in the Mezzano Lowland

The significant differences recorded in the physicochemical characteristics of the F and NF peaty soil profiles give insights on the magnitude of fire events in terms of their temperature, depth, and loss of carbon stock. The opposite trend of pH variation at depths of 14–73 cm (TOR1), 12–65 cm (TOR2), and 28–50 cm (TOR3) of the F with respect to the NF (TOR4 and TOR5) soil profiles suggests that burning modified the ML peaty soils at depth. The observed increase in pH in the F profiles at the intermediate depths mentioned above is consistent with the destabilization of organic acids and the enhanced contribution of carbonates and oxides, as a consequence of firing events (Granged et al., 2011a, 2011b; Kutiel et al., 1990; Ulery et al., 1995). The observed variation (3–4 pH units) in the F profiles suggests that they underwent high fire intensity (Ulery et al., 1995). The F profile horizons are also characterized by lower EC values compared with those of the NF profiles in the aforementioned depth intervals, likely due to the destruction of clay minerals and the formation of oxides at temperatures exceeding 500°C (Terefe et al., 2008). Low BD values (0.60–0.51 g $cm^{-3}$) noted in some horizons of the TOR1, TOR2, and TOR3 profiles can be ascribed to "unpacking" of particles (Ngole-Jeme, 2019) resulting from the loss of structure due to degradation of mineral and organic components.

The temperature to which the F profiles were exposed can be estimated by analyzing carbon fractions with different thermal stabilities. The thermally labile fraction ($TOC_{400}$) is always present in the superficial horizons of the F profiles, with average relative amounts ($TOC_{400}$%) of 90%, and is comparable to that observed in the NF profiles. The marked decrease in the $TOC_{400}$ fraction with depth (until it disappears) indicates that the F soil profiles were heated to over 400°C at depths of 14–73 cm (TOR1), 12–65 cm (TOR2), and 28–50 cm (TOR3) (Figure 30). The soil color change from dark brown (in the upper and lower horizons) to reddish at the intermediate depths also supports this finding, indicating burning temperatures of 300°C–500°C (Terefe et al., 2005, 2008). A sudden increase in the $TOC_{400}$ fraction at greater depths in the F soil profiles suggests a sharp decrease in the firing temperature downward.

The distribution of ROC along the F soil profiles is more variable. Only TOR1 records the total exhaustion of ROC at depths of 30–73 cm, whereas TOR2 and TOR3 show a significant decrease in the ROC content (down to 0.2 wt%) at depths of 12–65 and 30–50 cm, respectively. Such ROC content distribution indicates that the firing temperature exceeded 600°C only in TOR1, whereas TOR2 and TOR3 were subjected to maximum

temperatures of 400–600°C. These observations provide new insights into the thermal persistence of SOM, which was previously thought to disappear at temperatures of 450–500°C (Knoepp et al., 2005). The TIC fraction gradually decreases with depth in the F and NF profiles. The total exhaustion of TIC was only recorded in profile TOR1 at depths of 30–73 cm, suggesting that the layer was subjected to the maximum temperature (potentially exceeding 750°C) during the fire event. The significant correlation of TN with $TOC_{400}$ (and not with ROC) indicates that nitrogen is mostly volatilized at relatively low temperatures ($T < 400$°C) during firing events, as already reported in the literature (Turner et al., 2007). Moreover, the ubiquitous persistence of high $TOC_{400}$ and TN values in the superficial layers of the F profiles indicates that smoldering generally started and developed with variable intensity between depths of 10 and 70 cm.

Both the organic-rich (Op3) and organic-poor (Cg) horizons present similar thermal behavior of their carbon fractions. The total disappearance of the $TOC_{400}$ fraction (and TN) at heating temperatures over 400°C makes this fraction a robust thermal marker for the investigated profiles. Analogous conclusions can be made for the ROC fraction, which indicates heating temperatures below 600°C. The TIC fraction varied little in the experimental heating interval, and its presence in profiles TOR2 and TOR3 mainly implies that they did not undergo carbonate destabilization, which should occur at a temperature of approximately 750°C.

The bulk carbon isotopic composition of the experimentally heated NF horizons becomes less negative with increasing temperatures. This trend is similarly observed in the natural F profiles but does not imply the neoformation of carbonates during firing. The least negative values recorded in profile TOR2 at depths of 12–65 cm likely reflect the concentration of soil carbonates originally present in this horizon.

### 6.3.2 Triggering Mechanisms of Soil Burning in the Mezzano Lowland

Peat burning in the ML is not induced by surface flaming with downward propagation, as it is triggered at depth and develops in the 10–70 cm-deep soil horizons via smoldering combustion. This evidence suggests self-combustion of the organic-rich soils. Similar processes have been described in the literature, especially in dry and warm conditions (Restuccia et al., 2017), and are explained as the result of multiple reaction steps including drying, biological activity, and oxidation, that are necessary to trigger the spontaneous ignition of peat-soils (Yuan et al., 2021).

In the present case-study we suggest that the exothermal oxidation of methane (Christophersen et al., 2001; Pehme et al., 2020), which in the ML typically rises from the

deep stratigraphic layers, plays an additional role either in triggering the peat smoldering. The hypothesis is based on the fact that peat smoldering in the area is spatially associated to localized sectors characterized by high $CH_4$ seepage (with fluxes up to 120 g $m^{-2}$ $day^{-1}$, according to Cremonini et al., 2008). Soil heating occurs at depth where there is the transition between anoxic and oxic conditions with concomitant methanotrophic bacteria activity that promotes temperature well exceeding 40°C (Capaccioni et al., 2015), which is considered a thermal condition necessary for self-heating propensity (Yuan et al., 2021).
In this light, a possible strategy to minimize the peat-smoldering occurrence would require (a) the controlled collection of the upraising methane and (b) to maximize the irrigation efficiency of the area, that should be specifically planned to convey water at the soil depths where smoldering is effective.

### 6.3.3 Environmental Consequences of Peat Burning in the Mezzano Lowland

Peat burning implies environmental consequences in terms of release of greenhouse gases (Kohlenberg et al., 2018; Prosperi et al., 2020). The data described above allow the calculation of the soil organic carbon (SOC) stock in the F and NF profiles, and in turn the SOC stock is useful for estimating losses caused by burning events. The NF profile of TOR4 has a SOC stock of approximately 150 kg $m^{-2}$ for a thickness of 90 cm. These values are representative for ML soils unaffected by peat burning, as highlighted by the analyses of other soil profiles from the surroundings (Supplementary Table C2 in Appendix 6). A decrease in the SOC stock is observed in profiles TOR3 and TOR2 and, especially, in TOR1, characterized by the lowest SOC stock 38 kg $m^{-2}$ for a thickness of 96 cm. We infer that peat fires in the ML degraded up to two-thirds of the previous SOC stock. Although the extent of peat fire events is variable, we estimate that an average loss of the SOC stock within the first meter of depth is approximately 110 kg $m^{-2}$, potentially corresponding to approximately 580 kg $CO_2$ $m^{-3}$of emissions. As reported in Figure 34, the resulting emission coefficient is 725 g of $CO_2$ for kg of smoldered soil, a value that is compatible with what observed in other study-cases of smoldering peat soils in temperate climatic settings. However, carbon emissions plausibly include a wide spectrum of distinct components, where $CO_2$ is accompanied by CO, volatile organic components as well as by particulate matter (PM) having micrometer and sub-micrometer size range (Hu et al., 2018).

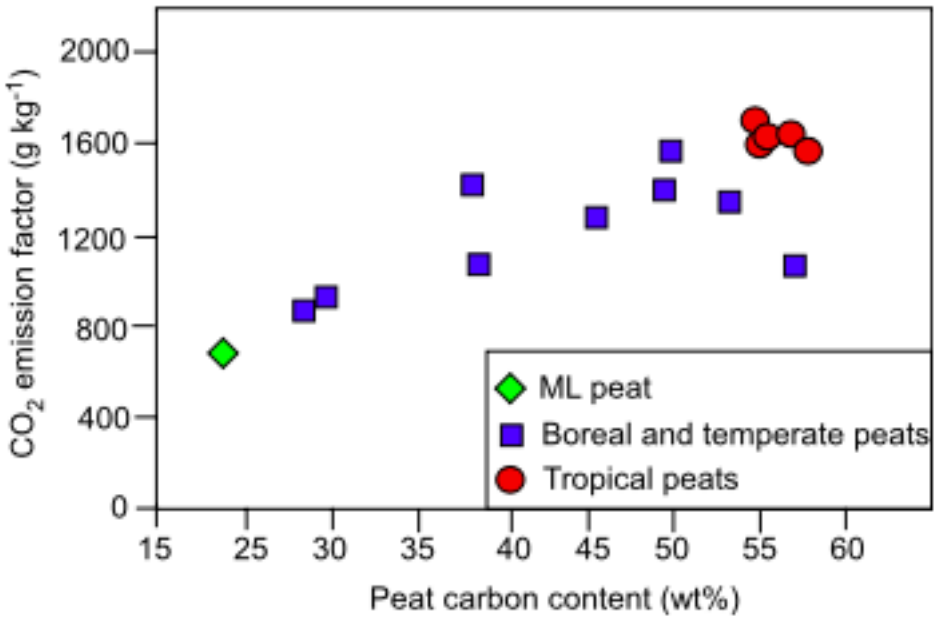


**Figure 34.** $CO_2$ emission of burning Mezzano Lowland peat-soils, compared with that of burning peat-soils from other areas.

### 6.3.4 Impacts of Peat Burning on the Human Health

The peat burning generates long-term smoke which is released in the air (Figure 11d, See section 3.1.3). These emissions are mainly composed by carbon monoxide, carbon dioxide, nitrate and sulfate, which are hazardous volatiles for the human health and if inhaled can trigger several symptoms from throat irritation, cough, and headaches to serious respiratory and cardiovascular problems, especially for people with existing asthma, emphysema, and heart disease (Hinwood and Rodriguez, 2005; Hu et al., 2018; Rappold et al., 2011).

Besides volatiles, the peat burning releases fine particles such as $PM_{10}$ and/or $PM_{2.5}$ depending on the predominance of coarse (particle diameter < 10 μm) or fine (particles diameter < 2.5 μm) soil fractions (Hinwood and Rodriguez, 2005). If inhaled $PM_{10}$ and $PM_{2.5}$ cause damages of lung tissue and respiratory and cardiovascular problems (Hu et al., 2018). The potential health risk of the smoke is even more serious considering the duration of the peat burning, as the prolonged or repeated smoke and particulate exposure by local people may aggravate the adverse health outcomes causing long-term health effects.

Additional concerns are related to elements potentially toxic (*e.g.,* several heavy metals such as Co, Cr, Cu, Ni, V, Zn, Pb, As, Mo, Se, Cd, Mo) that in the studied soils appear bounded in organo-metallic compounds (Di Giuseppe et al., 2014b, 2014c), because they could be released in the environment, in concomitance with the SOM destabilization, contaminating air, aquifers and soils (Kohlenberg et al., 2018).

In our view, the volatilization in the atmosphere or the dissolution in the hydrosphere of elements critical for the human health deserve further research on the peat-burning processes occurring in the Mezzano Lowland. In addition, the designed authorities should inform and educate locals about the health-risk of the peat smoke exposure.

## 6.4 Conclusions

Peat fires variously affect the first meter of soil profiles in the ML, and their intensity can be evaluated recording the differential consumption of the carbon pools with distinct thermal stabilities. The main damage to soil carbon budget occurs in the 10–70 cm-deep horizons, where smoldering temperatures of 400–600°C cause the total exhaustion of $TOC_{400}$ and variably decrease the ROC contents. Evidence of extreme temperatures overcoming the destabilization of carbonates (≥750°C) is limited to the inner horizons of the smoldering zone. The process appears spontaneous and shows analogies with what observed in other case-studies where peat self-combustion requires multiple reaction steps (drying, biological activity, and oxidative oxidation), but in the ML is possibly facilitated by the concomitant upraising of deep methane and its exothermal oxidation. The estimated carbon emission is 110 kg $m^{-2}$, corresponding to 580 kg $CO_2$ $m^{-3}$, that is, values in the same order of magnitude estimated in other temperate areas affected by smoldering peat-soils. The consequent release of significant amounts of greenhouse gases is coupled with a loss of soil structure, nutrients (*e.g.,* nitrogen), and possibly also toxic elements (*e.g.,* heavy metals). The consequences are surely negative for the environment, the agricultural activities and plausibly also for the health of the local people, and deserve further investigation to plan mitigation strategies for ongoing and future smoldering episodes.

Tables:

**Supplementary Table C1.** Additional data carried out to cross-check the reliability of SoliTOC data. * EA-IRMS analyses were performed on powdered samples and on powdered samples deprived of organic matter, *i.e.,* preliminary burnt in a muffle furnace at 550°C for 12h; the method measured Total Carbon (TC) and Total Inorganic Carbon (TIC), subsequently obtaining the Total Organic Carbon (TOC) for difference. **EA analyses were carried out on powders leached with hydrochloric acid that eliminate carbonates, thus measuring the TOC fraction.

| | | *TBS by EA-IRMS (Natali et al., 2018a; Catena, 164, 150-157) | | | **by EA after HCl leaching |
|---|---|---|---|---|---|
| | | *Measured* | | *Calculated* | |
| **Profile** | **Depth** | **TC** | **TIC** | **TOC** | **TOC** |
| | cm | (wt%) | (wt%) | (wt%) | (wt%) |
| **TOR 1** | 0-14 | 24.22 | 0.11 | 24.11 | 24.4 |
| | 14-17 | 2.52 | 0.08 | 2.44 | 2.49 |
| | 17-30 | 0.78 | 0.09 | 0.69 | |
| | 30-43 | 0.07 | 0.02 | 0.05 | 0.07 |
| | 43-65 | 0.05 | 0.03 | 0.02 | 0.05 |
| | 65-73 | 0.06 | 0.03 | 0.03 | 0.09 |
| | 73-84 | 10.14 | 0.03 | 10.11 | 10.2 |
| | 84-96+ | 2.65 | 0.04 | 2.61 | 2.66 |
| **TOR 2** | 0-12 | 15.76 | 0.66 | 15.10 | 15.3 |
| | 12-38 | 3.19 | 2.75 | 0.44 | 0.62 |
| | 38-48 | 9.21 | 8.54 | 0.67 | 0.42 |
| | 48-65 | 1.24 | 0.88 | 0.36 | 0.41 |
| | 65-72 | 22.62 | 0.03 | 22.59 | 22.9 |
| | 72-90 | 11.36 | | 11.36 | 12.1 |
| **TOR 3** | 0-28 | 18.51 | 1.46 | 17.05 | 18.3 |
| | 28-30 | 4.40 | 0.32 | 4.08 | 3.53 |
| | 30-40 | 1.09 | 0.41 | 0.68 | 0.49 |
| | 40-50 | 0.84 | 0.19 | 0.65 | 0.51 |
| | 50-70 | 25.16 | 0.04 | 25.12 | 27.2 |
| | 70-90 | 8.95 | 0.03 | 8.92 | 9.13 |
| **TOR 4** | 0-12 | 22.24 | 0.10 | 22.14 | 21.6 |
| | 12-25 | 22.46 | 0.10 | 22.36 | 22.1 |
| | 25-38 | 22.49 | 0.11 | 22.38 | 21.8 |
| | 38-47 | 22.34 | 0.02 | 22.32 | 21.4 |
| | 47-54 | 1.90 | 0.04 | 1.86 | 1.89 |
| | 54-63 | 31.54 | 0.04 | 31.50 | 31.7 |
| | 63-75 | 13.50 | 0.03 | 13.47 | 13.8 |
| | 75-85+ | 3.17 | 0.04 | 3.13 | 3.21 |
| **TOR 5** | 0-22 | 17.08 | 3.37 | 13.71 | 16.4 |
| | 22-30 | 17.42 | 1.93 | 15.49 | 17.6 |

| | | *TBS by EA-IRMS (Natali et al., 2018a; Catena, 164, 150-157) | | | **by EA after HCl leaching |
|---|---|---|---|---|---|
| | | *Measured* | | *Calculated* | |
| **Profile** | **Depth** | **TC** | **TIC** | **TOC** | **TOC** |
| | cm | (wt%) | (wt%) | (wt%) | (wt%) |
| | 30-36 | 21.95 | 0.06 | 21.89 | 22.8 |
| | 36-45 | 21.18 | 0.03 | 21.15 | 20.2 |
| | 45-60 | 7.79 | 0.03 | 7.76 | 8.23 |

**Supplementary Table C2.** Additional data concerning the Total Organic Carbon in soils of the Mezzano lowland surrounding the sites investigated in this study (Boschi and Spallacci, 1974).

| Profile | latitude | longitude | Depth | TOC |
|---|---|---|---|---|
| | | | cm | wt% |
| 64t | 44°4''18.0"" | 11°5''12.1"" | 0-50 | 8.8 |
| | | | 50-100 | 23.9 |
| 65t | 44°4''17.0"" | 12°0''9.3"" | 0-50 | 19.8 |
| | | | 50-100 | 23.8 |
| 66t | 44°4''15.9"" | 12°''54.7"" | 0-50 | 15.5 |
| | | | 50-100 | 25.2 |
| 79t | 44°4''37.4"" | 11°5''6.9"" | 0-50 | 13.1 |
| | | | 50-100 | 21.3 |
| 80t | 44°4''35.5"" | 12°0''6.4"" | 0-50 | 12.6 |
| | | | 50-100 | 23.9 |
| 81t | 44°4''35.4"" | 12°0''51.9"" | 0-50 | 10.5 |
| | | | 50-100 | 25.7 |
| 90t | 44°3''57.7"" | 11°5''10.6"" | 0-50 | 17.6 |
| | | | 50-100 | 23..5 |
| 91t | 44°3''55.5"" | 12°0''05.6"" | 0-50 | 10.6 |
| | | | 50-100 | 24.9 |
| 92t | 44°3''34.4"" | 11°5''06.0"" | 0-50 | 7.2 |
| | | | 50-100 | 18.7 |

# 7. A new geochemical-geophysical method for the SOC evaluation at farm scale: the Malborghetto di Boara case

Enclosed manuscript:

Carbon soil benchmark in a sustainable managed farm (Northeast Italy): application of geochemical and geophysical methods (*in prep*.)

Gian Marco Salani[a], Giacomo Fornasari[a], Valentina Brombin[a], Enzo Rizzo[a,b] , Gianluca Bianchini[a]

[a] Department of Physics and Earth Sciences, University of Ferrara, Ferrara, 44121, Italy

[b] Institute of Methodologies for Environmental Analysis, National Research Council, C.da S. Loja, Tito Scalo, 85050, Italy

## 7.1 Introduction

Nowadays soils are threatened by degradation due to land use and land use cover change (LULUCC). Consequently, one of the priorities of the Sustainable Development Goals (SDGs) is the protection of soils, as the worst projection estimate a mean soil erosion increase from 20% to 100% in Europe by 2050 (Panagos et al., 2021) with the loss of the most superficial soil layers hosting organic matter. In addition, the perpetration of conventional agricultural managements (*e.g.,* plough tillage) locally cause the decline of soil organic matter (SOM) (Turner et al., 2016). In order to contrast the current trend, the European Union, with an integration of the Common Agricultural Policy (CAP), is promoting the sustainable best-practices (*e.g.,* no- or minimu-tillage) in agriculture to preserve the SOM and the related organic carbon (OC). In fact, it is known that SOM globally stocks 1500 Pg of C in first meter of a soil, two and three times much more the C stored in the atmosphere and vegetation, respectively (Lal, 2004b). However, soil represents an open system, which can behave as a source or a sink of C. When the mineralization of the SOM due to the microbial activity is greater than its transformation into stable organic forms, soil releases C in the atmosphere as greenhouse gases (GHGs; *e.g.,* $CO_2$) with negative effects on climate (Blanco-Canqui and Lal, 2004; Oertel et al., 2016; Dai et al., 2017). This process is accelerated by unsustainable agricultural practices, like plough tillage which exposes the organic matter to the air, triggering the C oxidation (Figure 35a). On the other hand, if SOM is well managed through the application of sustainable agricultural practices, like agroforestry and no- or minimum tillage, the C is sequestered in the soils with benefits both for the environment and the human life (Figure 35b).

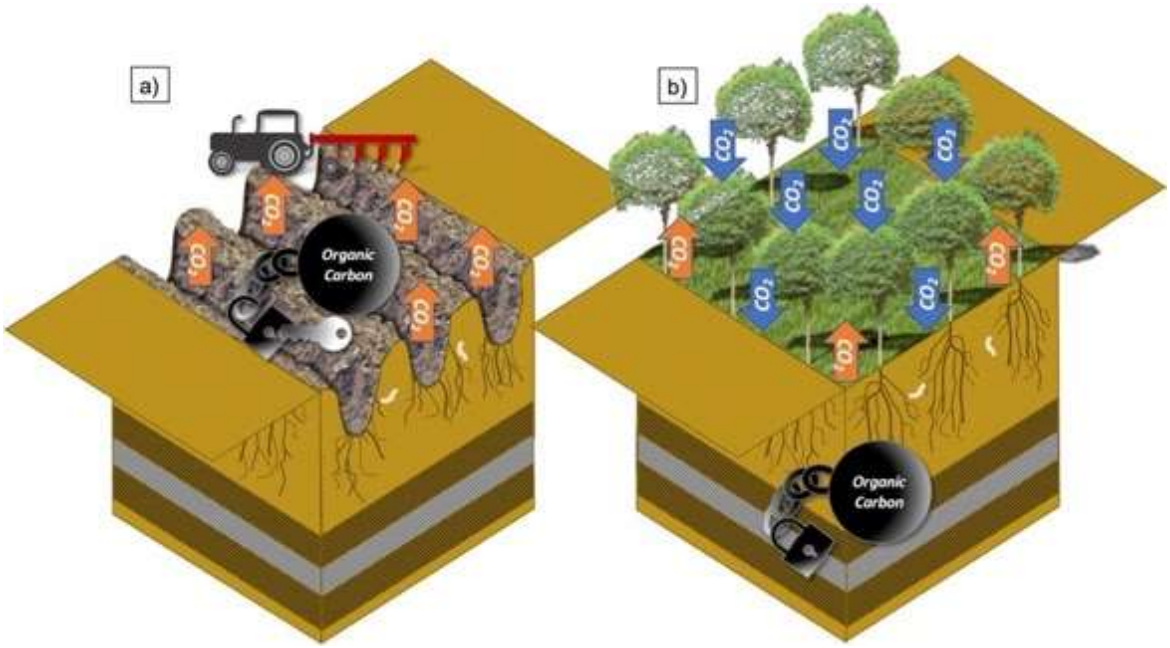


**Figure 35.** Simplified concept of C release and sequestration processes. Topsoil is like an open system, from which C is a) released in atmosphere as $CO_2$ as consequence of C oxidation triggered by the conventional practices or b) fixed by plants and sequestrated in agricultural soil, where sustainable practices are used.

Considering the delicate equilibrium of C in pedosphere-atmosphere-biosphere system, a regular monitoring of the soil health conditions should be adopted in each farm to verify the soil quality and consequently if OC is sequestered or released. This is the interest of the farmers, especially for those who want to turn toward more sustainable management. Following this line, the farmers should evaluate the current OC benchmark of their farm and monitor any changes of OC in a long period in order to take immediate actions to improve the C sequestration, and finally achieve the C neutrality. The certification of the soil conditions and the C sequestration will, also, allow to access to the CAP incentives for the reduction of $CO_2$ emission (Beka et al., 2022)

Thus, for this work, we defined the "carbon benchmark" of a conservative farm to verify, in the future, the soil OC sequestration. For this aim, we tested a new multidisciplinary approach, which involved both geochemical and geophysical analyses. The former measured the OC contents and the relative isotopic ratio ($^{13}C/^{12}C$) of soil samples in laboratory using an elemental analyzer coupled with a mass spectrometer (Natali et al., 2018a, 2018b; 2020). The latter were applied *in-situ* using non-invasive electromagnetic induction (EMI) to measure the apparent electrical conductivity (EC) for the estimation of soil physical properties (Doolittle et al., 2001; Corwin et al., 2003; Morari et al., 2009; Tromp-van Meerveld and McDonnell, 2009; Calamita et al., 2015; Boaga 2017). The results of these investigations were reported in a geochemical-geophysical map, which

represents a snapshot of the soil of the farm. The obtained map is useful to analyze the spatial variation of soil parameters (OC, SOM, $\delta^{13}C$, and EC) and to investigate in detail the situation of single farms that want to resolve specific issues and/or become more virtuous with the aim to reach the carbon neutrality.

## 7.2 Results

Thermo-gravimetric and bulk density results of the 15 sites are reported in Table 8.

**Table 8.** Results of sequential LOI (provided at temperature of 105°C, 550°C, and 1000°C) and the bulk density of soil samples.

| | | LOI | | | bulk density |
|---|---|---|---|---|---|
| **Sample** | **Class** | **105 °C (wt%)** | **550 °C (wt%)** | **1000 °C (wt%)** | **(g cm$^{-3}$)** |
| **MB06** | i | 1.29 | 3.83 | 6.19 | 1.4 |
| **MB11** | i | 1.56 | 4.55 | 6.09 | 1.5 |
| **MB14** | i | 1.24 | 4.15 | 6.25 | 1.4 |
| **MB15** | i | 1.48 | 4.80 | 6.28 | 1.4 |
| **MB02** | ii | 2.04 | 4.62 | 4.64 | 1.1 |
| **MB03** | ii | 1.87 | 4.22 | 5.50 | 1.3 |
| **MB04** | ii | 1.78 | 4.55 | 5.40 | 1.4 |
| **MB05** | ii | 1.74 | 4.13 | 6.08 | 1.4 |
| **MB09** | ii | 1.60 | 4.39 | 5.28 | 1.5 |
| **MB10** | ii | 1.55 | 4.57 | 5.47 | 1.4 |
| **MB01** | iii | 2.87 | 5.35 | 3.95 | 1.5 |
| **MB07** | iii | 2.51 | 5.32 | 4.23 | 1.3 |
| **MB08** | iii | 1.99 | 4.80 | 4.50 | 1.5 |
| **MB12** | iii | 2.70 | 5.84 | 4.24 | 1.5 |
| **MB13** | iii | 4.01 | 5.35 | 4.71 | 1.4 |

The soil hygroscopic water contents evaluated from the LOI at 105°C varied between 1.24 wt% (MB14) and 2.87 wt% (MB01), with the except of one value (4.01 wt%, MB13). The average is 1.87 wt% and standard deviation is 0.51 wt%. Soil organic matter represented by LOI at 550°C varied between 3.83 wt% (MB06) and 5.84 wt% (MB12), with an

average of 4.70 wt% and a standard deviation of 0.56 wt%. LOI measured at 1000 °C varied between 3.95 wt% (MB01) and 6.28 wt% (MB15), with an average of 5.25 wt% and a standard deviation of 0.82 wt%. The bulk density varied between 1.1 g $cm^{-3}$ (MB02) and 1.5 g $cm^{-3}$ (MB01, MB08, MB09, MB11, and MB12), with an average of 1.4 g $cm^{-3}$ and a standard deviation of 0.1 g $cm^{-3}$.

The elemental and isotopic C speciation results are reported in the Table 9 and Figure 36, whereas the SOC stock results are reported in Supplementary Figure D1 (se Appendix 7).

**Table 9.** Results of elemental contents and isotopic signatures of total (TC), organic carbon (OC), and inorganic (IC) carbon.

| Sample | TC (wt%) | OC (wt%) | IC (wt%) | $\delta^{13}C_{TC}$ (‰) | $\delta^{13}C_{OC}$ (‰) | $\delta^{13}C_{IC}$ (‰) |
|---|---|---|---|---|---|---|
| **MB01** | 1.89 | 1.21 | 0.68 | –15.3 | –22.3 | –2.7 |
| **MB02** | 2.10 | 1.10 | 1.00 | –12.2 | –22.4 | –0.9 |
| **MB03** | 2.20 | 0.99 | 1.21 | –10.4 | –21.4 | –1.5 |
| **MB04** | 2.33 | 1.15 | 1.18 | –11.4 | –21.8 | –1.1 |
| **MB05** | 2.34 | 0.96 | 1.39 | –9.0 | –20.7 | –0.9 |
| **MB06** | 2.36 | 0.93 | 1.43 | –8.6 | –20.8 | –0.7 |
| **MB07** | 2.04 | 1.22 | 0.82 | –14.4 | –22.3 | –2.6 |
| **MB08** | 2.05 | 1.12 | 0.93 | –13.0 | –22.3 | –1.9 |
| **MB09** | 2.26 | 1.04 | 1.22 | –10.6 | –21.3 | –1.4 |
| **MB10** | 2.22 | 0.99 | 1.23 | –10.6 | –22.1 | –1.5 |
| **MB11** | 2.34 | 0.93 | 1.41 | –9.1 | –20.9 | –1.3 |
| **MB12** | 1.97 | 1.22 | 0.75 | –14.2 | –21.4 | –2.4 |
| **MB13** | 2.09 | 1.14 | 0.95 | –12.4 | –21.3 | –1.7 |
| **MB14** | 2.25 | 0.79 | 1.45 | –7.8 | –19.7 | –1.3 |
| **MB15** | 2.40 | 0.93 | 1.46 | –8.9 | –20.6 | –1.5 |

Among the dataset, the TC varied between 1.89 wt% (MB01) and 2.40 wt% (MB15), with an average of 2.19 wt%. The isotopic $\delta^{13}C_{TC}$ showed values varying from –15.3‰ (MB01) to –7.8‰ (MB14), with an average of –11.2‰. The OC varied between 0.79 wt% (MB14) and 1.22 wt% (MB12), with an average of 1.05 wt%. The $\delta^{13}C_{OC}$ showed values varying

from –22.4‰ (MB02) to –19.7‰ (MB14), with an average of –21.4‰. The IC varied between 0.68 wt% (MB01) and 1.46 wt% (MB15), with an average of 1.14 wt%. The calculated $\delta^{13}C_{IC}$ showed values varying from –2.7‰ (MB01) to –0.7‰ (MB06), with an average of –1.6‰.

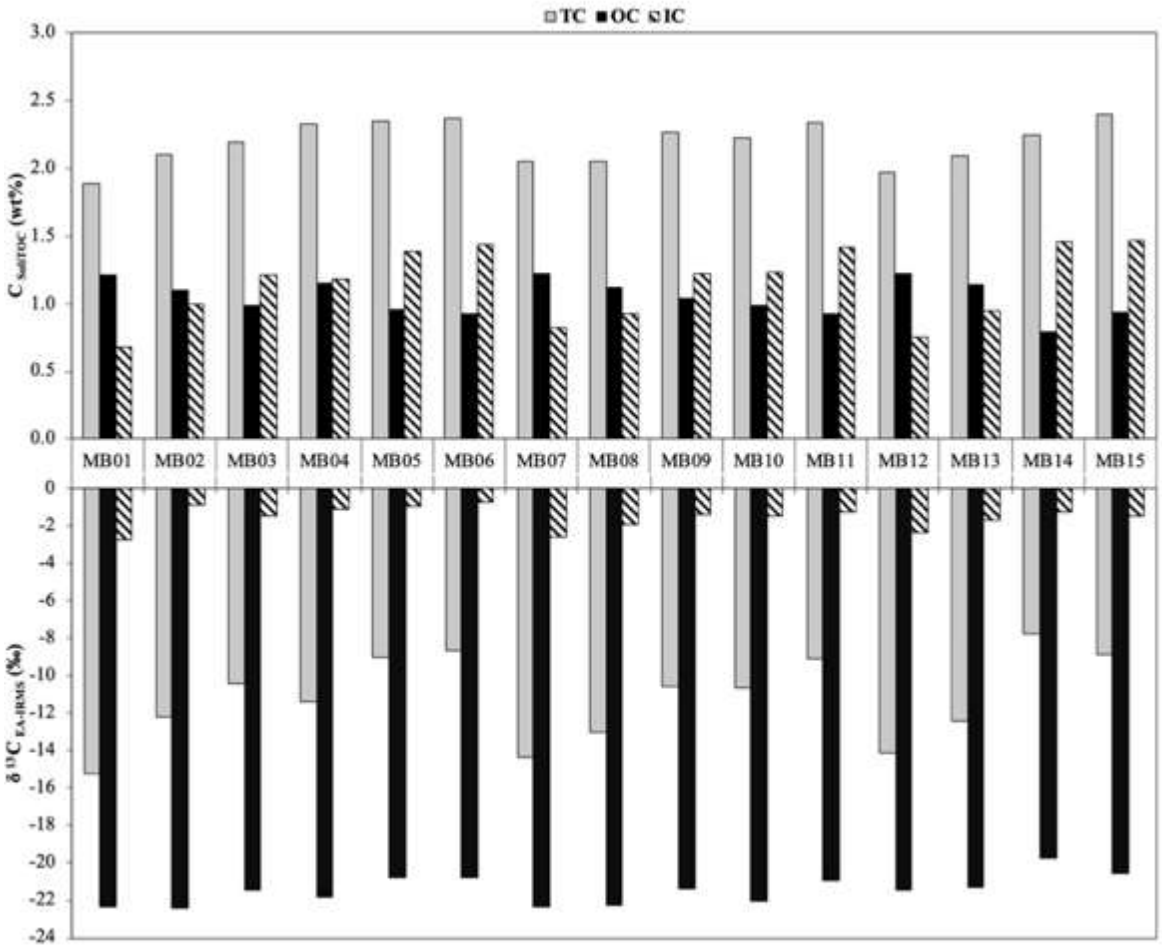


**Figure 36.** Elemental and isotopic composition of the total (TC), organic (OC), and inorganic (IC) carbon fractions of the soil samples.

In Figure 37 we investigated the variability of the physicochemical parameters of the soils with the OC contents. To observe any correlation between the predominance of the OC fraction and the physicochemical parameters, the soils samples were clustered on the basis of OC/IC as follows: "Class i" upper than the 75° percentile (OC/IC > 1.20; MB06, MB11, MB14, and MB15), "Class ii" between the 25° and 75° percentile (0.68 < OC/IC < 1.20; MB02, MB03, MB04, MB05, MB09, and MB10), and "Class iii" lower than the 25° percentile (OC/IC < 0.68; MB01, MB07, MB08, MB12, and MB13). The one-way ANOVA and the Tukey post-hoc results of the three classes are also reported.

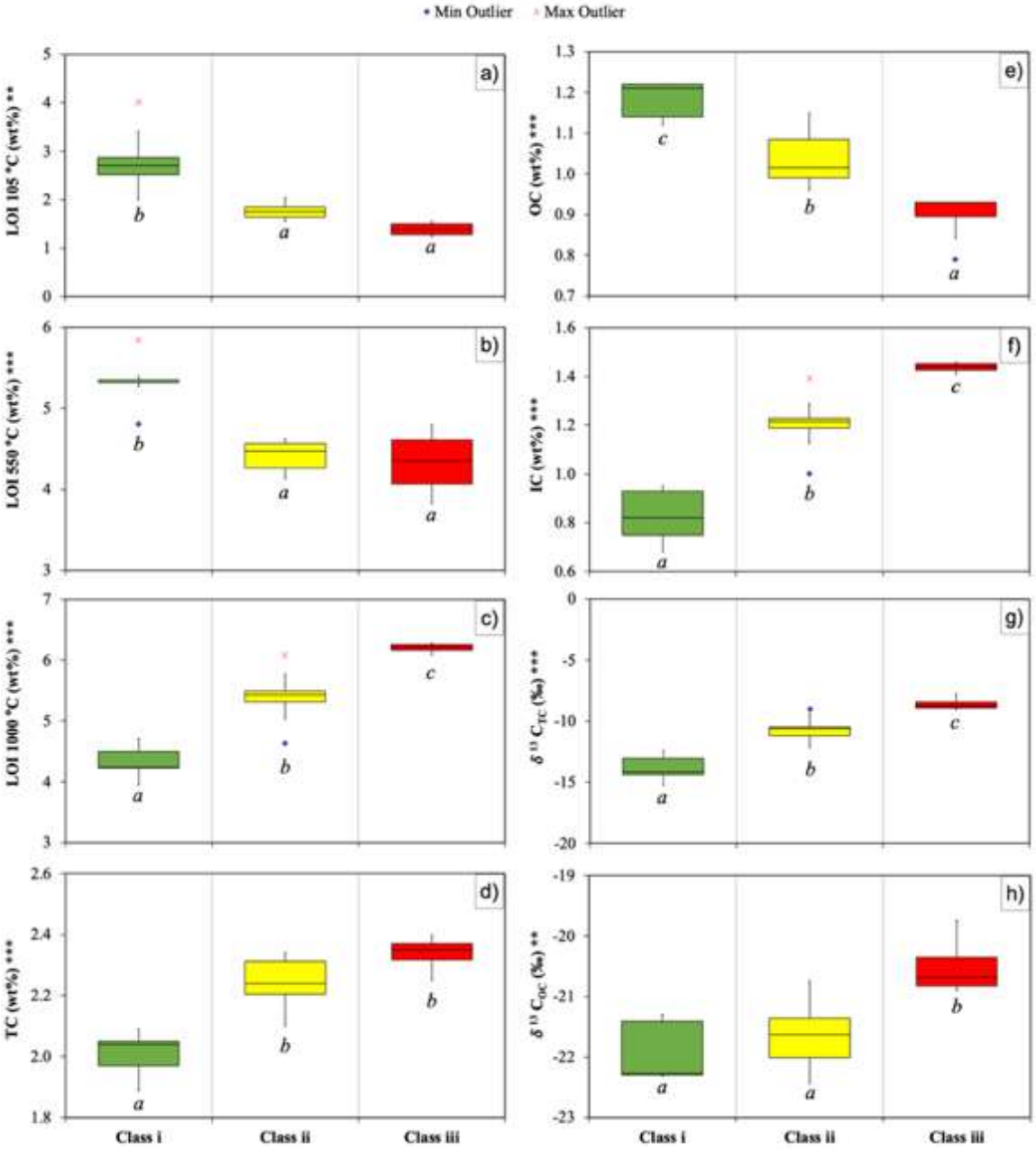


**Figure 37.** Boxplots of a) LOI 105°C, b) LOI 550°C, c) LOI 1000°C, d) TC, e) OC, f) IC, g) $\delta^{13}C_{TC}$, and h) $\delta^{13}C_{OC}$ of the samples divided in the three classes based on the OC/IC ratio (see the text for the detail). In each box plot the black line represent the median. Below the box plots the letters represent the results of the Tukey post-hoc test. Different letters denote significant differences among classes. The one-way ANOVA results are also reported (** $p < 0.001$; *** $p < 0.0001$).

The EC measurements acquired at 16, 14 and 10 kHz in 1999 locations in MB site, are described in Figure 38. The distribution of EC values at 16 kHz shows a median of 39 mS $dm^{-1}$, and a variation between 35 to 43 mS $dm^{-1}$. The distribution of EC values at 14 kHz shows a median of 35 mS $dm^{-1}$, and a variation between 32 to 40 mS $dm^{-1}$. The distribution of EC values at 10 kHz shows a median of 30 mS $dm^{-1}$, and a variation between 26 to 35

mS $dm^{-1}$. In this framework, the three acquisitions were useful to emphasize the site-specific variability of the soil also observed with the laboratory measurements.

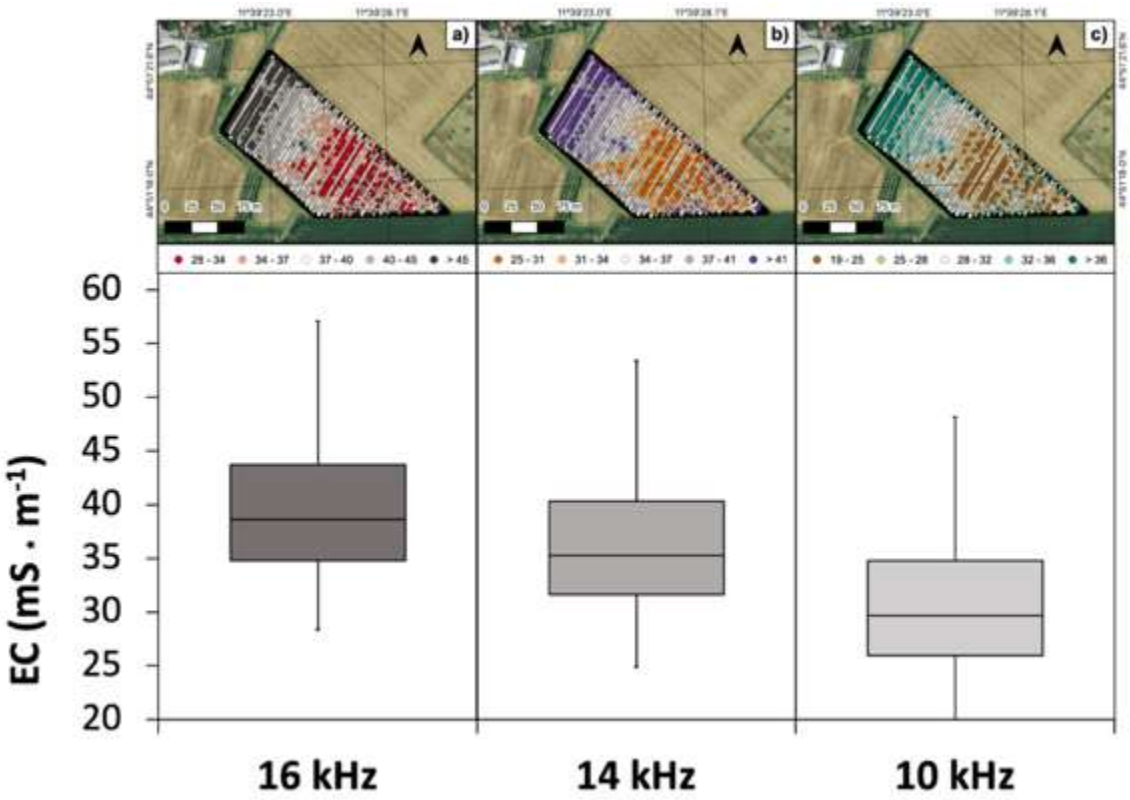


**Figure 38.** The EC measurement distributions acquired at a) 16, b) 14 and c) 10 kHz.

## 7.3 Discussion

### 7.3.1 Soil carbon elemental and isotopic speciation

The results of the TC vs $\delta^{13}C_{TC}$ of MB are comparable to the datasets described for the soils of the Ferrara province by Natali et al. (2018b) and Salani et al. (2021), and they are typical of mix of alluvial sediments of paleochannel and levee (Figure 39). In particular, the less negative values of $\delta^{13}C_{TC}$ are typical of samples (MB03, MB05, MB06, MB09, MB10, MB11, MB14, and MB15) collected within the levees of the paleochannel, whose sediments are characterized by coarse granulometry (*i.e.,* sand and silt). On the other hand, the most negative values are typical of samples collected in the interfluvial lowland located in the northwesternmost part of the field (MB01, MB02, MB07, MB08, MB12, and MB13; Figure 13; see section 3.1.4) and within the ancient bed of the paleochannel (MB04) where sediments are characterized by the finest granulometry (*i.e.,* clay). It is well known that

clay minerals are able to protect the SOM, and the related OC, from the microbial degradation more efficiently than coarse granulometry, due to the high adsorption capacity (von Lützow et al., 2006; Gunina and Kuzyakov, 2014; De Clercq et al., 2015; Guillaume et al., 2015; Sarkar et al., 2018). Therefore, in this study, the sites composed mainly by coarse granulometry record relatively low OC contents and less negative $\delta^{13}C_{TC}$ signature, indicative of soil with poor SOM, on the contrary the samples composed mainly by clay fraction record relatively higher OC contents and more negative $\delta^{13}C_{TC}$ signature, indicative of SOM conservation. Therefore, there is a clear relationship between the physicochemical characteristics of the soils and the OC contents.

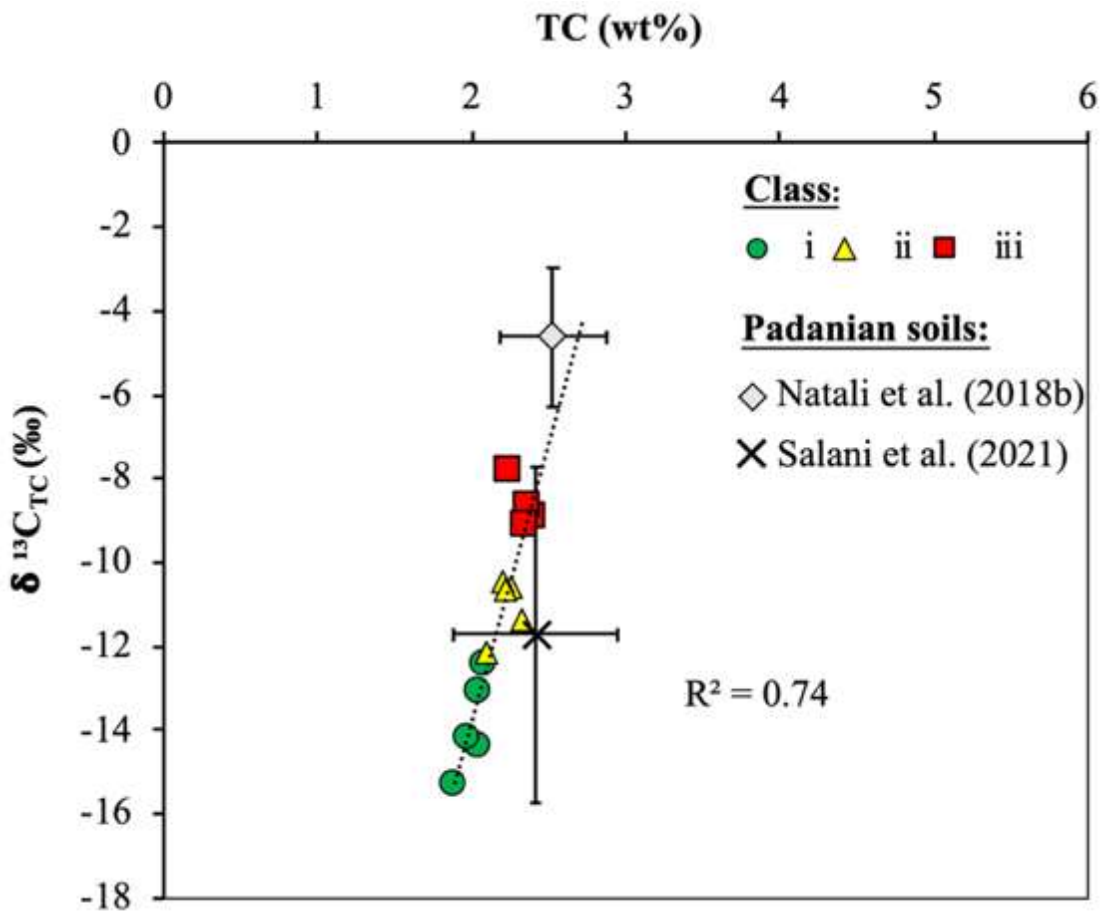


**Figure 39.** Elemental TC contents and $\delta^{13}C_{TC}$ of MB samples and average elemental TC contents and $\delta^{13}C_{TC}$ recognized as deposits of paleochannel and levee of easternmost Padanian plain soils studied by Natali et al. (2018b) and Salani et al. (2021).

According to the one-way ANOVA results the three classes are statistically different (*p*-value < 0.0001) for the LOI 550°C, LOI 1000°C, TC, OC, IC, and $\delta^{13}C_{TC}$ (Figure 37b, c, d, e, f, and g), and slightly less different (*p*-value < 0.001) for LOI 105°C and $\delta^{13}C_{OC}$ (Figure 37a and h). The Tukey post-hoc test better explored similarities and differences among the three classes. In detail, the two classes with low OC/IC (*i.e.,* Class ii and Class iii) have lower LOI 105°C, LOI 550°C, and OC, than the class with high OC/IC (*i.e.,* Class i) (Figure 37a, b, and e). This is indicative of a correlation between the soil hygroscopic water contents and soil organic matter. In fact, sites of Class i seem to have a condition of higher clay content on the basis of the relative higher values of soil hygroscopic water and organic matter. Another evident correlation is among LOI 1000°C and IC parameters, which are indicative of the presence of carbonatic minerals especially in samples of Class iii. Such evidence can be observed also for $\delta^{13}C_{TC}$ values that become less negative with the increase of the inorganic fraction in the Class iii. On the contrary, most negative $\delta^{13}C_{TC}$ values reflect the higher organic fraction in the Class i. Therefore, the $\delta^{13}C_{TC}$ signature is

influenced by the OC/IC ratio as shown in Figure 40, as samples characterized by the most negative $\delta^{13}C_{TC}$ signature also record the highest OC contents. Despite the different $\delta^{13}C_{TC}$ signature among the three classes, the samples show similar $\delta^{13}C_{IC}$ and $\delta^{13}C_{OC}$ values, indicating that the different $\delta^{13}C_{TC}$ values are ruled by the amount of organic and inorganic C contents, rather than the nature of the IC and OC. In fact, for all the samples the $\delta^{13}C_{IC}$ signature is close to 0‰, typical of geogenic carbonates. On the other hand, the average $\delta^{13}C_{OC}$ signature is –21.4‰, which represents a mix of SOM derived by plants with $C_3$ (~ −26‰) and $C_4$ (~ −15‰) photosynthetic pathways, typical of this area (Natali et al., 2018b; Brombin et al., 2020; Salani et al., 2021). Generally, as we reported, a $\delta^{13}C$ benchmarking is also useful to define a snapshot of the actual SOC conditions. Furthermore, in future a coupled elemental and isotopic C monitoring should be a systematic method to describe the evolution of the soil characteristics and to predict the carbon fluxes.

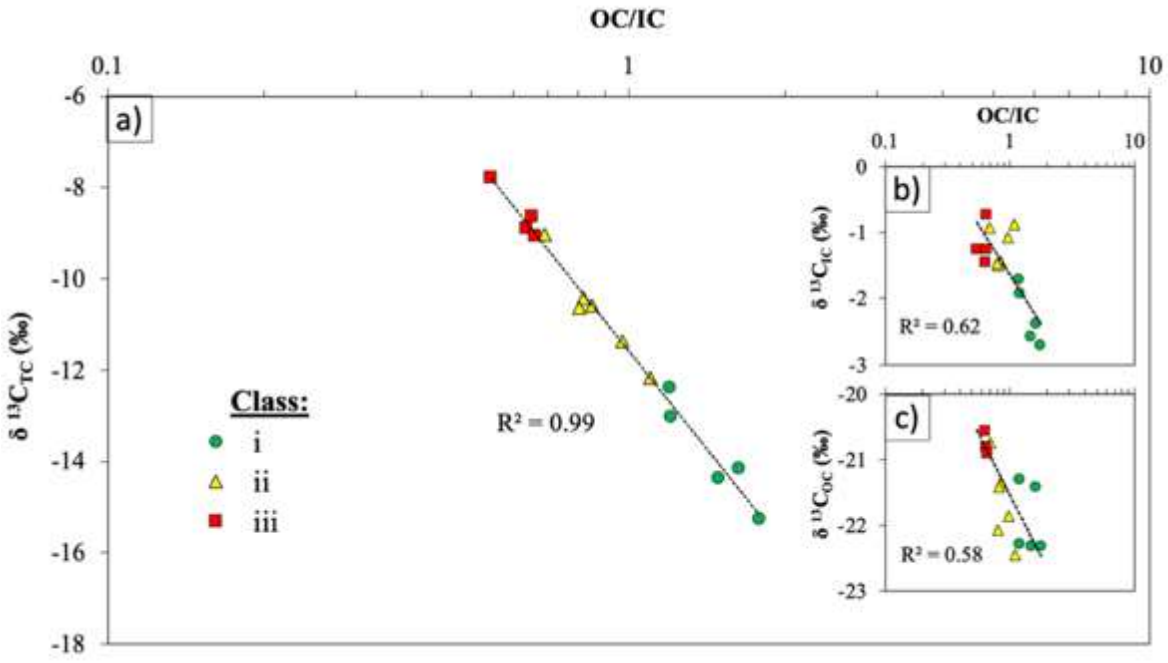


**Figure 40.** OC/IC (in logarithmic scale) versus $\delta^{13}C_{TC}$ shows a good negative correlation; the insets reproduce the relations between OC/IC, a) $\delta^{13}C_{IC}$, and b) $\delta^{13}C_{OC}$.

### 7.3.2 Insights from soil organic carbon and geophysical data

The principal component analysis (PCA) was calculated using the elemental fractions of C, the isotopic signature $\delta^{13}C_{TC}$, and the local electrical conductivity (EC) measured for each of the 15 samples at the frequencies of 16 kHz, 14 kHz, and 10 kHz (Figure 38). The

resulting PCA (Figure 41) explains more than 95% of the variance and well clusters the samples of Class i and Class iii which are characterized by the highest and the lowest OC/IC ratio, respectively. Accordingly, to the results of Figure 37 (e, f, and g) the samples of Class ii show intermediate characteristics between Class i and Class iii, therefore in the PCA plot they overlap over the other two clusters.

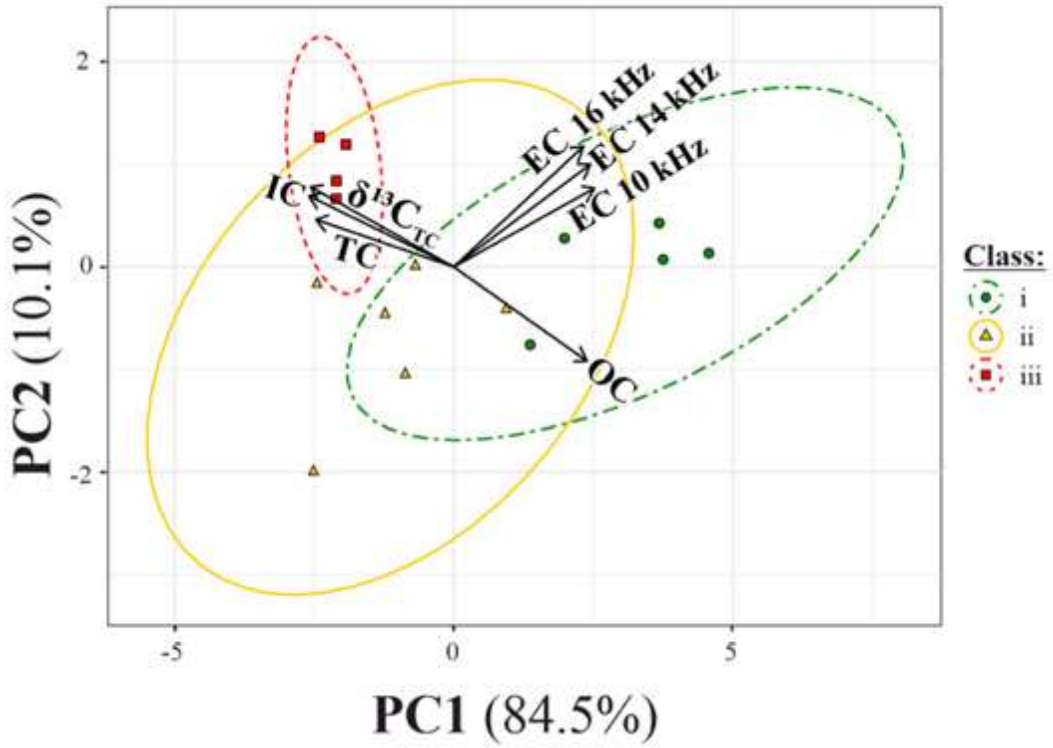


**Figure 41.** Principal Component Analysis (PCA) for $\delta^{13}C_{TC}$, OC, IC, TC, and EC (respectively measured at 16, 14, and 10 kHz), clustered in class i (green dots and dash-dotted line ellipse), class ii (yellow triangles and solid line ellipse), and class iii (red squares and dashed line ellipse).

In the MB context, the higher EC values are indicative of soil with the property to retain pore-fluids, that is correlated with the high cation exchange capacity of the finest sediment, *i.e.,* clay minerals (Katsube et al., 2003). Consequently, there is a correlation between EC and SOM, as the organic matter is generally hosted in clay minerals (Sarkar et al., 2018). Coherently, in Figure 42 the EC positively correlates with OC contents and OC/IC and negatively correlates with $\delta^{13}C_{TC}$, as the most negative values are typical of samples enriched in organic matter (Brombin et al., 2020). In particular the OC/IC exhibits the best index of correlation $R^2$ with the EC measured at 10 kHz (0.75). Also, OC and $\delta^{13}C_{TC}$ show the best $R^2$ values with the EC measured at 10 kHz (0.52 and 0.65, respectively).

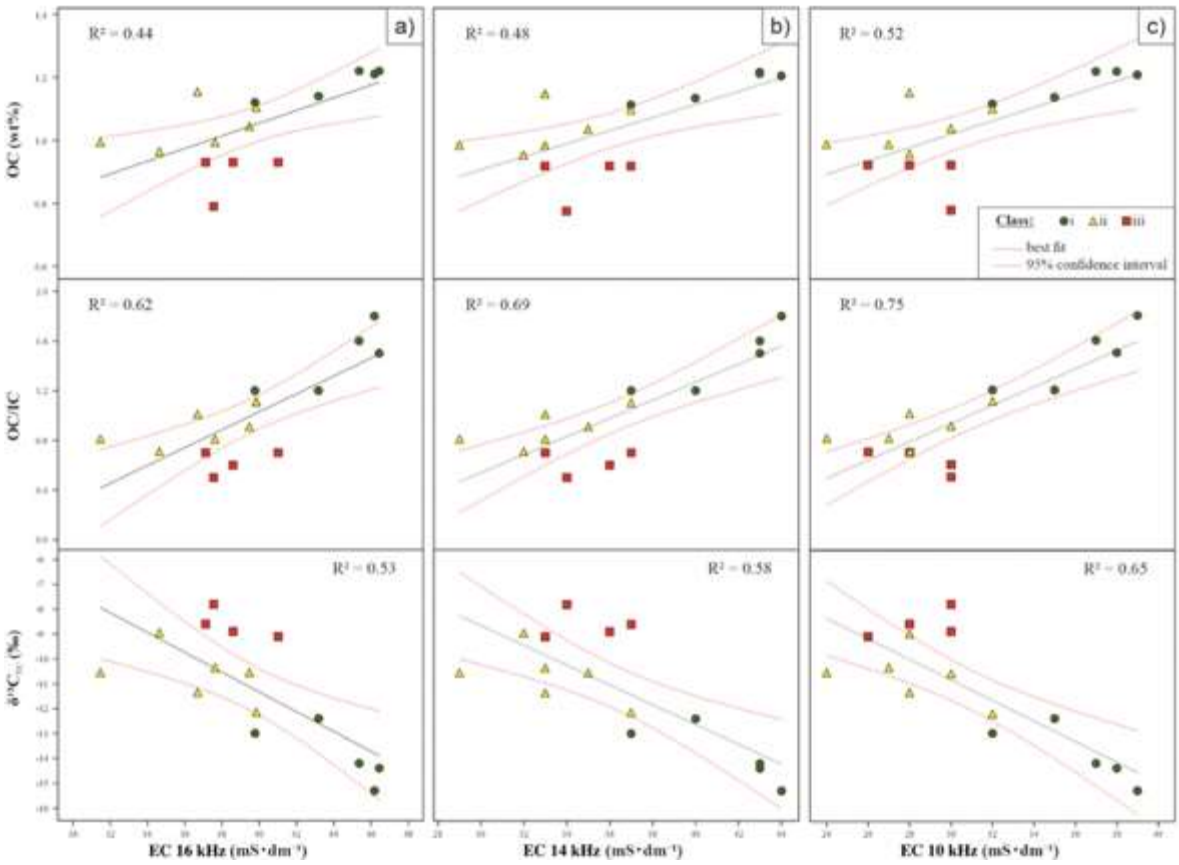


**Figure 42.** Linear regression graphics to observe the relations which OC, OC/IC, and $\delta^{13}C_{TC}$ show with the EC measured at a) 16 kHz, b) 14 kHz, and c) 10 kHz. The data are represented as green dots, yellow triangles, and red squares, for Class I, Class II, and Class III respectively. For each plot are represented the regression line (in black) and its equation, the $r^2$ value, and the 95% confidence intervals (the red curves).

Therefore, to evidence the spatial distributions of OC and the EC measured at 10 kHz, we generated the predictive maps using the interpolating method of ordinary kriging (Figure 43). Comparing Figure 43a and b it is evident that the OC content and EC variables are correlated as the northwesternmost part of the field show both the highest values of OC contents and EC as both organic matter and water are mainly hosted in the fine sediments of the soil (*i.e.,* clay). On the contrary the southeasternmost part, where coarse granulometry prevails (*i.e.,* sand), shows the lowest values of OC contents and EC, indicating the scarce sequester of OC and water contents in the soils of this area. Assuming as first variable the OC data and as covariate variable the EC data measured at 10 kHz, we predicted a new improved map of the OC surface (Figure 43c). This kind of map offers a snapshot of the amount of OC in the soils and it can be read easily also by farmers, which have not a scientific background, in order to take the right decisions to improve the OC sequester and plan the future crops.

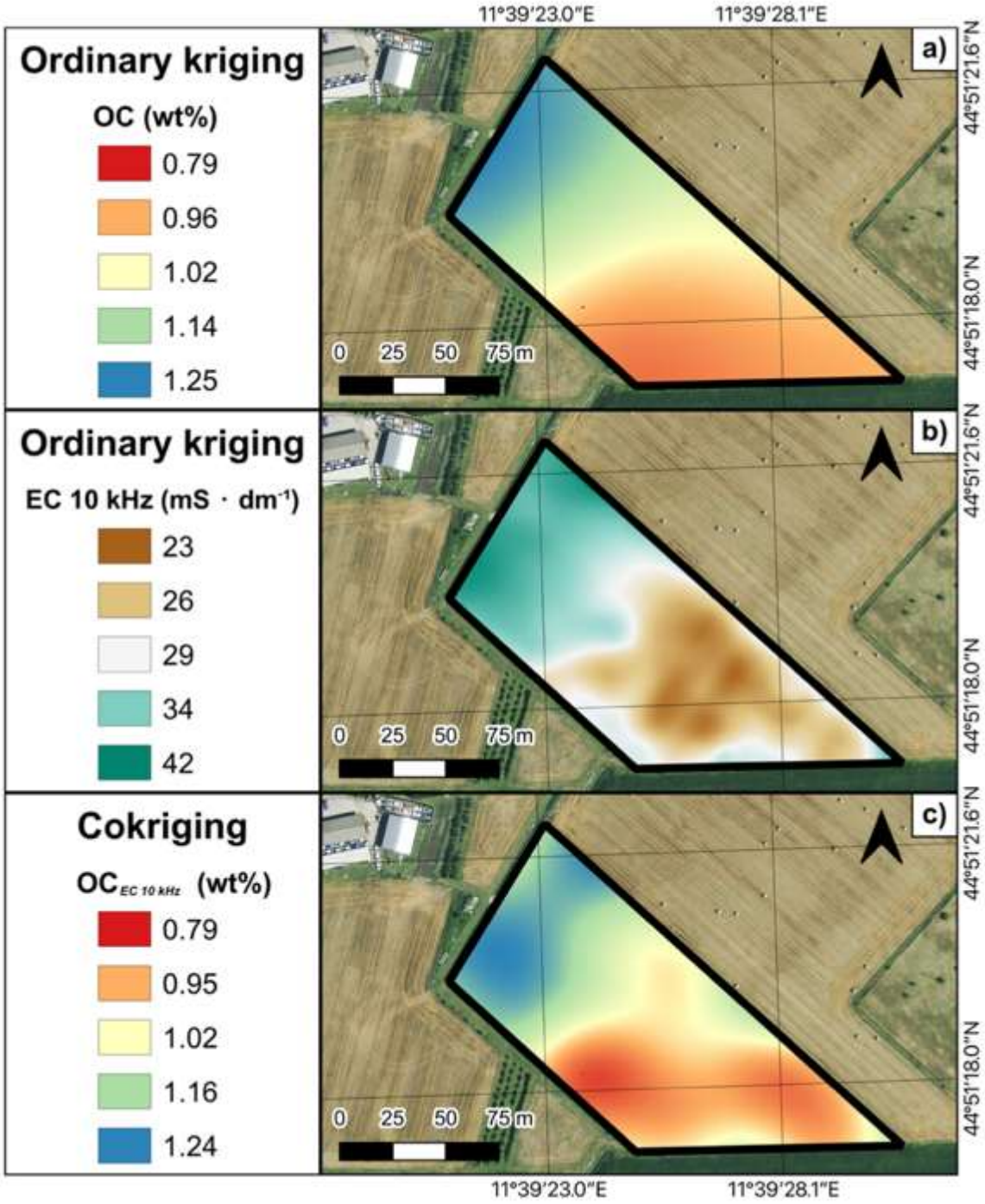


**Figure 43.** Predictive maps realized using the ordinary kriging on a) the OC values, and b) the EC values measured at 10 kHz, and the cokriging to predict c) a new OC surface using the OC values and the EC values at 10 kHz as a covariate variable. The legend values for each map represent a quantile classification.

## 7.4 Conclusions

The study demonstrates that a comprehensive geochemical and geophysical investigation of soil can provide detailed information of soil physicochemical parameters, which can be represented in a map useful to the farmers to evaluate health conditions of their fields. In this work the soil of a hazelnut crop in Emilia-Romagna region (Italy) was analyzed with i) geochemical analyses to evaluate the elemental total (TC), organic (OC), and inorganic (IC) carbon contents and the respective isotopic signatures of samples collected in the arable layer (0-30 cm), and ii) *in-situ* geophysical analyses to measure the electrical conductivity (EC) of the entire area, which is related with texture, salinity, porosity, and the presence of pore-fluids. We observed that the variability of the soil carbon along the site changes with the EC, in particular the OC concentration can be described by the EC measured at 10 kHz. In fact, the northwesternmost part of the field show the highest values of EC and the highest OC contents, as the finer sediments (*i.e.,* clay minerals) host both moisture and organic matter, whereas southeasternmost part of the field show the lowest values of EC and the lowest OC contents, due to the presence of coarse granulometry. Therefore, we demonstrate that geophysical non-destructive techniques can predict the OC contents allowing the mapping of an entire area in a short time.

In our opinion, a periodic verification of geochemical and geophysical parameters of the soils should be requested as ground-truth to each farm to monitor the soil health conditions and to promote the use of best-practices. The use of these approaches in a short-term period of monitoring (3-5 years) could be useful for farmers to evaluate any increase of C and point to obtain the incentives by CAP (*i.e.,* "carbon credits"; Figure 44). Then if the soil of is very well-managed, the farm can reach carbon neutrality.

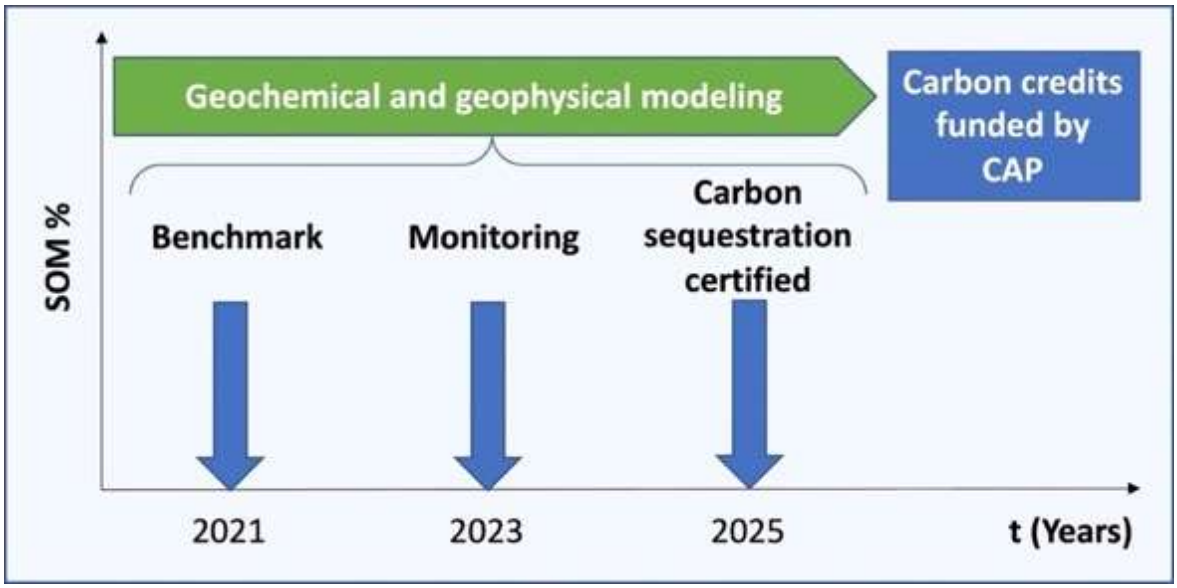

**Figure 44.** A short-term monitoring schedule for a better soil managing to increase SOM at a farm-scale. Carbon credits are achievable by the farmers after a certified carbon sequestration obtained by repeated measurements on field.

In the future, integrating this method with detailed stable carbon isotope ($^{13}C/^{12}C$) measurements will help to evaluate the soil OC stock of an area, identify carbon sources, and ultimately reconstruct soil $CO_2$ fluxes. In fact, during the degradation of soils, the $^{12}C$ tends more easily to be oxidized and released in the atmosphere than $^{13}C$, leaving the C isotopic signature of residual soil more enriched in $^{13}C$. As described by De Clercq et al. (2015), $\delta^{13}C_{OC}$ vary according to the soil managements, becoming negative signatures from conventional tillage to zero-tillage and to grass coverage as the amount of sequestrated SOC increase. In our case, we expect that OC contents will increase and the $\delta^{13}C_{OC}$ will become more negative in the MB site, where zero-tillage/grass cover practices are used. Unfortunately, as described by Menichetti et al. (2015) a plausible decay of soil OC, with increasing of $\delta^{13}C_{OC}$ signatures (between 1 and 3‰), due to the world climatic evolution is expectable for the future.

Appendix 7

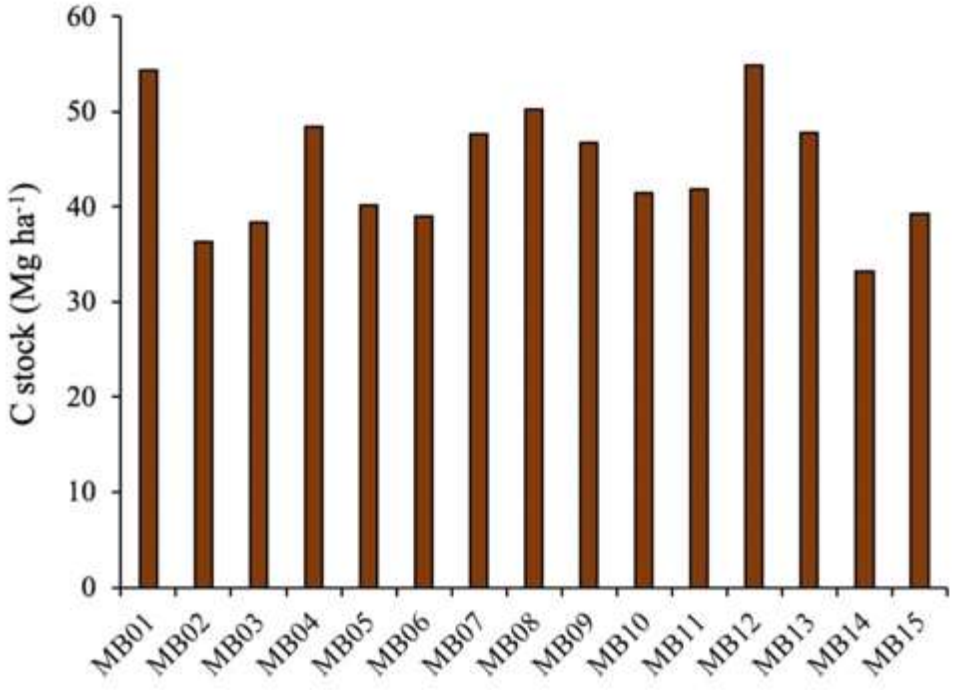


**Supplementary Figure D1.** Soil OC Stocks (0-30 cm) evaluated for the fifteen soil samples.

# 8. Assessing the soil organic carbon contents through a combination of geochemical soil investigations and remote-sensing by data of Sentinel-2 and PRISMA

Enclosed manuscript:

Organic Carbon estimation using an *ab initio* combined approach using geochemical and remotely sensed data: the case study of Ferrara (Northern Italy) (*in prep*.)

Gian Marco Salani[a], Michele Lissoni[b], Gianluca Bianchini[a], Valentina Brombin[a], Stefano Natali [c], Claudio Natali[d]

[a] Department of Physics and Earth Sciences, University of Ferrara, Ferrara, 44121, Italy

[b] Department of Geography, University of Colorado Boulder, Boulder, CO 80309, USA;

[c] SISTEMA GmbH, Vienna, Austria

[d] Department of Earth Sciences, University of Florence, Florence, 50121, Italy

## 8.1 Introduction

### 8.1.1 Soil Organic Carbon in the critical zone

The earth critical zone (CZ) is a variable thickness layer composed by soil, rocks, air, and biota, that is constrained between the treetops to the groundwater bottom (National Research Council, 2001; Xu and Liu, 2017). It has an evolving nature that is constantly modified by interactive water and biogeochemical processes (Chorover et al., 2007). In particular, within CZ many ecosystem processes, which provide a wide range of products and services to humans, are also supported by soil formation and water movement (Field et al., 2015). Only a thin part of the superficial CZ can be directly involved by human activities, in particular by the agriculture. In fact, intensive agricultural practices cause soil and vegetation degradation, interfering with processes of the CZ transformations. Thus, to increase the knowledge of such processes, a wide spectrum of disciplines such as physics, biology, geology, hydrology, soil science, ecology, geochemistry, and geomorphology are needed. In particular, geochemistry can offer a complete picture of the elemental distribution of all the involved CZ matrices, other than ensuring replicable methods to monitor changing conditions. Focusing on soil proprieties, soil organic carbon (SOC), which represents ~50% of soil organic matter (SOM), is considered a proxy of soil quality and fertility (Bünemann et al., 2018). Since the organic soil carbon pool includes the living and death residues of the organic materials, its presence facilitates soil aggregation and in turn affects soil erosion, aeration, water balance, temperature, roots growth, and biota activities, promoting crop productivity and climate change mitigation (Deb et al., 2015).

Although SOC geochemical investigation (*e.g.*, elemental analysis of C by dry combustion) is costly, time-consuming, and requires large numbers of soil samples, it is mandatory for the calibration and validation of new smart techniques (Smith et al., 2020).

In the last decade, some authors (Minasny et al., 2013; Scharlemann et al., 2014; Sanderman et al., 2017; Keskin et al., 2019; Sothe et al., 2022) described the rising interest on digital soil carbon mapping. In fact, the spatial distribution of soil carbon and related maps are useful to: i) define a baseline of carbon level, ii) provide soil information to farmers and policy makers, iii) identify areas affected by SOC gain and loss; and iv) feed models with new data. However, to predict SOC distributions and model a prevision for future concentrations, a number of covariates should also be taken into account (*e.g.*, bulk density, coarse mineral fragments, parent materials, climate, topography, and biotic factors). Therefore, use of physical proprieties measured *in situ* (*e.g.*, electrical conductivity using non-invasive electromagnetic induction; Salani et al., 2022) or using

spaceborne remote sensing (*e.g.*, spectroscopy as Visible Near Infrared –VNIR – reflectance; Biney et al., 2021; Vaudour et al., 2022) are spreading methods to achieve a prediction of SOC distribution. Among these indirect methods aimed at an economic, quick and accurate SOC quantification, spectroscopy is certainly one of the most promising (Ben-Dor et al., 2009; Nocita et al., 2015; Angelopoulou et al., 2019; Wang et al., 2022). Despite being rapid and cost effective, the spectroscopic approach also presents limiting factors such as the complex statistical processing and modelling (Li et al., 2022). In fact, Angelopoulou et al. (2019) suggested that although the sensor technology is constantly developing, the systematic exploitation of satellite imagery suffers of some limitations (*e.g.*, roughness, soil moisture, vegetation cover) that can preclude correct SOC estimations.

The spectroscopic analysis exploits spectral VNIR libraries used to predict OC distribution at large scale (*e.g.*, ISRIC World Soil Reference Collection (Batjes, 2009), LUCAS (Tóth et al., 2013), USDA Rapid Carbon Assessment (Wills et al., 2014; Viscarra Rossel et al., 2016). Because detailed spectral libraries are based on a collection of local studies built independently by different protocols for soil and spectral analyses, their application for SOC prediction in large areas provided results affected by a significantly lower accuracy with respect to those obtained by elemental analyses (Stevens et al., 2013). O'Rourke and Holden (2011) and Li et al. (2022) highlighted how approaches using this type of data to predict SOC need significant amounts of *in situ* data and predictions for large periods, and the cost of updating model can be a limitation. In addition, Sanderman et al. (2021) suggested that changes to soil carbon storage due to land use changes can made biased results of prediction that can only be avoided with accurate analysis of organic carbon fractions.

For these reasons, in this study we tried to merge the information derived by the spatial distribution of soil C fractions (total carbon – TC –, soil organic carbon – SOC –, and inorganic carbon – IC –) of 100 topsoil samples (0-15 cm in depth), with spectral data of the PRISMA satellite (Italian Space Agency Precursore IperSpettrale della Missione Applicative) (Pignatti et al., 2013), to predict OC contents using the machine learning technique of Artificial Neural Network (ANN). Using ADAM platform (https://adamplatform.eu) *in situ* NDVI product by Sentinel-2 was also obtained and compared to recognize phenological cycles.

### 8.1.2 Soil Organic Carbon changes in agricultural context

Nowadays agriculture is still the main human activity able to guarantee food production for global needs and the global products of crop can currently satisfy an overall of 9.7 billion of persons (global population expected in 2050; Berners-Lee et al., 2018). However, Sanderman et al. (2017) escribed that since the introduction of the agriculture (~8000 years ago), a large emission of Greenhouse gases (GHGs), as carbon dioxide ($CO_2$; ~550 Gt), were released in the atmosphere. Such huge emission corresponds to ~150 Gt of soil organic carbon (SOC) loss. In fact, the mineralization of soil organic matter (SOM), which lead to the SOC depletion and $CO_2$ emissions, is enhanced by agricultural practices that break down and expose to air the soil aggregates, promoting the microbial activity (Wang et al., 2011; Kibet et al., 2016). Globally, Lal et al. (2007) estimated that agricultural land could have lost from 30% to 75% of the pristine SOC stock. However, the land use change from stressed to a more sustainable managed agroforestry (*e.g.*, afforestation, carbon farming, no- and minimum-tillage) could also invert the role of the soil from source to sink of C (Lal, 2004a; Brombin et al., 2020; Khan and Chiti, 2022).

In any case, numerous studies currently verified the depletion in order to define loss of C at different scales as follow: from small scale (*e.g.*, Global: Friedlingstein et al., 2022; European: Carozzi et al., 2022, Ferreira et al., 2022; Italian: Khan and Chiti, 2022), to farm-detailed scale (*e.g.*, Brombin et al., 2020; Arunrat et al., 2022; Krauss et al., 2022) As suggested by Smith et al. (2020) and Mattila et al. (2022), monitoring of C gain or loss should be carried out every 3-5 years at farm scale, in order to establish effective solutions that limit GHG emissions.

In the Mediterranean area, characterized by warm and dry climate, SOM contents are typically low (<2%) and very low (<1%) (EIP-AGRI, 2015) and the SOC is particularly affected by oxidation processes (Ferreira et al., 2022). For these reasons the conservation of SOM in these vulnerable countries, including Italy, is a critical issue which should be tackled in order to guarantee the fertility of soils, as well as to limit the GHG emissions. Therefore, we attempted to predict SOC in the evolving context of agricultural soils from the easternmost sector of the Padanian plain (Ferrara province, Northern Italy) the biggest agrarian area of Italy.

## 8.2 Results and discussions

### 8.2.1 Laboratory analyses

Distributions of the soil parameters analyzed in JDS area are reported in Figure 45 as box and whiskers plots. The complete analytical dataset is reported in Supplementary table E1 (in appendix 8).

In particular, thermogravimetric analyses are revealed that LOI 105°C, which represents gypsum and hygroscopic water contents, varied between 0.30 wt% and 7.43 wt%, with an average of 2.23 wt%. LOI 550°C, which represents SOM contents, was between 2.14 wt% and 20.97 wt%, with an average of 7.40 wt%. LOI 1000°C, which represents carbonates and clay minerals, had a range between 1.96 wt% and 8.87 wt%, with an average of 5.25 wt% (Figure 45a).

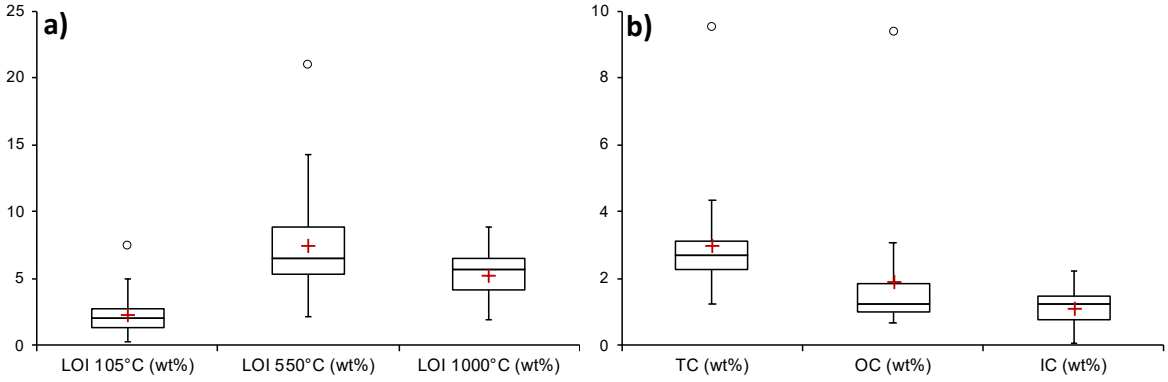


**Figure 45.** Box and whiskers distribution plots of the results of the analyzed topsoils: a) Thermogravimetric analyses (*i.e.,* LOI 105°C, LOI 550°C, and LOI 1000°C), and b) elemental carbon speciation (*i.e.,* TC, OC, and IC). Average (red cross) and median (black line) values are also reported.

The results of carbon speciation indicated that TC varied between 1.21 wt% and 9.50 wt%, with an average 2.96 wt%. OC values were between 0.68 wt% and 9.34 wt%, with an average 1.87 wt%. IC had a range between 0.05 wt% and 2.20 wt%, with an average of 1.09 wt% (Figure 45b).

### 8.2.2 Time series of the Sentinel-2 NDVI

For each investigated parcel a complete time series of the NDVI of Seninel-2 in the period December 2016 - December 2021 was downloaded from the ADAM platform. In general, in this period NDVI varied from –0.18 to 0.87, with an average of 0.28. Such values represent bare soul and dense vegetation conditions, respectively. In fact, NDVI values lower than 0.2 are typical of soil with no cover vegetation, on the contrary values higher

than 0.7 are typical of strength green vegetation at the peak of growth. For these reasons, using the time series we recognized bare soil conditions and the phenological cycle (Griffith et al., 2002; Zhong et al., 2015) of each crop that covered the investigated parcel of JDS. Therefore, the time series of the monthly averaged NDVI is reported in Figure 46a. Moreover, for the entire 2021 we recognized that 37/100 parcels were cultivated from before January to June with winter wheat (Figure 46b), on the contrary 47/100 parcel were covered by vegetation from May to October with maize, soybean, and rice (Figure 46c). Whereas the remaining 16/100 parcels were not cultivated, or with several phenological cycles (*i.e.,* horticulture crops).

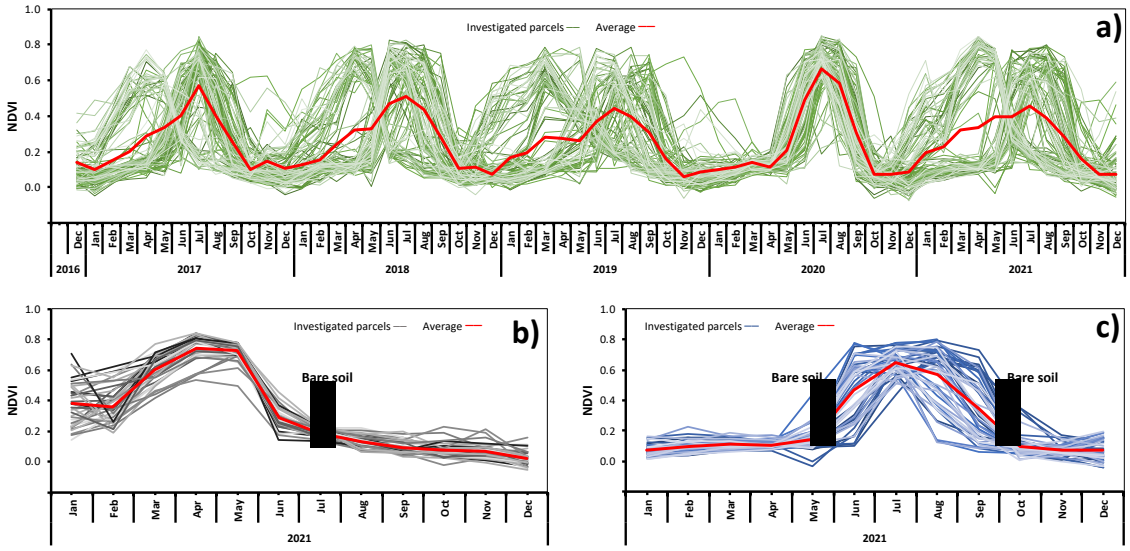


**Figure 46.** a) Sentinel-2 NDVI time series of the 100 investigated parcel for the period December 2016-December 2021; b) Sentinel-2 NDVI time series in 2021 of 37 investigated parcel that show a phenological cycle typical of winter wheat (bare soil conditions are under the brown field); c) Sentinel-2 NDVI time series in 2021 of 47 investigated parcel that show a phenological cycle typical of summer cultivars as maize soybean and rice (bare soil conditions are under the brown field). Averaged time series are represented by red curve.

For each investigated parcel the minimum NDVI values of Sentinel-2 are related to soil conditions. Despite the weak correlation, we can observe that the smaller the NDVI index, the smaller LOI 105°C, LOI 550°C, TC, and OC (Figure 47a, b, d, and e). On the contrary, NDVI correlates positively with both LOI 1000°C and IC (Figure 47c and f). Such conditions are probably imputable to the color of the bare soil. In particular high presence of black material, as occurs in the peaty soils of JDS or finer soils mainly composed by clay are related to the lower NDVI values. Meanwhile, soils with high presence of

carbonates and coarse material, which can cause SOM degradation and OC depletions, are related to higher NDVI values.

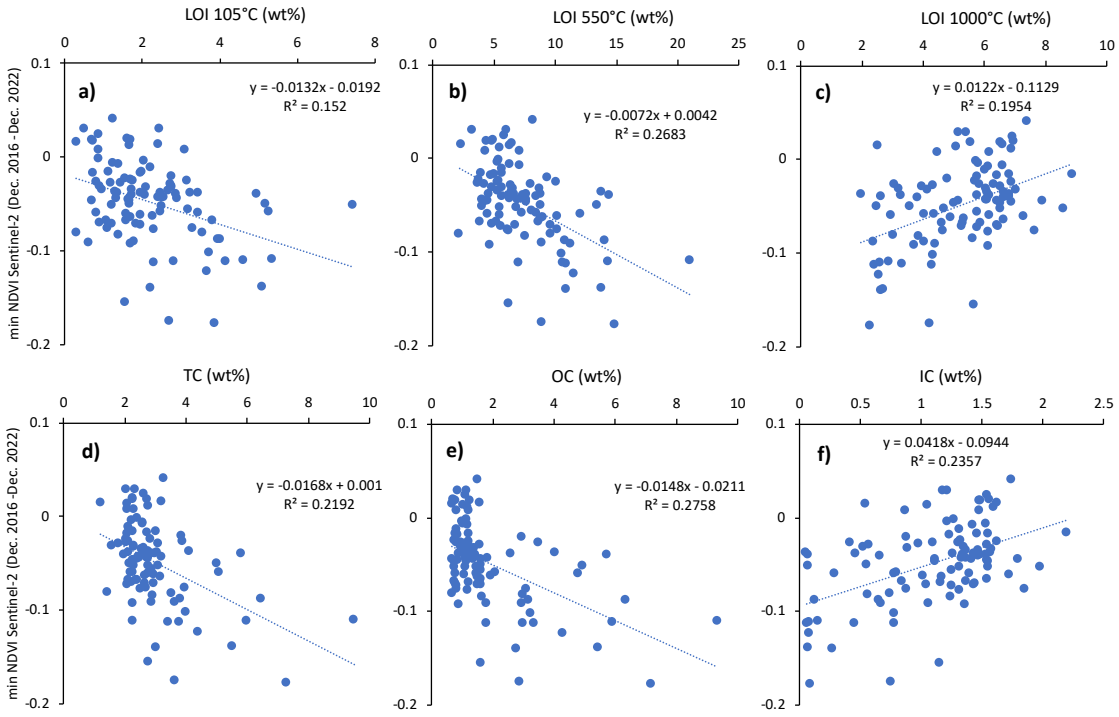


**Figure 47.** Minimum calculated Sentinel-2 NDVI (Period: December 2016-December 2021) vs: a) LOI 105°C, b) LOI 550°C, c) LOI 1000°C, d) TC, e) OC, and f) IC.

### 8.2.3 Artificial Neural Network results

Using the dataset of just 100 samples, we avoided setting a portion aside to act as validation data for ANN. In particular, we used 70% of the samples for ANN training and 30% for testing. Thus, we iterated the training and testing process multiple times, always making a different random selection of the training and testing data. To avoid excessive fluctuating results between one iteration and the next, we always performed 100 iterations. With the best results obtained with the configuration of 1 layer with 100 neurons. In Table 10 is reported for each parameter the resulting $R^2$ mean and standard deviation after 100 interactions. Overall, the best result obtained when using PRISMA spectra was the $R^2$ ~0.66 that we found by preprocessing and feeding to the ANN the first derivative of the PRISMA reflectance spectra taken from the 20200407 hyperspectral pixels corresponding to the locations from which we collected our 100 soil samples.

**Table 10.** Neural network performance with different soil quantities. The $R^2$ mean and standard deviation are computed over the 100 iterations.

| Quantity | $R^2$ | |
|---|---|---|
| | Mean | Std |
| OC (wt%) | 0.60 | 0.19 |
| LOI 550°C (wt%) | 0.52 | 0.20 |
| TC (wt%) | 0.50 | 0.24 |
| LOI 1000°C (wt%) | 0.48 | 0.13 |
| IC (wt%) | 0.45 | 0.14 |
| LOI 105°C (wt%) | 0.31 | 0.24 |

## 8.3 Conclusions

This study reported an *ab initio* approach to predict soil organic carbon in a territory with high soil variability. In fact, observing Figure 48, such variability of the organic contents (OC varies from 0.7 to 9.3 wt%), which can also occur in few meters (also within a pixel), also constrained the ANN results (max $R^2$ 0.6) and suggesting a future implementation of the dataset with other precise ground truth.

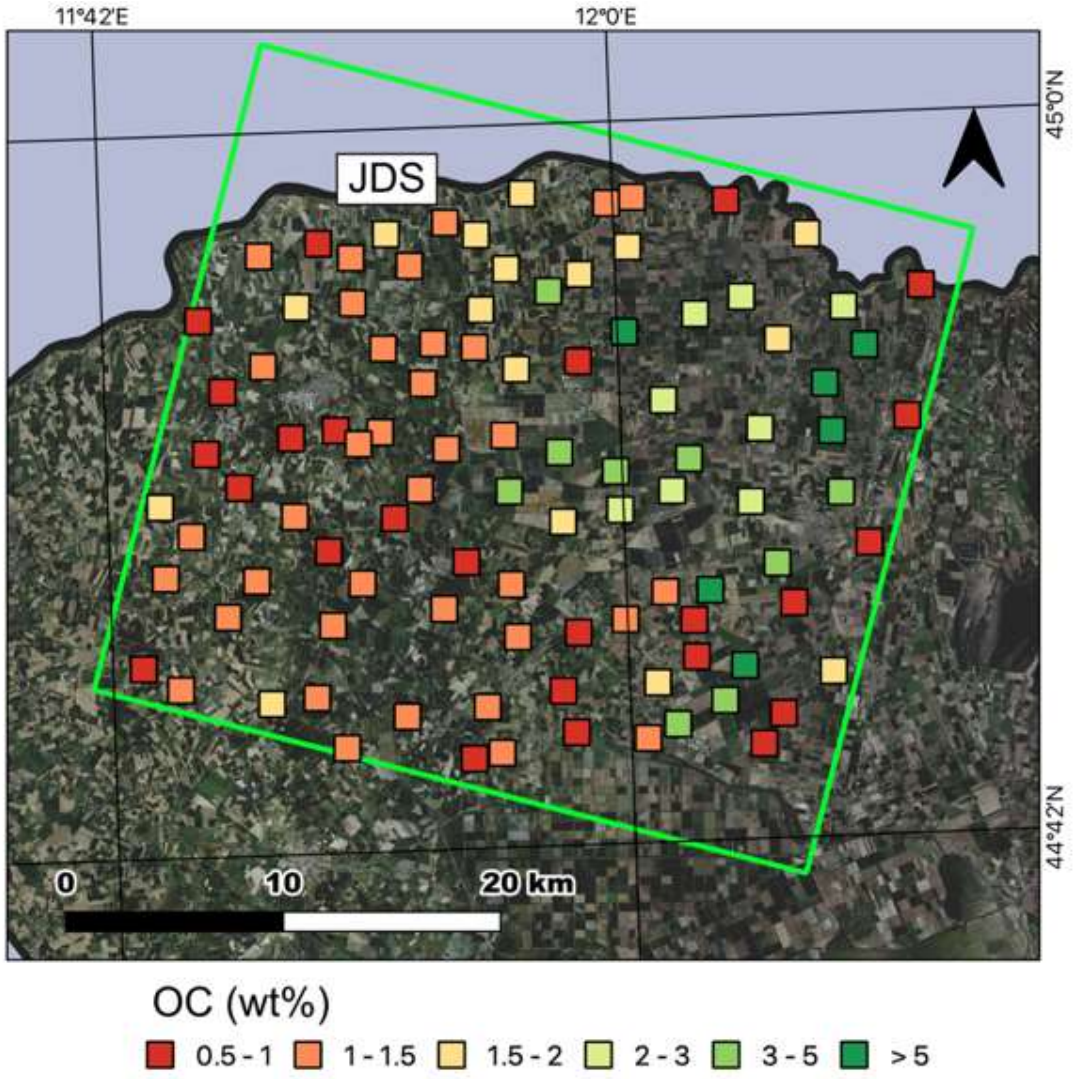


**Figure 48.** 100 topsoil OC contents in JDS.

We also provided that in future with the same procedure applied in this study we could achieve an $R^2$ ~0.8 (Figure 49). Thus, with a better resulting prediction we can create spectral libraries also to predict OC in a bigger area, such as the Ferrara province, and to estimate the soil degradation. This approach could be useful for policy makers and farmers to decide future land use and agricultural managements.

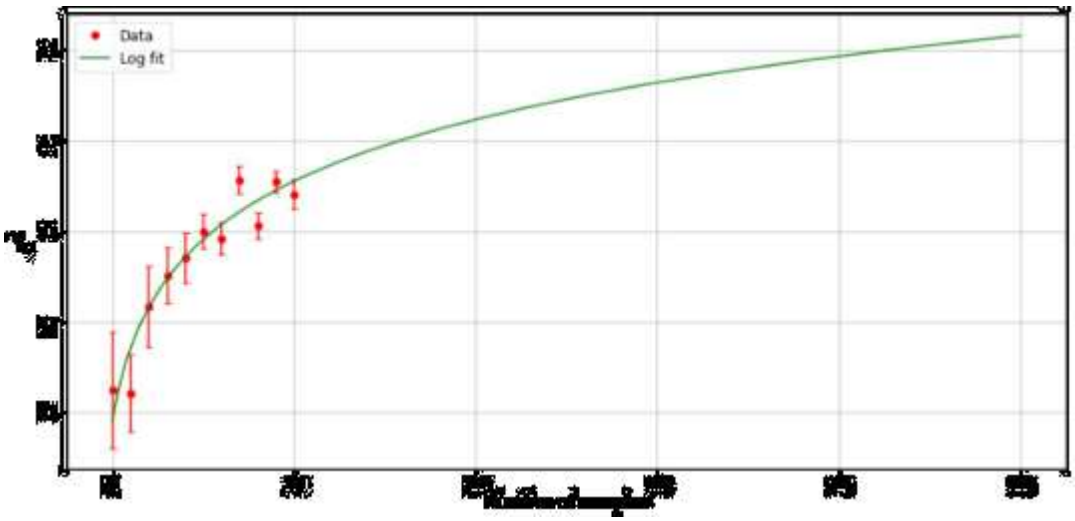


**Figure 49.** Training and testing dataset size vs $R^2$ averaged over 200 possible subsets with the given size of the main 100-sample dataset. The data are fitted with the curve $R^2 = 0.10 \log(N + 0.24) - 45.74$.

# Appendix 8

**Supplementary Table E1.** The complete dataset of the soil investigated in Jolanda di Savoia (JDS).

| Sample | Latit. | Long. | TC (wt%) | OC (wt%) | IC (wt%) | LOI 105°C (wt%) | LOI 550°C (wt%) | LOI 1000°C (wt%) |
|---|---|---|---|---|---|---|---|---|
| GMS22-01 | 44.95347 | 11.82749 | 2.18 | 0.79 | 1.40 | 0.81 | 4.50 | 6.17 |
| GMS22-02 | 44.94705 | 11.84639 | 2.66 | 1.49 | 1.17 | 2.28 | 8.96 | 5.32 |
| GMS22-03 | 44.95643 | 11.86723 | 2.68 | 1.63 | 1.04 | 1.84 | 9.60 | 5.27 |
| GMS21-01 | 44.94291 | 11.88035 | 1.96 | 1.30 | 0.66 | 1.73 | 8.42 | 3.80 |
| GMS21-02 | 44.96028 | 11.90197 | 2.61 | 1.19 | 1.42 | 1.38 | 7.07 | 6.11 |
| GMS21-03 | 44.95485 | 11.91966 | 2.96 | 1.94 | 1.02 | 1.96 | 10.16 | 4.90 |
| GMS21-04 | 44.94025 | 11.93648 | 2.27 | 1.81 | 0.46 | 2.80 | 7.02 | 3.30 |
| GMS21-05 | 44.97123 | 11.94750 | 3.27 | 1.52 | 1.75 | 1.25 | 8.16 | 7.40 |
| GMS21-06 | 44.93037 | 11.96075 | 4.11 | 4.05 | 0.05 | 2.67 | 13.75 | 1.96 |
| GMS12-01 | 44.93699 | 11.97897 | 2.91 | 1.67 | 1.25 | 1.38 | 7.59 | 5.64 |
| GMS12-02 | 44.96603 | 11.99626 | 2.59 | 1.06 | 1.54 | 1.24 | 6.32 | 6.61 |
| GMS12-03 | 44.94759 | 12.00776 | 2.87 | 1.82 | 1.06 | 1.80 | 8.93 | 4.41 |
| GMS12-04 | 44.96819 | 12.01146 | 3.09 | 1.11 | 1.98 | 1.22 | 5.47 | 8.58 |
| GMS12-05 | 44.91874 | 12.04571 | 3.64 | 2.97 | 0.67 | 0.61 | 11.27 | 3.71 |
| GMS12-06 | 44.96543 | 12.06601 | 2.31 | 0.76 | 1.55 | 0.71 | 4.17 | 6.54 |
| GMS12-07 | 44.92523 | 12.07299 | 3.78 | 3.00 | 0.78 | 2.31 | 10.86 | 4.29 |
| GMS11-01 | 44.90711 | 12.09327 | 2.16 | 1.60 | 0.55 | 1.68 | 8.81 | 3.55 |
| GMS11-02 | 44.95035 | 12.11237 | 3.16 | 1.61 | 1.55 | 1.71 | 8.83 | 6.64 |
| GMS11-03 | 44.91971 | 12.13222 | 3.03 | 2.76 | 0.27 | 2.22 | 10.86 | 2.64 |
| GMS11-04 | 44.90342 | 12.14368 | 6.46 | 6.33 | 0.13 | 4.02 | 14.06 | 2.39 |
| GMS11-05 | 44.92744 | 12.17779 | 2.06 | 0.85 | 1.22 | 0.50 | 3.18 | 5.17 |
| GMS23-01 | 44.92289 | 11.75622 | 2.30 | 0.82 | 1.48 | 0.87 | 4.31 | 6.17 |
| GMS23-02 | 44.89318 | 11.76888 | 2.68 | 0.83 | 1.85 | 1.09 | 6.13 | 7.65 |
| GMS23-03 | 44.94900 | 11.79278 | 2.30 | 1.41 | 0.89 | 2.10 | 8.74 | 4.13 |
| GMS23-04 | 44.90313 | 11.79300 | 2.78 | 1.21 | 1.57 | 1.29 | 6.44 | 6.80 |
| GMS23-05 | 44.92733 | 11.81369 | 3.11 | 1.56 | 1.54 | 1.44 | 8.03 | 6.51 |
| GMS23-06 | 44.92825 | 11.84646 | 2.27 | 1.15 | 1.12 | 1.67 | 7.62 | 5.01 |
| GMS24-01 | 44.87428 | 11.85987 | 2.85 | 1.23 | 1.63 | 1.69 | 5.40 | 6.89 |
| GMS24-02 | 44.90900 | 11.86336 | 2.86 | 1.38 | 1.48 | 2.87 | 7.35 | 6.73 |
| GMS24-03 | 44.89384 | 11.88576 | 2.70 | 1.26 | 1.43 | 2.46 | 6.69 | 6.16 |
| GMS24-04 | 44.91034 | 11.89257 | 2.58 | 1.11 | 1.47 | 2.06 | 5.62 | 6.63 |
| GMS24-05 | 44.86642 | 11.89807 | 2.98 | 1.44 | 1.53 | 1.97 | 6.18 | 6.82 |
| GMS24-06 | 44.90816 | 11.91650 | 2.08 | 1.22 | 0.87 | 3.09 | 7.13 | 4.45 |
| GMS24-07 | 44.92376 | 11.92089 | 3.21 | 1.59 | 1.62 | 0.72 | 6.51 | 6.61 |
| GMS24-08 | 44.87121 | 11.93198 | 2.37 | 1.22 | 1.16 | 1.60 | 5.17 | 5.31 |
| GMS24-09 | 44.89851 | 11.94035 | 2.73 | 1.62 | 1.11 | 2.56 | 6.93 | 5.15 |
| GMS13-01 | 44.86338 | 11.96374 | 5.08 | 4.79 | 0.29 | 3.43 | 12.08 | 2.94 |
| GMS13-02 | 44.90084 | 11.97647 | 2.11 | 0.74 | 1.37 | 1.08 | 3.84 | 5.87 |
| GMS13-03 | 44.85460 | 11.99610 | 3.43 | 3.37 | 0.06 | 4.16 | 10.59 | 2.40 |
| GMS13-04 | 44.91239 | 12.00407 | 9.50 | 9.34 | 0.16 | 5.36 | 20.97 | 2.87 |

| Sample | Latit. | Long. | TC (wt%) | OC (wt%) | IC (wt%) | LOI 105°C (wt%) | LOI 550°C (wt%) | LOI 1000°C (wt%) |
|---|---|---|---|---|---|---|---|---|
| GMS13-05 | 44.88340 | 12.02530 | 3.63 | 2.88 | 0.76 | 2.70 | 8.89 | 4.23 |
| GMS13-06 | 44.84578 | 12.02850 | 3.54 | 2.98 | 0.56 | 3.55 | 9.64 | 3.85 |
| GMS13-07 | 44.85885 | 12.03902 | 4.38 | 4.30 | 0.08 | 3.67 | 11.49 | 2.54 |
| GMS14-01 | 44.84013 | 12.07412 | 2.87 | 2.07 | 0.80 | 2.48 | 7.27 | 4.35 |
| GMS14-02 | 44.87038 | 12.08090 | 3.84 | 2.96 | 0.88 | 2.75 | 9.39 | 4.79 |
| GMS14-03 | 44.88809 | 12.11971 | 5.99 | 5.91 | 0.08 | 4.61 | 14.29 | 2.59 |
| GMS14-04 | 44.86830 | 12.12275 | 7.28 | 7.19 | 0.09 | 3.87 | 14.90 | 2.26 |
| GMS14-05 | 44.84270 | 12.12674 | 3.96 | 3.08 | 0.88 | 3.30 | 10.17 | 4.63 |
| GMS14-06 | 44.82144 | 12.14210 | 1.44 | 0.69 | 0.74 | 0.31 | 2.14 | 3.02 |
| GMS14-07 | 44.87334 | 12.16686 | 1.22 | 0.68 | 0.54 | 0.30 | 2.28 | 2.50 |
| GMS32-01 | 44.84605 | 11.73040 | 2.95 | 1.51 | 1.43 | 1.23 | 6.74 | 6.45 |
| GMS32-02 | 44.83354 | 11.74805 | 2.58 | 1.11 | 1.47 | 0.97 | 6.44 | 6.62 |
| GMS32-03 | 44.86754 | 11.75811 | 2.25 | 0.80 | 1.44 | 0.89 | 4.82 | 6.42 |
| GMS32-04 | 44.85316 | 11.77674 | 2.31 | 0.96 | 1.36 | 0.89 | 4.88 | 6.04 |
| GMS32-05 | 44.87301 | 11.80801 | 2.28 | 0.79 | 1.49 | 0.69 | 4.37 | 6.53 |
| GMS32-06 | 44.84041 | 11.80860 | 2.57 | 1.20 | 1.37 | 1.73 | 5.29 | 6.10 |
| GMS32-07 | 44.87563 | 11.83407 | 2.27 | 0.71 | 1.56 | 1.62 | 4.89 | 6.95 |
| GMS31-01 | 44.82560 | 11.82758 | 2.40 | 0.85 | 1.55 | 1.65 | 4.44 | 6.88 |
| GMS31-02 | 44.86969 | 11.84706 | 2.50 | 1.18 | 1.32 | 2.31 | 6.22 | 6.11 |
| GMS31-03 | 44.81176 | 11.84658 | 2.72 | 1.38 | 1.34 | 3.45 | 7.64 | 6.11 |
| GMS31-04 | 44.83837 | 11.86657 | 2.26 | 0.90 | 1.36 | 1.71 | 4.65 | 6.13 |
| GMS31-05 | 44.84998 | 11.88181 | 2.77 | 1.46 | 1.31 | 2.51 | 6.84 | 6.52 |
| GMS31-06 | 44.81918 | 11.90740 | 2.48 | 0.68 | 1.80 | 1.32 | 4.00 | 7.88 |
| GMS31-07 | 44.84789 | 11.93383 | 5.02 | 4.95 | 0.07 | 5.19 | 13.46 | 2.47 |
| GMS42-01 | 44.80919 | 11.93308 | 2.78 | 1.37 | 1.42 | 2.89 | 7.67 | 6.43 |
| GMS42-02 | 44.83448 | 11.96446 | 3.20 | 1.84 | 1.37 | 2.50 | 7.22 | 6.09 |
| GMS42-03 | 44.78828 | 11.97119 | 2.25 | 0.79 | 1.47 | 1.13 | 3.97 | 6.81 |
| GMS42-04 | 44.83859 | 11.99793 | 3.06 | 2.60 | 0.46 | 3.23 | 8.86 | 3.26 |
| GMS42-05 | 44.79306 | 11.99869 | 2.08 | 1.04 | 1.05 | 2.40 | 6.32 | 5.09 |
| GMS42-06 | 44.80386 | 12.02244 | 2.76 | 1.17 | 1.60 | 1.66 | 5.52 | 6.89 |
| GMS41-01 | 44.79173 | 12.03855 | 2.13 | 0.81 | 1.32 | 2.20 | 5.70 | 6.03 |
| GMS41-02 | 44.77656 | 12.03931 | 3.02 | 0.83 | 2.20 | 1.98 | 5.68 | 8.87 |
| GMS41-03 | 44.80396 | 12.04860 | 5.81 | 5.74 | 0.07 | 4.96 | 14.41 | 2.63 |
| GMS41-04 | 44.77222 | 12.06710 | 5.51 | 5.44 | 0.07 | 5.09 | 13.80 | 2.68 |
| GMS41-05 | 44.81420 | 12.08807 | 3.90 | 3.48 | 0.42 | 3.15 | 10.04 | 3.06 |
| GMS41-06 | 44.79755 | 12.09702 | 2.14 | 0.88 | 1.26 | 1.35 | 4.58 | 5.75 |
| GMS41-07 | 44.76853 | 12.11841 | 2.78 | 1.62 | 1.15 | 1.57 | 6.20 | 5.65 |
| GMS33-01 | 44.77921 | 11.71769 | 2.09 | 0.83 | 1.26 | 1.97 | 5.60 | 5.76 |
| GMS33-02 | 44.81641 | 11.73227 | 2.75 | 1.20 | 1.55 | 0.72 | 5.05 | 6.40 |
| GMS33-03 | 44.76994 | 11.73904 | 2.43 | 1.10 | 1.33 | 2.41 | 6.32 | 6.06 |
| GMS33-04 | 44.79951 | 11.76773 | 2.41 | 1.14 | 1.27 | 0.88 | 5.41 | 5.74 |
| GMS33-05 | 44.81416 | 11.78519 | 2.64 | 1.10 | 1.54 | 0.86 | 5.86 | 6.93 |
| GMS33-06 | 44.76299 | 11.79163 | 2.43 | 1.59 | 0.84 | 3.81 | 8.65 | 4.60 |
| GMS34-01 | 44.76491 | 11.81793 | 1.78 | 1.21 | 0.57 | 2.74 | 6.37 | 3.96 |

| Sample | Latit. | Long. | TC (wt%) | OC (wt%) | IC (wt%) | LOI 105°C (wt%) | LOI 550°C (wt%) | LOI 1000°C (wt%) |
|---|---|---|---|---|---|---|---|---|
| GMS34-02 | 44.79466 | 11.82857 | 2.26 | 1.49 | 0.78 | 5.28 | 8.46 | 4.02 |
| GMS34-03 | 44.74365 | 11.83439 | 2.78 | 1.06 | 1.72 | 1.59 | 5.46 | 7.27 |
| GMS34-04 | 44.75591 | 11.86997 | 2.05 | 1.07 | 0.98 | 1.18 | 4.17 | 4.33 |
| GMS34-05 | 44.80007 | 11.89351 | 2.23 | 1.01 | 1.22 | 2.03 | 5.33 | 5.82 |
| GMS43-01 | 44.73747 | 11.90806 | 2.11 | 0.81 | 1.31 | 1.76 | 5.27 | 5.85 |
| GMS43-02 | 44.75872 | 11.91673 | 2.73 | 1.25 | 1.48 | 1.71 | 4.80 | 5.56 |
| GMS43-03 | 44.73949 | 11.92432 | 2.34 | 1.16 | 1.18 | 2.43 | 6.05 | 5.41 |
| GMS43-04 | 44.78736 | 11.93576 | 2.62 | 1.04 | 1.58 | 2.75 | 6.56 | 7.04 |
| GMS43-05 | 44.76428 | 11.96106 | 2.06 | 0.73 | 1.32 | 1.55 | 3.80 | 5.70 |
| GMS43-06 | 44.74688 | 11.96791 | 2.08 | 0.85 | 1.23 | 1.95 | 4.79 | 5.78 |
| GMS43-07 | 44.74340 | 12.00944 | 1.59 | 1.07 | 0.53 | 2.76 | 5.67 | 3.21 |
| GMS43-08 | 44.76636 | 12.01615 | 2.88 | 1.62 | 1.26 | 3.18 | 8.07 | 5.75 |
| GMS44-01 | 44.74882 | 12.02706 | 4.02 | 3.24 | 0.78 | 3.73 | 10.49 | 4.33 |
| GMS44-02 | 44.75804 | 12.05484 | 3.83 | 3.17 | 0.65 | 3.95 | 10.78 | 4.03 |
| GMS44-03 | 44.73951 | 12.07659 | 2.07 | 0.98 | 1.09 | 0.81 | 3.70 | 6.31 |
| GMS44-04 | 44.75176 | 12.08854 | 2.29 | 0.74 | 1.55 | 7.43 | 4.06 | 4.70 |

# 9. General conclusions

This thesis represents an overview on the soil carbon contents and fluxes in Ferrara province (Northeastern Italy) using innovative and sophisticated methods. In this thesis the nature, as well as the spatial and temporal evolution of the Soil Organic Matter (SOM) in the Ferrara soils were investigated in detail. In addition, the distribution of the soil organic carbon (SOC) contents, the relative isotopic signature, and the $CO_2$ equivalent emissions were mapped in the entire Ferrara province.

The described topic is extremely interesting and not only brings scientific curiosity but also practical views.

First of all, the definition of Carbon (as well as Nitrogen and Sulphur) elemental contents and isotopic signatures in the Ferrara soils resulted to be a new useful proxy to assess the sediment provenance (*i.e.*, Alpine and Apennine contributions conveyed Po and Reno Rivers, respectively) and, in future, it could be a new tool to recognize anomalies due by pollutants, as they are related to the Cr-Ni backgrounds, already investigated in previous works.

Other legacies of this document can be resumed by the SOC data comparison of 1937 with those of 2022. Since XIX century, Ferrara province was affected by several reclamation processes and by a massive land-use land-cover-change. The comparison of the SOC data collected in 1937, before the last reclamations, and those collected today (in 2022), allowed us to verify the degradation of SOM in the Ferrara province occurred in 85 years. Such inventories were also useful to estimate the SOC stock loss and to calculate the amount of $CO_2$ eq released in the atmosphere. This topic demonstrates the consequence of the land-use and land-cover-change in the long term, as well as the importance of a long-monitoring of soils, in order to assess the SOM and SOC trends and take actions to prevent any ecosystem damage. Future studies to valorize the survey dataset could be an evaluation of microbial communities and fungal also to delineate current fingerprints and fate of the SOM.

This thesis also highlighted a particular case study of accelerate SOM degradation occurring in soil profiles of Mezzano Lowland (eastern part of Ferrara province), which host peatlands. In this area the natural peat burning process was documented: such phenomenon is a rare event in nature and it is due to the concomitant upraising of deep methane and its exothermal oxidation. In this particular context, a differential consumption of the carbon pools with distinct thermal stabilities were observed with a total consumption of the labile organic carbon and variably decrease of the residual oxidable carbon contents.

The burning of these soils induces i) the release of greenhouse gases, ii) the loss of soil structure and nutrients (*e.g.,* nitrogen), and possibly iii) the release of toxic elements (*e.g.,* heavy metals). Therefore, this unique case-study shed a light on the extreme consequences of the SOM depletion.

This thesis demonstrated the importance of the soil long-monitoring both at small- and large-scale; therefore, two pilot studies were introduced to provide fast techniques to monitor the quality and quantity of SOM both at the small-scale (*i.e.*, farm-scale) and at the large-scale (*i.e.*, the province scale).

For the small-scale SOC monitoring, a new method combining geochemical (elemental and isotopic carbon speciation) and *in-situ* geophysical method (electrical conductivity measurement) was tested to assess the SOC of a farm in Ferrara province. The SOC distribution was mapped in the entire area with kriging technique, also using the geophysical measurement of electrical conductivity (measured at 10 kHz) as covariate variable. This method could be employed to assess the OC benchmarking of an area and then to monitor the SOC stocks, in line with the Common Agriculture Policies of the European Union, which incentive the farmers to certify their capability of sequester C using agricultural best-practices.

Finally, for the large-scale SOC monitoring, this thesis presented a preliminary approach to predict in a fast and detailed way the OC content in the soils of the Ferrara province combining the geochemical soil analyses with the remote-sensing technologies and multi- and hyper-spectral data. Despite the use of artificial neural networks, this approach has proved to be bold. In fact, spectral libraries able to predict OC in a big area (*e.g.*, the Ferrara province) can be created only with a massive use of ground data, which still implies a large collection of soil samples and the related laboratory analyses.

In conclusion, this thesis demonstrates the relatively poor quality of the soils of the Ferrara province, which host low quantities of SOM and SOC, due to perpetuation of the massive land-use and land-cover-change activities, which are occurring since the XIX century. The depletion of SOM has induced, and is still promoting, the release of greenhouse gas emissions in the atmosphere with catastrophic long-term effects on climate. This situation is more concerning when soils particularly enriched in OM (*e.g.*, peatlands) are involved. Therefore, the development of fast, innovative, and cost-affordable techniques for a continuous soil-monitoring at both small- and large-scale should be encouraged.

## References


Abram, N.J., Henley, B.J., Gupta, S.A., Lippmann, T.J.R., Clarke, H., Dowdy, A.J., Sharples, J.J., Nolan, R.H., Zhang, T., Wooster, M.J., Wurtzel, J.B., Meissner, K.J., Pitman, A.J., Ukkola, A.M., Murphy, B.P., Tapper Nigel J. and Boer, M.M., 2021. Connections of climate change and variability to large and extreme forest fires in southeast Australia. *Communications Earth & Environment* 2, 8. https://doi.org/10.1038/s43247-020-00065-8

ADAM platform [WWW Document], n.d. URL https://adamplatform.eu (accessed 12.31.21).

Agnoletti, M., Cargnello, G., Gardin, L., Santoro, A., Bazzoffi, P., Sansone, L., Pezza, L., Belfiore, N., 2011. Traditional landscape and rural development: comparative study in three terraced areas in northern, central and southern Italy to evaluate the efficacy of GAEC standard 4.4 of cross compliance. *Italian Journal of Agronomy* 6, e16. https://doi.org/10.4081/ija.2011.6.s1.e16

Ahmed, Z.U., n.d. geospatial-r-github.io [WWW Document]. URL https://github.com/zia207/geospatial-r-github.io (accessed 3.29.22).

Ahmed, Z.U., Woodbury, P.B., Sanderman, J., Hawke, B., Jauss, V., Solomon, D., Lehmann, J., 2017. Assessing soil carbon vulnerability in the Western USA by geospatial modeling of pyrogenic and particulate carbon stocks. *Journal of Geophysical Research: Biogeosciences* 122, 354–369. https://doi.org/10.1002/2016JG003488

Allison, F.E., 1973. Soil Organic Matter and its role in crop production. Elsevier Scientific Publication Company, New York, N.Y.

Alvarez, C., Alvarez, C.R., Costantini, A., Basanta, M., 2014. Carbon and nitrogen sequestration in soils under different management in the semi-arid Pampa (Argentina). *Soil & Tillage Research* 142, 25–31. https://doi.org/10.1016/j.still.2014.04.005

Amorosi, A., 2012. Chromium and nickel as indicators of source-to-sink sediment transfer in a Holocene alluvial and coastal system (Po Plain, Italy). *Sedimentary Geology* 280, 260–269. https://doi.org/10.1016/j.sedgeo.2012.04.011

Amorosi, A., Barbieri, G., Bruno, L., Campo, B., Drexler, T.M., Hong, W., Rossi, V., Sammartino, I., Scarponi, D., Vaiani, S.C., Bohacs, K.M., 2019. Three-fold nature of coastal progradation during the Holocene eustatic highstand, Po Plain, Italy – close correspondence of stratal character with distribution patterns. *Sedimentology* 66, 3029–3052. https://doi.org/10.1111/sed.12621

Amorosi, A., Bruno, L., Campo, B., di Martino, A., Sammartino, I., 2021. Patterns of geochemical variability across weakly developed paleosol profiles and their role as regional stratigraphic markers (Upper Pleistocene, Po Plain). *Palaeogeography,*

*Palaeoclimatology, Palaeoecology* 574, 110413. https://doi.org/10.1016/j.palaeo.2021.110413

Amorosi, A., Centineo, M.C., Dinelli, E., Lucchini, F., Tateo, F., 2002. Geochemical and mineralogical variations as indicators of provenance changes in Late Quaternary deposits of SE Po Plain. *Sedimentary Geology* 151, 273–292. https://doi.org/10.1016/S0037-0738(01)00261-5

Anderson, D.W., 1988. The effect of parent material and soil development on nutrient cycling in temperate ecosystems. *Biogeochemistry* 5, 71–97. https://doi.org/10.1007/BF02180318

Angelopoulou, T., Tziolas, N., Balafoutis, A., Zalidis, G., Bochtis, D., 2019. Remote Sensing Techniques for Soil Organic Carbon Estimation: A Review. *Remote Sensing* 11, 676. https://doi.org/10.3390/rs11060676

Angileri, V., Loudjani, P., Serafini, F., 2011. GAEC implementation in the EU: situation and perspectives. *Italian Journal of Agronomy* 6, e2. https://doi.org/10.4081/ija.2011.6.s1.e2

Arneth, A., Sitch, S., Pongratz, J., Stocker, B.D., Ciais, P., Poulter, B., Bayer, A.D., Bondeau, A., Calle, L., Chini, L.P., Gasser, T., Fader, M., Friedlingstein, P., Kato, E., Li, W., Lindeskog, M., Nabel, J.E.M.S., Pugh, T.A.M., Robertson, E., Viovy, N., Yue, C., Zaehle, S., 2017. Historical carbon dioxide emissions caused by land-use changes are possibly larger than assumed. *Nature Geoscience* 10, 79–84. https://doi.org/10.1038/ngeo2882

Arunrat, N., Sereenonchai, S., Kongsurakan, P., Hatano, R., 2022. Soil organic carbon and soil erodibility response to various land-use changes in northern Thailand. *Catena* 219, 106595. https://doi.org/10.1016/j.catena.2022.106595

ASI, 2020. PRISMA Products Specification Document–- Issue 2.3. Agenzia Spaziale Italiana.

Bai, Z., Caspari, T., Gonzalez, M.R., Batjes, N.H., Mäder, P., Bünemann, E.K., de Goede, R., Brussaard, L., Xu, M., Ferreira, C.S.S., Reintam, E., Fan, H., Mihelič, R., Glavan, M., Tóth, Z., 2018. Effects of agricultural management practices on soil quality: A review of long-term experiments for Europe and China. *Agriculture, Ecosystems and Environment* 265, 1–7. https://doi.org/10.1016/j.agee.2018.05.028

Balabanova, B., Stafilov, T., Šajn, R., Tănăselia, C., 2016. Geochemical hunting of lithogenic and anthropogenic impacts on polymetallic distribution (Bregalnica river basin, Republic of Macedonia). *Journal of Environmental Science and Health, Part A* 51, 1180–1194. https://doi.org/10.1080/10934529.2016.1206389

Baldocchi, D., Ryu, Y., Keenan, T., 2016. Terrestrial Carbon Cycle Variability. *F1000Research* 5, 2371. https://doi.org/10.12688/f1000research.8962.1

Balesdent, J., Chenu, C., Balabane, M., 2000. Relationship of soil organic matter dynamics to physical protection and tillage. *Soil & Tillage Research* 53, 215–230. https://doi.org/10.1016/S0167-1987(99)00107-5

Ball, B.C., Scott, A., Parker, J.P., 1999. Field $N_2O$, $CO_2$ and $CH_4$ fluxes in relation to tillage, compaction and soil quality in Scotland. *Soil & Tillage Research* 53, 29–39. https://doi.org/10.1016/S0167-1987(99)00074-4

Barbieri, M., Sappa, G., Nigro, A., 2018. Soil pollution: Anthropogenic versus geogenic contributions over large areas of the Lazio region. *Journal of Geochemical Exploration* 195, 78–86. https://doi.org/10.1016/j.gexplo.2017.11.014

Bateman, A.S., Kelly, S.D., 2007. Fertilizer nitrogen isotope signatures. *Isotopes in Environmental and Health Studies* 43, 237–247. https://doi.org/10.1080/10256010701550732

Batjes, N.H., 2009. Harmonized soil profile data for applications at global and continental scales: updates to the WISE database. *Soil Use and Management* 25, 124–127. https://doi.org/10.1111/j.1475-2743.2009.00202.x

Batjes, N.H., 1996. Total carbon and nitrogen in the soils of the world. *European Journal of Soil Science* 47, 151–163. https://doi.org/10.1111/j.1365-2389.1996.tb01386.x

Bazzoffi, P., Zaccarini Bonelli, C., 2011. Cross compliance GAEC standards implemented in Italy: environmental effectiveness and strategic perspectives. *Italian Journal of Agronomy* 6, e1. https://doi.org/10.4081/ija.2011.6.s1.e1

Beccaluva, L., Bianchini, G., Natali, C., Siena, F., 2017. The alkaline-carbonatite complex of Jacupiranga (Brazil): Magma genesis and mode of emplacement. *Gondwana Research* 44, 157–177. https://doi.org/10.1016/j.gr.2016.11.010

Beka, S., Burgess, P.J., Corstanje, R., Stoate, C., 2022. Spatial modelling approach and accounting method affects soil carbon estimates and derived farm-scale carbon payments. *Science of the Total Environment* 827, 154164. https://doi.org/10.1016/j.scitotenv.2022.154164

Belyea, L.R., Malmer, N., 2004. Carbon sequestration in peatland: patterns and mechanisms of response to climate change. *Global Change Biology* 10, 1043–1052. https://doi.org/10.1111/j.1529-8817.2003.00783.x

Ben-Dor, E., Chabrillat, S., Demattê, J.A.M., Taylor, G.R., Hill, J., Whiting, M.L., Sommer, S., 2009. Using Imaging Spectroscopy to study soil properties. *Remote Sensing of Environment* 113, S38–S55. https://doi.org/10.1016/j.rse.2008.09.019

Berners-Lee, M., Kennelly, C., Watson, R., Hewitt, C.N., 2018. Current global food production is sufficient to meet human nutritional needs in 2050 provided there is radical societal

adaptation. *Elementa: Science of the Anthropocene* 6, 52. https://doi.org/10.1525/elementa.310

Bertolini, G., Cazzoli, M.A., Centineo, M.C., Cibin, U., Martini, A., 2008. The Geological Landscape of Emilia-Romagna scale 1:250.000.

Bianchini, G., Accorsi, C., Cremonini, S., De Feudis, M., Forlani, L., Salani, G.M., Vianello G., Vittori Antisari, L., 2022. Late Glacial and Holocene buried black soils in Emilia (northern Italy): genetic and paleoenvironmental insights. *Journal of Soils and Sediments* 22, 409–428. https://doi.org/10.1007/s11368-021-03088-6

Bianchini, G., Brombin, V., Carlino, P., Mistri, E., Natali, C., Salani, G.M., 2021. Traceability and authentication of manila clams from North-Western Adriatic lagoons using C and N stable isotope analysis. *Molecules*, 26, 1859. https://doi.org/10.3390/molecules26071859

Bianchini, G., Cremonini, S., Di Giuseppe, D., Gabusi, R., Marchesini, M., Vianello, G., Vittori Antisari, L., 2019. Late Holocene palaeo-environmental reconstruction and human settlement in the eastern Po Plain (northern Italy). *Catena* 176, 324–335. https://doi.org/10.1016/j.catena.2019.01.025

Bianchini, G., Cremonini, S., Di Giuseppe, D., Vianello, G., Vittori Antisari, L., 2014. Multiproxy investigation of a Holocene sedimentary sequence near Ferrara (Italy): clues on the physiographic evolution of the eastern Padanian Plain. *Journal of Soils and Sediments* 14, 230–242. https://doi.org/10.1007/s11368-013-0791-2

Bianchini, G., Di Giuseppe, D., Natali, C., Beccaluva, L., 2013. Ophiolite inheritance in the Po Plain sediments: Insights on heavy metals distribution and risk assessment. *Ofioliti* 38, 1–14. https://doi.org/10.4454/ofioliti.v38i1.412

Bianchini, G., Laviano, R., Lovo, S., Vaccaro, C., 2002. Chemical-mineralogical characterisation of clay sediments around Ferrara (Italy): a tool for an environmental analysis. *Applied Clay Science* 21, 165–176. https://doi.org/10.1016/S0169-1317(01)00086-2

Bianchini, G., Marrocchino, E., Moretti, A., Vaccaro, C., 2006. Chemical-mineralogical characterization of historical bricks from Ferrara: An integrated bulk and micro-analytical approach. *Geological Society, London, Special Publications* 257, 127–140. https://doi.org/10.1144/GSL.SP.2006.257.01.10

Bianchini, G., Natali, C., Di Giuseppe, D., Beccaluva, L., 2012. Heavy metals in soils and sedimentary deposits of the Padanian Plain (Ferrara, Northern Italy): characterisation and biomonitoring. *Journal of Soils and Sediments* 12, 1145–1153. https://doi.org/10.1007/s11368-012-0538-5

Biney, J.K.M., Saberioon, M., Borůvka, L., Houška, J., Vašát, R., Chapman Agyeman, P., Coblinski, J.A., Klement, A., 2021. Exploring the suitability of UAS-based multispectral iImages for estimating Soil Organic Carbon: comparison with proximal soil sensing and spaceborne imagery. *Remote Sensing* 13, 308. https://doi.org/10.3390/rs13020308

Blanco-Canqui, H., Lal, R., 2004. Mechanisms of Carbon sequestration in soil aggregates. Critical *Reviews in Plant Sciences* 23, 481–504. https://doi.org/10.1080/07352680490886842

Boaga, J., 2017. The use of FDEM in hydrogeophysics: A review. *Journal of Applied Geophysics* 139, 36–46. https://doi.org/10.1016/j.jappgeo.2017.02.011

Boehm, H.-D. v., Siegert, F., Riele, J.O., Page, S.E., Jauhiainen, J., Vasanser, H., Jaya, A., 2001. Fire impacts and carbon release on tropical peatlands in Central Kalimantan, Indonesia, in: *Proceedings of the 2nd Asian Conference on Remote Sensing*, Singapore.

Bondesan, M., 1989. Evoluzione geomorfologica ed idrografica della pianura ferrarese, in: Visser Travagli, A.M., Vighi, G. (Eds.), *Terre Ed Acqua-Le Bonifiche Ferraresi Nel Delta Del Po*. Corbo, G., Ferrara, pp. 13–20.

Bonzi, L., Ferrari, V., Martinelli, G., Norelli, E., Severi, P., 2017. Unusual geological phenomena in the Emilia-Romagna plain (Italy): gas emissions from wells and the ground, hot water wells, geomorphological variations. A review and an update of documented reports. *Bollettino di Geofisica Teorica ed Applicata* 58, 87–102. https://doi.org/10.4430/bgta0193

Borrelli, L., Colecchia, S., Troccoli, A., Caradonna, S., Papini, R., Ventrella, D., Dell'Abate, M.T., Galeffi, C., Tomasoni, C., Farina, R., 2011. Effectiveness of the GAEC standard of cross compliance Crop rotations in maintaining organic matter levels in soils. *Italian Journal of Agronomy* 6, e8. https://doi.org/10.4081/ija.2011.6.s1.e8

Boschi, V., Spallacci, P., 1974. Caratteristiche chimiche e agronomiche dei terreni salini della nuova bonifica del Mezzano. *Annali dell'Istituto Sperimentale Agronomico*. Sezione di Modena. Fasc. II. Pubbl. n. 4. 26

Bossio, D.A., Cook-Patton, S.C., Ellis, P.W., Fargione, J., Sanderman, J., Smith, P., Wood, S., Zomer, R.J., von Unger, M., Emmer, I.M., Griscom, B.W., 2020. The role of soil carbon in natural climate solutions. *Nature Sustainability* 2020 3, 391–398. https://doi.org/10.1038/s41893-020-0491-z

Bouchez, J., Gaillardet, J., France-Lanord, C., Maurice, L., Dutra-Maia, P., 2011. Grain size control of river suspended sediment geochemistry: Clues from Amazon River depth profiles. *Geochemistry, Geophysics, Geosystems* 12, 3. https://doi.org/10.1029/2010GC003380

Bouwman, A.F., 1990. Exchange of Greenhouse Gases between Terrestrial Ecosystems and the Atmosphere, in: Bouwman, A.F. (Ed.), *Soils and the Greenhouse Effect*. John Wiley and Sons, New York, pp. 61–127.

Bowen, G.J., 2010. Isoscapes: Spatial Pattern in Isotopic Biogeochemistry. *Annual Review of Earth and Planetary Sciences* 38, 161–187. https://doi.org/10.1146/annurev-earth-040809-152429

Box, G.E.P., Cox, D.R., 1964. An analysis of transformation. *Journal of the Royal Statistical Society*, 211–252.

Brombin, V., Mistri, E., Feudis, M. de, Forti, C., Salani, G.M., Natali, C., Falsone, G., Antisari, L.V., Bianchini, G., 2020. Soil carbon investigation in three pedoclimatic and agronomic settings of northern Italy. *Sustainability* 12, 1–19. https://doi.org/10.3390/su122410539

Bronick, C.J., Lal, R., 2005. Soil structure and management: a review. *Geoderma* 124, 3–22. https://doi.org/10.1016/j.geoderma.2004.03.005

Bünemann, E.K., Bongiorno, G., Bai, Z., Creamer, R.E., de Deyn, G., de Goede, R., Fleskens, L., Geissen, V., Kuyper, T.W., Mäder, P., Pulleman, M., Sukkel, W., van Groenigen, J.W., Brussaard, L., 2018. Soil quality – A critical review. *Soil Biology and Biochemistry* 120, 105–125. https://doi.org/10.1016/j.soilbio.2018.01.030

Burke, I., Elliott, E., Cole, C., 1995. Influence of macroclimate, landscape position, and management on Soil Organic Matter in agroecosystems. *Ecological Applications* 5, 124–131. https://doi.org/10.2307/1942057

Burke, J., Byrnes, R., Fankhauser, S., 2019. How to price carbon to reach net-zero emissions in the UK.

Calamita, G., Perrone, A., Brocca, L., Onorati, B., Manfreda, S., 2015. Field test of a multi-frequency electromagnetic induction sensor for soil moisture monitoring in southern Italy test sites. *Journal of Hydrology* 529, 316–329. https://doi.org/10.1016/j.jhydrol.2015.07.023

Camino-Serrano, M., Tifafi, M., Balesdent, J., Hatté, C., Peñuelas, J., Cornu, S., Guenet, B., 2019. Including Stable Carbon Isotopes to Evaluate the Dynamics of Soil Carbon in the Land-Surface Model ORCHIDEE. *Journal of Advances in Modeling Earth Systems* 11, 3650–3669. https://doi.org/10.1029/2018MS001392

Cammeraat, L.H., Imeson, A.C., 1999. The evolution and significance of soil–vegetation patterns following land abandonment and fire in Spain. *Catena* 37, 107–127. https://doi.org/10.1016/S0341-8162(98)00072-1

Campo, B., Bruno, L., Amorosi, A., 2020. Basin-scale stratigraphic correlation of late Pleistocene-Holocene (MIS 5e-MIS 1) strata across the rapidly subsiding Po Basin

(northern Italy). *Quaternary Science Reviews* 237, 106300. https://doi.org/10.1016/j.quascirev.2020.106300

Capaccioni, B., Tassi, F., Cremonini, S., Sciarra, A., Vaselli, O., 2015. Ground heating and methane oxidation processes at shallow depth in Terre Calde di Medolla (Italy): Observations and conceptual model. *Journal of Geophysical Research: Solid Earth* 120, 3048–3064. https://doi.org/10.1002/2014JB011635

Caporale, A.G., Violante, A., 2016. Chemical processes affecting the mobility of heavy metals and metalloids in soil environments. *Current Pollution Reports* 2, 15–27. https://doi.org/10.1007/s40726-015-0024-y

Carozzi, M., Martin, R., Klumpp, K., Massad, R.S., 2022. Effects of climate change in European croplands and grasslands: Productivity, greenhouse gas balance and soil carbon storage. *Biogeosciences* 19, 3021–3050. https://doi.org/10.5194/BG-19-3021-2022

CFI, 2011. Carbon Credits (Carbon Farming Initiative) Act.

Chen, L., Liu, L., Qin, S., Yang, G., Fang, K., Zhu, B., Kuzyakov, Y., Chen, P., Xu, Y., Yang, Y., 2019. Regulation of priming effect by soil organic matter stability over a broad geographic scale. *Nature Communications* 10, 1–10. https://doi.org/10.1038/s41467-019-13119-z

Chorover, J., Kretzschmar, R., Garcia-Pichel, F., Sparks, D.L., 2007. Soil Biogeochemical Processes within the Critical Zone. *Elements* 3, 321–326. https://doi.org/10.2113/gselements.3.5.321

Christophersen, M., Kjeldsen, P., Holst, H., Chanton, J., 2001. Lateral gas transport in soil adjacent to an old landfill: factors governing emissions and methane oxidation. *Waste Management & Research* 19, 595–612. https://doi.org/10.1177/0734242X0101900616

Cloern, J.E., Canuel, E.A., Harris, D., 2002. Stable carbon and nitrogen isotope composition of aquatic and terrestrial plants of the San Francisco Bay estuarine system. *Limnology and Oceanography* 47, 713–729. https://doi.org/10.4319/lo.2002.47.3.0713

Colombani, N., Salemi, E., Mastrocicco, M., Castaldelli, G., 2011. Groundwater nitrogen speciation in intensively cultivated lowland areas, in: *Advances in the Research of Aquatic Environment*. Springer Berlin Heidelberg, Berlin, Heidelberg, pp. 291–298. https://doi.org/10.1007/978-3-642-24076-8_34

Copland, S., 2020. Anti-politics and global climate inaction: the case of the Australian Carbon Tax. *Critical sociology* 46, 623–641. https://doi.org/10.1177/0896920519870230

Coplen, T.B., Qi, H., 2012. USGS42 and USGS43: Human-hair stable hydrogen and oxygen isotopic reference materials and analytical methods for forensic science and implications

for published measurement results. *Forensic Science International* 214, 135–141. https://doi.org/10.1016/j.forsciint.2011.07.035

Corbau, C., Simeoni, U., Zoccarato, C., Mantovani, G., Teatini, P., 2019. Coupling land use evolution and subsidence in the Po Delta, Italy: Revising the past occurrence and prospecting the future management challenges. *Science of the Total Environment* 654, 1196–1208. https://doi.org/10.1016/j.scitotenv.2018.11.104

Corwin, D.L., Kaffka, S.R., Hopmans, J.W., Mori, Y., van Groenigen, J.W., van Kessel, C., Lesch, S.M., Oster, J.D., 2003. Assessment and field-scale mapping of soil quality properties of a saline-sodic soil. *Geoderma* 114, 231–259. https://doi.org/10.1016/S0016-7061(03)00043-0

Costantini, E.A.C., Angelone, M., Napoli, R., 2002. Soil geochemistry and pedological processes. The case study of the quaternary soils of the Montagnola Senese (central Italy). *Alpine and Mediterranean Quaternary* 15, 111–120.

Craine, J.M., Elmore, A.J., Wang, L., Augusto, L., Baisden, W.T., Brookshire, E.N.J., Cramer, M.D., Hasselquist, N.J., Hobbie, E.A., Kahmen, A., Koba, K., Kranabetter, J.M., Mack, M.C., Marin-Spiotta, E., Mayor, J.R., McLauchlan, K.K., Michelsen, A., Nardoto, G.B., Oliveira, R.S., Perakis, S.S., Peri, P.L., Quesada, C.A., Richter, A., Schipper, L.A., Stevenson, B.A., Turner, B.L., Viani, R.A.G., Wanek, W., Zeller, B., 2015a. Convergence of soil nitrogen isotopes across global climate gradients. *Scientific Reports* 5, 1–8. https://doi.org/10.1038/srep08280

Craine, J.M., Ventures, J., Cramer, M D, Hasselquist, N J, Koba, K, Marin-Spiotta, E, Wang, L, 2015b. Ecological interpretations of nitrogen isotope ratios of terrestrial plants and soils. *Plant Soil* 396, 1–26. https://doi.org/10.1007/s11104-015-2542-1

Cremonini, S., 1989. Morfoanalisi della veteroidrografia centese. Approccio semiquantitativo ad un modello evolutivo del dosso fluviale, in: Insediamenti e Viabilità Nell'Alto Ferrarese Dall'eta Romana All'alto Medioevo. Ferrara, pp. 135–175.

Cremonini, S., Etiope, G., Italiano, F., Martinelli, G., 2008. Evidence of possible enhanced peat burning by deep-origin methane in the Po River delta plain (Italy). *Journal of Geology* 116, 401–413. https://doi.org/10.1086/588835

Crowther, T.W., Todd-Brown, K.E.O., Rowe, C.W., Wieder, W.R., Carey, J.C., MacHmuller, M.B., Snoek, B.L., Fang, S., Zhou, G., Allison, S.D., Blair, J.M., Bridgham, S.D., Burton, A.J., Carrillo, Y., Reich, P.B., Clark, J.S., Classen, A.T., Dijkstra, F.A., Elberling, B., Emmett, B.A., Estiarte, M., Frey, S.D., Guo, J., Harte, J., Jiang, L., Johnson, B.R., Kroël-Dulay, G., Larsen, K.S., Laudon, H., Lavallee, J.M., Luo, Y., Lupascu, M., Ma, L.N., Marhan, S., Michelsen, A., Mohan, J., Niu, S., Pendall, E., Peñuelas, J., Pfeifer-Meister,

L., Poll, C., Reinsch, S., Reynolds, L.L., Schmidt, I.K., Sistla, S., Sokol, N.W., Templer, P.H., Treseder, K.K., Welker, J.M., Bradford, M.A., 2016. Quantifying global soil carbon losses in response to warming. *Nature* 540, 104–108. https://doi.org/10.1038/nature20150

Dai, X., Wang, H., Fu, X., 2017. Soil microbial community composition and its role in carbon mineralization in long-term fertilization paddy soils. *Science of the Total Environment* 580, 556–563. https://doi.org/10.1016/j.scitotenv.2016.11.212

Davidson, E.A., Ackerman, I.L., 1993. Changes in soil carbon inventories following cultivation of previously untilled soils. *Biogeochemistry* 20, 161–193. https://doi.org/10.1007/BF00000786

de Brogniez, D., Ballabio, C., Stevens, A., Jones, R.J.A., Montanarella, L., van Wesemael, B., 2015. A map of the topsoil organic carbon content of Europe generated by a generalized additive model. *European Journal of Soil Science* 66, 121–134. https://doi.org/10.1111/ejss.12193

De Clercq, T., Heiling, M., Dercon, G., Resch, C., Aigner, M., Mayer, L., Mao, Y., Elsen, A., Steier, P., Leifeld, J., Merckx, R., 2015. Predicting soil organic matter stability in agricultural fields through carbon and nitrogen stable isotopes. *Soil Biology and Biochemistry* 88, 29–38. https://doi.org/10.1016/j.soilbio.2015.05.011

de Coninck, H., Revi, A., Babiker, M., Bertoldi, P., Buckeridge, M., Cartwright, A., Dong, W., Ford, J., Fuss, S., Hourcade, J.-C., Ley, D., Mechler, R., Newman, P., Revokatova, A., Schultz, S., Steg, L., Sugiyama, T., 2018. Strengthening and Implementing the Global Response, in: Global Warming of 1.5 °C an IPCC Special Report on the Impacts of Global Warming of 1.5 °c above pre-industrial levels and related global greenhouse gas emission pathways, in the context of strengthening the global response to the threat of climate change. *Intergovernmental Panel on Climate Change*.

Dean, W.E., 1974. Determination of carbonate and organic matter in calcareous sediments and sedimentary rocks by loss on ignition; comparison with other methods. *Journal of Sedimentary Research* 44, 242–248.

Deb, S., Bhadoria, P., Mandal, B., Rakshit, A., Singh, H., 2015. Soil organic carbon: Towards better soil health, productivity and climate change mitigation. *Climate Change and Environmental Sustainability* 3, 26–34. https://doi.org/10.5958/2320-642X.2015.00003.4

Di Giuseppe, D., Bianchini, G., Faccini, B., Coltorti, M., 2014a. Combination of wavelength dispersive X-ray fluorescence analysis and multivariate statistic for alluvial soils classification: a case study from the Padanian Plain (Northern Italy). *X-Ray Spectrometry* 43, 165–174. https://doi.org/10.1002/xrs.2535

Di Giuseppe, D., Bianchini, G., Vittori Antisari, L., Martucci, A., Natali, C., Beccaluva, L., 2014b. Geochemical characterization and biomonitoring of reclaimed soils in the Po River Delta (Northern Italy): Implications for the agricultural activities. *Environmental Monitoring and Assessment* 186, 2925–2940. https://doi.org/10.1007/s10661-013-3590-8

Di Giuseppe, D., Vittori Antisari, L., Ferronato, C., Bianchini, G., 2014c. New insights on mobility and bioavailability of heavy metals in soils of the Padanian alluvial plain (Ferrara Province, northern Italy). *Geochemistry* 74, 615–623. https://doi.org/10.1016/j.chemer.2014.02.004

Doetterl, S., Berhe, A.A., Nadeu, E., Wang, Z., Sommer, M., Fiener, P., 2016. Erosion, deposition and soil carbon: A review of process-level controls, experimental tools and models to address C cycling in dynamic landscapes. *Earth Science Reviews* 154, 102–122. https://doi.org/10.1016/j.earscirev.2015.12.005

Domeignoz-Horta, L.A., Shinfuku, M., Junier, P., Poirier, S., Verrecchia, E., Sebag D., DeAngelis, K. M., 2021. Direct evidence for the role of microbial community composition in the formation of soil organic matter composition and persistence. *ISME Communications* 1, 64. https://doi.org/10.1038/s43705-021-00071-7

Doolittle, J., Petersen, M., Wheeler, T., 2001. Comparison of two electromagnetic induction tools in salinity appraisals. *Journal of Soil and Water Conservation* 56, 257–262.

Dutta, K., Schuur, E.A.G., Neff, J.C., Zimov, S.A., 2006. Potential carbon release from permafrost soils of Northeastern Siberia. *Global Change Biology* 12, 2336–2351. https://doi.org/10.1111/j.1365-2486.2006.01259.x

European Commission, 2020. Caring for Soil is Caring for Life. Brussels.

Edwards, P.J., 1998. Sulfur cycling, retention, and mobility in soils: A review. *General Technical Report NE-250. Radnor, PA: U.S. Department of Agriculture, Forest Service, Northeastern Research Station*. 18 p. https://doi.org/10.2737/NE-GTR-250

Ehleringer, J.R., Buchmann, N., Flanagan, L.B., 2000. Carbon isotope ratios in belowground carbon cycle processes. *Ecological Applications* 412, 412–422.

EIP-AGRI, 2015. EIP-AGRI Focus Group on Soil Organic Matter content in Mediterranean regions: Final Report | EIP-AGRI [WWW Document]. URL https://ec.europa.eu/eip/agriculture/en/publications/eip-agri-focus-group-soil-organic-matter-content (accessed 11.2.22).

Emilia-Romagna region, 2015. Carbonio organico immagazzinato nei suoli — Ambiente [WWW Document]. URL https://ambiente.regione.emilia-romagna.it/it/geologia/suoli/proprieta-e-qualita-dei-suoli/carbonio-organico-immagazzinato-nei-suoli (accessed 11.2.22).

Emilia-Romagna region, 2011. 1853- Coperture vettoriali dell'uso del suolo storico- Edizione 2011 (poligoni) — Geoportale [WWW Document]. URL https://geoportale.regione.emilia-romagna.it/catalogo/dati-cartografici/pianificazione-e-catasto/uso-del-suolo/layer-5 (accessed 12.2.22).

ESRI, 2022. ArcMap 10.8.2 [WWW Document]. URL https://my.esri.com/#/my-profile/overview (accessed 11.2.22).

Evans, J., Sharkey, T., Berry, J., Farquhar, G., 1986. Carbon isotope discrimination measured concurrently with gas exchange to investigate $CO_2$ diffusion in leaves of higher plants. *Functional Plant Biology* 13, 281–292. https://doi.org/10.1071/PP9860281

Evans, M.C., 2018. Effective incentives for reforestation: lessons from Australia's carbon farming policies. *Current Opinion in Environmental Sustainability* 32, 38–45. https://doi.org/10.1016/j.cosust.2018.04.002

Fantappié, M., L'Abate, G., Costantini, E.A.C., 2011. The influence of climate change on the soil organic carbon content in Italy from 1961 to 2008. *Geomorphology* 135, 343–352. https://doi.org/10.1016/J.GEOMORPH.2011.02.006

Farina, R., Seddaiu, G., Orsini, R., Steglich, E., Roggero, P.P., Francaviglia, R., 2011. Soil carbon dynamics and crop productivity as influenced by climate change in a rainfed cereal system under contrasting tillage using EPIC. *Soil & Tillage Research* 112, 36–46. https://doi.org/10.1016/j.still.2010.11.002

Ferrari, C., Fiano, E., Sandri, G., 1937. I terreni della provincia di Ferrara. *Annali della sperimentazione agraria* 27.

Ferreira, C.S.S., Seifollahi-Aghmiuni, S., Destouni, G., Ghajarnia, N., Kalantari, Z., 2022. Soil degradation in the European Mediterranean region: Processes, status and consequences. *Science of the Total Environment* 805, 150106. https://doi.org/10.1016/j.scitotenv.2021.150106

Field, J.P., Breshears, D.D., Law, D.J., Villegas, J.C., López-Hoffman, L., Brooks, P.D., Chorover, J., Barron-Gafford, G.A., Gallery, R.E., Litvak, M.E., Lybrand, R.A., McIntosh, J.C., Meixner, T., Niu, G.-Y., Papuga, S.A., Pelletier, J.D., Rasmussen, C.R., Troch, P.A., 2015. Critical zone services: expanding context, constraints, and currency beyond ecosystem services. *Vadose Zone Journal* 14, vzj2014.10.0142. https://doi.org/10.2136/vzj2014.10.0142

Finlay, J.C., Kendall, C., 2007. Stable isotope tracing of temporal and spatial variability in organic matter sources to freshwater ecosystems, in: Michener, R.H., Lajtha, K. (Eds.), *Stable Isotopes in Ecology and Environmental Science*. Blackwell Publishing Ltd, Oxford, UK, pp. 283–333. https://doi.org/10.1002/9780470691854.ch10

Franko, U., Spiegel, H., 2016. Modeling soil organic carbon dynamics in an Austrian long-term tillage field experiment. *Soil & Tillage Research* 156, 83–90. https://doi.org/10.1016/j.still.2015.10.003

Friedlingstein, P., Jones, M.W., O'Sullivan, M., Andrew, R.M., Hauck, J., Peters, G.P., Peters, W., Pongratz, J., Sitch, S., le Quéré, C., dBakker, O.C.E., Canadell1, J.G., Ciais1, P., Jackson, R.B., Anthoni1, P., Barbero, L., Bastos, A., Bastrikov, V., Becker, M., Bopp, L., Buitenhuis, E., Chandra, N., Chevallier, F., Chini, L.P., Currie, K.I., Feely, R.A., Gehlen, M., Gilfillan, D., Gkritzalis, T., Goll, D.S., Gruber, N., Gutekunst, S., Harris, I., Haverd, V., Houghton, R.A., Hurtt, G., Ilyina, T., Jain, A.K., Joetzjer, E., Kaplan, J.O., Kato, E., Goldewijk, K.K., Korsbakken, J.I., Landschützer, P., Lauvset, S.K., Lefèvre, N., Lenton, A., Lienert, S., Lombardozzi, D., Marland, G., McGuire, P.C., Melton, J.R., Metzl, N., Munro, D.R., Nabel, J.E.M.S., Nakaoka, S.I., Neill, C., Omar, A.M., Ono, T., Peregon, A., Pierrot, D., Poulter, B., Rehder, G., Resplandy, L., Robertson, E., Rödenbeck, C., Séférian, R., Schwinger, J., Smith, N., Tans, P.P., Tian, H., Tilbrook, B., Tubiello, F.N., van der Werf, G.R., Wiltshire, A.J., Zaehle, S., 2019. Global carbon budget 2019. *Earth System Science Data* 11, 1783–1838. https://doi.org/10.5194/ESSD-11-1783-2019

Friedlingstein, P., O'Sullivan, M., Jones, M.W., Andrew, R.M., Gregor, L., Hauck, J., le Quéré, C., Luijkx, I.T., Olsen, A., Peters, G.P., Peters, W., Pongratz, J., Schwingshackl, C., Sitch, S., Canadell, J.G., Ciais, P., Jackson, R.B., Alin, S.R., Alkama, R., Arneth, A., Arora, V.K., Bates, N.R., Becker, M., Bellouin, N., Bittig, H.C., Bopp, L., Chevallier, F., Chini, L.P., Cronin, M., Evans, W., Falk, S., Feely, R.A., Gasser, T., Gehlen, M., Gkritzalis, T., Gloege, L., Grassi, G., Gruber, N., Gürses, Ö., Harris, I., Hefner, M., Houghton, R.A., Hurtt, G.C., Iida, Y., Ilyina, T., Jain, A.K., Jersild, A., Kadono, K., Kato, E., Kennedy, D., Klein Goldewijk, K., Knauer, J., Korsbakken, J.I., Landschützer, P., Lefèvre, N., Lindsay, K., Liu, J., Liu, Z., Marland, G., Mayot, N., McGrath, M.J., Metzl, N., Monacci, N.M., Munro, D.R., Nakaoka, S.-I., Niwa, Y., O'Brien, K., Ono, T., Palmer, P.I., Pan, N., Pierrot, D., Pocock, K., Poulter, B., Resplandy, L., Robertson, E., Rödenbeck, C., Rodriguez, C., Rosan, T.M., Schwinger, J., Séférian, R., Shutler, J.D., Skjelvan, I., Steinhoff, T., Sun, Q., Sutton, A.J., Sweeney, C., Takao, S., Tanhua, T., Tans, P.P., Tian, X., Tian, H., Tilbrook, B., Tsujino, H., Tubiello, F., van der Werf, G.R., Walker, A.P., Wanninkhof, R., Whitehead, C., Willstrand Wranne, A., Wright, R., Yuan, W., Yue, C., Yue, X., Zaehle, S., Zeng, J., Zheng, B., 2022. Global Carbon Budget 2022. *Earth System Science Data* 14, 4811–4900. https://doi.org/10.5194/ESSD-14-4811-2022

Fumagalli, M., Acutis, M., Mazzetto, F., Vidotto, F., Sali, G., Bechini, L., 2011. An analysis of agricultural sustainability of cropping systems in arable and dairy farms in an intensively

cultivated plain. *European Journal of Agronomy* 34, 71–82. https://doi.org/10.1016/j.eja.2010.11.001

Galán, E., González, I., Romero, A., Aparicio, P., 2014. A methodological approach to estimate the geogenic contribution in soils potentially polluted by trace elements. Application to a case study. *Journal of Soils and Sediments* 14, 810–818. https://doi.org/10.1007/s11368-013-0784-1

Gambolati, G., Putti, M., Teatini, P., Camporese, M., Ferraris, S., Gasparetto Stori, G., Nicoletti, V., Silvestri, S., Rizzetto, F., Tosi, L., 2005. Peat land oxidation enhances subsidence in the Venice watershed. *Eos, Transactions American Geophysical Union* 86, 217–220. https://doi.org/10.1029/2005EO230001

Gambolati, G., Putti, M., Teatini, P., Gasparetto Stori, G., 2006. Subsidence due to peat oxidation and impact on drainage infrastructures in a farmland catchment south of the Venice Lagoon. *Environmental Geology* 49, 814–820. https://doi.org/10.1007/S00254-006-0176-6

Gao, Y., Tian, J., Pang, Y., Liu, J., 2017. Soil Inorganic Carbon sequestration following afforestation is probably induced by pedogenic carbonate formation in Northwest China. *Frontiers in Plant Science* 8, 1282. https://doi.org/10.3389/fpls.2017.01282

Garcia, A.K., Cavanaugh, C.M., Kacar, B., 2021. The curious consistency of carbon biosignatures over billions of years of Earth-life coevolution. *ISME Journal* 15, 2183–2194. https://doi.org/10.1038/S41396-021-00971-5

Gardi, C., Sconosciuto, F., 2007. Evaluation of carbon stock variation in Northern Italian soils over the last 70 years. *Sustainability Science* 2, 237–243. https://doi.org/10.1007/s11625-007-0034-9

Garzanti, E., Resentini, A., Vezzoli, G., Ando, S., Malusa, M., Padoan, M., 2012. Forward compositional modelling of Alpine orogenic sediments. *Sedimentary Geology* 280, 149–164. https://doi.org/10.1016/j.sedgeo.2012.03.012

Géron, A., 2019. Hands-on Machine Learning with Scikit-Learn and TensorFlow: Concepts, Tools, and Techniques to Build Intelligent Systems, 2nd ed. O'Really Media, Sebastopol, CA, USA.

Gonfiantini, R., Stichler, W., Rozanski, K., 1995. Standards and intercomparison materials distributed by the International Atomic Energy Agency for stable isotope measurements, in: Stichler, W. (Ed.), *Reference and Intercomparison Materials for Stable Isotopes of Light Elements*. IAEA, Vienna, pp. 13–29.

Gonzalez-Vila, F.J., Galmendros, G., 2003. Thermal transformation of soil organic matter by natural fires and laboratory-controlled heatings, in: Ikan, R. (Ed.), *Natural and laboratory-simulated thermal geochemical processes*. pp. 153–200.

Gougoulias, C., Clark, J., Shaw, L., 2014. The role of soil microbes in the global carbon cycle: tracking the below-ground microbial processing of plant-derived carbon for manipulating carbon dynamics in agricultural systems. *Journal of the Science of Food and Agriculture* 94, 2362–2371. https://doi.org/10.1002/jsfa.6577

Granged, A.J.P., Jordan, A., Zavala, L.M., Munoz-Rojas, M., Mataix-Solera, J., 2011a. Short-term effects of experimental fire for a soil under eucalyptus forest (SE Australia). *Geoderma* 167–68, 125–134. https://doi.org/10.1016/j.geoderma.2011.09.011

Granged, A.J.P., Zavala, L.M., Jordan, A., Barcenas-Moreno, G., 2011b. Post-fire evolution of soil properties and vegetation cover in a Mediterranean heathland after experimental burning: A 3-year study. *Geoderma* 164, 85–94. https://doi.org/10.1016/j.geoderma.2011.05.017

Gregorich, E., Greer, K., Anderson, D., Liang, B., 1998. Carbon distribution and losses: erosion and deposition effects. *Soil & Tillage Research* 47, 291–302. https://doi.org/10.1016/S0167-1987(98)00117-2

Griffith, J.A., Martinko, E.A., Whistler, J.L., Price, K.P., 2002. Interrelationships among landscapes, NDVI, and stream water quality in the U.S. central plains. *Ecological Applications* 12, 1702–1718. https://doi.org/10.1890/1051-0761(2002)012[1702:IALNAS]2.0.CO;2

Guillaume, T., Damris, M., Kuzyakov, Y., 2015. Losses of soil carbon by converting tropical forest to plantations: erosion and decomposition estimated by $\delta^{13}C$. *Global Change Biology* 21, 3548–3560. https://doi.org/10.1111/gcb.12907

Gulde, S., Chung, H., Amelung, W., Chang, C., Six, J., 2008. Soil Carbon Saturation Controls Labile and Stable Carbon Pool Dynamics. *Soil Science Society of America Journal* 72, 605–612. https://doi.org/10.2136/sssaj2007.0251.

Gunina, A., Kuzyakov, Y., 2014. Pathways of litter C by formation of aggregates and SOM density fractions: Implications from $^{13}C$ natural abundance. *Soil Biology and Biochemistry* 71, 95–104. https://doi.org/10.1016/j.soilbio.2014.01.011

Guo, Q., Zhu, G., Strauss, H., Peters, M., Chen, T., Yang, J., Wei, R., Tian, L., Han, X., 2016. Tracing the sources of sulfur in Beijing soils with stable sulfur isotopes. *Journal of Geochemical Exploration* 161, 112–118. https://doi.org/10.1016/j.gexplo.2015.11.010

Habicht, K.S., Canfield, D.E., 2001. Isotope fractionation by sulfate-reducing natural populations and the isotopic composition of sulfide in marine sediments. *Geology* 29, 555. https://doi.org/10.1130/0091-7613(2001)029<0555:IFBSRN>2.0.CO;2

Halas, S., Szaran, J., 2001. Improved thermal decomposition of sulfates to SO2 and mass spectrometric determination of ?34S of IAEA SO-5, IAEA SO-6 and NBS-127 sulfate standards. *Rapid Communications in Mass Spectrometry* 15, 1618–1620. https://doi.org/10.1002/rcm.416

Hinwood, A.L., Rodriguez, C.M., 2005. Potential health impacts associated with peat smoke: A review. *Journal of the Royal Society of Western Australia* 88, 133–138.

Hobbie, E.A., Ouimette, A.P., 2009. Controls of nitrogen isotope patterns in soil profiles. *Biogeochemistry* 95, 355–371. https://doi.org/10.1007/s10533-009-9328-6

Hoffland, E., Kuyper, T.W., Comans, R.N.J., Creamer, R.E., 2020. Eco-functionality of organic matter in soils. *Plant Soil* 455, 1–22. https://doi.org/10.1007/s11104-020-04651-9

Horowitz, J.K., Gottlieb, J., 2010. The Role of Agriculture in Reducing Greenhouse Gas Emissions. https://doi.org/10.22004/AG.ECON.138910

Hu, Y., Fernandez-Anez, N., Smith, T.E.L., Rein, G., 2018. Review of emissions from smouldering peat fires and their contribution to regional haze episodes. *International Journal of Wildland Fire* 27, 293–312. https://doi.org/10.1071/WF17084

IPCC, 2014a. Agriculture, forestry and other land use (AFOLU). Climate Change 2014: Mitigation of Climate Change: Working Group III Contribution to the IPCC Fifth Assessment Report (2015).

IPCC, 2014b. Climate Change 2014: Synthesis, Report Contribution of Working Groups I, II and III to the Fifth Assessment Report of the Intergovernmental Panel on Climate Change. Geneva.

IPCC, 2007. Climate change 2007, in: The Physical Science Basis Contribution of Working Group I to the Fourth Assessment Report of the Intergovernmental Panel on Climate Change. Cambridge University Press, Cambridge, UK, pp. 1–966.

Jackson, R.B., Lajtha, K., Crow, S.E., Hugelius, G., Kramer, M.G., Piñeiro, G., 2017. The ecology of Soil Carbon: pools, vulnerabilities, and biotic and abiotic controls. *Annual Review of Ecology, Evolution, and Systematics* 48, 419–445. https://doi.org/10.1146/annurev-ecolsys-112414-054234

Janzen, H.H., Ellert, B.H., Anderson, D.W., 2018. Soil Organic Matter (SOM): Landscape. *Encyclopedia of soil science*.

Johnston, A.E., Poulton, P.R., Coleman, K., 2009. Chapter 1 Soil Organic Matter. Its Importance in Sustainable Agriculture and Carbon Dioxide Fluxes. *Advances in Agronomy* 101, 1–57. https://doi.org/10.1016/S0065-2113(08)00801-8

Joosten, H., Clarke, D., 2002. Wise use of mires and peatlands. *International Mire Conservation Group/International Peat Society*, Saarijärvi, Finland.

Kanstrup, M., Thomsen, I.K., Andersen, A.J., Bogaard, A., Christensen, B.T., 2011. Abundance of $^{13}C$ and $^{15}N$ in emmer, spelt and naked barley grown on differently manured soils: towards a method for identifying past manuring practice. *Rapid Communications in Mass Spectrometry* 25, 2879–2887. https://doi.org/10.1002/rcm.5176

Kassambara, F.M., 2017. Factoextra: Extract and Visualize the Results of Multivariate Data Analyses. R Package Version 1.0.7 [WWW Document]. URL https://CRAN.R–project. org/package=factoextra (accessed 6.22.20).

Katsube, T.J., Klassen, R.A., Das, Y., Ernst, R., Calvert, T., Cross, G., Hunter, J., Best, M., DiLabio, R., Connell, S., 2003. Prediction and validation of soil electromagnetic characteristics for application in landmine detection, in: Harmon, R.S., Holloway, Jr., J.H., Broach, J.T. (Eds.), *Proc. SPIE 5089, Detection and Remediation Technologies for Mines and Minelike Targets VIII, (11 September 2003)* p. 1219. https://doi.org/10.1117/12.486983

Keskin, H., Grunwald, S., Harris, W.G., 2019. Digital mapping of soil carbon fractions with machine learning. *Geoderma* 339, 40–58. https://doi.org/10.1016/j.geoderma.2018.12.037

Khan, M.Z., Chiti, T., 2022. Soil carbon stocks and dynamics of different land uses in Italy using the LUCAS soil database. *Journal of Environmental Management* 306, 114452. https://doi.org/10.1016/j.jenvman.2022.114452

Kibet, L.C., Blanco-Canqui, H., Jasa, P., 2016. Long-term tillage impacts on soil organic matter components and related properties on a Typic Argiudoll. *Soil & Tillage Research* 155, 78–84. https://doi.org/10.1016/J.STILL.2015.05.006

Kirkels, F., de Boer, H., Concha Hernández, P., Martes, C., van der Meer, M., Basu, S., Usman, M., Peterse, F., 2022. Carbon isotopic ratios of modern C3 and C4 vegetation on the Indian peninsula and changes along the plant-soil-river continuum - implications for vegetation reconstructions. *Biogeosciences* 19, 4107–4127. https://doi.org/10.5194/bg-19-4107-2022

Knoepp, J.D., Debano, L.F., Neary, D.G., 2005. Soil chemistry, in: Neary, D.G., Ryan, K.C., Debano, L.F. (Eds.), *Wildland Fire in Ecosystems*: Effects of Fire on Soil and Water. Ogden, UT, pp. 53–71.

Köchy, M., Hiederer, R., Freibauer, A., 2015. Global distribution of soil organic carbon – Part 1: Masses and frequency distributions of SOC stocks for the tropics, permafrost regions, wetlands, and the world. *Soil* 1, 351–365. https://doi.org/10.5194/soil-1-351-2015

Kohlenberg, A.J., Turetsky, M.R., Thompson, D.K., Branfireun, B.A., Mitchell, C.P.J., 2018. Controls on boreal peat combustion and resulting emissions of carbon and mercury. *Environmental Research Letters* 13, 035005. https://doi.org/10.1088/1748-9326/aa9ea8

Kohn, M., 2010. Carbon isotope compositions of terrestrial C3 plants as indicators of (paleo)ecology and (paleo)climate. *Proceedings of the National Academy of Sciences of the United States of America* 107, 19691–19695.

Kragt, M.E., Pannell, D.J., Robertson, M.J., Thamo, T., 2012. Assessing costs of soil carbon sequestration by crop-livestock farmers in Western Australia. *Agricultural Systems* 112, 27–37. https://doi.org/10.1016/j.agsy.2012.06.005

Krauss, M., Wiesmeier, M., Don, A., Cuperus, F., Gattinger, A., Gruber, S., Haagsma, W.K., Peigné, J., Palazzoli, M.C., Schulz, F., van der Heijden, M.G.A., Vincent-Caboud, L., Wittwer, R.A., Zikeli, S., Steffens, M., 2022. Reduced tillage in organic farming affects soil organic carbon stocks in temperate Europe. *Soil & Tillage Research* 216, 105262. https://doi.org/10.1016/j.still.2021.105262

Kreye, J.K., Varner, J.M., Knapp, E.E., 2011. Effects of particle fracturing and moisture content on fire behaviour in masticated fuelbeds burned in a laboratory. *International Journal of Wildland Fire* 20, 308–317. https://doi.org/10.1071/WF09126

Kumar, P., Le, P.V.V., Papanicolaou, A.N.T., Rhoads, B.L., Anders, A.M., Stumpf, A., Wilson, C.G., Bettis, E.A., Blair, N., Ward, A.S., Filley, T., Lin, H., Keefer, L., Keefer, D.A., Lin, Y.F., Muste, M., Royer, T. v., Foufoula-Georgiou, E., Belmont, P., 2018. Critical transition in critical zone of intensively managed landscapes. *Anthropocene* 22, 10–19. https://doi.org/10.1016/j.ancene.2018.04.002

Kusaka, S., Nakano, T., 2014. Carbon and oxygen isotope ratios and their temperature dependence in carbonate and tooth enamel using a GasBench II preparation device. *Rapid Communications in Mass Spectrometry* 28, 563–567. https://doi.org/10.1002/rcm.6799

Kutiel, P., Naveh, Z., Kutiel, H., 1990. The effect of a wildfire on soil nutrients and vegetation in an Aleppo pine forest on Mount Carmel, Israel, in: Goldammer, J.G., Jenkins, M.J. (eds.), *Fire in ecosystem dynamics: Mediterranean and Northern perspectives*. pp. 85–94.

Laceby, J.P., Olley, J., Pietsch, T.J., Sheldon, F., Bunn, S.E., 2015. Identifying subsoil sediment sources with carbon and nitrogen stable isotope ratios. *Hydrological Processes* 29, 1956–1971. https://doi.org/10.1002/hyp.10311

Lal, R., 2018a. Digging deeper: A holistic perspective of factors affecting soil organic carbon sequestration in agroecosystems. *Global Change Biology* 24, 3285–3301. https://doi.org/10.1111/gcb.14054

Lal, R., 2018b. Soil Organic Matter (SOM). *Encyclopedia of soil science*.

Lal, R., 2008. Sequestration of atmospheric $CO_2$ in global carbon pools. *Energy & Environmental Science* 1, 86–100. https://doi.org/10.1039/B809492F

Lal, R., 2004a. Soil carbon sequestration to mitigate climate change. *Geoderma* 123, 1–22. https://doi.org/10.1016/j.geoderma.2004.01.032

Lal, R., 2004b. Soil carbon sequestration impacts on global climate change and food security. *Science* 304, 1623–1627. https://doi.org/ 10.1126/science.1097396

Lal, R., 2001. Soil conservation for C-sequestration. In: Steinhardt, G.C. (Ed.), Sustaining the Global Farm: Selected Papers from the 10th International Soil Conservation Organization Meeting held May 24–29, 1999 at Purdue University and the USDA-ARS National Soil Erosion Research Laboratory, pp. 459–465

Lal, R., 2003. Soil erosion and the global carbon budget. *Environment International* 29, 437–450. https://doi.org/10.1016/S0160-4120(02)00192-7

Lal, R., 1993. Tillage effects on soil degradation, soil resilience, soil quality, and sustainability. *Soil & Tillage Research* 27, 1–8. https://doi.org/10.1016/0167-1987(93)90059-X

Lal, R., Follett, R.F., Stewart, B.A., Kimble, J.M., 2007. Soil carbon sequestration to mitigate climate change and advance food security. *Soil Science* 172, 943–956. https://doi.org/10.1097/ss.0b013e31815cc498

Lal, R., Kimble, J., Follett, R.F., 1998. Pedospheric Processes and the Carbon Cycle, in: Lal, R., Kimble, J.M., Follett, R.F., Stewart, B.A. (Eds*.), Soil Processes and the Carbon Cycle*. CRC Press, Boca Raton, FL, USA, pp. 1–8.

Lal, R., Kimble, J.M., Stewart, B.A., Eswaran, H., 1999. Global climate change and pedogenic carbonates. CRC Press.

Lal, R., Negassa, W., Lorenz, K., 2015. Carbon sequestration in soil. *Current Opinion in Environmental Sustainability* 15, 79–86. https://doi.org/10.1016/j.cosust.2015.09.002

Langmann, B., Heil, A., 2004. Release and dispersion of vegetation and peat fire emissions in the atmosphere over Indonesia 1997/1998. *Atmospheric Chemistry and Physics* 4, 2145–2160. https://doi.org/10.5194/acp-4-2145-2004

Le Quéré, C., Andrew, R.M., Canadell, J.G., Sitch, S., Ivar Korsbakken, J., Peters, G.P., Manning, A.C., Boden, T.A., Tans, P.P., Houghton, R.A., Keeling, R.F., Alin, S., Andrews, O.D., Anthoni, P., Barbero, L., Bopp, L., Chevallier, F., Chini, L.P., Ciais, P., Currie, K., Delire, C., Doney, S.C., Friedlingstein, P., Gkritzalis, T., Harris, I., Hauck, J.,

Haverd, V., Hoppema, M., Klein Goldewijk, K., Jain, A.K., Kato, E., Körtzinger, A., Landschützer, P., Lefèvre, N., Lenton, A., Lienert, S., Lombardozzi, D., Melton, J.R., Metzl, N., Millero, F., Monteiro, P.M.S., Munro, D.R., Nabel, J.E.M.S., Nakaoka, S.I., O'Brien, K., Olsen, A., Omar, A.M., Ono, T., Pierrot, D., Poulter, B., Rödenbeck, C., Salisbury, J., Schuster, U., Schwinger, J., Séférian, R., Skjelvan, I., Stocker, B.D., Sutton, A.J., Takahashi, T., Tian, H., Tilbrook, B., van der Laan-Luijkx, I.T., van der Werf, G.R., Viovy, N., Walker, A.P., Wiltshire, A.J., Zaehle, S., 2016. Global Carbon Budget 2016. *Earth System Science Data* 8, 605–649. https://doi.org/10.5194/ESSD-8-605-2016

Le, S., Josse, J., Husson, F., 2008. FactoMineR: An R package for multivariate analysis. *Journal of Statistical Software* 25, 1–18. https://doi.org/10.18637/jss.v025.i01

Lefèvre, C., Rekik, F., Alcantara, V., Wiese-Rozanov, L., 2017. Soil organic carbon: the hidden potential burial of organic matter for carbon sequestration: Potentials, processes and long-term effects.

Li, S., Viscarra Rossel, R.A., Webster, R., 2022. The cost-effectiveness of reflectance spectroscopy for estimating soil organic carbon. *European Journal of Soil Science* 73, e13202. https://doi.org/10.1111/ejss.13202

Li, S., Xia, X., Zhang, S., Zhang, L., 2020. Source identification of suspended and deposited organic matter in an alpine river with elemental, stable isotopic, and molecular proxies. *Journal of Hydrology* 590, 125492. https://doi.org/10.1016/j.jhydrol.2020.125492

Libohova, Z., Seybold, C., Wysocki, D., Wills, S., Schoeneberger, P., Williams, C., Lindbo, D., Stott, D., Owens, P.R., 2018. Reevaluating the effects of soil organic matter and other properties on available water-holding capacity using the National Cooperative Soil Survey Characterization Database. *Journal of Soil and Water Conservation* 73, 411–421. https://doi.org/10.2489/jswc.73.4.411

Liu, Y., Ge, T., van Groenigen, K.J., Yang, Y., Wang, P., Cheng, K., Zhu, Z., Wang, J., Li, Y., Guggenberger, G., Sardans, J., Penuelas, J., Wu, J., Kuzyakov, Y., 2021. Rice paddy soils are a quantitatively important carbon store according to a global synthesis. *Communications Earth & Environment* 2, 154. https://doi.org/10.1038/s43247-021-00229-0

Macintosh, A., Waugh, L., 2012. An introduction to the Carbon Farming Initiative: key principles and concepts.

Mäkelä, J., Arppe, L., Fritze, H., Heinonsalo, J., Karhu, K., Liski, J., Oinonen, M., Straková, P., Viskari, T., 2022. Implementation and initial calibration of carbon-13 soil organic matter decomposition in the Yasso model. *Biogeosciences* 19, 4305–4313. https://doi.org/10.5194/BG-19-4305-2022

Manzi, V., Roveri, M., Gennari, R., Bertini, A., Biffi, U., Giunta, S., Iaccarino, S.M., Lanci, L., Lugli, S., Negri, A., Riva, A., Rossi, M.E., Taviani, M., 2007. The deep-water counterpart of the Messinian Lower Evaporites in the Apennine foredeep: The Fanantello section (Northern Apennines, Italy). *Palaeogeography, Palaeoclimatology, Palaeoecology* 251, 470–499. https://doi.org/10.1016/j.palaeo.2007.04.012

Marchina, C., Bianchini, G., Knoeller, K., Natali, C., Pennisi, M., Colombani, N., 2016. Natural and anthropogenic variations in the Po river waters (northern Italy): insights from a multi-isotope approach. *Isotopes in Environmental and Health Studies* 52, 649–672. https://doi.org/10.1080/10256016.2016.1152965

Marchina, C., Bianchini, G., Natali, C., Pennisi, M., Colombani, N., Tassinari, R., Knoeller, K., 2015. The Po river water from the Alps to the Adriatic Sea (Italy): new insights from geochemical and isotopic ($\delta^{18}$O-δD) data. *Environmental Science and Pollution Research* 22, 5184–5203. https://doi.org/10.1007/s11356-014-3750-6

Marchina, C., Natali, C., Bianchini, G., 2019. The Po River water isotopes during the drought Ccondition of the year 2017. *Water* 11, 150. https://doi.org/10.3390/w11010150

Marchina, C., Natali, C., Fahnestock, M.F., Pennisi, M., Bryce, J., Bianchini, G., 2018. Strontium isotopic composition of the Po river dissolved load: Insights into rock weathering in Northern Italy. *Applied Geochemistry* 97, 187–196. https://doi.org/10.1016/j.apgeochem.2018.08.024

Marchina, C., Natali, C., Fazzini, M., Fusetti, M., Tassinari, R., Bianchini, G., 2017. Extremely dry and warm conditions in northern Italy during the year 2015: effects on the Po river water. Rendiconti Lincei. Scienze Fisiche e Naturali 28, 281–290. https://doi.org/10.1007/s12210-017-0596-0

Marraccini, E., Debolini, M., di Bene, C., Rapey, H., Bonari, E., 2012. Factors affecting soil organic matter conservation in Mediterranean hillside winter cereals-legumes cropping systems. *Italian Journal of Agronomy* 7, 283–292. https://doi.org/10.4081/ija.2012.e38

Martinelli, G., Cremonini, S., Samonati, E., 2013. The peat fires of Italy. In: Stracher, G.B., Prakash, A., Sokol, E.V. (Eds.), *Coal and Peat Fires, a Global Perspective*, Volume 2: Photographs and Multimedia Tours. Elsevier, Amsterdam, pp. 205–216 https://doi.org/10.1016/B978-0-444-59412-9.00013-2

Martinelli, G., Cremonini, S., Samonati, E., Stracher, G.B., 2015. Italian Peat and Coal fires, in: Stracher, G.B., Prakash, A., Rein G. (Eds.), *Coal and Peat Fires: A Global Perspective*, Volume 4: Peat-Geology Combustion and Case Studies. Elsevier, Amsterdam, pp. 40–73. https://doi.org/10.1016/B978-0-444-59510-2.00003-3

Mastrocicco, M., Colombani, N., Salemi, E., Castaldelli, G., 2010. Numerical assessment of effective evapotranspiration from maize plots to estimate groundwater recharge in lowlands. *Agricultural Water Management* 97, 1389–1398. https://doi.org/10.1016/j.agwat.2010.04.005

Mattila, T.J., Hagelberg, E., Söderlund, S., Joona, J., 2022. How farmers approach soil carbon sequestration? Lessons learned from 105 carbon-farming plans. *Soil & Tillage Research* 215, 105204. https://doi.org/10.1016/J.STILL.2021.105204

Meier, H.A., Driese, S.G., Nordt, L.C., Forman, S.L., Dworkin, S.I., 2014. Interpretation of Late Quaternary climate and landscape variability based upon buried soil macro- and micromorphology, geochemistry, and stable isotopes of soil organic matter, Owl Creek, central Texas, USA. *Catena* 114, 157–168. https://doi.org/10.1016/j.catena.2013.08.019

Meng, X., Bao, Y., Liu, J., Liu, H., Zhang, X., Zhang, Y., Wang, P., Tang, H., Kong, F., 2020. Regional soil organic carbon prediction model based on a discrete wavelet analysis of hyperspectral satellite data. *International Journal of Applied Earth Observation and Geoinformation* 89, 102111. https://doi.org/10.1016/j.jag.2020.102111

Menichetti, L., Houot, S., van Oort, F., Kätterer, T., Christensen, B.T., Chenu, C., Barré, P., Vasilyeva, N.A., Ekblad, A., 2015. Increase in soil stable carbon isotope ratio relates to loss of organic carbon: results from five long-term bare fallow experiments. Oecologia 177, 811–821. https://doi.org/10.1007/s00442-014-3114-4

Minasny, B., Malone, B.P., McBratney, A.B., Angers, D.A., Arrouays, D., Chambers, A., Chaplot, V., Chen, Z.S., Cheng, K., Das, B.S., Field, D.J., Gimona, A., Hedley, C.B., Hong, S.Y., Mandal, B., Marchant, B.P., Martin, M., McConkey, B.G., Mulder, V.L., O'Rourke, S., Richer-de-Forges, A.C., Odeh, I., Padarian, J., Paustian, K., Pan, G., Poggio, L., Savin, I., Stolbovoy, V., Stockmann, U., Sulaeman, Y., Tsui, C.C., Vågen, T.G., van Wesemael, B., Winowiecki, L., 2017. Soil carbon 4 per mille. *Geoderma* 292, 59–86. https://doi.org/10.1016/j.geoderma.2017.01.002

Minasny, B., McBratney, A.B., Malone, B.P., Wheeler, I., 2013. Digital Mapping of Soil Carbon. *Advances in Agronomy* 118, 1–47. https://doi.org/10.1016/B978-0-12-405942-9.00001-3

Miola, A., Bondesan, A., Corain, L., Favaretto, S., Mozzi, P., Piovan, S., Sostizzo, I., 2006. Wetlands in the Venetian po plain (northeastern Italy) during the last glacial maximum: Interplay between vegetation, hydrology and sedimentary environment. *Review of Palaeobotany and Palynology* 141, 53–81. https://doi.org/10.1016/j.revpalbo.2006.03.016

Mistri, E., De Feudis, M., 2021. L'importanza del carbonio organico per la salvaguardia del suolo. *Sapere, Scienza* 36–40.

Moinet, G.Y.K., Moinet, M., Hunt, J.E., Rumpel, C., Chabbi, A., Millard, P., 2020. Temperature sensitivity of decomposition decreases with increasing soil organic matter stability. *Science of the Total Environment* 704, 135460. https://doi.org/10.1016/j.scitotenv.2019.135460

Mondini, C., Coleman, K., Whitmore, A.P., 2012. Spatially explicit modelling of changes in soil organic C in agricultural soils in Italy, 2001–2100: potential for compost amendment. *Agriculture, Ecosystems, and Environment* 153, 24–32. https://doi.org/10.1016/j.agee.2012.02.020

Monroe, M.C., Watts, A.C., Kobziar, L.N., 2009. Where there's fire, there's smoke: Air quality and prescribed burning in Florida Gainesville.

Morari, F., Castrignanò, A., Pagliarin, C., 2009. Application of multivariate geostatistics in delineating management zones within a gravelly vineyard using geo-electrical sensors. *Computers and Electronics in Agriculture* 68, 97–107. https://doi.org/10.1016/j.compag.2009.05.003

Mörchen, R., Lehndorff, E., Diaz, F.A., Moradi, G., Bol, R., Fuentes, B., Klumpp, E., Arnelung, W., 2019. Carbon accrual in the Atacama Desert. *Global and Planetary Change* 181, 102993. https://doi.org/10.1016/j.gloplacha.2019.102993

Moreno, L., Jimenez, M.-E., Aguilera, H., Jimenez, P., de la Losa, A., 2011. The 2009 Smouldering Peat Fire in Las Tablas de Daimiel National Park (Spain). *Fire Technology* 47, 519–538. https://doi.org/10.1007/s10694-010-0172-y

Moyano, F.E., Vasilyeva, N., Bouckaert, L., Cook, F., Craine, J., Curiel Yuste, J., Don, A., Epron, D., Formanek, P., Franzluebbers, A., Ilstedt, U., Kätterer, T., Orchard, V., Reichstein, M., Rey, A., Ruamps, L., Subke, J.-A., Thomsen, I.K., Chenu, C., 2012. The moisture response of soil heterotrophic respiration: interaction with soil properties. *Biogeosciences* 9, 1173–1182. https://doi.org/10.5194/bg-9-1173-2012

Murray, E., 2012. Australia's Carbon Farming Initiative in building resilience for adaptation to climate change in the agriculture sector, in: Meybeck, A., Lankoski, J., Redfern, S., Azzu, N., Gitz, V. (Eds.), Joint FAO/OECD Workshop. Food and Agriculture Organization of the United Nations (FAO), Rome, Italy, pp. 343–344.

Natali, C., Bianchini, G., 2015. Thermally based isotopic speciation of carbon in complex matrices: a tool for environmental investigation. *Environmental Science and Pollution Research* 22, 12162–12173. https://doi.org/10.1007/s11356-015-4503-x

Natali, C., Bianchini, G., Carlino, P., 2020. Thermal stability of soil carbon pools: Inferences on soil nature and evolution. *Thermochimica Acta* 683, 178478. https://doi.org/10.1016/J.TCA.2019.178478

Natali, C., Bianchini, G., Cremonini, S., Salani, G.M., Vianello, G., Brombin, V., Ferrari, M., Vittori Antisari, L., 2021. Peat Soil Burning in the Mezzano Lowland (Po Plain, Italy): Triggering mechanisms and environmental consequences. *GeoHealth* 5, e2021GH000444. https://doi.org/10.1029/2021GH000444

Natali, C., Bianchini, G., Vittori Antisari, L., 2018a. Thermal separation coupled with elemental and isotopic analysis: A method for soil carbon characterisation. *Catena* 164, 150–157. https://doi.org/10.1016/j.catena.2018.02.022

Natali, C., Bianchini, G., Vittori Antisari, L., Natale, M., Tessari, U., 2018b. Carbon and nitrogen pools in Padanian soils (Italy): Origin and dynamics of soil organic matter. *Geochemistry* 78, 490–499. https://doi.org/10.1016/j.chemer.2018.09.001

National Research Council, 2001. Basic Research Opportunities in Earth Science; National Academy. National Academy Press, Washington, DC.

Nelson, D.W., Sommers, L.E., 1996. Total carbon, organic carbon, and organic matter, in: Page, A.L. (Ed.), Methods of Soil Analysis, Part 2. John Wiley & Sons, Madison, WI, USA, pp. 961–1010.

Ngole-Jeme, V.M., 2019. Fire-Induced Changes in soil and implications on soil sorption capacity and remediation methods. *Applied Sciences* 9, 3447. https://doi.org/10.3390/app9173447

Nocita, M., Stevens, A., van Wesemael, B., Aitkenhead, M., Bachmann, M., Barthès, B., ben Dor, E., Brown, D.J., Clairotte, M., Csorba, A., Dardenne, P., Demattê, J.A.M., Genot, V., Guerrero, C., Knadel, M., Montanarella, L., Noon, C., Ramirez-Lopez, L., Robertson, J., Sakai, H., Soriano-Disla, J.M., Shepherd, K.D., Stenberg, B., Towett, E.K., Vargas, R., Wetterlind, J., 2015. Soil Spectroscopy: An Alternative to Wet Chemistry for Soil Monitoring. *Advances in Agronomy* 132, 139–159. https://doi.org/10.1016/bs.agron.2015.02.002

Nordt, L.C., Hallmark, C.T., Wilding, L.P., Boutton, T.W., 1998. Quantifying pedogenic carbonate accumulations using stable carbon isotopes. *Geoderma* 82, 115–136. https://doi.org/10.1016/S0016-7061(97)00099-2

Norman, A.L., Giesemann, A., Krouse, H.R., Jäger, H.J., 2002. Sulphur isotope fractionation during sulphur mineralization: results of an incubation–extraction experiment with a Black Forest soil. *Soil Biology & Biochemistry* 34, 1425–1438. https://doi.org/10.1016/S0038-0717(02)00086-X

Nyobe, J.M., Sababa, E., Bayiga, E.C., Ndjigui, P.-D., 2018. Mineralogical and geochemical features of alluvial sediments from the Lobo watershed (Southern Cameroon): Implications

for rutile exploration. *Comptes Rendus Geoscience* 350, 119–129. https://doi.org/10.1016/j.crte.2017.08.003

Oertel, C., Matschullat, J., Zurba, K., Zimmermann, F., Erasmi, S., 2016a. Greenhouse gas emissions from soils-A review. *Geochemistry* 76, 327–352. https://doi.org/10.1016/j.chemer.2016.04.002

O'Leary, M.H., 1988. Carbon Isotopes in Photosynthesis Fractionation techniques may reveal new aspects of carbon dynamics in plants. *Bioscience* 38, 328–336. https://doi.org/10.2307/1310735

O'Rourke, S.M., Holden, N.M., 2011. Optical sensing and chemometric analysis of soil organic carbon – a cost effective alternative to conventional laboratory methods? *Soil Use and Management* 27, 143–155. https://doi.org/10.1111/J.1475-2743.2011.00337.X

Page, S.E., Siegert, F., Rieley, J.O., Boehm, H.D. v, Jaya, A., Limin, S., 2002. The amount of carbon released from peat and forest fires in Indonesia during 1997. *Nature* 420, 61–65. https://doi.org/10.1038/nature01131

Plante, A., Conant, R.T., 2014. Chapter 37. Soil Organic Matter Dynamics, Climate Change Effects. *Global Environmental Change* 317–323. https://doi.org/10.1007/978-94-007-5784-4_3.

Panagos, P., Ballabio, C., Himics, M., Scarpa, S., Matthews, F., Bogonos, M., Poesen, J., Borrelli, P., 2021. Projections of soil loss by water erosion in Europe by 2050. *Environmental Science & Policy* 124, 380–392. https://doi.org/10.1016/j.envsci.2021.07.012

Paul, E.A., 2014. Soil microbiology, ecology, and biochemistry, Academic Press pp. 582.

Paustian, K., 2014. Soil: Carbon Sequestration in Agricultural Systems. *Encyclopedia of Agriculture and Food Systems* 140–152. https://doi.org/10.1016/B978-0-444-52512-3.00093-0

Pehme, K.-M., Orupold, K., Kuusemets, V., Tamm Ottar and Jani, Y., Tamm, T., Kriipsalu, M., 2020. Field study on the efficiency of a methane degradation layer composed of fine fraction soil from landfill mining. *Sustainability* 12, 6209. https://doi.org/10.3390/su12156209

Pellizzari, M., 2020. Cyperus-dominated vegetation in the eastern Po river. *Plant Sociology* 57, 1–16. https://doi.org/10.3897/pls2020571/06

Pignatti, S., Palombo, A., Pascucci, S., Romano, F., Santini, F., Simoniello, T., Umberto, A., Vincenzo, C., Acito, N., Diani, M., Matteoli, S., Corsini, G., Casa, R., de Bonis, R., Laneve, G., Ananasso, C., 2013. The PRISMA hyperspectral mission: Science activities and opportunities for agriculture and land monitoring, in: *2013 IEEE International*

*Geoscience and Remote Sensing Symposium- IGARSS. IEEE*, pp. 4558–4561. https://doi.org/10.1109/IGARSS.2013.6723850

Poeplau, C., Don, A., 2015. Carbon sequestration in agricultural soils via cultivation of cover crops – A meta-analysis. *Agriculture, Ecosystems & Environment* 200, 33–41. https://doi.org/10.1016/j.agee.2014.10.024

Powlson, D.S., Bhogal, A., Chambers, B.J., Coleman, K., Macdonald, A.J., Goulding, K.W.T., Whitmore, A.P., 2012. The potential to increase soil carbon stocks through reduced tillage or organic material additions in England and Wales: A case study. *Agriculture, Ecosystems & Environment* 146, 23–33. https://doi.org/10.1016/j.agee.2011.10.004

Prasad, J.V.N.S., Srinivasa Rao, C., Srinivas, K., Naga Jyothi, C., Venkateswarlu, B., Ramachandrappa, B.K., Dhanapal, G.N., Ravichandra, K., Mishra, P.K., 2016. Effect of ten years of reduced tillage and recycling of organic matter on crop yields, soil organic carbon and its fractions in Alfisols of semi arid tropics of southern India. *Soil & Tillage Research* 156, 131–139. https://doi.org/10.1016/j.still.2015.10.013

Prăvălie, R., Patriche, C., Bandoc, G., 2017. Quantification of land degradation sensitivity areas in Southern and Central Southeastern Europe. New results based on improving DISMED methodology with new climate data. *Catena* 158, 309–320. https://doi.org/10.1016/j.catena.2017.07.006

Pries, H.C.E., Castanha, C., Porras, R.C., Torn, M.S., 2017. The whole-soil carbon flux in response to warming. *Science* 355, 6332. https://doi.org/10.1126/science.aal131

Prosperi, P., Bloise, M., Tubiello, F.N., Conchedda, G., Rossi, S., Boschetti, L., Salvatore, M., Bernoux, M., 2020. New estimates of greenhouse gas emissions from biomass burning and peat fires using MODIS Collection 6 burned areas. *Climatic Change* 161, 415–432. https://doi.org/10.1007/s10584-020-02654-0

Puttock, A., Dungait, J.A.J., Bol, R., Dixon, E.R., Macleod, C.J.A., Brazier, R.E., 2012. Stable carbon isotope analysis of fluvial sediment fluxes over two contrasting C4 -C3 semi-arid vegetation transitions. *Rapid Communications in Mass Spectrometry* 26, 2386–2392. https://doi.org/10.1002/rcm.6257

QGIS.org, 2021. QGIS Geographic Information System [WWW Document]. QGIS Association. URL http://www.qgis.org

Qin, S., Chen, L., Fang, K., Zhang, Q., Wang, J., Liu, F., Yu, J., Yang, Y., 2019. Temperature sensitivity of SOM decomposition governed by aggregate protection and microbial communities. *Sciences Advanced* 5, eaau1218. https://doi.org/10.1126/sciadv.aau1218

Qiu, L., Zhang, Q., Zhu, H., Reich, P. B., Banerjee, S., van der Heijden, M. G. A., Sadowsky, M J., Satoshi, I., Jia, X., Shao, M., Liu, B., Jiao, H., Li, H., Wei, X., 2021. Erosion reduces

soil microbial diversity, network complexity and multifunctionality. *The ISME Journal* 15, 2474–2489. https://doi.org/10.1038/s41396-021-00913-1

Quideau, S.A., 2018. Soil Organic Matter (SOM): Landscape. Encyclopedia of soil science.

R Core Team, 2017. R: a language and environment for statistical computing [WWW Document]. URL https://www.R–project.org/ (accessed 6.22.20).

Rappold, A.G., Stone, S.L., Cascio, W.E., Neas, L.M., Kilaru, V.J., Carraway, M.S., Szykman James J. and Ising, A., Cleve, W.E., Meredith, J.T., Vaughan-Batten, H., Deyneka, L., Devlin, R.B., 2011. Peat Bog Wildfire Smoke Exposure in Rural North Carolina Is Associated with Cardiopulmonary Emergency Department Visits Assessed through Syndromic Surveillance. *Environmental Health Perspectives* 119, 1415–1420. https://doi.org/10.1289/ehp.1003206

Raven, M.R., Adkins, J.F., Werne, J.P., Lyons, T.W., Sessions, A.L., 2015. Sulfur isotopic composition of individual organic compounds from Cariaco Basin sediments. *Organic Geochemistry* 80, 53–59. https://doi.org/10.1016/j.orggeochem.2015.01.002

Reicosky, D.C., Lindstrom, M.J., Schumacher, T.E., Lobb, D.E., Malo, D.D., 2005. Tillage-induced CO2 loss across an eroded landscape. *Soil & Tillage Research* 81, 183–194. https://doi.org/10.1016/j.still.2004.09.007

Rein, G., 2015. Smoldering-Peat Megafires, in: *Coal and Peat Fires: A Global Perspective*. Elsevier, pp. 1–11. https://doi.org/10.1016/B978-0-444-59510-2.00001-X

Rein, G., 2009. Smouldering combustion phenomena in science and technology. *Review of Chemical Engineering* 1, 3–18.

Rein, G., Cleaver, N., Ashton, C., Pironi Paolo and Torero, J.L., 2008. The severity of smouldering peat fires and damage to the forest soil. *Catena* 74, 304–309. https://doi.org/10.1016/j.catena.2008.05.008

Restuccia, F., Huang, X., Rein, G., 2017. Self-ignition of natural fuels: Can wildfires of carbon-rich soil start by self-heating? *Fire Safety Journal* 91, 828–834. https://doi.org/10.1016/j.firesaf.2017.03.052

Roddaz, M., Viers, J., Moreira-Turcq, P., Blondel, C., Sondag, F., Guyot, J.-L., Moreira, L., 2014. Evidence for the control of the geochemistry of Amazonian floodplain sediments by stratification of suspended sediments in the Amazon. *Chemical Geology* 387, 101–110. https://doi.org/10.1016/j.chemgeo.2014.07.022

Ruiz-Colmenero, M., Bienes, R., Eldridge, D., Marques, M.J., 2013. Vegetation cover reduces erosion and enhances soil organic carbon in a vineyard in the central Spain. *Catena* 104, 153–160. https://doi.org/10.1016/j.catena.2012.11.007

Sage, R., 2004. The evolution of C4 photosynthesis. *New Phytologist* 161, 341–370. https://doi.org/10.1111/j.1469-8137.2004.00974.x

Salani, G.M., Brombin, V., Natali, C., Bianchini, G., 2021. Carbon, nitrogen, and sulphur isotope analysis of the Padanian Plain sediments: Backgrounds and provenance indication of the alluvial components. *Applied Geochemistry* 135, 105130. https://doi.org/10.1016/j.apgeochem.2021.105130

Salani, G.M., Fornasari, G., Brombin, V., Rizzo, E., Bianchini, G., 2022. Definizione del benchmark del carbonio di un suolo agricolo: Relazione tra sostanza organica e conducibilità elettrica del suolo, in: XVI Convegno GIT-SI. Fondi, Latina.

Salomão, G.N., Dall'Agnol, R., Sahoo, P.K., Angélica, R.S., de Medeiros Filho, C.A., Ferreira Júnior, J. da S., Sousa da Silva, M., Souza Filho, P.W.M. e, Nascimento Junior, W. da R., da Costa, M.F., Guilherme, L.R.G., Siqueira, J.O. de, 2020. Geochemical mapping in stream sediments of the Carajás Mineral Province: Background values for the Itacaiúnas River watershed, Brazil. *Applied Geochemistry* 118, 104608. https://doi.org/10.1016/j.apgeochem.2020.104608

Sanderman, J., Baldock, J.A., Dangal, S.R.S., Ludwig, S., Potter, S., Rivard, C., Savage, K., 2021. Soil organic carbon fractions in the Great Plains of the United States: an application of mid-infrared spectroscopy. *Biogeochemistry* 156, 97–114. https://doi.org/10.1007/s10533-021-00755-1

Sanderman, J., Hengl, T., Fiske, G.J., 2017. Soil carbon debt of 12,000 years of human land use. *Proceedings of the National Academy of Sciences* 114, 9575–9580. https://doi.org/10.1073/pnas.1706103114

Santos, R. v, Clayton, R.N., 1995. Variations of oxygen and carbon isotopes in carbonatites–- a study of Brazilian alkaline complexes. *Geochimica et Cosmochimica Acta* 59, 1339–1352. https://doi.org/10.1016/0016-7037(95)00048-5

Sarkar, B., Singh, M., Mandal, S., Churchman, G.J., Bolan, N.S., 2018. Clay Minerals—Organic Matter Interactions in Relation to Carbon Stabilization in Soils, in: *The Future of Soil Carbon*. Elsevier, pp. 71–86. https://doi.org/10.1016/B978-0-12-811687-6.00003-1

Scharlemann, J.P., Tanner, E.V., Hiederer, R., Kapos, V., 2014. Global soil carbon: understanding and managing the largest terrestrial carbon pool. *Carbon Management* 5, 81–91. https://doi.org/10.4155/cmt.13.77

Schidlowski, M., 2001. Carbon isotopes as biogeochemical recorders of life over 3.8 Ga of Earth history: evolution of a concept. *Precambrian Research* 106, 117–134. https://doi.org/10.1016/S0301-9268(00)00128-5

Schimel, D., Coleman, D., Horton, K., 1985. Soil organic matter dynamics in paired rangeland and cropland toposequences in North Dakota. *Geoderma* 36, 201–214. https://doi.org/10.1016/0016-7061(85)90002-3

Schmidt, M.W.I., Torn, M.S., Abiven, S., Dittmar, T., Guggenberger, G., Janssens, I.A., Kleber, M., Kögel-Knabner, I., Lehmann, J., Manning, D.A.C., Nannipieri, P., Rasse, D.P., Weiner, S., Trumbore, S.E., 2011. Persistence of soil organic matter as an ecosystem property. *Nature* 478, 49–56. https://doi.org/10.1038/nature10386

Schoeneberger, P.J., Wysocki, D.A., Benham, E.C., Soil Survey Staff, 2012. Field book for describing and sampling soils, version 3.0. Natural Resources Conservation Service, National Soil Survey Center, Lincoln, NE, USA.

Shukla, P.R., Skea, J., Calvo Buendia, E., Masson-Delmotte, V., Pörtner, H.O., Roberts, D.C., Zhai, P., Slade, R., Connors, S., van Diemen, R., 2019. IPCC, 2019: Climate Change and Land: an IPCC Special Report on Climate Change, Desertification, Land Degradation, Sustainable Land Management, Food Security, and Greenhouse Gas Fluxes in Terrestrial Ecosystems.

Simeoni, U., Corbau, C., 2009. A review of the Delta Po evolution (Italy) related to climatic changes and human impacts. *Geomorphology* 107, 64–71. https://doi.org/10.1016/j.geomorph.2008.11.004

Six, J., Elliott, E.T., Paustian, K., Doran, J.W., 1998. Aggregation and Soil Organic Matter accumulation in cultivated and native grassland soils. *Soil Science Society of America Journal* 62, 1367–1377. https://doi.org/10.2136/sssaj1998.03615995006200050032x

Smith, C., Chalk, P., 2021. Carbon ($\delta^{13}C$) dynamics in agroecosystems under traditional and minimum tillage systems: a review. *Soil Research* 59, 661–672. https://doi.org/10.1071/SR21056

Smith, L.C., MacDonald, G.M., Velichko, A.A., Beilman, D.W., Borisova, O.K., Frey, K.E., Kremenetski, K. v, Sheng, Y., 2004. Siberian peatlands a net carbon sink and global methane source since the early Holocene. *Science* 303, 353–356. https://doi.org/10.1126/science.1090553

Smith, P., Soussana, J., Angers, D., Schipper, L., Chenu, C., Rasse, D.P., Batjes, N.H., Egmond, F., McNeill, S., Kuhnert, M., Arias-Navarro, C., Olesen, J.E., Chirinda, N., Fornara, D., Wollenberg, E., Álvaro-Fuentes, J., Sanz-Cobena, A., Klumpp, K., 2020. How to measure, report and verify soil carbon change to realize the potential of soil carbon sequestration for atmospheric greenhouse gas removal. *Global Change Biology* 26, 219–241. https://doi.org/10.1111/gcb.14815

Smith, W.N., Desjardins, R.L., Grant, B., 2001. Estimated changes in soil carbon associated with agricultural practices in Canada. *Canadian Journal of Soil Science* 81, 221–227. https://doi.org/10.4141/S00-033

Soane, B.D., van Ouwerkerk, C., 1995. Implications of soil compaction in crop production for the quality of the environment. *Soil & Tillage Research* 35, 5–22. https://doi.org/10.1016/0167-1987(95)00475-8

Søballe, D.M., Kimmel, B.L., 1987. A large-scale comparison of factors influencing phytoplankton abundance in rivers, lakes, and impoundments. *Ecology* 68, 1943–1954. https://doi.org/10.2307/1939885

Solomon, D., Lehmann, J., Zech, W., 2000. Land use effects on soil organic matter properties of chromic luvisols in semi-arid northern Tanzania: carbon, nitrogen, lignin and carbohydrates, *Agriculture, Ecosystems & Environment* 78, 203–213. https://doi.org/10.1016/S0167-8809(99)00126-7

Sothe, C., Gonsamo, A., Arabian, J., Kurz, W.A., Finkelstein, S.A., Snider, J., 2022. Large soil carbon storage in terrestrial ecosystems of Canada. *Global Biogeochemical Cycles* 36. https://doi.org/10.1029/2021GB007213

Stefani, M., Vincenzi, S., 2005. The interplay of eustasy, climate and human activity in the late Quaternary depositional evolution and sedimentary architecture of the Po Delta system. *Marine Geology* 222–223, 19–48. https://doi.org/10.1016/J.MARGEO.2005.06.029

Stevens, A., Nocita, M., Tóth, G., Montanarella, L., van Wesemael, B., 2013. Prediction of soil organic carbon at the European scale by Visible and Near Infrared Reflectance Spectroscopy. *pLoS One* 8, e66409. https://doi.org/10.1371/journal.pone.0066409

Stevenson, F., 1994. Humus Chemistry: Genesis, Composition, Reactions. *Humus Chemistry* 72, 512.

Still, C., Berry, J., Collatz, G., DeFries, R., 2003. Global distribution of C3 and C4 vegetation: Carbon cycle implications. *Global Biogeochemical Cycles* 17, 6-1–6-14. https://doi.org/10.1029/2001GB001807

Strauss, H., 1997. The isotopic composition of sedimentary sulfur through time. *Palaeogeography, Palaeoclimatology, Palaeoecology* 132, 97–118. https://doi.org/10.1016/S0031-0182(97)00067-9

Svensson, J., Waisman, H., Vogt-Schilb, A., Bataille, C., Aubert, P.M., Jaramilo-Gil, M., Angulo-Paniagua, J., Arguello, R., Bravo, G., Buira, D., Collado, M., de La Torre Ugarte, D., Delgado, R., Lallana, F., Quiros-Tortos, J., Soria, R., Tovilla, J., Villamar, D., 2021. A low GHG development pathway design framework for agriculture, forestry and land use. *Energy Strategy Reviews* 37, 100683. https://doi.org/10.1016/J.ESR.2021.100683

Szpak, P., 2014. Complexities of nitrogen isotope biogeochemistry in plant-soil systems: implications for the study of ancient agricultural and animal management practices. *Frontiers in Plant Science* 5. https://doi.org/10.3389/fpls.2014.00288

Tamm, C.O., 1991. Introduction: geochemical occurrence of Nitrogen. Natural Nitrogen cycling and anthropogenic Nitrogen emissions. *Nitrogen in Terrestrial Ecosystems* 1–6. https://doi.org/10.1007/978-3-642-75168-4_1

Targetti, S., Raggi, M., Zavalloni, M., Viaggi, D., 2021. Perceived benefits from reclaimed rural landscapes: Evidence from the lowlands of the Po River Delta, Italy. *Ecosystem Services* 49, 101288. https://doi.org/10.1016/J.ECOSER.2021.101288

Telford, W.M., Geldart, L.P., Sheriff, R.E., Keys, D.A., 1976. Applied Geophysics. Cambridge University Press.

Terefe, T., Mariscal, S.-I., Gomez, V., Espejo, R., 2005. Relationship between soil color and temperature in the surface horizon of mediterranean soils. *Soil Science* 170, 495–503. https://doi.org/10.1097/01.ss.0000175341.22540.93

Terefe, T., Mariscal, S.-I., Peregrina, F., Espejo, R., 2008. Influence of heating on various properties of six Mediterranean soils. A laboratory study. *Geoderma* 143, 273–280. https://doi.org/10.1016/j.geoderma.2007.11.018

Thiébeau, P., Girardin, C., Recous, S., 2021. Water interception and release of soluble carbon by mulches of plant residues under contrasting rain intensities. *Soil & Tillage Research* 208, 104882. https://doi.org/10.1016/j.still.2020.104882

Tiessen, H., Cuevas, E., Chacon, P., 1994. The role of soil organic matter in sustaining soil fertility. *Nature* 371, 783–785. https://doi.org/10.1038/371783a0

Tóth, G., Jones, A., Montanarella, L., 2013. The LUCAS topsoil database and derived information on the regional variability of cropland topsoil properties in the European Union. *Environmental Monitoring and Assessment* 185, 7409–7425. https://doi.org/10.1007/s10661-013-3109-3

Tromp-van Meerveld, H.J., McDonnell, J.J., 2009. Assessment of multi-frequency electromagnetic induction for determining soil moisture patterns at the hillslope scale. *Journal of Hydrology* 368, 56–67. https://doi.org/10.1016/j.jhydrol.2009.01.037

Turner, K.G., Anderson, S., Gonzales-Chang, M., Costanza, R., Courville, S., Dalgaard, T., Dominati, E., Kubiszewski, I., Ogilvy, S., Porfirio, L., Ratna, N., Sandhu, H., Sutton, P.C., Svenning, J.-C., Turner, G.M., Varennes, Y.-D., Voinov, A., Wratten, S., 2016. A review of methods, data, and models to assess changes in the value of ecosystem services from land degradation and restoration. *Ecological Modelling* 319, 190–207. https://doi.org/10.1016/j.ecolmodel.2015.07.017

Turner, M.G., Smithwick, E.A.H., Metzger, K.L., Tinker, D.B., Romme, W.H., 2007. Inorganic nitrogen availability after severe stand-replacing fire in the Greater Yellowstone ecosystem. *Proceedings of the National Academy of Sciences* 104, 4782–4789. https://doi.org/10.1073/pnas.0700180104

Uda, S.K., Hein, L., Atmoko, D., 2019. Assessing the health impacts of peatland fires: a case study for Central Kalimantan, Indonesia. *Environmental Science and Pollution Research* 26, 31315–31327. https://doi.org/10.1007/s11356-019-06264-x

Ulery, A.L., Graham, R.C., Chadwick, O.A., Wood, H.B., 1995. Decade-scale changes of soil carbon, nitrogen and exchangeable cations under chaparral and pine. *Geoderma* 65, 121–134. https://doi.org/10.1016/0016-7061(94)00034-8

Ungaro, F., Calzolari, C., Tarocco, P., Giapponesi, A., Sarno, G., 2005. Quantifying spatial uncertainty of soil organic matter content using conditional sequential simulations: A case study in Emilia Romagna Plain (Northern Italy). *Canadian Journal of Soil Science* 85, 499–510. https://doi.org/10.4141/S04-084

Usup, A., Hashimoto, Y., Takahashi, H., Hayasaka, H., 2004. Combustion and thermal characteristics of peat fire in tropical peatland in Central Kalimantan, Indonesia. *Tropics* 14, 1–19. https://doi.org/10.3759/tropics.14.1

van der Wal, A., de Boer, W., 2017. Dinner in the dark: Illuminating drivers of soil organic matter decomposition. *Soil Biology and Biochemistry* 105, 45–48. https://doi.org/10.1016/j.soilbio.2016.11.006

Vaudour, E., Gholizadeh, A., Castaldi, F., Saberioon, M., Borůvka, L., Urbina-Salazar, D., Fouad, Y., Arrouays, D., Richer-de-Forges, A.C., Biney, J., Wetterlind, J., van Wesemael, B., 2022. Satellite imagery to map topsoil organic carbon content over cultivated areas: an overview. *Remote Sensing* 14, 2917. https://doi.org/10.3390/rs14122917

Védère, C., Lebrun, M., Honvault, N., Aubertin, M.-L., Girardin, C., Garnier, P., Dignac, M.-F., Houben, D., Rumpel, C., 2022. How does soil water status influence the fate of soil organic matter? A review of processes across scales. *Earth Science Reviews* 234, 104214. https://doi.org/10.1016/j.earscirev.2022.104214

Verschuuren, J., 2017. Towards a regulatory design for reducing emissions from agriculture: lessons from Australia's carbon farming initiative. *Climate Law* 7, 1–51. https://doi.org/10.1163/18786561-00701001

Vicente, V.A.S., Pratas, J.A.M.S., Santos, F.C.M., Silva, M.M.V.G., Favas, P.J.C., Conde, L.E.N., 2021. Geochemical anomalies from a survey of stream sediments in the Maquelab area (Oecusse, Timor-Leste) and their bearing on the identification of mafic-ultramafic

chromite rich complex. *Applied Geochemistry* 126, 104868. https://doi.org/10.1016/j.apgeochem.2020.104868

Viscarra Rossel, R., Behrens, T., Ben-Dor, E., Brown, D., Demattê, J., Shepherd, K., Shi, Z., Stenberg, B., Stevens, A., Adamchuk, V., Aïchi, H., Barthès, B., Bartholomeus, H., Bayer, A., Bernoux, M., Böttcher, K., Brodský, L., Du, C., Chappell, A., Fouad, Y., Genot, V., Gomez, C., Grunwald, S., Gubler, A., Guerrero, C., Hedley, C., Knadel, M., Morrás, H., Nocita, M., Ramirez-Lopez, L., Roudier, P., Campos, E., Sanborn, P., Sellitto, V., Sudduth, K., Rawlins, B., Walter, C., Winowiecki, L., Hong, S., Ji, W., 2016. A global spectral library to characterize the world's soil. *Earth-Science Reviews* 155, 198–230. https://doi.org/10.1016/J.EARSCIREV.2016.01.012

Vittori Antisari, L., Bianchini, G., Cremonini, S., Di Giuseppe, D., Falsone, G., Marchesini, M., Marvelli, S., Vianello G., 2016. Multidisciplinary study of a Late glacial-Holocene sedimentary sequence near Bologna (Italy): insights on natural and anthropogenic impacts on the landscape dynamics. *Journal of Soils and Sediments* 16, 645–662. https://doi.org/10.1007/S11368-015-1266-4

von Lützow, M., Kögel-Knabner, I., Ekschmitt, K., Matzner, E., Guggenberger, G., Marschner, B., Flessa, H., 2006. Stabilization of organic matter in temperate soils: mechanisms and their relevance under different soil conditions–- a review. *European Journal of Soil Science* 57, 426–445. https://doi.org/10.1111/j.1365-2389.2006.00809.x

Wada, E., 2009. Stable $\delta^{15}N$ and $\delta^{13}C$ isotope ratios in aquatic ecosystems. *Proceedings of the Japan Academy, Ser. B, Physical and Biological Sciences* 85, 98. https://doi.org/10.2183/PJAB.85.98

Wang, C., Houlton, B.Z., Liu, D., Hou, J., Cheng, W., Bai, E., 2018. Stable isotopic constraints on global soil organic carbon turnover. *Biogeosciences* 15, 987–995. https://doi.org/10.5194/BG-15-987-2018

Wang, G., Jia, Y., Li, W., 2015. Effects of environmental and biotic factors on carbon isotopic fractionation during decomposition of soil organic matter. *Scientific Reports* 5, 1–11. https://doi.org/10.1038/srep11043

Wang, S., Guan, K., Zhang, C., Lee, D., Margenot, A.J., Ge, Y., Peng, J., Zhou, W., Zhou, Q., Huang, Y., 2022. Using soil library hyperspectral reflectance and machine learning to predict soil organic carbon: Assessing potential of airborne and spaceborne optical soil sensing. *Remote Sensing of Environment* 271, 112914. https://doi.org/10.1016/j.rse.2022.112914

Wang, Y., Tu, C., Cheng, L., Li, C., Gentry, L. F., Hoyt, G. D., Zhang, X., Hu, S., 2011. Long-term impact of farming practices on soil organic carbon and nitrogen pools and microbial

biomass and activity. *Soil and Tillage Research* 17, 8–16. https://doi.org/10.1016/j.still.2011.08.002

Watts, A.C., Kobziar, L.N., 2013. Smoldering combustion and ground fires: ecological effects and multi-scale significance. *Fire Ecology* 9, 124–132. https://doi.org/10.4996/fireecology.0901124

Wills, S., Loecke, T., Sequeira, C., Teachman, G., Grunwald, S., West, L.T., 2014. Overview of the U.S. Rapid Carbon Assessment Project: Sampling Design, Initial Summary and Uncertainty Estimates, in: Hartemink, A., McSweeney, K. (eds) *Soil Carbon. Progress in Soil Science*. Springer, Cham. 95–104. https://doi.org/10.1007/978-3-319-04084-4_10

Wisniewski, J., Sampson, R.N., 1993. Terrestrial Biospheric Carbon Fluxes: Quantification of Sinks and Sources of $CO_2$. Kluwer Academic Publishers, Dordrecht.

Wu, J., 2011. Carbon accumulation in paddy ecosystems in subtropical China: evidence from landscape studies. *European Journal of Soil Science* 62, 29–34. https://doi.org/10.1111/j.1365- 2389.2010.01325.x

Xu, G., Fan, X., Miller, A.J., 2012. Plant Nitrogen assimilation and use efficiency. *Annual Review of Plant Biology* 63, 153–182. https://doi.org/10.1146/annurev-arplant-042811-105532

Xu, X., Liu, W., 2017. The global distribution of Earth's critical zone and its controlling factors. *Geophysical Research Letters* 44, 3201–3208. https://doi.org/10.1002/2017GL072760

Yuan, H., Restuccia, F., Rein, G., 2021. Spontaneous ignition of soils: a multi-step reaction scheme to simulate self-heating ignition of smouldering peat fires. *International Journal of Wildland Fire* 30, 440–453. https://doi.org/10.1071/WF19128

Zakeri, A., Dehghanian, F., Fahimnia, B., Sarkis, J., 2015. Carbon pricing versus emissions trading: A supply chain planning perspective. *International Journal of Production Economics* 164, 197–205. https://doi.org/10.1016/j.ijpe.2014.11.012

Zethof, J.H.T., Bettermann, A., Vogel, C., Babin, D., Cammeraat, E.L.H., Sole-Benet, A., Lazaro, R., Luna, L., Nesme, J., Woche, S.K., Sorensen, S.J., Smalla, K., Kalbitz, K., 2020. Prokaryotic community composition and extracellular polymeric substances affect soil microaggregation in carbonate containing semiarid grasslands. *Frontiers in Environmental Science* 8. https://doi.org/10.3389/fenvs.2020.00051

Zethof, J.H.T., Leue, M., Vogel, C., Stoner, S.W., Kalbitz, K., 2019. Identifying and quantifying geogenic organic carbon in soils – the case of graphite. *Soil* 5, 383–398. https://doi.org/10.5194/soil-5-383-2019

Zhong, C., Wang, C., Wu, C., 2015. MODIS-Based Fractional Crop Mapping in the U.S. Midwest with Spatially Constrained Phenological Mixture Analysis. *Remote Sensing* 7, 512–529. https://doi.org/10.3390/rs70100512

## Acknowledgments

With these few words I would like to spend my gratitude to the people who helped me and filled my life during these three years. My intention is to remember everyone.
First of all, my gratitude goes to my supervisor, Prof. Gianluca Bianchini, who with his research experience and his calm approach has provided me with fundamental elements to grow my profile. A constant in my PhD course was Dr. Valentina Brombin, whose precise and reliable suggestions gave me the right ingredients to correct and improve my work. I also want to be grateful to her and to Prof. Costanza Bonadiman, for the human comprehension I received from them during the darkest period of my PhD. For the hospitality I received in Vienna during my experience abroad, I want to thank Dr. Stefano Natali and his collaborators. At the same time, I want to thank all the persons that collaborate with me such as: Prof. Claudio Natali, Dr. Chiara Marchina, Maura Mancinelli, Enrico Mistri, Giacomo Fornasari, Michele Lissoni, Dr. Flavio Fornasier (also for his lab teaching), Prof. Annalisa Martucci, Prof. Enzo Rizzo, Prof. Gilmo Vianello, Dr. Stefano Cremonini, and Prof. Livia Vittori Antisari.
I thank the personnel of our department as: Dr. Renzo Tassinari, Dr. Massimo Verde, and Francesco Droghetti. I also want to remember all the girls and guys I met during my PhD period. Thanks to Edo (old strong rock!), Jack, Giulio, Valeria and Luca, Silvia, Sahara, Nicola, Claudia and Andrea, Lorenzo, Simone, Claudia, Giacomo, Sara, Francesca, and Alessia.
Obviously, I embrace the person with whom I want to share my life, my little heart, Giulia.
For the last but not the least, I want remember my family, my father Davide, my mother Floriana, my grandfather Erino, and, in particular, my grandmother Rita. I want to believe this: I hope that she will come home healed in a few days, we need you! I also want to be happy to remember with all my friends that they spent pleasant moments with me.